NIR Active Squaraine Dyes for Dye-Sensitized Solar Cells: Modulating Aggregation, Orientation and Electronic Properties of the Dyes

Thesis Submitted to AcSIR

For the Award of the Degree of

DOCTOR OF PHILOSOPHY

In Chemical Sciences

By
Rajesh Bisht
(Registration Number: 10CC12A26015)

Under the guidance of
Dr. Jayaraj Nithyanandhan

Physical and Materials Chemistry Division
CSIR-National Chemical Laboratory
Pune-411008, India

May 2018

To My Family

For their love, endless support, encouragement & sacrifices

सीएसआईआर - राष्ट्रीय रासायनिक प्रयोगशाला
(वैज्ञानिक तथा औद्योगिक अनुसंधान परिषद)
डॉ. होमी भाभा मार्ग, पुणे - 411 008, भारत
CSIR - NATIONAL CHEMICAL LABORATORY
(Council of Scientific & Industrial Research)
Dr. Homi Bhabha Road, Pune - 411 008, India

CERTIFICATE

This is to certify that the work incorporated in this Ph.D. thesis entitled "**NIR Active Squaraine Dyes for Dye-Sensitized Solar Cells: Modulating Aggregation, Orientation and Electronic Properties of the Dyes**" submitted by **Mr. Rajesh Bisht** to Academy of Scientific and Innovative Research (AcSIR) in fulfilment of the requirements for the award of the Degree of Doctor of Philosophy in Chemical Sciences, embodies original research work under my supervision. I further certify that this work has not been submitted to any other University or Institution in part or full for the award of any degree or diploma. Research material obtained from other sources has been duly acknowledged in the thesis. Any text, illustration, table etc., used in the thesis from other sources, have been duly cited and acknowledged.

Research Student
Rajesh Bisht

Research guide
Dr. Jayaraj Nithyanandhan
Senior Scientist

Communication Channels
NCL Level DID : 2590
NCL Board No. : +91-20-25902000
EPABX : +91-20-25893300
: +91-20-25893400
FAX
Director's Office : +91-20-25902601
COA's Office : +91-20-25902660
SPO's Office : +91-20-25902664
WEBSITE
www.ncl-india.org

DECLARATION

I, hereby declare that the research work in this thesis entitled, "**NIR Active Squaraine Dyes for Dye-Sensitized Solar Cells: Modulating Aggregation, Orientation and Electronic Properties of the Dyes**" submitted for the degree of Doctor of Philosophy in Chemical Sciences to the Academy of Scientific & Innovative Research (AcSIR), has been carried out at the Physical and Materials Chemistry Division of CSIR-National Chemical Laboratory, Pune, India under the guidance of **Dr. Jayaraj Nithyanandhan**. Research material obtained from other sources has been duly cited and acknowledged in the thesis. The work is original and has not been submitted in part or full by me for any other degree or diploma to other University.

Date: 7/5/18

Physical and Materials Chemistry Division
CSIR-National Chemical Laboratory,
Pune - 411008, India.

Rajesh Bisht
Research Student

CONTENTS

Acknowledgments **v**
Abbreviations **vii**
Abstract **ix**

Chapter 1: Introduction

1.1. Global Energy Crisis……..……. 3
1.2. Solar Energy…… 3
1.3. Photovoltaic……. 4
1.3.1. First Generation Solar Cells……. 4
1.3.2. Second Generation Solar Cells…….…… 5
1.3.3. Third Generation Solar Cells……..... 6
1.4. Dye-sensitized solar cells……..... 8
1.4.1. Operating Principles of dye-sensitized solar cells…… 9
1.4.2. Key parameters……. 10
1.4.3. Key components……... 13
1.5. Sensitizers for Dye-sensitized solar cells……..... 16
1.6. Near-infrared (NIR) active dyes in DSSCs……. 19
1.6.1. Zinc- Porphyrins (Zn-Por)……..……. 19
1.6.2. Phthalocyanines (Pcs)…….…….……. 21
1.6.3. Squaraine dyes……..…… 23
1.6.4. Aggregation in Squaraine dyes……..… 26
1.7. Objectives of the Thesis…….……...….. 29
1.8. References……... 30

Chapter 2: Unsymmetrical Squaraine Dyes with Benzodithiophene (BDT) as π-Spacer for Dye-sensitized Solar Cells

2.1. Introduction……. 41
2.2. Results and Discussion……..... 44

2.2.1. Synthesis…….. 44

2.2.2. Optical and Electrochemical Properties……... 46

2.2.3. Computational Studies…….. 49

2.2.4. Photovoltaic Performance……..……... 51

2.2.5. Electrochemical Impedance Spectroscopy (EIS) …… 54

2.2.6. Open circuit voltage Decay (OCVD)…...…… 56

2.3. Summary……. 57

2.4. Experimental……... 57

2.5. NMR Spectra……... 65

2.6. References……... 76

Chapter 3: Fluorenylindolenine based Unsymmetrical Squaraine Dyes for Dye-sensitized Solar Cells

3.1. Introduction……. 81

3.2. Results and Discussion…… 83

3.2.1. Synthesis……... 83

3.2.2. Optical and Electrochemical Properties……... 85

3.2.3. Computational Studies…….. 89

3.2.4. Photovoltaic Performance…….… 91

3.2.5. Electrochemical Impedance Spectroscopy (EIS)……. 96

3.3. Summary…….…. 98

3.4. Experimental…… 98

3.5. NMR Spectra……... 106

3.6. References……... 117

Chapter 4: Indenoquinaldine based Unsymmetrical Squaraine Dyes for Near-Infrared Responsive Dye-sensitized Solar Cells

4.1. Introduction……. 121

4.2. Results and Discussion…… 123

4.2.1. Synthesis……... 123

4.2.2. Optical and Electrochemical Properties……...… 124

4.2.3. Computational Studies…….. 128

4.2.4. Photovoltaic Performance……. 130

4.2.5. Electrochemical Impedance Spectroscopy (EIS)……. 136

4.3. Summary…….. 138

4.4. Experimental…… 138

4.5. NMR Spectra……... 146

4.6. References……... 157

Chapter 5: Extended Hetero-Acyloin Phototrigger and their Application in Organic Electronics: Efforts towards Developing a Photoinitiated Method for Processing Organic Molecules

5.1. Introduction……. 161

5.2. Results and Discussion…… 169

5.2.1. Synthesis……..... 169

5.2.2. Photophysical and Photochemical Investigation……...…... 170

5.2.3. Organic Field Effect Transistors (OFETs) Characteristics…….. 178

5.3. Summary……..…… 182

5.4. Experimental……..……. 182

5.5. NMR Spectra…….....…... 192

5.6. References……..... 206

Chapter 6: Summary and Future Outlooks

6.1. Summary…….. 211

6.2. Future Outlooks……... 213

List of Publications 215

Erratum 216

ACKNOWLEDGMENTS

There are many people I would like to thank for their support, guidance, and friendship over the course of this Ph.D. First of all, I would like to express my profound gratitude and sincere thanks to my supervisor Dr. J. Nithyanandhan for his invaluable advice, inspiration and continuous support throughout my Ph.D. His guidance and encouragement are gratefully acknowledged.

My sincere appreciation goes to Dr. Kothandam Krishnamoorthy for helping me begin my research by providing lab space and access to the required instruments, specially during the initial days of my research. I also thank him for helpful discussions and suggestions on scientific problems in our weekly research review meetings. As a member of my Doctoral Advisory Committee (DAC), his constructive criticism also helped me in improving my research progress. Great appreciation is extended to other members of my DAC, Dr. Prakash P. Wadgaonkar, and Dr. D. Srinivasa Reddy, who encouraged me with their valuable suggestions and advice during my work presentations.

I sincerely thank the Council of Scientific and Industrial Research (CSIR) for my Ph.D. fellowship. I would also like to thank Director, CSIR-National Chemical Laboratory (CSIR-NCL) and Head of Physical and Materials Chemistry Division, for providing the infrastructure and advanced facilities for research.

I wish to appreciate and acknowledge my seniors and past members from Dr. Krishnamoorthy's group: Dr. Arulkashmir, Dr.Bhanprakash, Dr. Chayanika, Dr. Manik, Dr. Mrinmoy, Dr. Rajashree, Dr. Satej and Dr. Saumya, who made me feel at home when I joined NCL.

I am thankful to all of my past and present lab-members: Neeta, Manik, Munavvar, Punitharasu, Ananthan, Kubandiran, Supriya, Ambarish, Amrita, and Indrajeet, for always being supportive and creating a pleasant atmosphere in the lab. I acknowledge the efforts put in by Kubandiran, Munavvar, and Manik, in setting up the lab in the beginning. I particularly thank Neeta for helpful discussions and support, whenever needed. I would like to specially thank Kubandiran for mentoring me in my initial days in the lab, Munnavar for help with DSSC fabrication and Dr. Saumya Singh for OFET fabrication; in my various research projects. I appreciate the help and support provided by Renjith, Rincy, Saranya, Swapnali, Supriya, Dhanashri, Neel, Ashwath, Bhavisha, and Jenny, in their short stay in our lab.

I also thank current members of Dr. Krishnamoorthy's lab: Gunawant, Anup, Kumar, Jagdish, Gitanjali, and Sudhakar, for providing all the required help.

Last but not least, without my family, I would not have come this far. I would like to express my deepest appreciation and gratitude to my parents for their unconditional love, blessings, and sacrifice. I also thank my brothers for constant encouragement and guidance throughout my life. Finally, I would like to thank my wife, Vartika, for her understanding and love. Her enduring support and encouragement was in the end what made this thesis possible.

Rajesh Bisht

List of Abbreviations

AM	Air mass
BDT	Benzodithiophene
CDCA	Chenodeoxycholic acid
CV	Cyclic Voltammetry
DFT	Density functional theory
DPV	Differential Pulse Voltammetry
DSSCs	Dye-sensitized solar cells
D-π-A	Donor-π-bridge-acceptor
EIS	Electrochemical Impedance Spectroscopy
FET	Field effect transistor
FMO	Frontier molecular orbital
FTO	Fluorine-doped-tin oxide
HOMO	Highest occupied molecular orbital
HR-MS	High resolution mass spectrometry
ICT	Intramolecular charge transfer
IPCE	Incident photon-to-current conversion efficiency
IR	Infrared
IL	Ionic liquid
NIR	Near Infrared
J-V	Current-Voltage
LHE	Light harvesting efficiency
LUMO	Lowest unoccupied molecular orbital
MALDI-TOF	Matrix-assisted laser desorption ionization-time of flight
MLCT	Metal-to-ligand charge transfer
OFET	Organic field effect transistor
OPV	Organic photovoltaic
P3HT	Poly(3-hexylthiophene)
PCE	Power conversion efficiency
PV	Photovoltaic
PEDOT	Poly(3,4-ethylenedioxythiophene)
SSDSCs	Solid-state dye-sensitized solar cells
TCO	Transparent conductive oxide
TD-DFT	Time dependent density functional theory
UV-Vis	Ultraviolet-visible
NMR	Nuclear magnetic resonance
DCM	Dichloromethane

DMF	N,N-Dimethylformamide
EtOAc	Ethyl acetate
THF	Tetrahydrofuran
$CDCl_3$	Chloroform-*d*
MeOH-d_4	Methanol-d_4
DMSO-d_6	Dimethyl sulfoxide-d_6
E_g	Energy band gap
E_{CB}	Conduction band edge
ff	Fill factor
J_{SC}	Short-circuit currentdensity
V_{OC}	Open-circuit voltage
R_{ct}	Charge transfer resistance
C_μ	Chemical capacitance
η	Power conversion efficiency
τ	Electron lifetime
ε	Extinction coefficient
s	Singlet
d	Doublet
t	Triplet
m	Multiplet
MS	Mass spectrometry
M^+	Molecular ion
mmol	Millimole
MHz	Megahertz
ppm	Parts per million
Å	Angstrom
λ	Wavelength
eV	Electron volt
^oC	Degree Celsius
min	Minute(s)
h	Hour (s)
g	Gram
mg	Miligram
mL	Mililitre
kW	Kilowatt
GW	Gigawatt

ABSTRACT

The sensitizer or dye is an essential component of Dye-sensitized solar cells (DSSCs) which contains a light absorbing moiety and an anchoring group which helps it to bind to metal-oxide semiconductor (TiO_2) surface. Dye-TiO_2 interface plays a vital role in power conversion efficiency (PCE) as it controls the charge injection and charge recombination process in DSSC. Considerable efforts have been devoted to developing new and efficient sensitizers to improve the performance of DSSCs. Several sensitizers, such as metal-organic complexes, metal-free organic dyes, Zn–porphyrin, and Zn–phthalocyanine dyes have been used successfully in DSSC. While most of the dye absorbs very well in the visible region, there are limited chromophores which absorb in near infra-red (NIR) region, which includes porphyrins, phthalocyanine, and polymethine. The absorption in NIR region is essential to harvest the maximum incident photons and improve the current density.

Squaraine dyes are a subclass of polymethine dyes, which owing to its low band gap and strong absorption ($\varepsilon > 10^5\ M^{-1}\ cm^{-1}$) in the far-red and NIR region have found application in dye-sensitized solar cells. While the squaraine dyes have excellent absorption in the far-red region, the exciton quenching by aggregation limits its overall performance in dye-sensitized solar cells. The aggregates form when the dipoles of the molecules interact with each other due to π-π interaction. When a molecule absorbs light and reaches excited state, the photo-excited electron in the LUMO state hops between the neighboring molecules instead of injecting electron in the metal oxide semiconductor. Thus aggregation may hamper the efficiency of DSSC by quenching the exciton which leads to low electron injection on TiO_2. Thus it is desirable to have such a design for dyes which can help in controlling aggregation and promote charge injection efficiency in squaraine dyes. It is also beneficial to shift the absorption of squaraine dyes further towards NIR to utilize maximum available photons. It can be achieved by extension of conjugation which can be done either towards the anchoring end or the non-anchoring end.

Hence, we designed and synthesized squaraines based dye for DSSC with focus on modulating electronic and steric properties of dyes to enhance absorption in NIR region and avoid aggregation on TiO_2 surface respectively. To achieve this, we used moieties like benzodithiophene (BDT), fused fluorenylindolenine and fused indenoquinalidne to enhance

absorption and also several in-plane and out-of-the plane alkyl chains were integrated to control aggregation.

Chapter 1 reviews the importance of NIR-responsive sensitizers for DSSCs; significance and synthesis of squaraine dyes; and squaraine based systems reported for DSSCs. It begins with the general description of dye-sensitized solar cells, its working principle, and parameters involved in measurement of it electronic, physical and photovoltaic properties. The role of sensitizers and effect of aggregation on the performance of DSSCs are discussed in details. This chapter concludes with the overview of scope and objectives of the thesis.

Chapter 2 deals with the impact of alkyl chains and extension of conjugation on electronic, physical and photovoltaic properties. In this work, we have linked the benzodithiophene (BDT) to indole-based squaraine by direct arylation method to extend the conjugation towards anchoring group and substituted O-methyl and O-ethylhexyl side chain on the BDT to compare the effect of alkyl chains on aggregation. The optical, electrochemical and photovoltaic properties of the dyes were studied in meticulous detail. The photovoltaic performance was measured and compared. One of the dyes (RSQ2) showed the best photovoltaic performance with power conversion efficiency of 6.72% with panchromatic incident photon-to-current conversion efficiency (IPCE) response extending up to 775 nm.

Chapter 3 describes a strategy to increase conjugation towards the non-anchoring side of squaraine dyes and to incorporate out-of-plane alkyl chains on the dye. A fluorene-indolenine based fused donor, fluorenylindolenine was synthesized to induce planarity and increase absorption towards the non-anchoring end of the molecule, and the two sp^3-carbon present on fluorenylindolenine were utilized to incorporate four out-of-plane branched chains on the dyes to avoid aggregation induced self-quenching. The fused donor was condensed with carboxyindolenine and carboxybenzindolenine based semisquaric acid towards anchoring side to give a series of dyes (XSQ1-4). XSQ2 gave the maximum PCE of 6.57% with IPCE onset up to 800 nm.

Chapter 4 depicts the incorporation of quinaldine as a strong donor to fuse with fluorene to further shift absorption of squaraine dyes towards NIR. The sp^3-carbon available

on fluorene unit was used to install C-12 alkyl chain to control aggregation. The fluorene-quinladine (indenoquinaldine) donor was condensed with carboxyindolenine, carboxybenzindole and quinaldine based semisquaric acid to give a series of NIR-responsive squaraine dyes (ISQ1-3). ISQ3 showed good IPCE response in the NIR region with onset up to 880 nm and showed the highest efficiency of 4.1 % in the presence of 10 equiv CDCA

The molecular packing and the morphology of nanostructures play a vital role in determining the charge transport properties of small molecules and polymers respectively. In terms of small molecules, the solubility of semiconducting motif limits the unitization of solution processed methods. Hence thermal and chemical reaction initiated methods have been utilized to process the same. In an attempt to develop a photochemical reaction to afford a conjugated organic molecule, 3'-5' dimethoxybenzoin ester capped phototrigger have been utilized as a soluble precursor, which could afford conjugated molecules upon photo irradiation.

So in **Chapter 5,** we describe the design and synthesis of a series of benzoin based phototrigger with phenyl, furan, thiophene, bithiophene moieties. Smaller triggers formed the cyclized benzofuran derivatives when irradiated with UV light in acetonitrile solution. In case of extended phototrigger, only trace amount of cyclized product formation occurred, but the reactivity changed when the reaction was carried out in the presence of triethylamine. When 1 equivalent of triethylamine (TEA) was added, the yield of cyclized product improved to over 60% and the deacetoxylated product was also obtained. Upon further addition of TEA, the yield of cyclized product diminished whereas the yield for the deacetoxylated product enhanced. The benzofuran capped cyclized product of extended trigger were used in Organic field effect transistor (OFET)

Chapter 6 summarizes essential results from all chapters with respect to design and synthesis, as well as physical, electronic, and photovoltaic properties of squaraine dyes. Modulated photoreactivity of benzoin type extended phototriggers, and their possible application in organic electronic in chapter 5 is also summarized. This chapter also includes the future outlooks on the basis of the findings reported in the thesis work.

Chapter 1

Introduction

1.1. Global Energy Crisis

The global population is increasing rapidly with 83 million additions per year.[1] The currently accessible energy is not sufficient for a large fraction of people due to their poor economic status and weak development profile of their country. Even in today's world 1.1 billion people do not have access to electricity and 85% of them live in rural areas.[2] On the other hand, growth in income, dependence on technology and improved standard of the lifestyle of the urban population have skyrocketed their appetite for energy. With the economic growth of highly populated countries like India and China, the continuous access to the energy has become even more important in order to convert this growth into sustainable development. The energy demand is, therefore, increasing rapidly to meet the requirements of a growing global population and to support economic growth. Fossil fuels such as coal, oil, and gas have been fulfilling energy requirements of humans for ages; however, the unbridled exploitation of fossil fuels in the quest of energy has brought the world to face two major challenges, energy security, and climate change. It is, therefore, vital to invest in renewable energy sources such as wind energy, hydropower, solar energy, and geothermal for the benefit of the future generation.

1.2. Solar Energy

Renewable sources of energy are naturally restored without being exhausted from the earth and give us a chance to reduce the emission of greenhouse gases and control global warming. Among the renewables, the solar energy is the most promising source of energy due to its sheer abundance. The Sun emits energy at the rate of 3.8×10^{23} kW, out of which the earth receives approximately 1.8×10^{14} kW.[3] In other words, the Sun provides the earth with as much energy in one hour as the whole humanity uses in one year. Thus, it is a great challenge as well as an opportunity for the mankind to tap into this huge energy reservoir for sustainable development. Due to increased technological advancement and computerization of machines electricity has become one of the key forms of energy. Whether it is the small household appliances like computers and refrigerators or heavy machineries like trains and electric vehicles, the electricity has become a preferable source of power for all purposes. The fact that photovoltaic cells are the only devices that directly convert sunlight into electrical energy gives great encouragement for solar electricity production.

Taking cognizance of the possible energy crisis in the future, governments around the globe have increased their solar energy production. In 2016, total global photovoltaic (PV) installed capacity has exceeded 300 GW. China was the biggest contributor to a total grid-connected solar capacity of 77.9 GW (**Figure 1**).[4] Recently, India has launched an ambitious strategy to target 174 GW of renewable energy capacity by 2022, which includes 100 GW of solar power. A total solar capacity of 20 GW had been achieved earlier this year (January 2018).[5]

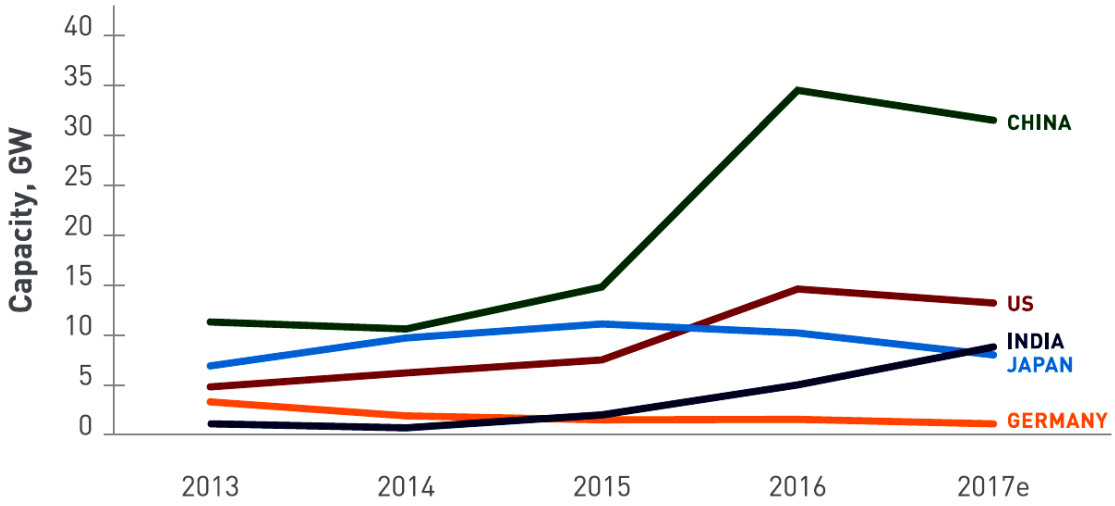

Figure 1. Global annual solar capacity addition in leading international markets (India Solar Handbook 2017).

1.3. Photovoltaics

A photovoltaic (PV) cell is a device which converts light into electricity, and the phenomenon is called the photovoltaic effect. The photovoltaic effect was first discovered in 1839 by a French scientist named Edmond Becquerel. Later, Charles Fritts, an American inventor, coated selenium with a thin layer of gold and created the first solar cell which achieved a solar-to-electricity conversion efficiency of 1–2%. In the 1950s, the Bell Laboratories invented the first practical solar cell by using silicon as it was more efficient than selenium. The rapid advance of silicon electronic industry further promoted the growth of the photovoltaic sector as we know it today.

Several kinds of photovoltaic devices have been invented until today which can be classified broadly into three generations.

1.3.1. First Generation Solar Cells (Silicon Solar cells)

The first generation solar cells are the most widely used photovoltaic technology. These cells use a thick crystalline film of semiconductor (mainly Si) and provide an excellent solar energy to current conversion efficiency. The primary working mechanism of silicon-based solar cells is demonstrated in **Figure 2**. Two layers of silicon semiconductor, one n-doped and other p-doped are fused together in direct contact. When the light falls upon the depleted region of the p-n junction, the excited electrons move towards the n-type region under in-built potential bias. The electrons travel to an external circuit and pass through the load to arrive at the p-doped layer. There are two types of crystalline silicon which are commonly used: mono-crystalline and multicrystalline silicon. The solar cells based on mono-crystalline silicon are more efficient compared to the multi-crystalline silicon solar cells.

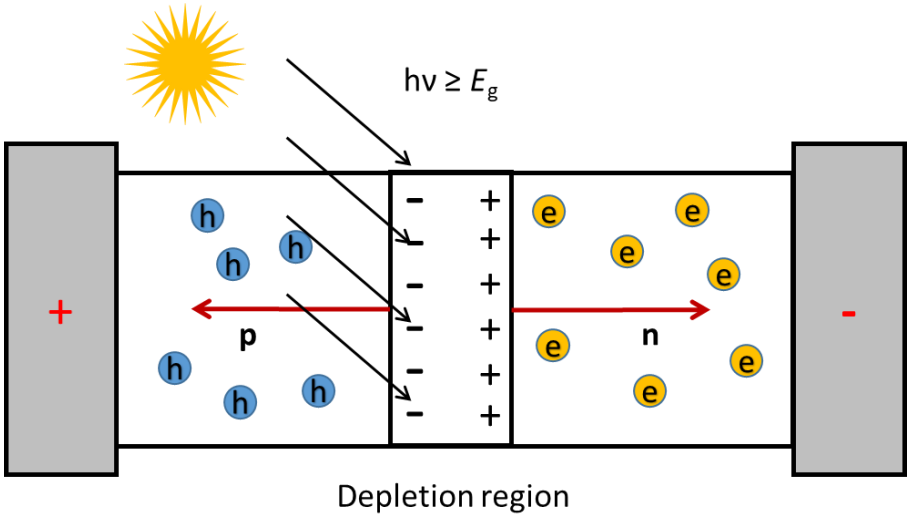

Figure 2. The fundamental working principle of silicon solar cells.

The crystalline silicon-based solar cells have an efficiency between 15-25%. Though the silicon is found in abundance of earth crust, the process to purify it into a usable form is expensive which results in its high cost. Thus next generations of solar cells deal with the reduction of cost while maintaining the good efficiency.

1.3.2. Second Generation Solar Cells (Thin Film Technologies)

The second generation solar cells were developed with the aim of reducing the cost of solar panels through the utilization of thin film technology. They are made from layers of semiconductor materials with a thickness of a few micrometers and hence require less

material which leads to the reduction in manufacturing cost. Based on the active materials, there are generally three types of solar cells that are considered in this category, amorphous silicon, and non-silicon materials based cadmium telluride (CdTe), and copper indium gallium diselenide (CIGS). While the cost issues associated with thick films were addressed in the second generation PV cell, the performance was poor compared to first generation PV cells. Hence even today, the first generation solar cells are the most popular for commercial purpose.

1.3.3. Third Generation Solar Cells

Third generation solar cells explore the application of alternative materials instead of silicon as a light harvester, and they are not directly related to the single p-n junction. The significant efforts were devoted to the understanding of the charge and energy transfer processes across the various interfaces and the respective methods to optimize charge collection, thereby increasing the energy harvesting within the solar spectrum. The major technologies in this generation include organic/polymer solar cells; quantum dots sensitized solar cells, dye-sensitized solar cells, and perovskite solar cells.

(a) Organic/ Polymer Solar Cells

Organic solar cells utilized organic polymers or small molecules with semiconducting properties as charge transport materials. Analogous to silicon solar cells, p-type and n-type organic semiconductor with different HOMO-LUMO levels are used to create in-built potential at their interfaces. The p-type material (usually polymer based) is generally called donor, and the n-type material (usually fullerene-based) is known as acceptor. Upon irradiation, the excitons are generated which dissociates into electron and hole at the interface of donor and acceptor materials. Thus, the charge transports to the anode and cathode through bicontinuous networks of the donor (hole-transporting) and acceptor (electron-transporting) polymers. The efficiency up to 13% have been achieved with organic solar cells.[6]

(b) Dye-Sensitized Solar Cells

Dye-sensitized solar cells (DSSCs) have different mechanism and configuration compared to silicon solar cells. In DSSC light absorption and carrier generation occurs in separate medium i.e. dye, whereas the carrier transport occurs in a metal-oxide based semiconductors on which the dye is anchored. The major advantage of DSSC over other photovoltaic technology is that

it can generate charge carriers even in low light conditions due to high extinction coefficients of the dyes used in DSSCs. The low sensitivity to the incident angle of the light radiation makes them ideal for indoor power generation. DSSCs have successfully achieved efficiency up to 14%.[7]

(c) Quantum Dot Sensitized Solar Cells

Quantum dots sensitized solar cells (QDSSCs) have the working mechanism similar to DSSC in which semiconducting nanocrystals (Quantum dots) are used as sensitizers. The advantage of using quantum dots is that the bandgap of materials can be tuned by varying the size of nano-particles. Lead-sulfide is one of the commonly used materials to synthesize quantum dots. Quantum dot solar cells have accomplished an efficiency over 13%.[8]

(d) Perovskite Solar Cells

Perovskite solar cells are the latest entrant in the field of photovoltaic. It consists of three-dimensional organic-inorganic hybrid perovskite structured compounds, such as methylammonium lead halides, as a light absorbing unit. While the kinetics and working principle of perovskite solar cells are still under investigation, it seems that perovskite behaves as a charge carrier as well as light harvesting material. The perovskite solar cells have generated huge interest in the photovoltaic circle due to their higher efficiency compared to other non-silicon solar cells, and for the lead-based perovskite cell, the record efficiency is over 20%.[9] Despite the good photovoltaic performance, the poor stability and lead toxicity are some of the major hurdles in progress of perovskite solar cells.

(e) Multijunction or Tandem Solar Cells)

According to the Shockley-Queisser limit, a single p-n junction solar cell with a band gap of 1.1 eV cannot attain efficiency greater than 33%, using air mass (AM) 1.5G solar spectrum. The third generation solar cells also focused on crossing the Shockley-Queisser limit by introducing the multijunction cell (tandem solar cells) where cells with materials of different bandgaps are arranged on top of each other to utilize the maximum portion of the solar spectrum. Recently, four-junction solar cells have been reported to give the efficiencies as high as 45%.[10]

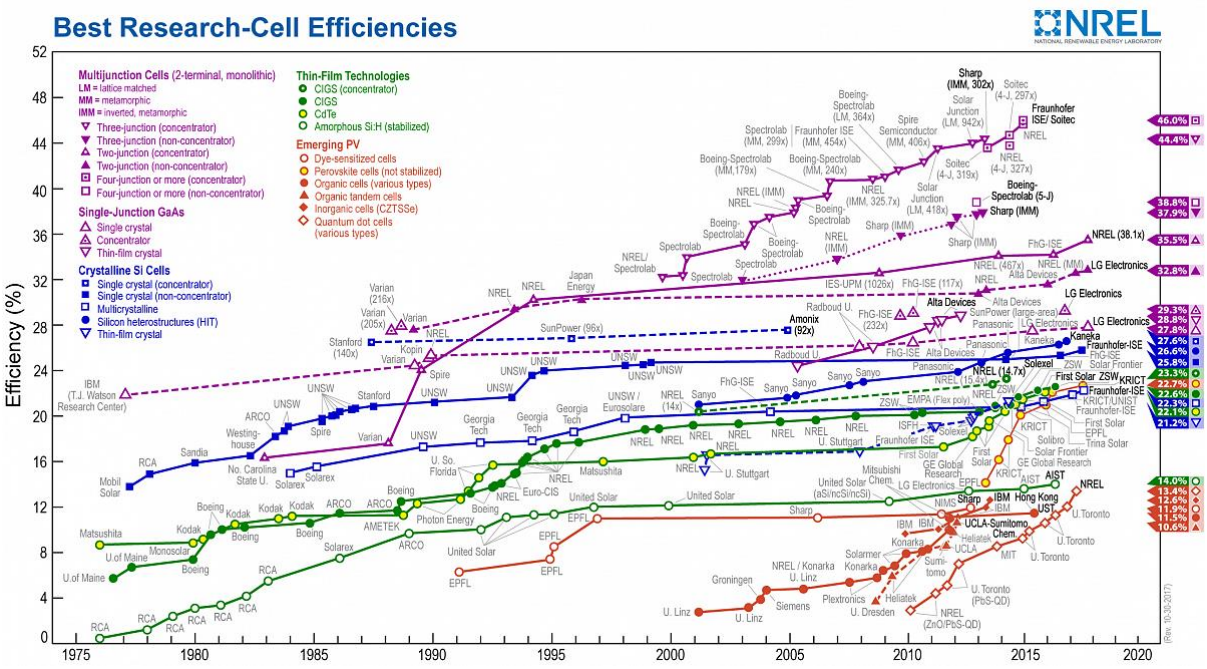

Figure 3. Research Cell Efficiency Records, National Renewable Energy Laboratory (2017).

1.4. Dye-sensitized Solar Cells

In 1991, O'Regan and Grätzel invented a modern version of dye-sensitized solar cells by using ruthenium-based sensitizer and a mesoporous TiO_2 as a semiconductor.[11] This device produced power conversion efficiency of ca. 7% which was much greater than the previously reported efficiencies of photoelectrochemical solar cells.[12–14] The discovery by Grätzel attracted as considerable attention in the scientific community and accelerated dedicated research in DSSCs.[15]

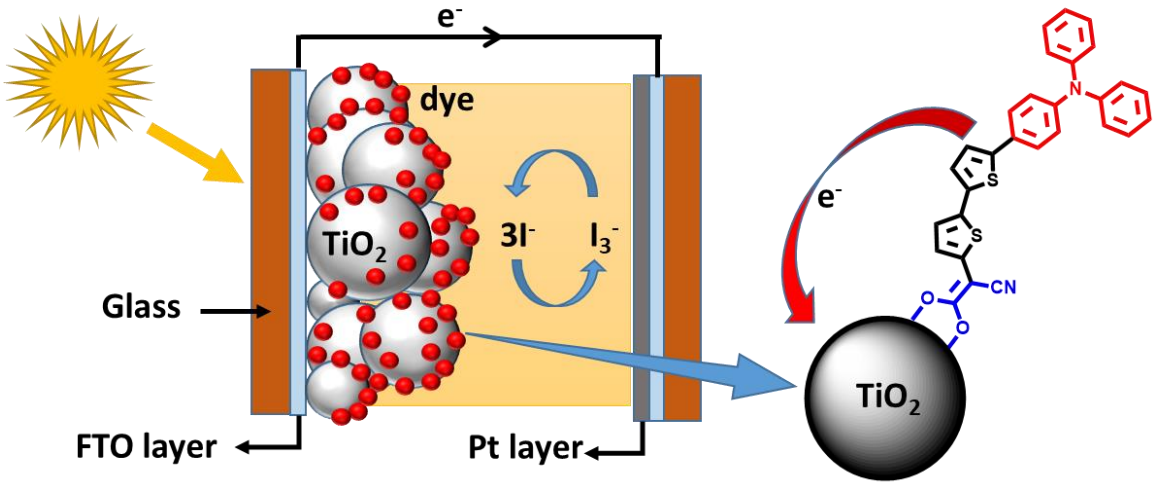

Figure 4. The basic structure of the dye-sensitized solar cell.

A typical n-type liquid DSSC consists of photoanode which is made of a thin layer of transparent conducting oxide (TCO) is deposited on a glass substrate. Fluorine-doped tin oxide (FTO) is one of the most common transparent conducting metal-oxide that is used for this purpose (**Figure 4**). On the top of the FTO-glass substrate, a layer of mesoporous semiconducting metal-oxide of the wide bandgap (TiO_2, SnO_2, ZnO, etc.) is deposited. A dye or sensitizer binds to this metal-oxide layer with the help of anchoring groups (such as –COOH or $–PO_3H$) and forms a sensitized photo-anode. An FTO-glass coated with a thin layer of Platinum nanoparticles is generally used as a counter electrode. The two electrodes are sandwiched together with a spacer in between. A liquid electrolyte is filled between the two electrodes which complete the construction of DSSC.

1.4.1. Operating Principle of Dye-sensitized Solar Cells

The mechanism and operating principle of dye-sensitized solar cells are illustrated in **Figure 5**. When the DSSC is exposed to light, the dye anchored on the surface of semiconducting metal-oxide goes over an electronic state change from the ground (S) to the excited state (S*) (eq 1).

$$S + h\nu \rightarrow S^* \text{ (Photo-excitation)} \qquad (1)$$

The internal electric field of the metal-oxide nanoparticles helps the dye release the electron into the conduction band (E_{CB}) of the semiconductor (eq 2).

$$S^* \rightarrow S^+ + e^-_{\text{ injected}} \text{ (electron injection)} \qquad (2)$$

This process is fast and takes place within 100 fs-100 ps. For effective injection of electrons into the semiconductor, the LUMO of the sensitizer should be above 0.2 V.[16] After injection the electron diffuses through the mesoporous network of TiO_2 particles and reaches conducting FTO surface. The electron injection leaves the sensitizer in the oxidized state which needs to be regenerated. The reduced iodide ion in the redox mediator refills the highest occupied molecular orbital (HOMO) of the dye and makes it ready to generate electrons again (eq 3). Thus, the device components do not experience any permanent physical or chemical damage.

$$2S^+ + 3I^- \rightarrow 2S + I_3^- \text{ (Dye regeneration)} \qquad (3)$$

For efficient dye regeneration, the HOMO of the dye should be lower than the redox potential of the electrolyte. The offset ≥ 0.15 eV is considered adequate. The electron travels the through the external circuit and reaches Pt-coated FTO counter electrode. Here the platinum layer performs as an electrocatalyst for reduction and reduces the triiodide species in the electrolyte (eq 4).

$$I_3^- + 2e^- \rightarrow 3I^- \quad \text{(Electrolyte regeneration)} \qquad (4)$$

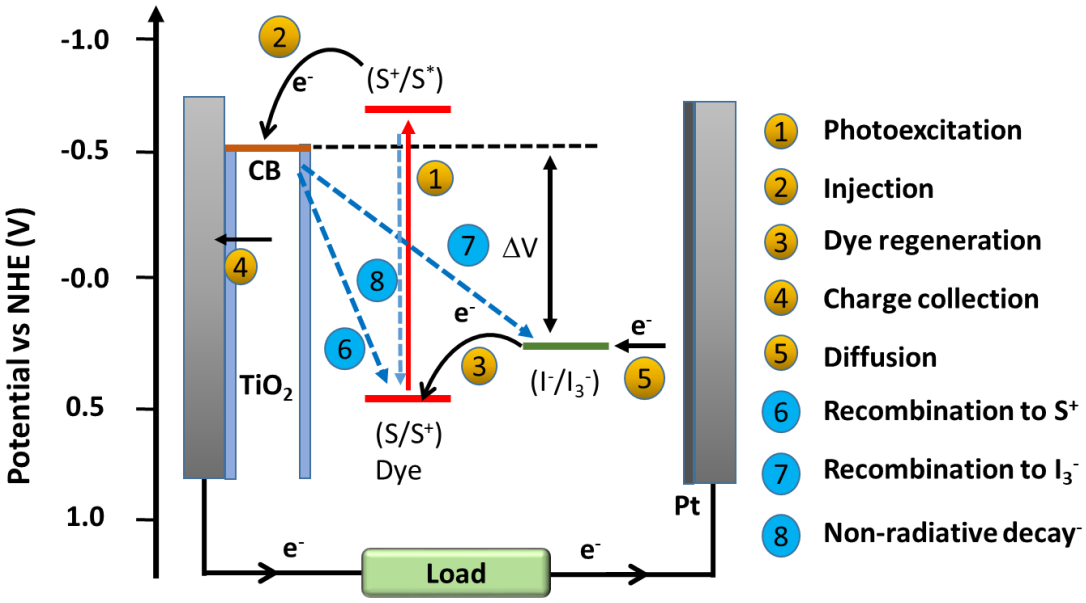

Figure 5. Operating principle and processes involved in the dye-sensitized solar cell.

The driving force for the charge movement in DSSC comes from the potential difference between the quasi-Fermi level of the working electrode when illuminated, and the redox potential of the redox species present in the electrolyte. There are some unfavorable processes (charge recombination) which can reduce the efficiency of DSSCs. These include the recombination of the injected electrons in the conduction band of the TiO_2 back to the electrolyte (process 7, **Figure 5**) and the recombination of injected electrons with the oxidized dye before the dye is regenerated (process 6, **Figure 5**). The decay or quenching of the excited state of dyes before the electron injection into TiO_2 may also lead to a loss in efficiency (process 8, **Figure 5**). For an efficient DSSC, the rate of forward (charge injection) reactions should be greater than the rate of backward (charge recombination) reactions.

1.4.2. Key Parameters in DSSC

(a) Air Mass (AM)

The Sun emits light of wide range of wavelengths with maximum intensity in the visible region. However, when the solar radiation travels through earth's atmosphere, the intensity in some wavelengths decreases due to absorption by several gases and dust/particles present in the atmosphere. Also, the intensity of solar radiation reaching the earth surface varies with the locations. The air mass measures the reduction in the intensity of light as it passes through the atmosphere which describes the direct optical path length through the earth's atmosphere.

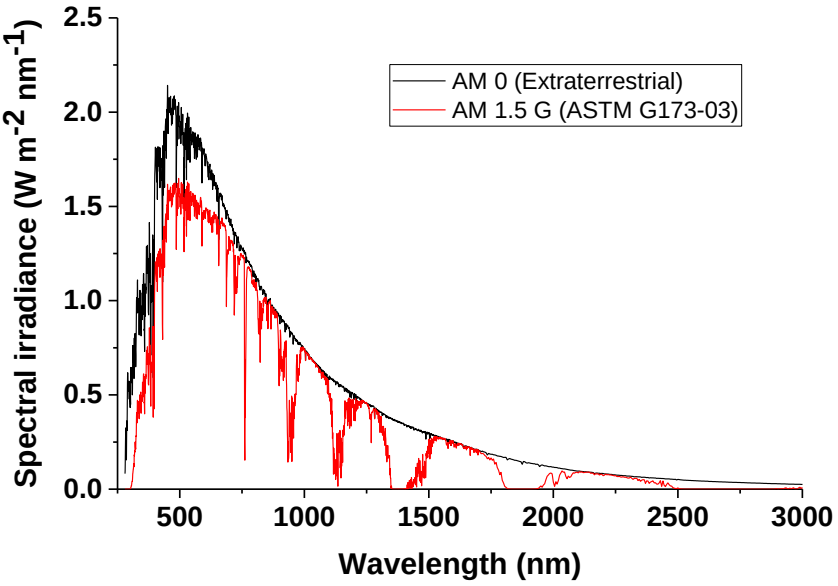

Figure 6. Spectral irradiance of AM 0 and AM 1.5 G.

The air mass is defined as:

$$AM = 1/\cos\theta \quad (5)$$

where θ is the angle between the Sun and the vertical, i.e., the zenith angle (z). The air mass becomes equal to 1 when the direction of solar radiation is normal to the surface of the earth. Since the intensity and spectrum of solar radiation varies with the time and location, a standard spectrum and power density is necessary to make a correct comparison between the solar cells measured at different times and locations. For this purpose, a standard solar spectral irradiance with air mass coefficient of 1.5 (AM 1.5 G) is considered, which is derived from zenith angle (θ) of 48.2^o (the G stands for global) (**Figure 6**).

(b) Incident Photon-to-Current Conversion Efficiency (IPCE)

The incident photon-to-current conversion efficiency is one of the important parameters of the solar cell which measures the efficiency with which the device converts the light of specific wavelength into photocurrent (**Figure 7b**). The IPCE is also called external quantum yield (EQE) and is defined by the eq 6.

$$IPCE = LHE.\Phi_{inj}.\eta_{reg}.\eta_{cc} \qquad (6)$$

LHE is the light harvesting efficiency; Φ_{inj} is the quantum yield of charge injection into TiO_2, η_{reg} is dye regeneration efficiency, and η_{cc} is the charge collection efficiency of DSSC.

(c) Short-Circuit Photocurrent Density (*J*sc)

The J_{SC} is the value of the photocurrent which is obtained when DSSC under irradiation is short-circuited. It is the maximum current that can be obtained from a solar cell its unit is milliampere per unit area (mA cm^{-2}). J_{SC} is the direct consequence of the IPCE and can be calculated by integrating IPCE spectra according to eq 7

$$J_{SC} = q \int IPCE\,(\lambda)\phi(\lambda)d\lambda \qquad (7)$$

Where q is the charge of the electron and $\phi(\lambda)$ is the photon flux at wavelength λ under standard AM 1.5 simulated sunlight.

(d) Open-Circuit Voltage (*V*OC)

The difference between the electrical potential at the two terminal of a solar cell under illumination when no current is drawn is known as open circuit potential (V_{OC}). Ideally, the V_{OC} of the DSSC is dependent on the conduction band of the TiO_2 and the electrochemical potential of the redox mediator which can be expressed by the eq 8.

$$V_{OC} = \frac{E_{CB}}{e} + \frac{k_B T}{e} ln\left(\frac{n}{N_{CB}}\right) - E_{redox} \qquad (8)$$

where e is the elementary charge, n is the number of the electrons present in TiO_2, k_B is the Boltzmann constant, T is the absolute temperature, N_{CB} is the total number of effective density of states, and E_{redox} is the potential of the redox mediator. Thus, theoretically, the V_{OC} of a DSSC is the difference between the conduction band energy level (E_{CB}) of TiO_2 and the energy level of the redox mediator (I_3^-/I^-) present in the electrolyte. However, the V_{OC}

obtained from the working DSSC is always lower than the theoretical values due to several recombination losses.

(e) Fill Factor (*ff*)

The fill factor measures the quality of the device and can be estimated from the J-V curve. It is expressed as the ratio of the maximum power output ($J_{mp}V_{mp}$) to the product of J_{SC} and V_{OC}.

$$ff = \frac{J_{mp}V_{mp}}{J_{SC}V_{OC}} \qquad (9)$$

The theoretically maximum obtainable value of fill factor is 1. However, such value cannot be realized in practical solar cells due to high inner resistances such as sheet resistances of the photoanodes and counter electrode, ion transport resistance, and the charge-transfer resistance at the counter electrode. The fill factors can be improved by decreasing the series resistance (R_s) and increasing the shunt resistance (R_{sh}).

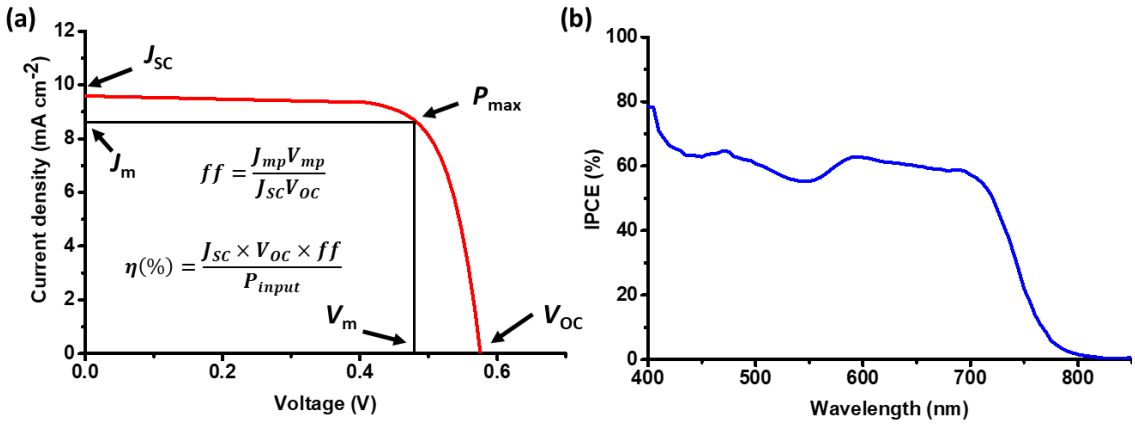

Figure 7. A typical a) *J*–*V* curve, b) IPCE curve of DSSC.

(f) Solar Energy to Electricity Conversion Efficiency (η)

The overall solar energy to electricity conversion efficiency of a solar cell is determined by open-circuit voltage (V_{OC}), short-circuit current density (J_{SC}), fill factor (*ff*), and incident solar radiation power (I_0) (generally at AM 1.5 G, 100 mW cm^{-2})

$$\eta(\%) = \frac{J_{SC} \times V_{OC} \times ff}{I_o} \qquad (10)$$

Thus, to obtain high values efficiency, the J_{SC}, V_{OC} an *ff* should be as high as possible. The great improvements have been achieved in the efficiency of DSSC by significant development in sensitizer designing as well as device fabrication.

1.4.3. Key components in DSSC

(a) Semiconductor

Photo-anodes are generally made by depositing a mesoporous layer of metal-oxide semiconductor on transparent conducting oxide (TCO). TiO_2 and ZnO are the commonly explored metal-oxide for DSSC but some other metal-oxide system such as SnO_2, Nb_2O_3 have also been tested.[17–19] These metal-oxides have a wide band gap and usually does not absorb in the visible region. Hence a sensitizer is necessary to harvest the visible region of the solar spectrum and absorb the electron injected by the dyes. TiO_2 has been the most efficient among all the semiconductors and used extensively in DSSC.[20] TiO_2 is a stable and non-toxic oxide which gives it an additional advantage over other metal-oxides. Two major crystal form of TiO_2, i.e., rutile and anatase have been explored in DSSC. Though rutile is thermodynamically more stable than anatase, anatase has larger bandgap (3.2 eV) [20] and high conduction band edge (E_{CB}) which makes it preferable to rutile. The metal-oxides such as ZnO and SnO_2 have also been investigated. ZnO has a bandgap and conduction band edge similar to TiO_2 and has better electron mobility which supports electron transport. The major disadvantage of ZnO is its chemical instability, and it dissolves rather easily compared to TiO_2 in acidic and basic conditions which make them less preferable to TiO_2. In a typical DSSC device, a paste of TiO_2 particles is applied to deposit a nanocrystalline TiO_2 film on FTO substrate by doctor blading or screen printing.[21] The size of TiO_2 particles is around 20 nm. The TiO_2 coated FTO substrate is sintered around 400-500 $^{\circ}$C which remove organic additives to induce porosity. The porosity is essential to increase the surface area to ensure higher loading of dye on TiO_2. A layer of larger particles of TiO_2 which is called the scattering layer is often applied on the top to enhance light absorption by reflecting light back into the cell.

(b) Counter Electrode

The counter electrode (CE) is essential to reduce the oxidized species of the redox couple present in the electrolyte. These are generally made by depositing a platinum layer on FTO

substrate by pyrolysis, sputtering, and vapor deposition. Platinum is very good electrocatalyst for dye regeneration due to fast reversible electron transfer with very low charge transfer resistance (~ 1 Ω cm^2).[22] However, Platinum is an expensive and scarce metal; as a result, the non-Pt materials have also been explored. The carbonaceous materials are the most researched Pt- free CE materials and the materials such as graphite,[23–25] carbon black,[26] carbon nanotubes,[26] activated carbon on FTO-glass and organic ion-doped conducting polymers of poly(3,4-ethylenedioxythiophene) (PEDOT) coated on TCOs, have been proposed as CEs in DSSCs. The highest PCE (14.3%) in DSSCs was obtained by counter electrode based on the FTO/Au/GNP (graphene nanoplatelet).[7]

(c) Electrolyte

The electrolyte is one of the vital components in DSSCs which helps in transporting the inner charge carrier between electrodes and continuous regeneration of the dye and itself during DSSC operation. A typical liquid electrolyte contains I_3^-/I^- couple in suitable organic solvent usually acetonitrile and some additives. The choice of solvent used in the electrolyte is critical. Several kinds of solvents such as alcohols, propylene carbonate, -butyrolactone, tetrahydrofuran, N, N-dimethylformamide,[27–29] as well as different types of nitrile solvent[30] have been studied for the electrolyte in DSSC. However, acetonitrile has been the most successful so far due to its low viscosity and good solubility to dissolve electrolyte components. The power conversion efficiency (PCE) up to 12% has been recorded for an ACN-based DSSC.[31,32] Acetonitrile is a volatile solvent (boiling point at 82 ºC) and hence liable to evaporation and leakage. Ionic liquids (ILs) possess high ionic conductivity with very low vapor pressure which made it a potential candidate for replacing the volatile organic solvents.[32,33] However, due to their high viscosity and mass-transport limitation, they show low efficiencies and photocurrent. To counter the mass-transport limitations, binary mixtures of tetrahydrothiophenium-based ionic liquids with low viscosity have also been used to form stable DSSCs.[34]

The iodide/triiodide based redox couple have an optimal redox potential and allows rapid dye regeneration and hence has been used extensively since the beginning of DSSC development. The couple also possesses several other advantageous features such as good solubility, high conductivity, and good penetration into the mesoporous semiconductor film.[35] The redox potential of the I_3^-/I^- the couple is, however, much higher (less positive) than required

compared to the HOMO level of most sensitizers which can bring a significant loss in the open-circuit voltage (V_{OC}) (**Figure 8**). Several iodine-free alternatives to redox mediator were explored. The bromide/tribromides,[36–38] interhalogen systems[39] and pseudohalogen system[40,41] have redox potential lower than I_3^-/I^-, but high corrosion and toxicity of these electrolytes restricted further exploration.

Cobalt(II/III) polypyridyl complexes have also been tested as an alternative redox couple due to their lower redox potential which can be tuned by modifying the ligands coordinated to Cobalt.[42–45] Besides being noncorrosive and non-volatile, Cobalt complexes are generally less colored than iodine solutions and doesn't interfere with absorption of the sensitizer. Co (II/III) polypyridyl based complex proved to be most successful redox couple after I_3^-/I^- and produced efficiency of over 12% with V_{OC} approaching 1 V (0.965 V) in combination with porphyrin dyes as reported by Yella et al.[32] Recently, the efficiency of 13% (V_{OC} = 0.91 V) with was achieved, proving that the Cobalt based complex can become a viable alternative to tradition I_3^-/I^{--} redox couple.[46]

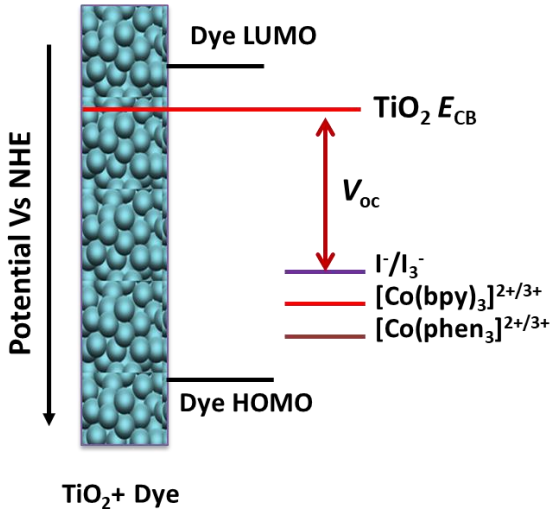

Figure 8. The redox potential of various electrolyte and effect on V_{OC}.

1.5. Sensitizers for Dye-sensitized Solar Cells

A sensitizer or dye is the light harvesting component of DSSC and plays the crucial role in converting the incident light into photocurrent. It not only absorbs the light but also injects the electron in the TiO_2 and thereby directly affecting the overall power conversion efficiency. Following properties are desirable in an ideal sensitizer:

i) It should have a high extinction coefficient (ε) with broad absorption covering a wide range of the solar spectrum to generate high photocurrent.

ii) It should have anchoring groups such as carboxylates or phosphonates to attach itself to TiO_2 surface. It also helps in electron injection by keeping the dye in close proximity to TiO_2.

iii) The dyes must have LUMO level higher than the conduction band of the TiO_2 for efficient electron injection, and HOMO levels should be lower than the electrochemical potential of the redox mediator for efficient dye regeneration.

iv) It should possess long-term photostability along with thermal and electrochemical stability.

The sensitizers are generally divided into two major groups−Metal complexes which include Ruthenium (II), Metal-porphyrin, Metal-phthalocyanine, and Metal-free dyes. Ruthenium complexes have been widely researched as photosensitizers at the beginning of DSSC due to their favorable photovoltaic properties such as broad absorption spectra, the longer exciton lifetime and chemical stability (**Figure 9**).[47]

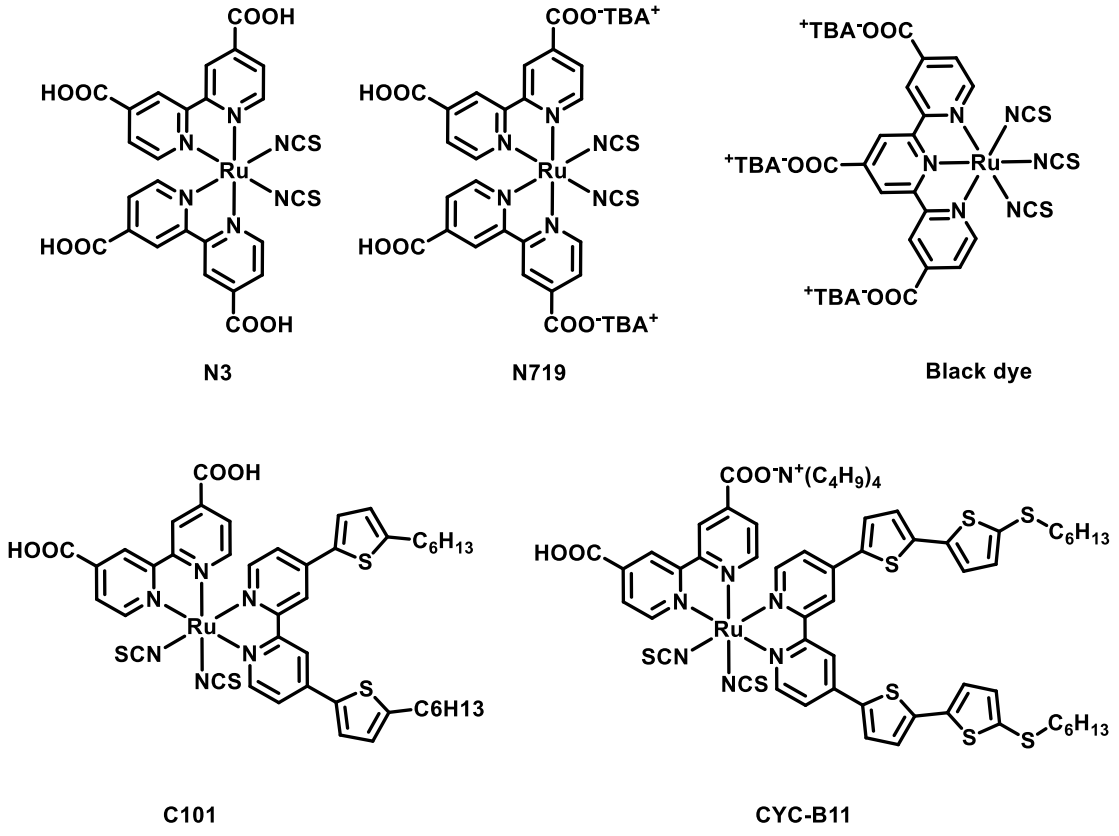

Figure 9. Ruthenium polypyridyl complexes used as sensitizers in DSSC.

These complexes have broad absorption, ranging from the visible to the near-infrared region of the solar spectrum, which originates from metal-to-ligand charge transfer. In Ru-polypyridyl complexes, the HOMO is localized on the Ru and electron donating ligands, and the LUMO is spread over the polypyridyl ligand. Both the absorption and HOMO-LUMO levels can be tuned by suitable modifications in ancillary ligands such as bipyridine or terpyridine ligands. DSSCs based on ruthenium(II)- polypyridyl complexes as the light harvesting materials have achieved overall power conversion efficiencies over 11% under standard (AM 1.5G) illumination[48,49]. Zinc-porphyrins are another example of metal-based sensitizers and have been very successful recently.[50–53] These sensitizers have excellent absorption in visible as well as far-red region due to Soret band and Q-band. Recently, a record efficiency of 13% was achieved by Zn-Porphyrin dyes sensitized DSSC in combination with Co(II/III) electrolyte.[46] Zn-phthalocyanines are structurally similar to porphyrin and also show Soret and Q-band in the absorption spectrum. Unlike Zn-Porphyrins, the DSSC based on Zn-phthalocyanine have not been able to achieve high efficiency mostly due to excessive aggregation.[54,55] Despite the high energy conversion efficiency of the metal complex dyes, the high costs, complicated synthetic routes, and the limited absorptivity has led the focus to metal-free dyes.

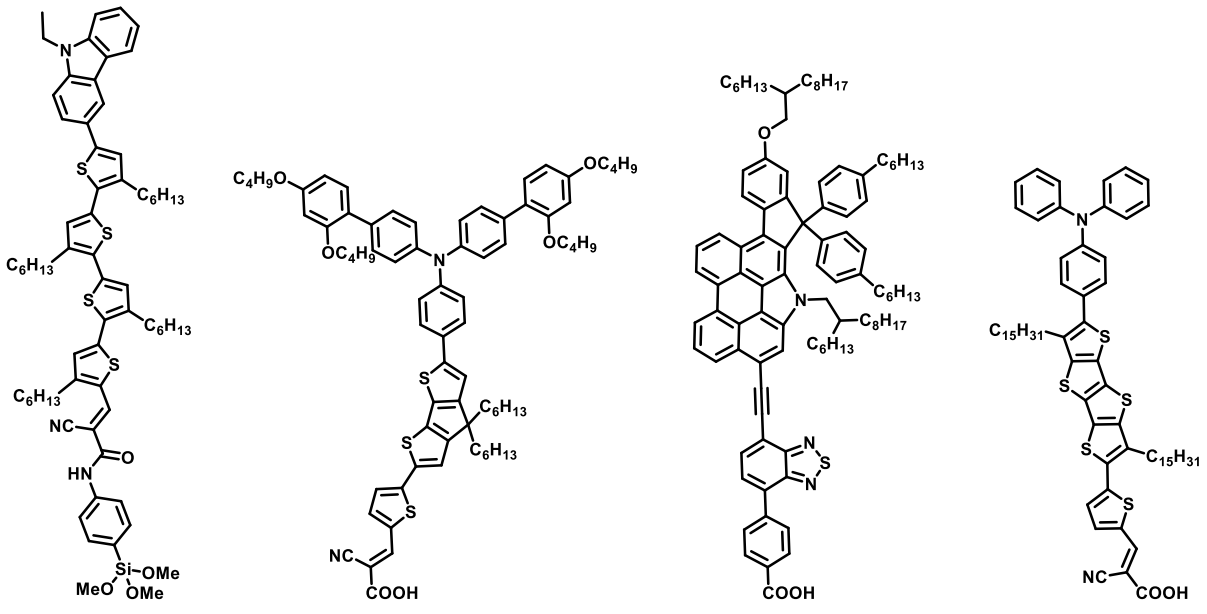

Figure 10. High performance metal-free organic dyes used in DSSC.

The metal-free dyes have been widely explored for DSSCs due to their simple synthesis, good flexibility in molecular design, economical purification, easy large-scale production, and extremely high molar extinction coefficients.[56] Metal-free organic dyes consists triarylamine,[57] indolines,[58] coumarins,[59] and fluorene[60], phenothiazine,[61] hemicyanine[62] dye, squaraine[63], etc. as conjugated chromophores for light harvesting. The skeleton of most of the organic sensitizers consists of electron donor (D), a π-conjugated spacer (π) and electron acceptor (A) moieties, which is designated as D–π–A configuration.[64,65] Such molecules exhibit intramolecular charge transfer (ICT) from the donor to acceptor through π-conjugated space due to the push-pull structure. (**Figure 10**). Recently, the D-A-π-A configuration have also been investigated where an electron acceptor is placed between donor and p-spacer.[66–68] Substantial efforts have been dedicated towards modifying the different components of metal-free dyes to optimize the DSSC performance. Currently, several organic dyes have achieved efficiencies over 10%.[69]

1.6. Near-infrared (NIR) Active dyes in DSSCs

The absorption over a broad solar spectral range (panchromatic absorption) is one of the most desirable features in the dyes for DSSC.

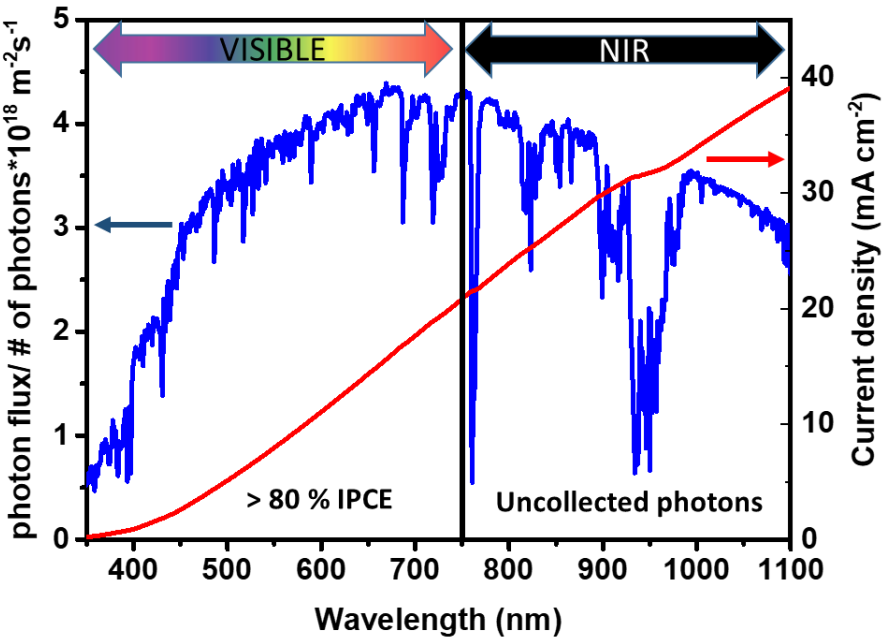

Figure 11. Solar light spectrum (blue) and calculated photocurrent (red) with an assumed IPCE of 100% integrated from 300 nm to the corresponding wavelength at the band gap.

Most high-performance DSSCs efficiently converts photons to electricity from 400-700 nm; however, a significant portion of energy available in the longer wavelength is lost due to lack of efficient absorber in NIR region (**Figure 11**). Porphyrin, Phthalocyanine, and squaraine based dyes are the major examples of NIR absorbing sensitizers in DSSC.

1.6.1. Zinc-Porphyrins (Zn-Por)

Porphyrins are the conjugated macrocycles which are instrumental in many bio-activities in animals as well as plants. Porphyrins have been considered potential sensitizers since the beginning of DSSC as they have broad and intense absorption between 400-450 (soret band) and 500-700 nm (Q-band).[70–72] However, the efficiencies of the earlier porphyrins based designs were low due to inefficient light harvesting around 500 nm and beyond 600 nm. Considerable efforts have been made to overcome this bottleneck by using push-pull structure and elongation of porphyrin π-conjugated system (**Figure 12**).

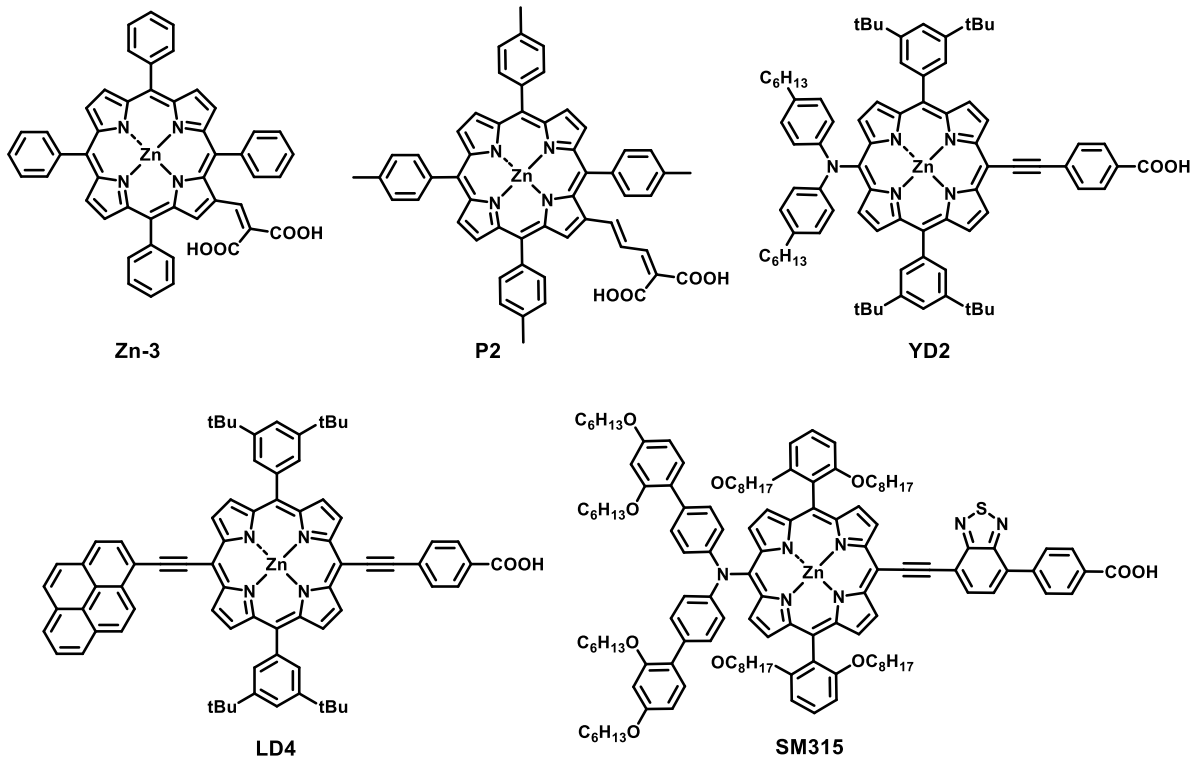

Figure 12. Zinc-Porphyrin based dyes used in DSSC.

In 2004, Grätzel and Officer used a zinc porphyrin dye (P2) which is a tetraphenylporphyrin with a β-substituted styrylcarboxylic acid. The dye produced the efficiency of 4.8% [73] and a

year later the same group reported efficiency of 5.6% with Zn-3 which has β-substituted cyanoacrylic acid as an anchoring group.[74] Replacing cyanoacrylic acid with malonic acid group facilitated a stronger binding to the semiconductor surface which improved the efficiency to 7.1% with panchromatic IPCE up to 710 nm.[75] These results opened a new avenue for the porphyrin-based sensitizer as a potential successor to ruthenium dyes. Yeh and Diau designed a promising YD2 which consists of an electron-releasing diarylamino group attached at the meso position of the porphyrin ring and the meso-substituted phenylethynyl carboxyl anchoring group at the opposite end. This push-pull porphyrin configuration gave efficiency up to 6.8% when co-adsorbed with CDCA.[76] A set of fluorene/pyrene-modified porphyrin with aromatic substituents at the meso-position of porphyrin ring were synthesized by Lin and Diau. Fluorene-functionalized LD22[77] featured an impressive efficiency of 8.1% whereas the pyrene-functionalized LD4[78] displayed efficiency up to 10.1% due to broad IPCE response from 300 to 800 nm. Further attempts to increase the absorption by extending conjugation by synthesizing dimeric porphyrin could not increase the efficiency due to self-quenching induced by aggregation.[79–83] To counter this the problem Imahori and co-workers reported ortho-substituted zinc porphyrins sensitizer with alkyl groups (methyl and ethyl) to reduce the dye aggregation for improved charge injection and suppress charge recombination.[84,85] Hupp and co-workers reported porphyrin-based dyes with two phenyl groups attached at the 5,15-meso-positions of porphyrin ring, bearing dodecyl ($–OC_{12}H_{25}$) groups at the ortho-position of each phenyl group to restrict aggregation.[86,87] Further work along this line improved the performance of DSSC constructed using a push-pull zinc porphyrin-based dye, YD2-OC8,[32] which has four *ortho*-substituted octyloxy side chains in the each of the *meso*-phenyls of porphyrin. The particular molecular design helped greatly to control the aggregation and YD2-OC8 based device produced an efficiency of 11.9% under standard irradiation. The co-sensitization of YD2-OC8 with the previously reported organic dye, Y123, produced an efficiency of 12.3%. Recently, DSSCs based on similar designs of porphyrins, SM315 and GY50, exhibited exceptionally high efficiencies of 13% and 12.7% respectively with IPCE up to 775 nm.[46,88]

1.6.2. Zinc-Phthalocyanines (Zn-Pc)

Phthalocyanines (Pcs) are planar 18 π-electron macro-heterocycles which are structurally related to porphyrin but even more extended conjugation which results in the absorption in the far visible/near-IR region. The UV-Vis spectrum of metallophthalocyanines shows a

Soret band at 300–400 nm and a Q band centered around 650–700 nm which makes them potential panchromatic sensitizer (**Figure 13**).

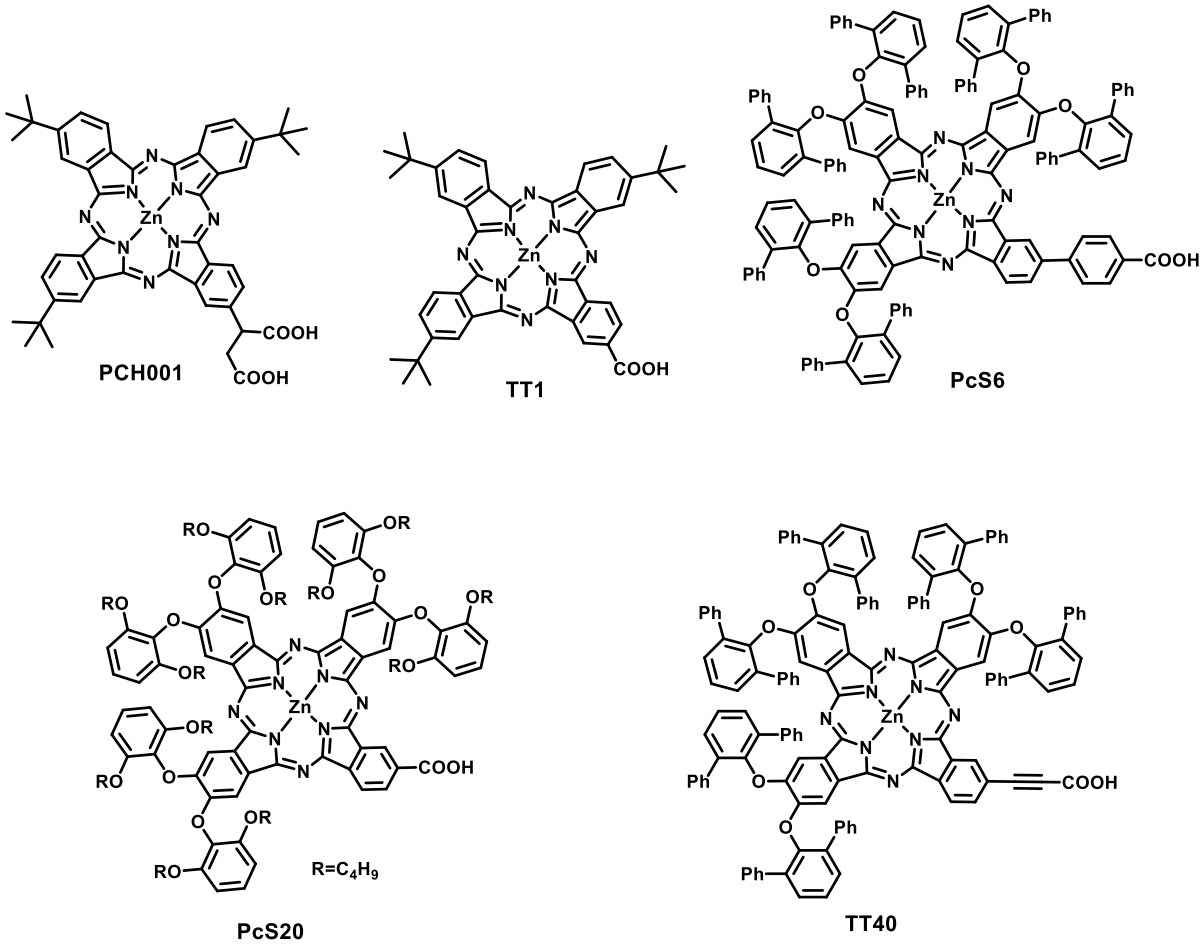

Figure 13. Zinc-Phthalocyanine based dyes used in DSSC.

Earlier attempts to use phthalocyanine as the light harvester in DSSC fared poorly, and it could not surpass 1% overall efficiency. The main reason behind the low performance was the strong aggregation of the dye due to the extended planarity of phthalocyanine and absence of directionality of the symmetrical dyes in combination with the poor coupling of the LUMO with the conduction band of TiO_2.[89,90] The first breakthrough came with the Zn-Pc sensitizers PCH001[91,92] and TT1 where the periphery of the phthalocyanines was functionalized with bulky alkyl groups to suppress the aggregation. The difference in the two dyes was the number of carboxylic acid anchoring groups (PCH0001 with two carboxylic group and TT1 with one carboxylic group), and the resulting PCEs were 3.05% for PCH001 and 3.5% for TT1. The greater performance of TT1 over PCH001 could be ascribed to attachment of

carboxylic acid directly to the conjugated skeleton which brought directionality in the charge movement flow from the dye to the TiO_2, due to its "push-pull" nature, resulting in an outstanding IPCE of 80% at 700 nm. A number of modifications were done on PCH001 and TT1 which includes changes in bulky alkyl groups and linkage of carboxylic acid, but the efficiency could not be improved. Mori, Kimura, et al. used even bulkier 2,6-diphenylphenoxy groups at the periphery which lie normal to the plane of Pc macrocycle, succeeding in suppressing the aggregation efficiently. Their dye PcS6 achieved an excellent efficiency of 4.6% with a 78 % IPCE at the Q-band maximum which extends up to ca. 750 nm.[93] Further exploration and modification of structural features of Pc macrocycle led to the synthesis of many more dyes with improved efficiency. TT40 which has carboxylic acid linked to the Pc ring through a triple bond (carboxyethynyl) with 2,6-diphenylphenoxy groups provided improved efficiency of 6.01%.[94] Currently, the record of highest efficiency (η = 6.4%) in Zn-Pc dyes is held by Pcs20 which has an n-butoxy chain on the 2,6-diphenylphenoxy group to prevent aggregation.[95]

1.6.3. Squaraine Dyes

Squaraine dyes belong to the family of polymethine dyes and comprise of resonance-stabilized zwitterionic structures. Due to strong absorption (e > 10 5 M-1) in visible, far red and NIR region, squaraine dyes have found applications in wide range of areas such as imaging,[96–99] ion sensing,[100,101]nonlinear optics,[102,103] photodynamic therapy[104,105], and photovoltaics.[63,106] Squaraine dyes, in general, are synthesized by the condensation of electron-rich aromatic/heterocyclic compounds with squaric acid. Aromatic compounds such as *N*, *N*-dialkylanilines, indolenines, benzothiazoles, quinolines, phenols, azulenes, pyrroles, etc. have been used to synthesized squaraine based dyes.[101,107] By choosing aromatic and heteroaromatic systems of varying donor strength, the squaraine dyes of diverse optical and electrochemical properties can be synthesized (**Figure 14**).

The sensitization behavior of squaraine dye was investigated first time by Kamat and coworkers in 1993.[108] They observed a very low IPCE for these dyes primarily due to high back electron transfer and low singlet fluorescence quantum yields. Zhao and co-workers synthesized indole-based symmetric squaraine dyes with sulphonic acid anchoring group which was attached to N-atom through propyl chain.[109] The DSSC based on the dye gave the efficiency of 2.16% which initiated an extensive investigation of squaraine dyes for DSSCs.

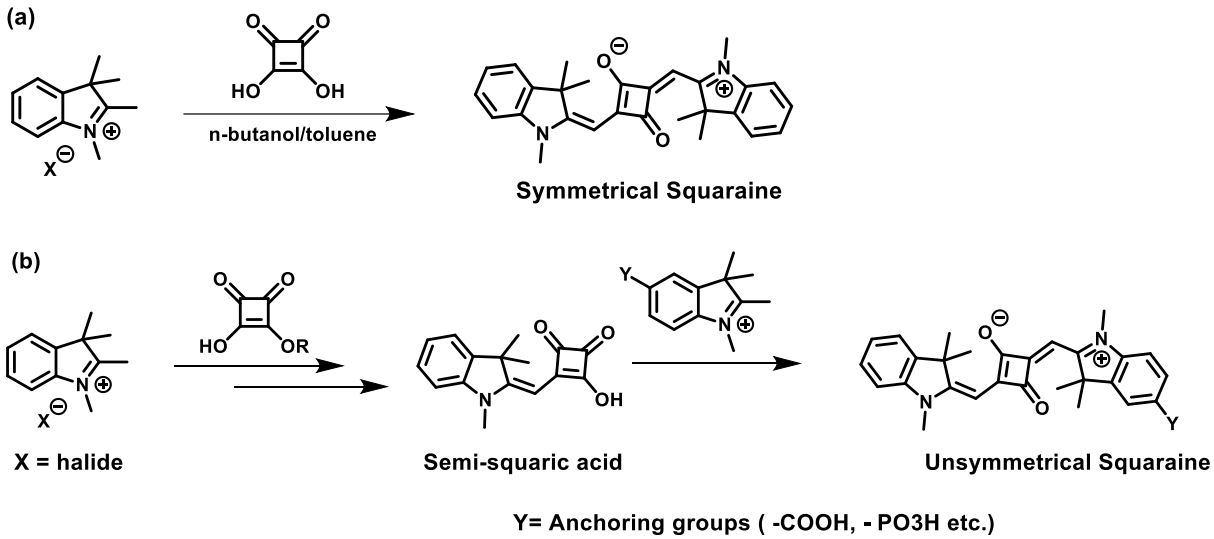

Figure 14. The general scheme for the synthesis of a) symmetrical squaraine and b) unsymmetrical squaraine dyes.

The same group later synthesized a series of aniline-based symmetric dye where they used carboxylic acid as an anchoring group which gave the efficiency of 3.4%.[110] Several symmetrical squaraine based dyes were explored and synthesized, but no significant improvement in efficiency was observed. Yum et al. provided a breakthrough by developing an unsymmetrical squaraine dye where the carboxylic group is directly attached to the conjugated backbone.[111]Their unsymmetrical design brought the directionality of the charge movement within the molecule which was evident in the DFT calculation. Efficient charge separation and electron injection improved the IPCE and efficiency of 4.5% were obtained. Geiger et al. improved the above design by replacing indole with benz[e]indole moiety which further red-shifted the spectrum of dye.[112] It gave rise to improved light harvesting and broadened IPCE spectrum which yielded the efficiency of 5.4%. A bulky spirobifluorene or hexyloxyphenyl motif was introduced into the squaraine framework by Choi et al. The large steric group helped to suppress dye aggregation efficiency and impressive overall efficiency of 4.2% was achieved.[113] Shi et al. extended the conjugation of indoline base squaraine dye by covalently attaching the thiophene unit on end of the squaraine unit. Moreover, the carboxylic group was replaced by a stronger electron withdrawing cyanoacrylic acid anchoring group. This dye exhibited not only the extended absorption at longer wavelength but also an additional higher energy band. These features led to the significantly high efficiency of 6.74% with J_{SC} of 14.8 mA cm^{-2}.[114]This design strategy seems to be very

effective to achieve the red-shifted maximum as well as panchromatic absorption which inspired a significant improvement in performance of squaraine based DSSC.

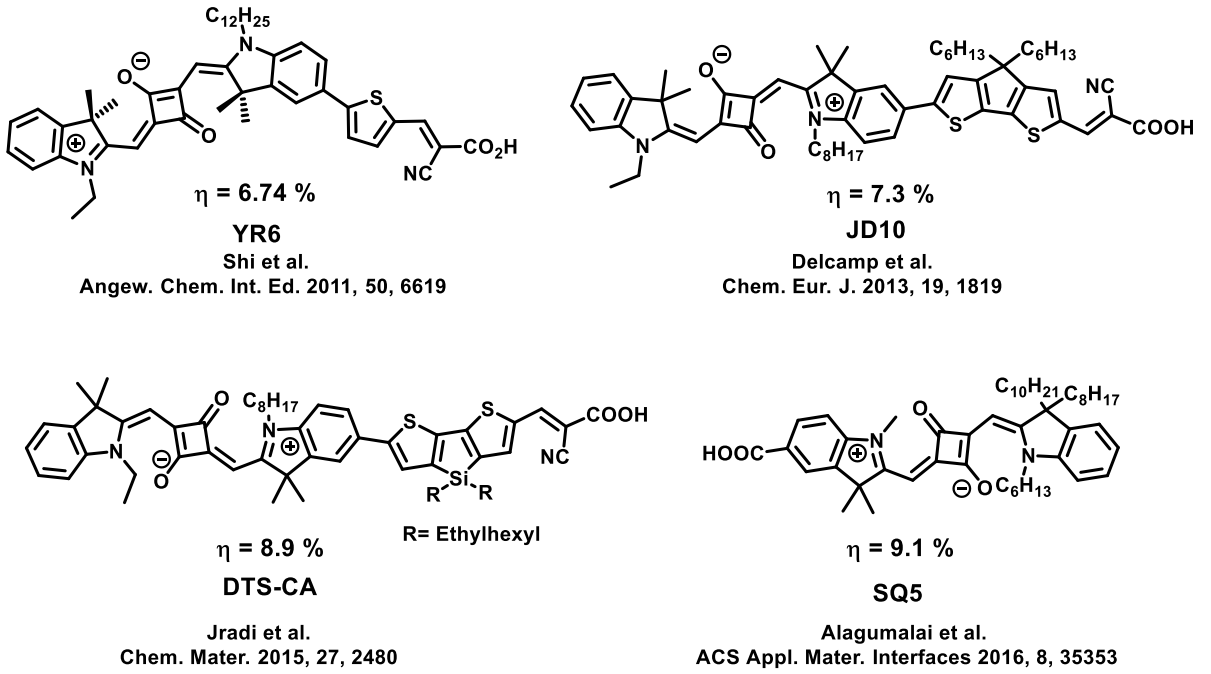

Figure 15. High-performance squaraine dyes in DSSC.

Recently, Jradi et al. reported a squaraine dye DTS-CA, where squaraine unit is extended by DTS bearing out-of-plane ethylhexyl chain. This design effectively suppressed aggregation as well as generated panchromatic IPCE response which produced a high efficiency of 8.9%.[115] The detailed understanding of structure-property relationship has significantly improved the squaraine dyes based DSSC and efficiency up to 9% have been achieved till recently. However, the absorption of the successful squaraine dyes is still limited up to 750 nm. There are very few squaraine dyes which absorb beyond 750 nm, and the examples of such dyes are shown with their IPCE onset in **Figure 16**. Several modifications and molecular engineering were carried out to enhance the absorption of SQ dyes in NIR. The increase in conjugation was attempted by either attaching extra aromatic unit covalently to the squaraine structure or by including π-extended fused heteroaromatic moieties as a donor instead of indole unit. Both the methods helped to push the absorption of SQ dyes and successfully increased the IPCE onset. However, the increased absorbance in the NIR region of squaraine dyes could not be translated into improved performance. Barring JK-217, DTS-CA, HSQ4, and YR6, no other dyes could achieve efficiency of more than 3%. The major challenge faced while reducing the band gap of dyes is to maintain the proper energy level of HOMO and LUMO.

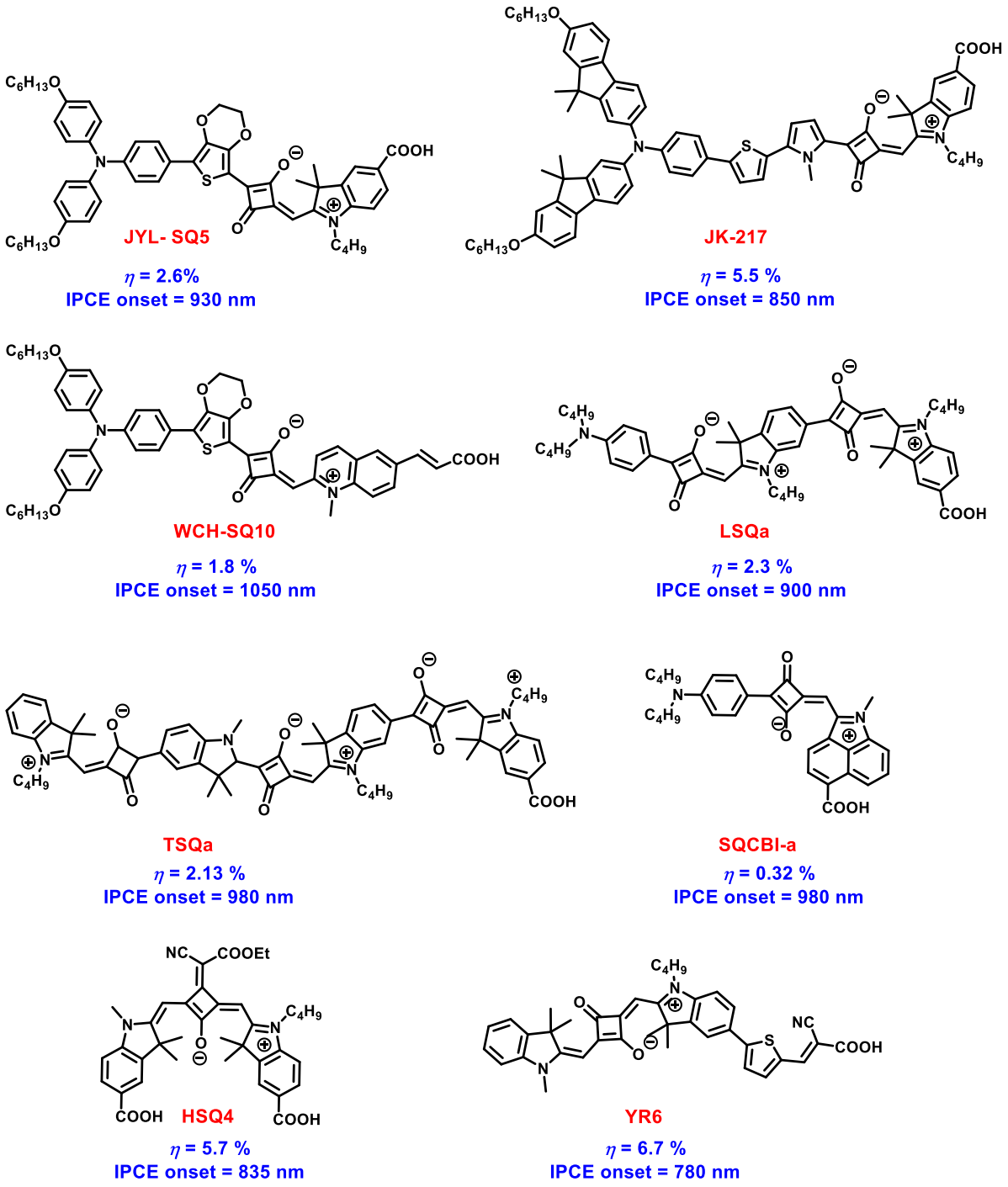

Figure 16. NIR responsive squaraine dyes with IPCE onset greater than 750 nm.

Extending the conjugation can either bring down the LUMO close to CB of TiO_2 leading to poor injection, or it can push the HOMO upwards leading to poor dye regeneration. Another major problem is extensive aggregation on TiO_2 surface. Attempts to increase absorption by including π-extended moieties in the dyes also induced planarity in extended π-backbone

which encourage the formation of aggregates. As a result, despite having very good absorption in the NIR region, these dyes failed to perform satisfactorily.

1.6.4. Aggregation in DSSCs

The aggregation of dyes is a common phenomenon in dye chemistry which can occur in solution or the solid state. It originates due to strong intermolecular van der Waals-like attractive forces which brings the molecules together to self-assemble. Squaraine dyes also show strong aggregation properties in both in solution and solid form. The aggregates display characteristic changes in the absorption band in comparison to the monomeric species. The H-type aggregates are formed when molecules align in face-to-face (or head-to-head) fashion, and J-type aggregates are formed due to edge-to-edge (head-to-tail) alignment. These aggregates can be distinctly observed by UV-Vis absorption spectroscopy where H-aggregates appears as blue-shifted band whereas the J-aggregates shows bathochromic shift compared to the monomer (**Figure 17**). Origin of the spectral behavior of the aggregates has been explained by Kasha's molecular exciton theory.[116–118]

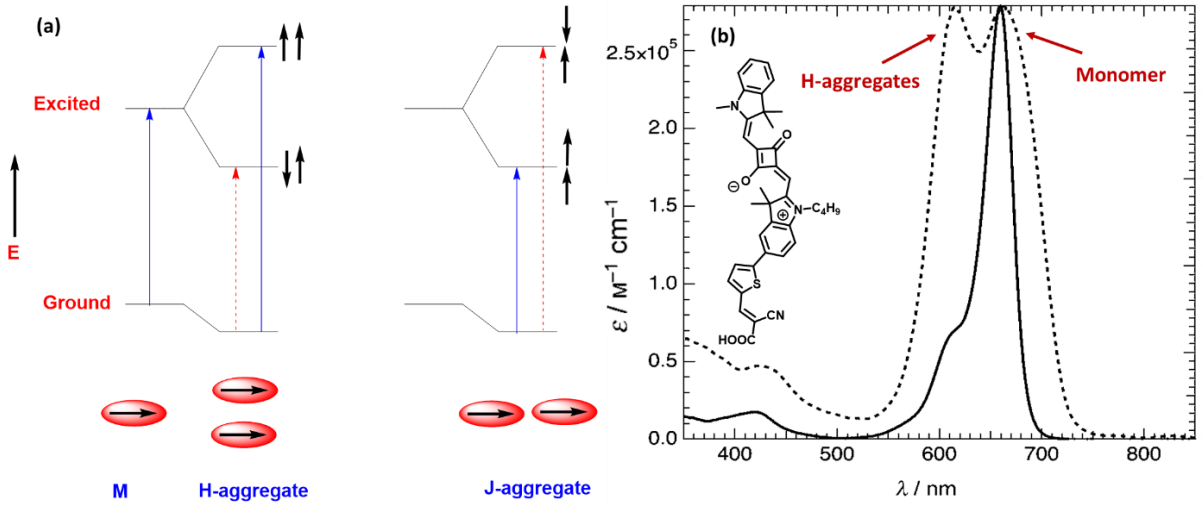

Figure 17. (a) Simplified schematic of exciton theory to explain the different absorption behaviors of H- and J-aggregates. (b) Formation of aggregates in squaraine dye (YR6) when adsorbed on TiO_2 film (dotted) solution (adapted from reference no.114).

According to molecular exciton theory when two monomer molecules interact to form a dimer, the energy of the excited dimer becomes non-degenerate due to the coupling which leads to exciton-splitting.

In general, aggregates hamper the performance of DSSC by exciton quenching. The early designs of dyes could not produce high efficiency despite strong absorption because of aggregate formation on the TiO_2 surface.[119] To explain the effect of aggregation on electron injection a time-resolved laser spectroscopy measurements were done by Ziółek et al.[120] The study revealed that electron injection rate of monomer was quite higher compared to H-aggregates, which show that H-aggregation hinders electron injection rate. Nevertheless, there are a few reports that show H-aggregation may extend the spectral range of absorption spectra with respect to the monomeric form, thus augmenting the light harvesting and device efficiency of the dyes.[121,122]. In comparison to H-aggregates, J-aggregates are considered helpful for light absorption due to their ability to capture low energy photons (far-red and NIR) which is more suitable for improving solar cell performance.[123,124] However, numbers of such reports are quite few, and in major consensus, the aggregation is considered harmful for DSSC performance. Some methods have been developed to restrain the formation of dye aggregates which are discussed below.

a) Addition of co-adsorbing agents. It is one of the most common methods of suppressing aggregation in which an optically transparent bulky molecule such as a chenodeoxycholic acid (CDCA) is co-adsorbed along with sensitizing dye on TiO_2 surface. When TiO_2 coated electrodes are dipped in a solution containing both the dye and co-adsorbent, both species contend for anchoring spaces on the TiO_2 surface. This is one of the very effective methods to control aggregation, but the amount of CDCA that can be added is limited as high CDCA amount can reduce the dye loading on the TiO_2 surface leading to low light harvesting efficiency.

b) Modification in dye structure. Planarity of molecules induces the aggregation as it provides large π-surface to interact. Several reports suggested the twisting the conjugation to induces non-planarity in molecules which improved the PCE. However, these methods hinder conjugation restricts the absorption at longer wavelengths.

c) Attaching alkyl groups and bulky substituents to the dye. Introducing long-chain alkyl groups stops the dye molecules to come close to each other and hence restricts the formation of aggregates. This is the best method so far as it allows the dyes to control aggregation at the molecular level without compromising on the planarity. Additionally, the performance of the

dyes can be tweaked by optimizing the chain length of alkyl groups. Jradi et al. obtained a PCE of 8.9% by introducing out-of-plane alkyl chain on squaraine dyes.

d) Dye co-sensitization. In this method, two or more chemically different dyes are sensitized onto the surface of a TiO_2 thin film. In contrast to optically transparent co-adsorber such as CDCA, co-sensitizing with a dye does not hamper light harvesting as both the components can absorb light. By employing the dye with complementary absorption spectrum, the light harvesting can be improved efficiently over the broad spectral range.

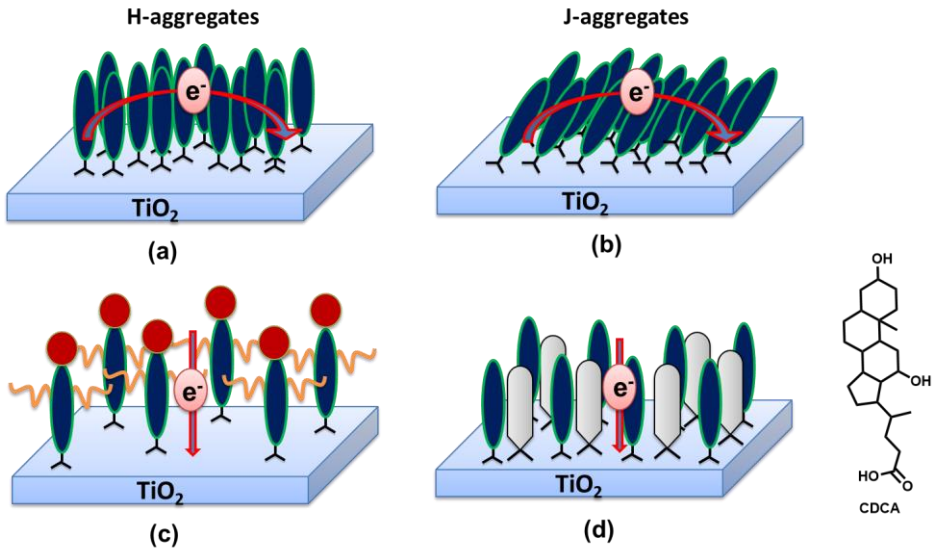

Figure 18. (a, b) Orientation of H- and J- aggregates, (c) suppressing aggregation by incorporating alkyl chains on the dyes (d) suppressing aggregation using CDCA.

1.7. Objectives of the Thesis

The extensive literature survey presented above shows the importance of sensitizers in dye-sensitized solar cells. The photovoltaic performances of DSSCs have been improved over the years by applying new sensitizers, optimizing the device components and carrying out some fundamental studies. However, the absorption in the NIR region of the sensitizers still lacks which has created a bottleneck in the progress of DSSCs. Squaraines are one of the metal-free dyes, which have the potential to absorb in the NIR region with a very high extinction coefficient. The work in this thesis attempts the design and synthesis of NIR responsive squaraine based dyes and their application in dye-sensitized solar cells. The broad objective of the present work is directed towards increasing the pool of NIR responsive dyes, addressing the intricate problems associated with them such as aggregation; and ultimately, increasing the efficiency of squaraine based DSSCs. Also, this research assists to gain more

insight into the structure-property relationship of squaraine dyes, and the photovoltaic performance of DSSCs devices based on these squaraine based sensitizers.

The specific objectives are as follows:

1) To synthesize squaraine based dye with extended conjugation towards anchoring end by incorporating a π-spacer to increase absorption in longer wavelength, with variation in alkyl chain to understand the impact of the side chain on aggregation and recombination.

2) To synthesize squaraine dyes with out-of-plane alkyl chains where conjugation is extended towards the non-anchoring end as well as towards anchoring end to understand the effect of the electronic and structural modification on photovoltaic parameters of DSSCs.

3) To incorporate fused π-extended heterocyclic moieties in the squaraine unit to extend the absorption further into the NIR region.

4) To fabricate dye-sensitized solar cells (DSSCs) using these dyes and study their photovoltaic and charge transport properties to establish a structure-property relationship in squaraine based materials.

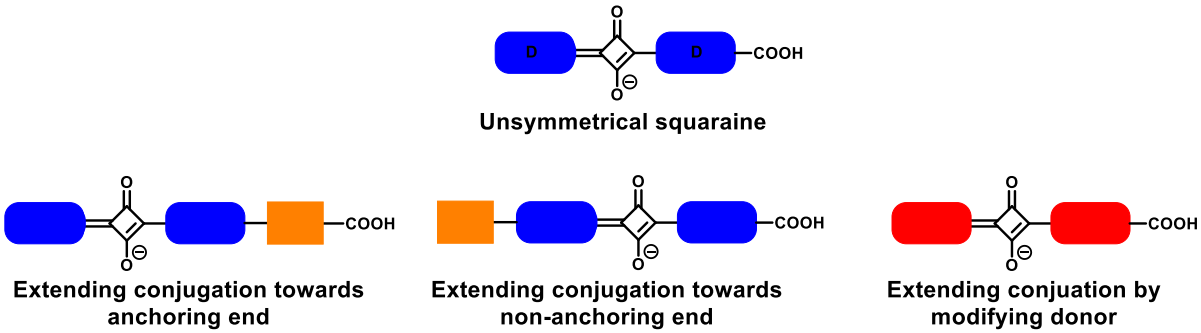

Figure 19. Various strategies to synthesize NIR absorbing squaraine dyes.

1.8. REFERENCES

(1) *World Population Prospects 2017*. United Nations, New York.

(2) *International Energy Agency*. Energy Access Outlook 2017.

(3) Kannan, N.; Vakeesan, D. *Renew. Sustain. Energy Rev.* **2016**, *62*, 1092–1105.

(4) *REN21*. Renewables 2017 Global Status Report 2017.

(5) *Press Information Bureau, Government of India*. Year End Review 2017 –MNRE.

(6) Zhao, W.; Li, S.; Yao, H.; Zhang, S.; Zhang, Y.; Yang, B.; Hou, J. *J. Am. Chem. Soc.* **2017**, *139*, 7148–7151.

(7) Kakiage, K.; Aoyama, Y.; Yano, T.; Oya, K.; Fujisawa, J.; Hanaya, M. *Chem Commun* **2015**.

(8) Sanehira, E. M.; Marshall, A. R.; Christians, J. A.; Harvey, S. P.; Ciesielski, P. N.; Wheeler, L. M.; Schulz, P.; Lin, L. Y.; Beard, M. C.; Luther, J. M. *Sci. Adv.* **2017**, *3*, eaao4204.

(9) Yang, W. S.; Park, B.-W.; Jung, E. H.; Jeon, N. J.; Kim, Y. C.; Lee, D. U.; Shin, S. S.; Seo, J.; Kim, E. K.; Noh, J. H.; Seok, S. I. *Science* **2017**, *356*, 1376–1379.

(10) France, R. M.; Geisz, J. F.; García, I.; Steiner, M. A.; McMahon, W. E.; Friedman, D. J.; Moriarty, T. E.; Osterwald, C.; Ward, J. S.; Duda, A.; Young, M.; Olavarria, W. J. *IEEE J. Photovolt.* **2016**, *6*, 578–583.

(11) O'Regan, B.; Grätzel, M. *Nature* **1991**, *353*, 737–740.

(12) Matsumura, M.; Nomura, Y.; Tsubomura, H. *Bull. Chem. Soc. Jpn.* **1977**, *50*, 2533–2537.

(13) Willig, F.; Eichberger, R.; Sundaresan, N. S.; Parkinson, B. A. *J. Am. Chem. Soc.* **1990**, *112*, 2702–2707.

(14) Desilvestro, J.; Graetzel, M.; Kavan, L.; Moser, J.; Augustynski, J. *J. Am. Chem. Soc.* **1985**, *107*, 2988–2990.

(15) Hagfeldt, A.; Boschloo, G.; Sun, L.; Kloo, L.; Pettersson, H. *Chem. Rev.* **2010**, *110*, 6595–6663.

(16) Hara, K.; Sato, T.; Katoh, R.; Furube, A.; Ohga, Y.; Shinpo, A.; Suga, S.; Sayama, K.; Sugihara, H.; Arakawa, H. *J. Phys. Chem. B* **2003**, *107*, 597–606.

(17) Hamann, T. W.; Jensen, R. A.; Martinson, A. B. F.; Ryswyk, H. V.; Hupp, J. T. *Energy Environ. Sci.* **2008**, *1*, 66–78.

(18) Pagliaro, M.; Palmisano, G.; Ciriminna, R.; Loddo, V. *Energy Environ. Sci.* **2009**, *2*, 838–844.

(19) Jose, R.; Thavasi, V.; Ramakrishna, S. *J. Am. Ceram. Soc.* **2009**, *92*, 289–301.

(20) Peter, L. M. *Phys. Chem. Chem. Phys.* **2007**, *9*, 2630–2642.

(21) Peng, B.; Jungmann, G.; Jäger, C.; Haarer, D.; Schmidt, H.-W.; Thelakkat, M. *Coord. Chem. Rev.* **2004**, *248*, 1479–1489.

(22) Papageorgiou, N.; Maier, W. F.; Grätzel, M. *J. Electrochem. Soc.* **1997**, *144*, 876–884.

(23) Kay, A.; Grätzel, M. *Sol. Energy Mater. Sol. Cells* **1996**, *44*, 99–117.

(24) Lindström, H.; Holmberg, A.; Magnusson, E.; Lindquist, S.-E.; Malmqvist, L.; Hagfeldt, A. *Nano Lett.* **2001**, *1*, 97–100.

(25) Imoto, K.; Takahashi, K.; Yamaguchi, T.; Komura, T.; Nakamura, J.; Murata, K. *Sol. Energy Mater. Sol. Cells* **2003**, *79*, 459–469.

(26) Murakami, T. N.; Ito, S.; Wang, Q.; Nazeeruddin, M. K.; Bessho, T.; Cesar, I.; Liska, P.; Humphry-Baker, R.; Comte, P.; Péchy, P.; Grätzel, M. *J. Electrochem. Soc.* **2006**, *153*, A2255–A2261.

(27) Hara, K.; Horiguchi, T.; Kinoshita, T.; Sayama, K.; Arakawa, H. *Sol. Energy Mater. Sol. Cells* **2001**, *70*, 151–161.

(28) Kato, N.; Takeda, Y.; Higuchi, K.; Takeichi, A.; Sudo, E.; Tanaka, H.; Motohiro, T.; Sano, T.; Toyoda, T. *Sol. Energy Mater. Sol. Cells* **2009**, *93*, 893–897.

(29) Law ChunHung; Pathirana Shehan C.; Li Xaioe; Anderson Assaf Y.; Barnes Piers R. F.; Listorti Andrea; Ghaddar Tarek H.; O′Regan Brian C. *Adv. Mater.* **2010**, *22*, 4505–4509.

(30) Yu, Z.; Vlachopoulos, N.; Gorlov, M.; Kloo, L. *Dalton Trans.* **2011**, *40*, 10289-.

(31) Yu, Q.; Wang, Y.; Yi, Z.; Zu, N.; Zhang, J.; Zhang, M.; Wang, P. *ACS Nano* **2010**, *4*, 6032–6038.

(32) Yella, A.; Lee, H.-W.; Tsao, H. N.; Yi, C.; Chandiran, A. K.; Nazeeruddin, M. K.; Diau, E. W.-G.; Yeh, C.-Y.; Zakeeruddin, S. M.; Grätzel, M. *Science* **2011**, *334*, 629–634.

(33) Shi, D.; Pootrakulchote, N.; Li, R.; Guo, J.; Wang, Y.; Zakeeruddin, S. M.; Grätzel, M.; Wang, P. *J. Phys. Chem. C* **2008**, *112*, 17046–17050.

(34) Xi, C.; Cao, Y.; Cheng, Y.; Wang, M.; Jing, X.; Zakeeruddin, S. M.; Grätzel, M.; Wang, P. *J. Phys. Chem. C* **2008**, *112*, 11063–11067.

(35) Boschloo, G.; Hagfeldt, A. *Acc. Chem. Res.* **2009**, *42*, 1819–1826.

(36) Wang, Z.-S.; Sayama, K.; Sugihara, H. *J. Phys. Chem. B* **2005**, *109*, 22449–22455.

(37) Teng, C.; Yang, X.; Yuan, C.; Li, C.; Chen, R.; Tian, H.; Li, S.; Hagfeldt, A.; Sun, L. *Org. Lett.* **2009**, *11*, 5542–5545.

(38) Ning, Z.; Zhang, Q.; Wu, W.; Tian, H. *J. Organomet. Chem.* **2009**, *694*, 2705–2711.

(39) Gorlov, M.; Pettersson, H.; Hagfeldt, A.; Kloo, L. *Inorg. Chem.* **2007**, *46*, 3566–3575.

(40) Oskam, G.; Bergeron, B. V.; Meyer, G. J.; Searson, P. C. *J. Phys. Chem. B* **2001**, *105*, 6867–6873.

(41) Bergeron, B. V.; Marton, A.; Oskam, G.; Meyer, G. J. *J. Phys. Chem. B* **2005**, *109*, 937–943.

(42) Wang, M.; Grätzel, C.; Zakeeruddin, S. M.; Grätzel, M. *Energy Environ. Sci.* **2012**, *5*, 9394–9405.

(43) Nelson, J. J.; Amick, T. J.; Elliott, C. M. *J. Phys. Chem. C* **2008**, *112*, 18255–18263.

(44) Feldt, S. M.; Gibson, E. A.; Gabrielsson, E.; Sun, L.; Boschloo, G.; Hagfeldt, A. *J. Am. Chem. Soc.* **2010**, *132*, 16714–16724.

(45) Bella, F.; Galliano, S.; Gerbaldi, C.; Viscardi, G. *Energies* **2016**, *9*, 384.

(46) Mathew, S.; Yella, A.; Gao, P.; Humphry-Baker, R.; Curchod, B. F. E.; Ashari-Astani, N.; Tavernelli, I.; Rothlisberger, U.; Nazeeruddin, M. K.; Grätzel, M. *Nat. Chem.* **2014**, *6*, 242–247.

(47) Kohle, O.; Grätzel, M.; Meyer, A. F.; Meyer, T. B. *Adv. Mater.* **2004**, *9*, 904–906.

(48) Nazeeruddin, M. K.; De Angelis, F.; Fantacci, S.; Selloni, A.; Viscardi, G.; Liska, P.; Ito, S.; Takeru, B.; Grätzel, M. *J. Am. Chem. Soc.* **2005**, *127*, 16835–16847.

(49) Chen, C.-Y.; Wang, M.; Li, J.-Y.; Pootrakulchote, N.; Alibabaei, L.; Ngoc-le, C.; Decoppet, J.-D.; Tsai, J.-H.; Grätzel, C.; Wu, C.-G.; Zakeeruddin, S. M.; Grätzel, M. *ACS Nano* **2009**, *3*, 3103–3109.

(50) Birel, Ö.; Nadeem, S.; Duman, H. *J. Fluoresc.* **2017**, *27*, 1075–1085.

(51) Higashino, T.; Imahori, H. *Dalton Trans.* **2014**, *44*, 448–463.

(52) Li, L.-L.; Diau, E. W.-G. *Chem. Soc. Rev.* **2012**, *42*, 291–304.

(53) Urbani, M.; Grätzel, M.; Nazeeruddin, M. K.; Torres, T. *Chem. Rev.* **2014**, *114*, 12330–12396.

(54) Ragoussi, M.-E.; Ince, M.; Torres, T. *Eur. J. Org. Chem.* **2013**, *2013*, 6475–6489.

(55) Martín-Gomis, L.; Fernández-Lázaro, F.; Sastre-Santos, Á. *J. Mater. Chem. A* **2014**, *2*, 15672–15682.

(56) Mishra, A.; Fischer, M. K. R.; Bäuerle, P. *Angew. Chem. Int. Ed.* **2009**, *48*, 2474–2499.

(57) Liang, M.; Chen, J. *Chem. Soc. Rev.* **2013**, *42*, 3453–3488.

(58) Ito S.; Zakeeruddin S. M.; Humphry-Baker R.; Liska P.; Charvet R.; Comte P.; Nazeeruddin M. K.; Péchy P.; Takata M.; Miura H.; Uchida S.; Grätzel M. *Adv. Mater.* **2006**, *18*, 1202–1205.

(59) Hara, K.; Sayama, K.; Ohga, Y.; Shinpo, A.; Suga, S.; Arakawa, H. *Chem. Commun.* **2001**, *0*, 569–570.

(60) Thomas, K. R. J.; Lin, J. T.; Hsu, Y.-C.; Ho, K.-C. *Chem. Commun.* **2005**, *0*, 4098–4100.

(61) Huang, Z.-S.; Meier, H.; Cao, D. *J. Mater. Chem. C* **2016**, *4*, 2404–2426.

(62) Chen, Y.-S.; Li, C.; Zeng, Z.-H.; Wang, W.-B.; Wang, X.-S.; Zhang, B.-W. *J. Mater. Chem.* **2005**, *15*, 1654–1661.

(63) Qin, C.; Wong, W.-Y.; Han, L. *Chem. – Asian J.* **2013**, *8*, 1706–1719.

(64) Gabrielsson, E.; Ellis, H.; Feldt, S.; Tian, H.; Boschloo, G.; Hagfeldt, A.; Sun, L. *Adv. Energy Mater.* **2013**, *3*, 1647–1656.

(65) Yang, J.; Ganesan, P.; Teuscher, J.; Moehl, T.; Kim, Y. J.; Yi, C.; Comte, P.; Pei, K.; Holcombe, T. W.; Nazeeruddin, M. K.; Hua, J.; Zakeeruddin, S. M.; Tian, H.; Grätzel, M. *J. Am. Chem. Soc.* **2014**, *136*, 5722–5730.

(66) Zhu, W.; Wu, Y.; Wang, S.; Li, W.; Li, X.; Chen, J.; Wang, Z.; Tian, H. *Adv. Funct. Mater.* **2011**, *21*, 756–763.

(67) Cui, Y.; Wu, Y.; Lu, X.; Zhang, X.; Zhou, G.; Miapeh, F. B.; Zhu, W.; Wang, Z.-S. *Chem. Mater.* **2011**, *23*, 4394–4401.

(68) Wu, Y.; Zhu, W.-H.; Zakeeruddin, S. M.; Grätzel, M. *ACS Appl. Mater. Interfaces* **2015**, *7*, 9307–9318.

(69) Zhou, N.; Prabakaran, K.; Lee, B.; Chang, S. H.; Harutyunyan, B.; Guo, P.; Butler, M. R.; Timalsina, A.; Bedzyk, M. J.; Ratner, M. A.; Vegiraju, S.; Yau, S.; Wu, C.-G.; Chang, R. P. H.; Facchetti, A.; Chen, M.-C.; Marks, T. J. *J. Am. Chem. Soc.* **2015**, *137*, 4414–4423.

(70) Campbell, W. M.; Burrell, A. K.; Officer, D. L.; Jolley, K. W. *Coord. Chem. Rev.* **2004**, *248*, 1363–1379.

(71) Imahori, H.; Umeyama, T.; Ito, S. *Acc. Chem. Res.* **2009**, *42*, 1809–1818.

(72) Martínez-Díaz, M. V.; Torre, G. de la; Torres, T. *Chem. Commun.* **2010**, *46*, 7090–7108.

(73) Nazeeruddin, M. K.; Humphry-Baker, R.; Officer, D. L.; Campbell, W. M.; Burrell, A. K.; Grätzel, M. *Langmuir* **2004**, *20*, 6514–6517.

(74) Wang, Q.; Campbell, W. M.; Bonfantani, E. E.; Jolley, K. W.; Officer, D. L.; Walsh, P. J.; Gordon, K.; Humphry-Baker, R.; Nazeeruddin, M. K.; Grätzel, M. *J. Phys. Chem. B* **2005**, *109*, 15397–15409.

(75) Campbell, W. M.; Jolley, K. W.; Wagner, P.; Wagner, K.; Walsh, P. J.; Gordon, K. C.; Schmidt-Mende, L.; Nazeeruddin, M. K.; Wang, Q.; Grätzel, M.; Officer, D. L. *J. Phys. Chem. C* **2007**, *111*, 11760–11762.

(76) Lu, H.-P.; Tsai, C.-Y.; Yen, W.-N.; Hsieh, C.-P.; Lee, C.-W.; Yeh, C.-Y.; Diau, E. W.-G. *J. Phys. Chem. C* **2009**, *113*, 20990–20997.

(77) Wu, C.-H.; Pan, T.-Y.; Hong, S.-H.; Wang, C.-L.; Kuo, H.-H.; Chu, Y.-Y.; Diau, E. W.-G.; Lin, C.-Y. *Chem. Commun.* **2012**, *48*, 4329–4331.

(78) Wang, C.-L.; Chang, Y.-C.; Lan, C.-M.; Lo, C.-F.; Diau, E. W.-G.; Lin, C.-Y. *Energy Environ. Sci.* **2011**, *4*, 1788–1795.

(79) Jiao, C.; Zu, N.; Huang, K.-W.; Wang, P.; Wu, J. *Org. Lett.* **2011**, *13*, 3652–3655.

(80) Tanaka, M.; Hayashi, S.; Eu, S.; Umeyama, T.; Matano, Y.; Imahori, H. *Chem. Commun.* **2007**, *0*, 2069–2071.

(81) Hayashi, S.; Tanaka, M.; Hayashi, H.; Eu, S.; Umeyama, T.; Matano, Y.; Araki, Y.; Imahori, H. *J. Phys. Chem. C* **2008**, *112*, 15576–15585.

(82) Mozer, A. J.; Griffith, M. J.; Tsekouras, G.; Wagner, P.; Wallace, G. G.; Mori, S.; Sunahara, K.; Miyashita, M.; Earles, J. C.; Gordon, K. C.; Du, L.; Katoh, R.; Furube, A.; Officer, D. L. *J. Am. Chem. Soc.* **2009**, *131*, 15621–15623.

(83) Liu, Y.; Lin, H.; Dy, J. T.; Tamaki, K.; Nakazaki, J.; Nakayama, D.; Uchida, S.; Kubo, T.; Segawa, H. *Chem. Commun.* **2011**, *47*, 4010–4012.

(84) Imahori, H.; Hayashi, S.; Hayashi, H.; Oguro, A.; Eu, S.; Umeyama, T.; Matano, Y. *J. Phys. Chem. C* **2009**, *113*, 18406–18413.

(85) Mathew, S.; Iijima, H.; Toude, Y.; Umeyama, T.; Matano, Y.; Ito, S.; Tkachenko, N. V.; Lemmetyinen, H.; Imahori, H. *J. Phys. Chem. C* **2011**, *115*, 14415–14424.

(86) Lee, C. Y.; Hupp, J. T. *Langmuir* **2010**, *26*, 3760–3765.

(87) Lee, C. Y.; She, C.; Jeong, N. C.; Hupp, J. T. *Chem. Commun.* **2010**, *46*, 6090–6092.

(88) Yella Aswani; Mai Chi-Lun; Zakeeruddin Shaik M.; Chang Shu-Nung; Hsieh Chi-Hung; Yeh Chen-Yu; Grätzel Michael. *Angew. Chem. Int. Ed.* **2014**, *53*, 2973–2977.

(89) Nazeeruddin MD. K.; Humphry-Baker R.; Grätzel M.; Wöhrle D.; Schnurpfeil G.; Schneider G.; Hirth A.; Trombach N. *J. Porphyr. Phthalocyanines* **1999**, *3*, 230–237.

(90) He, J.; Benkö, G.; Korodi, F.; Polívka, T.; Lomoth, R.; Åkermark, B.; Sun, L.; Hagfeldt, A.; Sundström, V. *J. Am. Chem. Soc.* **2002**, *124*, 4922–4932.

(91) Reddy, P. Y.; Giribabu, L.; Lyness, C.; Snaith, H. J.; Vijaykumar, C.; Chandrasekharam, M.; Lakshmikantam, M.; Yum, J.-H.; Kalyanasundaram, K.; Grätzel, M.; Nazeeruddin, M. K. *Angew. Chem. Int. Ed.* **2007**, *46*, 373–376.

(92) Cid, J.-J.; Yum, J.-H.; Jang, S.-R.; Nazeeruddin, M. K.; Martínez-Ferrero, E.; Palomares, E.; Ko, J.; Grätzel, M.; Torres, T. *Angew. Chem. Int. Ed.* **2007**, *46*, 8358–8362.

(93) Mori, S.; Nagata, M.; Nakahata, Y.; Yasuta, K.; Goto, R.; Kimura, M.; Taya, M. *J. Am. Chem. Soc.* **2010**, *132*, 4054–4055.

(94) Ragoussi, M.-E.; Yum, J.-H.; Chandiran, A. K.; Ince, M.; Torre, G. de la; Grätzel, M.; Nazeeruddin, M. K.; Torres, T. *ChemPhysChem* **2014**, *15*, 1033–1036.

(95) Ikeuchi, T.; Nomoto, H.; Masaki, N.; Griffith, M. J.; Mori, S.; Kimura, M. *Chem. Commun.* **2014**, *50*, 1941–1943.

(96) Law, K. Y. *Chem. Rev.* **1993**, *93*, 449–486.

(97) Luo, S.; Zhang, E.; Su, Y.; Cheng, T.; Shi, C. *Biomaterials* **2011**, *32*, 7127–7138.

(98) Pansare, V. J.; Hejazi, S.; Faenza, W. J.; Prud'homme, R. K. *Chem. Mater.* **2012**, *24*, 812–827.

(99) Escobedo, J. O.; Rusin, O.; Lim, S.; Strongin, R. M. *Curr. Opin. Chem. Biol.* **2010**, *14*, 64–70.

(100) Chithra, P.; Varghese, R.; Divya, K. P.; Ajayaghosh, A. *Chem. – Asian J.* **2008**, *3*, 1365–1373.

(101) Ajayaghosh, A. *Acc. Chem. Res.* **2005**, *38*, 449–459.

(102) Dirk, C. W.; Herndon, W. C.; Cervantes-Lee, F.; Selnau, H.; Martinez, S.; Kalamegham, P.; Tan, A.; Campos, G.; Velez, M. *J. Am. Chem. Soc.* **1995**, *117*, 2214–2225.

(103) Prabhakar, C.; Bhanuprakash, K.; Rao, V. J.; Balamuralikrishna, M.; Rao, D. N. *J. Phys. Chem. C* **2010**, *114*, 6077–6089.

(104) Ramaiah, D.; Eckert, I.; Arun, K. T.; Weidenfeller, L.; Epe, B. *Photochem. Photobiol.* **2002**, *76*, 672–677.

(105) Yuan, A.; Wu, J.; Tang, X.; Zhao, L.; Xu, F.; Hu, Y. *J. Pharm. Sci.* **2013**, *102*, 6–28.

(106) Chen, G.; Sasabe, H.; Igarashi, T.; Hong, Z.; Kido, J. *J. Mater. Chem. A* **2015**, *3*, 14517–14534.

(107) Sreejith, S.; Carol, P.; Chithra, P.; Ajayaghosh, A. *J. Mater. Chem.* **2008**, *18*, 264–274.

(108) Kamat, P. V.; Hotchandani, S.; Lind, M. de; Thomas, K. G.; Das, S.; George, M. V. *J. Chem. Soc. Faraday Trans.* **1993**, *89*, 2397–2402.

(109) Zhao, W.; Jun Hou, Y.; Song Wang, X.; Wen Zhang, B.; Cao, Y.; Yang, R.; Bo Wang, W.; Rui Xiao, X. *Sol. Energy Mater. Sol. Cells* **1999**, *58*, 173–183.

(110) Li, C.; Wang, W.; Wang, X.; Zhang, B.; Cao, Y. *Chem. Lett.* **2005**, *34*, 554–555.

(111) Yum, J.-H.; Walter, P.; Huber, S.; Rentsch, D.; Geiger, T.; Nüesch, F.; De Angelis, F.; Grätzel, M.; Nazeeruddin, M. K. *J. Am. Chem. Soc.* **2007**, *129*, 10320–10321.

(112) Geiger, T.; Kuster, S.; Yum, J.-H.; Moon, S.-J.; Nazeeruddin, M. K.; Grätzel, M.; Nüesch, F. *Adv. Funct. Mater.* **2009**, *19*, 2720–2727.

(113) Choi, H.; Kim, J.-J.; Song, K.; Ko, J.; Nazeeruddin, M. K.; Grätzel, M. *J. Mater. Chem.* **2010**, *20*, 3280–3286.

(114) Shi, Y.; Hill, R. B. M.; Yum, J.-H.; Dualeh, A.; Barlow, S.; Grätzel, M.; Marder, S. R.; Nazeeruddin, M. K. *Angew. Chem. Int. Ed.* **2011**, *50*, 6619–6621.

(115) Jradi, F. M.; Kang, X.; O'Neil, D.; Pajares, G.; Getmanenko, Y. A.; Szymanski, P.; Parker, T. C.; El-Sayed, M. A.; Marder, S. R. *Chem. Mater.* **2015**, *27*, 2480–2487.

(116) Kasha, M.; Rawls, H. R.; Ashraf, E.-B. M. *Pure Appl. Chem.* **2009**, *11*, 371–392.

(117) Bardeen, C. J. *Annu. Rev. Phys. Chem.* **2014**, *65*, 127–148.

(118) Sauer, M.; Hofkens, J.; Enderlein, J. Wiley-VCH, Weinheim, Germany,*Handbook of Fluorescence Spectroscopy and Imaging: From Single Molecules to Ensembles*, 2011.

(119) Zhang, L.; Cole, J. M. *J. Mater. Chem. A* **2017**.

(120) Ziółek, M.; Karolczak, J.; Zalas, M.; Hao, Y.; Tian, H.; Douhal, A. *J. Phys. Chem. C* **2014**, *118*, 194–205.

(121) Mulhern, K. R.; Detty, M. R.; Watson, D. F. *J. Phys. Chem. C* **2011**, *115*, 6010–6018.

(122) Mulhern, K. R.; Orchard, A.; Watson, D. F.; Detty, M. R. *Langmuir* **2012**, *28*, 7071–7082.

(123) Okada, S.; Segawa, H. *J. Am. Chem. Soc.* **2003**, *125*, 2792–2796.

(124) Würthner, F.; Kaiser, T. E.; Saha-Möller, C. R. *Angew. Chem. Int. Ed.* **2011**, *50*, 3376–3410.

Chapter 2

Unsymmetrical Squaraine Dyes with Benzodithiophene (BDT) as π-Spacer for Dye-sensitized Solar Cells

---

This chapter is adapted from:

Bisht, R.; M. K., M. F.; Singh, A. K.; Nithyanandhan, J. "Panchromatic Sensitizer for Dye-Sensitized Solar Cells: Unsymmetrical Squaraine Dyes Incorporating Benzodithiophene π-Spacer with Alkyl Chains to Extend Conjugation, Control the Dye Assembly on TiO_2, and Retard Charge Recombination" . J. Org. Chem. **2017**, *82*, 1920–1930

2.1. INTRODUCTION

Sensitizers or dyes are one of the critical constituents of dye-sensitized solar cells (DSSCs) which absorb the light and inject electrons into the conduction band of the semiconductor. The persisting investigation on the structure-property relationship of the dyes has led to the synthesis of some high-performance dyes for DSSCs.[1,2] Ruthenium (II) polypyridyl complex based dye **CYC-B11** have achieved the PCE of 11.5% with I^-/I_3^- redox couple[3] whereas Mathew et al.[4] reported the highest efficiency of 13% for Zn (II)-porphyrin complex (**SM-315**) in the presence of Co (II/III) redox couple. Among the metal-free organic dyes, tetrathienoacene based dye (TPA-TTART-A)[5] gave PCE of 10.1% whereas N-annulated indenoperylene (**C275**) based dye[6] produced the efficiency of 12.5% with Co(II/III) based electrolyte. Recently, an efficiency (PCE) of >14% was achieved by a metal-free organic dye bearing silyl anchoring group through co-sensitization.[7] The metal-free D-π-A dyes even though are efficient, their photoresponse in far-red and near-infrared (NIR) region is still limited. NIR absorbing dyes are always desirable in DSSCs as it helps to utilize the maximum photons from the solar spectrum.

Squaraine based dyes are among the few chromophores which can absorb in far red and NIR region with high extinction coefficient ($\varepsilon > 10^5$ $M^{-1}cm^{-1)}$. However, these dyes have not been used up to their full potential as there is only a handful of squaraine based DSSCs which gives photoresponse over 750 nm. The preliminary results of the squaraine based DSSCs were poor due to lack of directionality and extensive aggregation on metal oxide surface.[8–11] These dyes have a strong tendency to form aggregates on TiO_2 surface which are known to reduce the photocurrent through self-quenching process and deactivation of the excited state.[8,9,12]. However, the aggregation may help in broadening the absorption spectra which can increase the light harvesting efficiency.[13–15] These aggregates can be studied by UV-Vis spectroscopy as blue shifted peak (H-type aggregates) or red-shifted peak (J-type aggregates) with respect to monomer absorption peak. J-aggregates, in particular, are considered to be beneficial in DSSCs as it broadens the absorption towards the longer wavelength.

Yum et al.[16] brought the major breakthrough in the squaraine based DSSCs by reporting an indole-based unsymmetrical squaraine dye (**SQ1**) where the carboxylic group

was attached to the indolium group. The unsymmetrical nature of dye facilitated the unidirectional charge transfer from the excited dye to the conduction band of the TiO_2 and increased the photocurrent. To further improve the performance of squaraine based DSSCs, several efforts have been made to increase the absorption in the far-red region as well as to avoid aggregation by tuning the structural design. Extending the conjugation by covalently attaching a π-spacer followed by an acceptor such as cyanoacrylic acid, to indole-based squaraine, is one of the strategies to extend absorption in NIR region.[17–22] A thiophene bridge with cyanoacrylic acid as an anchoring group was incorporated in squaraine dye (**YR6**) by Shi et al. to enhance the absorption in the NIR region.[17] The dye displayed λ_{max} at 659 nm with a ε of 2.79×10^5 $M^{-1}cm^{-1}$ and IPCE response up to 780 nm. The YR6-sensitized cell gave a J_{SC} of 14.8 mA cm^{-2} and V_{OC} of 0.642 *V* which led to an overall PCE of 6.74%. Delcamp and coworkers[18] investigated various π-bridges such as gem-di-n-hexyl-substituted CPDT, N-(n-hexyl) dithienopyrrole (DTP), thiophene, benzene, ethynyl thiophene and ethynyl benzene groups with indole-based squaraine dyes. **JD-10** with CPDT π-bridge exhibited the best performance and produced PCE of 7.3%, with J_{SC} of 16.4 mA cm^{-2} and V_{OC} of 0.635 V. The out-of-plane hexyl chains on CPDT helped to reduce dye aggregation as well as enhance the absorption towards NIR region with IPCE extending up to 780 nm. Taking inspiration from this design, Jradi et al.[19] reported a dye, **DTS-CA**, comparable to **JD-10**, in which they have 4-bis(2-ethylhexyl)-4Hsilolo[3,2-b:4,5-b]dithiophene (DTS) linked to a squaraine as a π-bridge. The two branched out-of-plane 2-ethylhexyl chains (on DTS) successfully avoided aggregation which led to high photocurrent with IPCE onset at 850 nm with the response of 90% at 700 nm and 82% at 500 nm. The DSSC fabricated using the dye performed exceptionally well and gave J_{SC} of 19.1 mA cm^{-2} and V_{OC} of 0.682 V to yield efficiency of 8.9%. These results suggest that dye aggregation and light harvesting ability can significantly influence the performance of squaraine dyes in DSSC, hence modulating these properties by suitable design is very critical.

Benzodithiophene (BDT) based dyes in DSSC

Benzodithiophene (BDT) is a heterocyclic structure in which two thiophenes are fused to a benzene unit. The BDT unit can be functionalized readily like thiophene, and it is also fairly easy to synthesize in large scale. BDT has an excellent charge transport ability and has been used extensively as a donor in Donor-Acceptor (D-A) copolymers and small molecules for organic electronics and photovoltaics[23,24]. BDT has been used in DSSC very rarely, but there

are few reports available where it is utilized as a π-bridge in D-π-A type DSSC (**Figure 1**).[25–27] The first report of DSSC based on BDT is published by Hao et al.[28] They incorporated BDT as π-spacer with triphenyl amine as a donor and cyanoacrylic acid as an acceptor to design a novel dye (**XS32**).

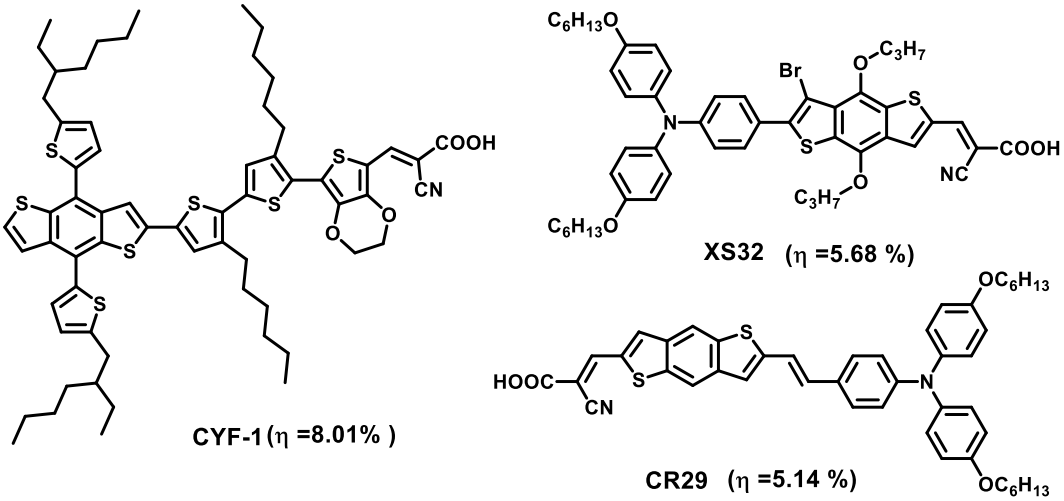

Figure 1. Examples of BDT based dyes used in DSSC.

It has a broad absorption range from 400 nm to 700 nm with 89% maximum IPCE at 497 which helped this dye to attain an efficiency of 5.68%. Longhi et al. synthesized **CR29** dye[26] with BDT as rigid π spacer with PCE of 5.14%. Chen et al. used BDT as a donor in D-π-A type DSSC with bithiophene and EDOT as π-bridge to synthesize a new dye **CYF-1** which produced an efficiency of 8.01%.[27]

In this study, we report the synthesis of squaraine based dyes (**RSQ1** and **RSQ2**) with BDT as π-spacer to extend the conjugation for improved light absorption in the NIR region. BDT was chosen to extend the conjugation due to its fused structure which enhances conjugation. We incorporated methyl and ethylhexyl group on the BDT to understand the effect of alkyl chains on aggregation and device performance in these dyes. Squaraine unit was coupled to BDT with the help of palladium-catalyzed direct hetero-arylation instead of traditional C-C bond cross couplings like Suzuki, Negishi and Stille coupling (**Figure 2**). Although conventional C-C bond couplings are efficient and consistent, they involve the synthesis of organometallic intermediates like boronic acids derivatives and organotin compounds from the starting precursor, which takes additional synthetic steps. In contrast,

direct arylation can form a C-C bond directly to the activated carbon on aromatic or heteroaromatic compounds, and no additional organometallic components are required. Recently, direct arylation has emerged as a useful alternative to conventional cross-coupling and has been used to synthesize organic molecules for organic electronic and photovoltaic,[29–31] however, its application in squaraine based molecules are rarely reported.

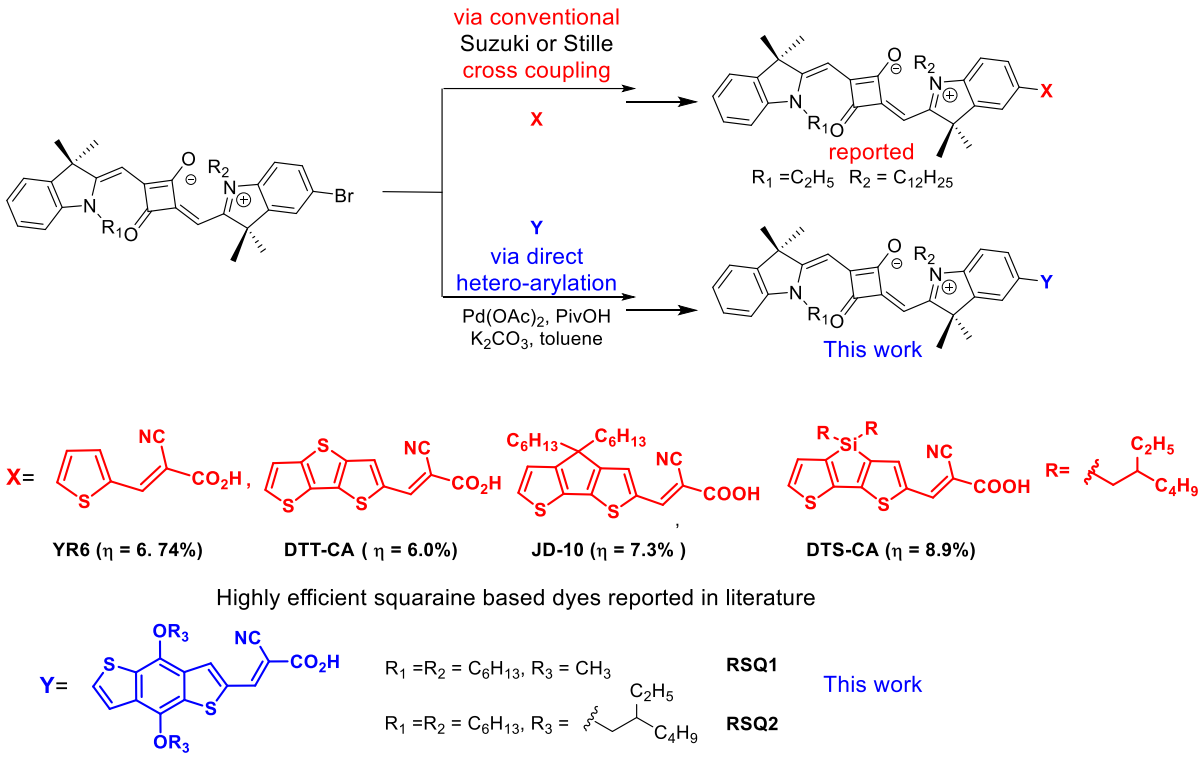

Figure 2. Reported squaraine dyes synthesized via the conventional method and RSQ dyes synthesized via direct (hetero)arylation method for DSSCs.

2.2. RESULTS AND DISCUSSION

2.2.1. Synthesis

Synthetic route to **RSQ1** and **RSQ2** is depicted in **Scheme 1.** The precursors **1** and **5** were heated with hexyl iodide to give the corresponding N-hexylated indolenine derivatives **2** and **6,** respectively. The indolium derivative **2** was reacted with 3,4-dibutoxy-3-cyclobutene-1,2-dione in the presence of triethylamine to give semi-squaraine, **3** which was then hydrolyzed with 2N HCl in acetone to give semi-squaric acid **4**, quantitatively as a yellow solid.

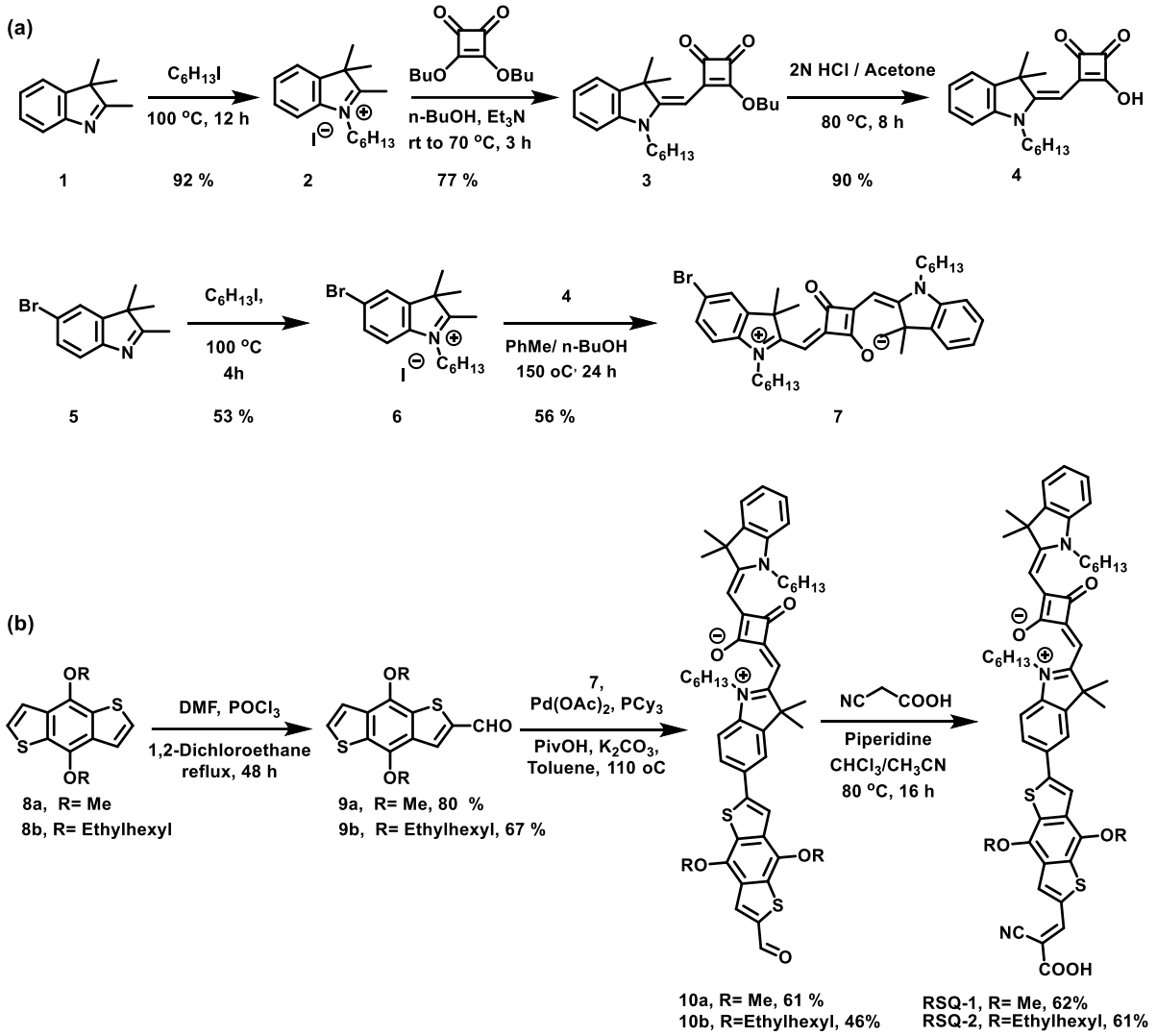

Scheme 1. a) Synthesis of bromo-functionalized unsymmetrical squaraine, **7** and b) Synthesis of **RSQ1** and **RSQ2** dyes involving palladium catalyzed direct (hetero)arylation.

The bromo-indolium derivative, **6** was condensed with the semi-squaric acid **4** in a mixture of *n*-butanol and toluene by azeotropic distillation of water employing Dean-Stark apparatus to afford bromo-functionalized unsymmetrical squaraine dye **7** in moderate yield as a blue solid. BDT derivatives **8a** and **8b** were reacted with $POCl_3$ and DMF in 1,2-dichloroethane under Vilsmeier Haack formylation reaction conditions for 48 h to afford corresponding BDT based aldehyde derivatives **9a** and **9b**. Before this, the formylation of BDT has been carried out by lithiation of BDT derivative followed by quenching with DMF. However, this method needs the strict moisture free environment and affords low reaction conversion.[25,32] We have optimized the Vilsmeier-Haack formylation conditions for the two **9a**, and **9b** derivatives,

without strict anhydrous conditions. Bromo functionalized unsymmetrical squaraine derivative, **7** was coupled with **9a** and **9b** via $Pd(OAc)_2$ catalyzed direct arylation with Fagnou's protocol,[33] with PCy_3 as a co-ligand and pivalic acid as an additive in PhMe to provide the corresponding aldehyde precursors **10a**, and **10b** in moderate yield as green solid. Knoevenagel condensation of the aldehyde precursors **10a** and **10b** with cyanoacetic acid afforded the final compounds, **RSQ1,** and **RSQ2** respectively in moderate yields as green solid. The SQ-BDT dyes **RSQ1** and **RSQ2** are entirely soluble in chlorinated solvents such as $CHCl_3$, CH_2Cl_2; **RSQ1** is soluble in acetone and ethanol, in which **RSQ2** is not soluble. All the synthesized compounds were duly characterized by NMR and mass spectrometry.

2.2.2. Optical and Electrochemical Properties

The UV-Vis absorption and emission spectra of **RSQ1** and **RSQ2** in $CHCl_3$ solution are shown in **Figure 3a-b**. Both the dyes show identical absorption spectra in solution indicating that the side chain does not affect the energy levels. The dyes exhibit intense absorption band in the range of 500 nm to700 nm and have λ_{max} at 664 nm corresponding to intramolecular charge transfer (ICT) transition, with a high molar absorption coefficient (ε) of $2.18\times10^5$and 2.39×10^5 $M^{-1}cm^{-1}$ for **RSQ1** and **RSQ2** respectively (**Table 1**). A low-intensity band stretching from 400 to 500 nm was observed for **RSQ1** and **RSQ2** with an extinction coefficient of 1.71×10^4 and 1.53×10^4 $M^{-1}cm^{-1}$ (at 455 nm) respectively. The presence of low-intensity band had been observed previously when the squaraine units were electronically extended with π-spacer[18,19]. Such spectral features help to absorb visible photons besides harvesting NIR photons.

To understand the self-assembly of dyes on TiO_2 film, the titania coated glass was immersed in a 0.1 mM dye solution for 30 minutes. The absorption spectra of dye anchored on TiO_2 film displayed spectral broadening (**Figure 3c**) which generally occurs due to two major reasons— (i) interaction of carboxylic acid anchoring group (-COOH) with Ti center of TiO_2 and (ii) formation of aggregates on the TiO_2 surface due to the π-π stacking of dye molecules.[34,35] In addition to the monomeric peak at 663 nm, peaks at 619 nm for **RSQ1** and 624 nm for **RSQ2** were observed. The appearance of peaks at shorter wavelength indicates the formation of H-type aggregates on TiO_2 film which has been reported for squaraine based dyes.[36,37] In the case of **RSQ2**, the high energy aggregate peak was narrower and less prominent, suggesting the suppression of aggregation by branched alkyl chains.

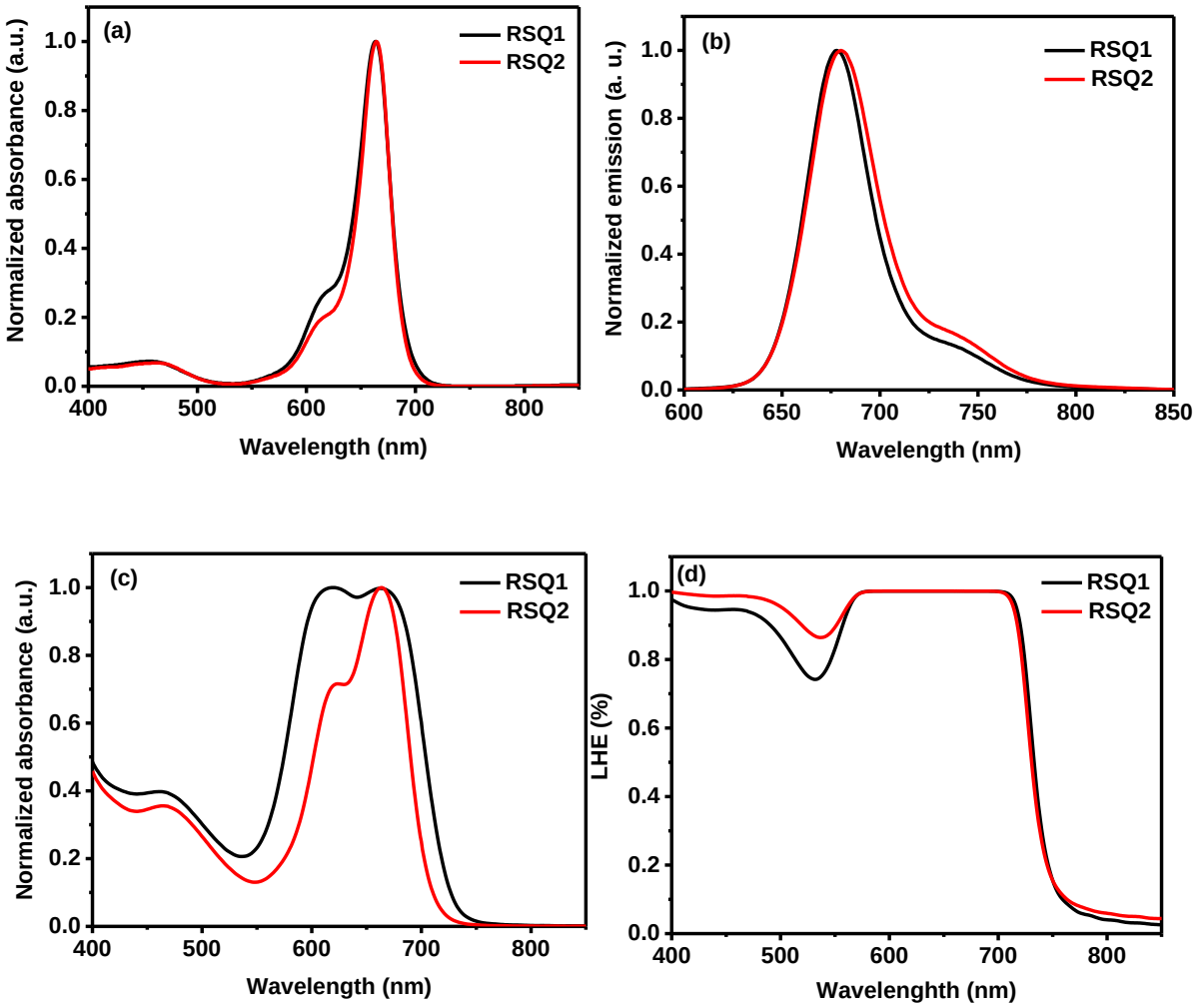

Figure 3. (a) Absorption and (b) emission spectra of **RSQ** dyes in $CHCl_3$ solution, (c) Normalized absorbance of RSQ dyes adsorbed at the surface of 6 μm thick TiO_2 film. (d) Light harvesting efficiency of **RSQ** dyes on TiO_2 film

The light harvesting efficiency (LHE = $1\text{-}10^{-A}$)[38] was calculated by measuring absorption in transmittance mode of dye adsorbed film which was obtained by immersing the TiO_2 film in the dye solution for an extended period of 6 h (**Figure 3d**). LHE of dyes anchored on TiO_2 indicates the fraction of the light absorbed by dyes across the solar spectrum. LHE profiles show that all the dyes are able to harvest the photons from visible as well as NIR region which makes these sensitizers suitable candidates for panchromatic absorption. Both **RSQ** dyes showed more than 90% LHE from 400 to 750 nm except for a small decrease around 540 nm. **RSQ2** shows better light harvesting efficiency in the region

of 400 to 550 nm in comparison to **RSQ1** but overlaps in the region 600-800 nm for both the dyes.

To evaluate the feasibility of charge injection and dye regeneration process for **RSQ1-3** dyes, differential pulse voltammetry (DPV) was carried out in a CH_2Cl_2 solution with tetrabutylammonium perchlorate ($TBAClO_4$) as electrolyte and ferrocene as an external reference (**Figure 4**). The differential pulse voltammograms of **RSQ** dyes exhibit two-electron oxidation peaks, which is characteristic of squaraine dyes.

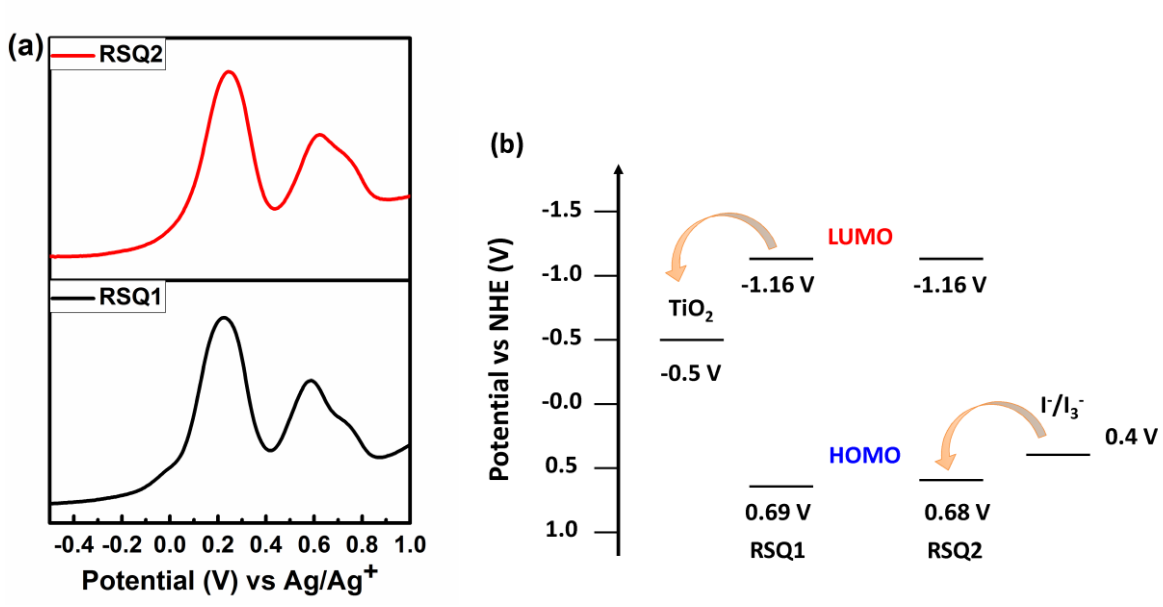

Figure 4. a) Differential pulse voltammograms (DPV) of RSQ dyes measured in CH_2Cl_2. (b) Energy level diagram for **RSQ1** and **RSQ2** with DSSC device components

For an effective electron transfer from excited dye to TiO_2, the excited state potential (LUMO) of the dye should be more negative than conduction band (CB) edge (-0.5 V vs. NHE) of TiO_2 (by at least 0.2 eV),[39] whereas ground state potential (HOMO) of the dye should be more positive than the redox potential (0.4 V vs. NHE) of iodide/triiodide (by at least 0.15 eV)[40] to provide sufficient driving force for efficient regeneration of oxidized dye. The HOMO energy levels (E_{HOMO}) were calculated from the first oxidation peak and found to be at 0.69 V and 0.68 V vs. NHE for **RSQ1** and **RSQ2** respectively, which are lower than the electrochemical potential of I^-/I_3^- to ensure the dye regeneration (**Table 1** and **Figure 4b**). The LUMO energy levels (E_{LUMO}) were calculated by subtracting $E_{0\text{-}0}$ from E_{HOMO} and are

found at -1.16 V for both **RSQ1** and **RSQ2**. These values lie well above the conduction band edge of TiO_2 which predicts efficient charge injection into TiO_2. The optical bandgaps or excited state energies ($E_{0\text{-}0}$) were calculated from the intersecting point of absorption and emission curve and found to be 1.84 eV and 1.85 eV for **RSQ1** and **RSQ2** respectively.

Table 1. Optical and Electrochemical Data of **RSQ** dyes

Dyes	λ_{abs} /CH_2Cl_2 (nm)[a]	ε x10^4 ($M^{-1}cm^{-1}$)[a]	λ_{em} (nm)[a]	$\lambda_{abs/}$ /TiO_2 (nm)[b]	$E_{g/DFT}$ (eV)	$E_{ox/onset}$ (V vs Ag/Ag^+)[c]	E_{HOMO} (V vs NHE)[c]	$E_{0\text{-}0}$ (eV)[d]	E_{LUMO} (V *vs* NHE)[e]
RSQ1	455, 664	1.71, 21.8	678	619, 663	1.85	0.2154	0.69	1.85	-1.16
RSQ2	455, 664	1.53, 23.9	680	624, 664	1.85	0.2050	0.68	1.84	-1.16

[a]Absorption spectra, emission spectra (λ_{exc} = 580 nm), molar extinction coefficients (ε) were measured in CH_2Cl_2. [b]6 μm transparent film was dipped in 0.1 mM of dye in CH_2Cl_2 for 30 min. [c]The oxidation potentials were measured in CH_2Cl_2 solutions with tetrabutylammonium perchlorate ($TBAClO_4$) as supporting electrolyte, ferrocene/ferrocenium (Fc/Fc^+) as an internal reference and converted to NHE by addition of 0.63 V. [d]Optical energy gaps ($E_{0\text{-}0}$) were calculated from the intersection of absorption and emission spectra, $E_{0\text{-}0}$ (eV) = 1240/λ. [e]E_{LUMO} was calculated from E_{LUMO} (V *vs.* NHE) =E_{HOMO}- $E_{0–0.}$

2.2.3. Computational Studies

Optimized molecular geometries and electronic distribution of frontier molecular orbitals in **RSQ** dyes were computed by density functional theory (DFT) in Gaussian 09 using B3LYP functional with 6-31G** basis set[41]. The isodensity plots show the electron density distribution in the frontier molecular orbitals of the dyes under investigation (**Figure 5a)**. The electron density in HOMO of both the dye is located mostly in central squaraine unit whereas the BDT unit is devoid of electron density. In LUMO energy level, there is a clear shift of the electron density from the squaraine unit towards anchoring group for both the dyes. Such electron distribution in HOMO and LUMO suggests the effective electron transfer from donor to anchoring unit which is significant for the facile charge transfer to ensure the

efficient injection of electrons from the excited dye molecule into the conduction band of the TiO_2.

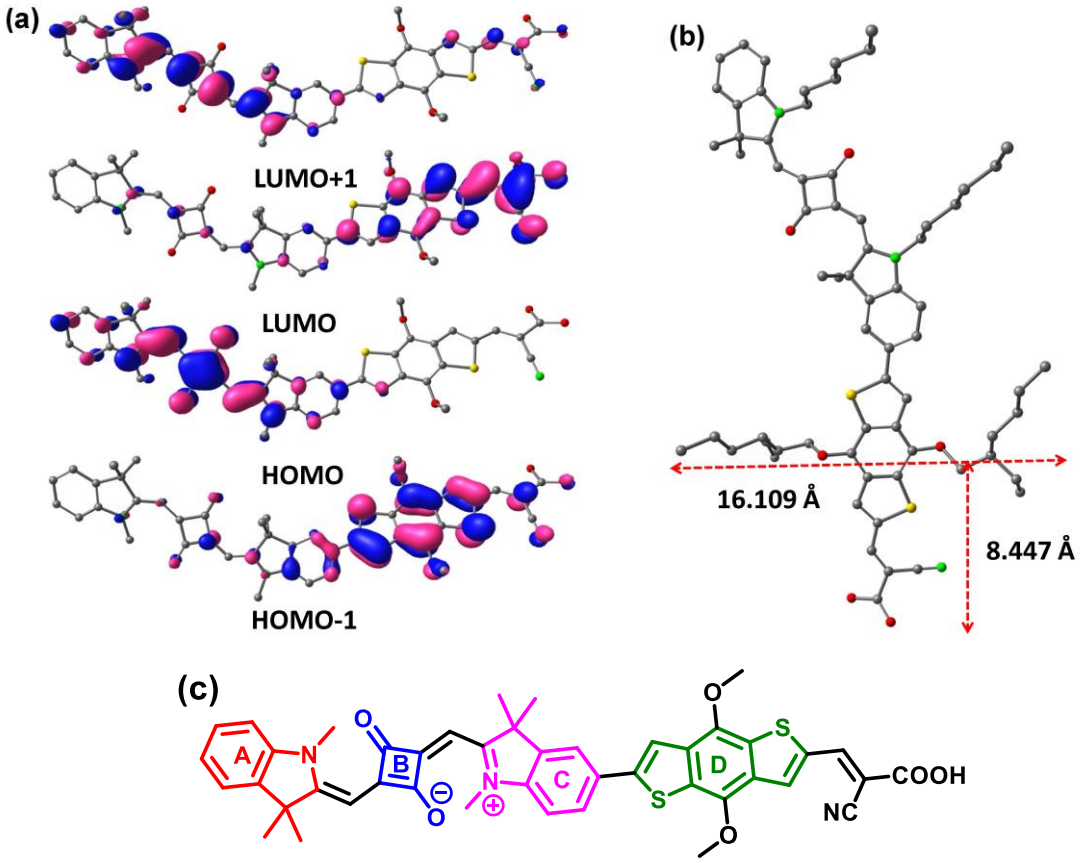

Figure 5. (a) Isodensity surface plots of HOMO-1, HOMO, LUMO and LUMO+1 of **RSQ** dye (Hydrogen atoms and alkyl chains are removed for clarity) (b) DFT optimized structure of **RSQ2**. (c) Dihedral planes are shown as A, B, C and D on RSQ dye (alkyl chains are removed for clarification).

The optimized geometry of **RSQ2** is shown in **Figure 5b**. The ethylhexyl chain around the RSQ2 extends up to 16.1 Å along the plane of the molecule and 6.9 Å in the out-of-plane direction and is at the distance of about 8.4 Å away from TiO_2. These structural features improve the charge injection by avoiding the dye aggregation and reduce the charge recombination by surface passivation due to hydrophobic alkyl chains near to TiO_2. In general, the degree of conjugation in the molecule is dependent on the planarity of the molecule to some extent, which can be predicted from the dihedral angle between squaraine and BDT unit in this particular case. Dihedral angles for the dyes were calculated from the optimized ground state geometry for the planes between indolenine units and squaric acid

unit (A-B and B-C) and between BDT and SQ units (C-D) (**Figure 5c**). ∠**A-B** and ∠**B-C** show that squaraine unit is almost planar in itself whereas ∠**C-D** of 20.1º (**RSQ1**) and 25.5º (**RSQ2**) predicts that BDT is slightly out of the plane which shows slight restriction in the conjugation (**Table 2**).

Table 2. Dihedral angles between dihedral planes of RSQs were calculated from the optimized ground state geometry.

RSQ Dyes	**Dihedral angle (degree)**		
	∠A-B	**∠B-C**	**∠C-D**
RSQ1	4.4	-2.9	-25.5
RSQ2	1.8	-1.3	-20.1

2.2.4. Photovoltaic Performance

Photovoltaic characterization of the RSQ based dye-sensitized solar cells was carried out under an irradiance of 100 mW cm^{-2} simulated AM 1.5G sunlight. The current density−voltage (*J*−*V*) characteristics of DSSCs are shown in **Figure 6a**, and device performance data with and without co-adsorbent are summarized in **Table 3**.

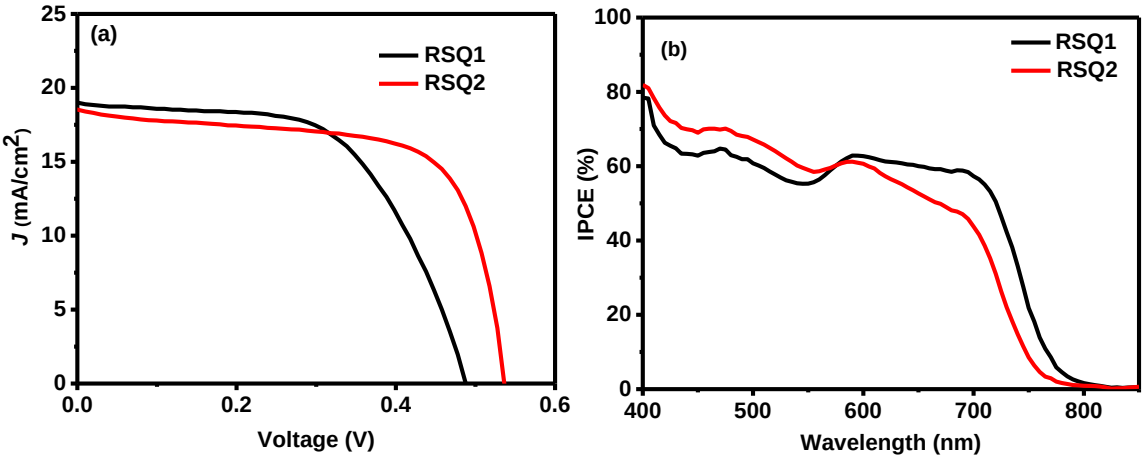

Figure 6. (a) *J*–*V* curve and (b) IPCE spectrum (solid lines) and LHE spectrum (dotted lines) of RSQ sensitizers without co-adsorbent. ([Dye] = 0.1 mM, in CH_2Cl_2, dipping time 5 h, TiO_2 active area = 0.22 cm^2).

RSQ2 sensitized cells performed better than **RSQ1** based cells in the absence of co-adsorbent, and achieved an overall power conversion efficiency (η) of 6.72% with a J_{SC} of 18.53 mA cm^{-2}, fill factor (*ff*) of 67.4% and V_{OC} of 0.538 V. The efficiency (η) of 5.43% was obtained by **RSQ1** sensitized solar cell with J_{SC} of 19.03 mA cm^{-2}, *ff* of 58.3% and V_{OC} of 0.490 V. The **RSQ2** gave better performance due to the enhanced V_{OC} and *ff* in comparison to **RSQ1** which could be attributed to the controlled assembly of the dyes on TiO_2 surface.

Table 3. Photovoltaic data of **RSQ** dyes with CDCA and without CDCA under 1 sun illumination.

SQ Dyes	V_{OC} (V)	J_{SC} (mA cm^{-2})	*ff* (%)	η (%)[a]
RSQ1	0.490	19.03	58.3	5.43
RSQ1/CDCA (1:1)	0.488	18.25	59.4	5.29
RSQ1/CDCA (1:5)	0.494	15.08	58.6	4.36
RSQ1/CDCA (1:10)	0.495	9.47	58.5	2.74
RSQ2	0.538	18.53	67.4	6.72
RSQ2/CDCA (1:1)	0.539	18.77	67.7	6.84
RSQ2/CDCA (1:5)	0.545	15.53	68.8	5.82
RSQ2/CDCA (1:10)	0.539	14.14	68.5	5.22

[a]Photovoltaic performance of **RSQ** cells, thickness of electrode: 8+4 μm (transparent + scattering) layer of TiO_2, Electrolyte: 0.5 M DMII, 0.1 M LiI, 0.1 M I_2 and 10 mM TBP in CH_3CN. [Dye] = 0.1 mM in CH_2Cl_2, dipping time was 6 h, Active area of 0.22 cm^2 and measurements were carried out under 1 sun intensity (100 mW cm^{-2}).

To understand the effect of aggregation on DSSC performance, the dye was co-adsorbed in the presence of (3α,7α-dihydroxy-5β-cholanic acid, (CDCA). CDCA is an optically transparent molecule which is generally co-adsorbed on TiO_2 along with dyes to boost the performance of DSSC by minimizing the aggregation. When 1 equiv of CDCA was

added, the efficiency of the **RSQ2** dye improved to 6.84% with J_{SC} of 18.77 mA cm^{-2} and V_{OC} of 0.539 V, but for the **RSQ1** it reduced to 5.29% with J_{SC} 18.25 mA cm^{-2} and V_{OC} of 0.448 V (**Figure 7a** and **7c**). Here, the difference in the PCE after addition of 1 equiv of CDCA appeared because of the slight perturbation in the dye assembly. Further addition of CDCA reduced the device efficiencies as shown in **Table 3**. PCE of **RSQ1** depleted to 4.36% when 5 equiv of CDCA was added due to a decrease in short circuit current density (J_{SC} = 15.08 mA cm^{-2}), and for **RSQ2,** PCE was decreased to 5.82% with J_{SC} of 15.53 mA cm^{-2}. PCE further decreased to 2.74% and 5.22% when 10 equiv of CDCA are added for **RSQ1** and **RSQ2,** respectively. This drop in performance could be the result of reduced adsorption of the dye on the TiO_2 surface due to competitive adsorption of CDCA over dyes. To confirm the hypothesis, dye loading on TiO_2 films were calculated by dye desorption study. The amount of dye loaded on TiO_2 for **RSQ1** and **RSQ2** sensitized DSSC was found to be 2.07 × 10^{-7} mol cm^{-2} and 1.21 × 10^{-7} mol cm^{-2} respectively.

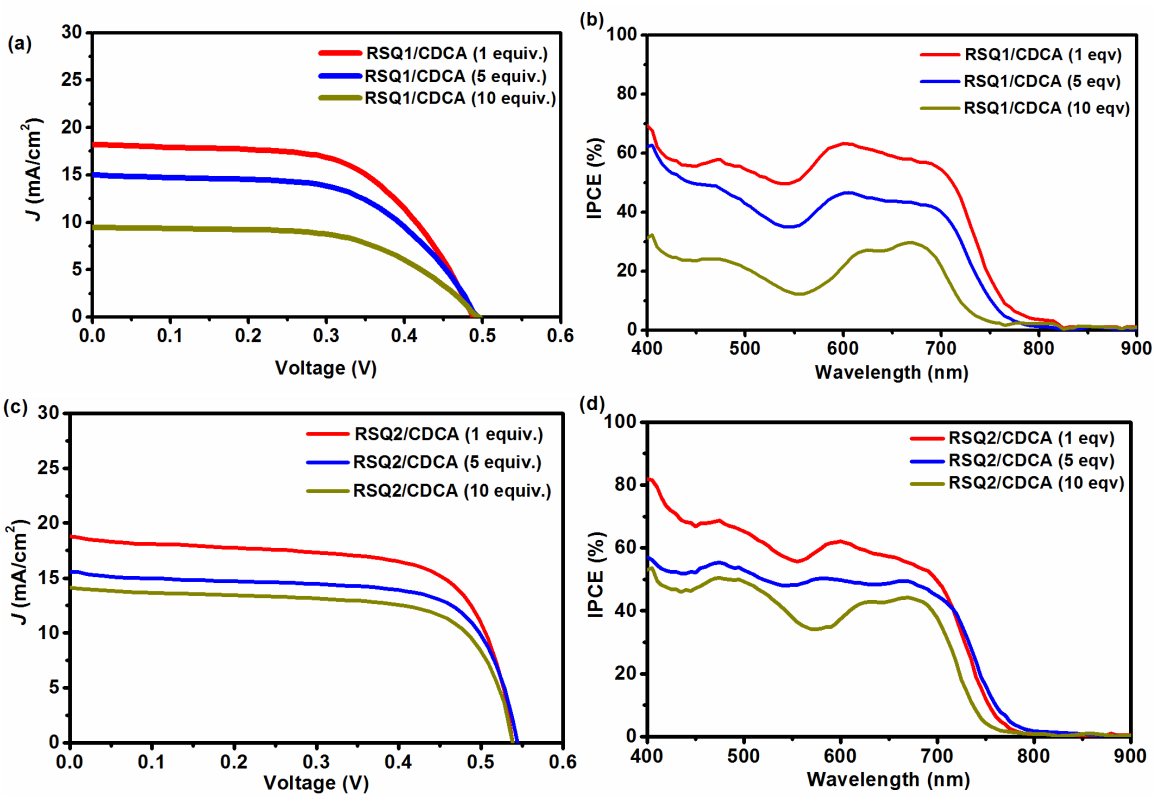

Figure 7. *J–V* curve and IPCE spectrum of **RSQ** sensitizers (solid lines) in the presence of CDCA.

A severe decrease in dye loading is observed for **RSQ1** (1.09×10^{-7} mol cm^{-2}) when 10 equivalent of CDCA was added whereas in case of **RSQ2** the decrease in dye adsorption (0.67×10^{-7} mol cm^{-2}) was comparatively moderate. This differential adsorption of dye on the addition of CDCA could be attributed to the presence of bulky alkyl chains on **RSQ2** which can sterically hinder the adsorption of CDCA on TiO_2.

The variation in J_{SC} can be explained from the IPCE spectrum of **RSQ** dyes as it is the direct consequence of IPCE and can be expressed as eq 1.

$$J_{SC} = q \int \text{IPCE}(\lambda)\, \phi(\lambda)\, d\lambda \qquad (1)$$

If we compare the IPCE spectra of the two dyes without CDCA (**Figure 6b**), the **RSQ1** based DSSC has better IPCE response in the region of 600 – 800 nm which corresponds to the absorption by monomers and aggregates whereas the **RSQ2** compensates for this with greater IPCE between 400-560 nm, which corresponds to the absorption from the π-spacer. Consequently, **RSQ1** and **RSQ2** have comparable J_{SC} of 19.03 mA cm^{-2} and 18.53 mA cm^{-2} respectively (**Figure 6b**). A steady decrease in IPCE is observed with increasing concentration of CDCA, due to competitive binding of CDCA on TiO_2 (**Figure 7b**, **7d**). When 5 equivalents of CDCA were added, the IPCE dropped to 46% and 49% at 600 nm for **RSQ1** and **RSQ2** respectively. Addition of 10 equivalents of CDCA further decreased IPCE due to the reduction in dye content which is particularly severe in case of **RSQ1**, as a result, IPCE is only 20% at 600 nm while it is 40% for **RSQ2**. Even though the de-aggregating effect of CDCA could be observed from the IPCE trace, any expected improvement in IPCE is negated by the huge decrease in the dye loading especially in **RSQ1** sensitized devices.

2.2.5. Electrochemical Impedance Spectroscopy (EIS)

Since both the dyes exhibited similar J_{SC} in the absence of CDCA, the greater PCE in **RSQ2** sensitized device could be ascribed to the distinct improvement in V_{OC}. In DSSC, changes in the Fermi level of electrons in the TiO_2 and redox potential of electrolyte critically affect the V_{OC} and J_{SC}. As the device architecture and electrolytes; including fabrication conditions, are similar for all the cells, the factors that influence the V_{OC} for a set of dyes can be estimated by evaluating the electron transport resistance (R_{ct}) in the device across TiO_2/Dye/electrolyte interface and lifetime of electrons injected in the conduction band of

TiO_2 (E_{CB}). To understand the correlation between the charge transfer processes at the interfaces (TiO_2/dye/electrolyte) and the V_{OC}, EIS analysis was carried out in the dark without perturbing the self-assembled monolayer of dyes. The Nyquist plots of the devices based on the **RSQ1-2** dyes under an applied bias of −0.45 V are shown in **Figure 8a**.

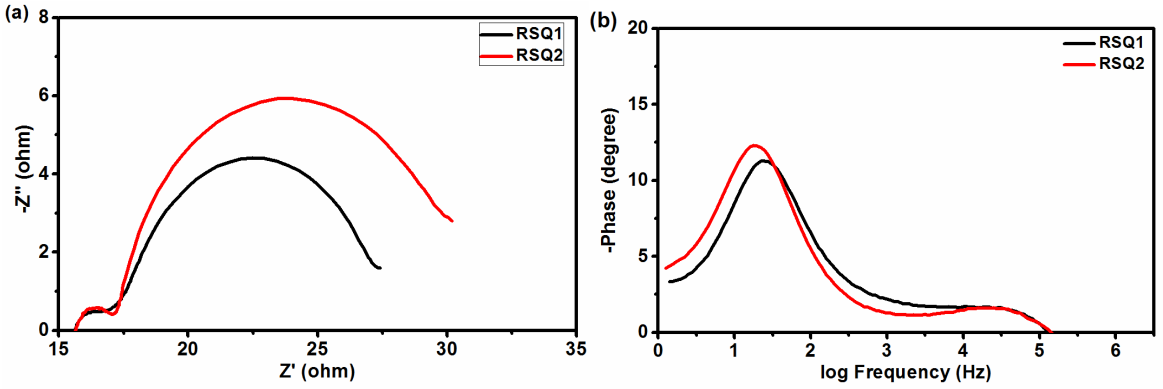

Figure 8. EIS data of **RSQ1-2** dye cells. (a) Nyquist plot (applied bias of −0.45 V in the dark) and (b) Bode phase plot (electron lifetime is described as $\tau = 1/2\pi f$)

The smaller semicircle in the high-frequency region is ascribed to the charge transfer processes at the interface of Pt electrode and electrolyte, whereas the larger semicircle in intermediate frequency region gives the information regarding charge recombination dynamics between dye-sensitized TiO_2 and electrolyte.[42,43] Larger the radius of the semicircle, larger is the resistance and hence smaller dark current. The radius of the larger semicircle for **RSQ2** (12.73 Ω) is greater than **RSQ1** (9.53 Ω), indicating greater electron recombination resistance at TiO_2/electrolyte interface which correlates with the greater V_{OC} **(Table 4)**. This indicates that the bulky ethylhexyl group helped to passivate the TiO_2 surface which reduced electron recombination in **RSQ2** sensitized DSSC. The lifetime of electrons on TiO_2 is calculated from the peak frequency of the low-frequency peak in Bode phase plots (**Figure 8b**). It is reciprocal of the peak frequency and hence lower the peak frequency longer is the lifetime. **RSQ2** (τ = 8.97 ms) displayed longer electron lifetime compared to **RSQ1** (τ = 6.35 ms) which further supports the higher V_{OC} for **RSQ2**.

Table 4. EIS data for **RSQ** dyes.

Dyes	R_{ct} (Ω)	C_{μ} (mF)	f (Hz)	τ (ms)
RSQ1	9.53	0.775	25.06	6.35
RSQ2	12.73	0.833	17.74	8.97

2.2.6. Open Circuit Voltage Decay Study (OCVD)

The electron recombination kinetics of **RSQ** dyes based DSSCs were studied under simulated sunlight (AM 1.5G, 100 mW cm^{-2}) by photovoltage decay method. Open-circuit voltage decay profile (OCVD) reflects the electron recombination kinetics after generating triiodide species at the proximity of TiO2/dye/electrolyte interface via regeneration of oxidized dyes on TiO_2. The devices were illuminated under simulated light for 10 seconds, then the light was turned off using a shutter, and open-circuit voltage decay profiles were measured. **RSQ2** displayed the slower voltage decay than **RSQ1** (**Figure 8**). This further supports the strong ability of ethylhexylated BDT π-linker to attenuate the charge recombination process and increase the V_{OC} of **RSQ2** which in turn resulted in the high PCE of 6.72%.

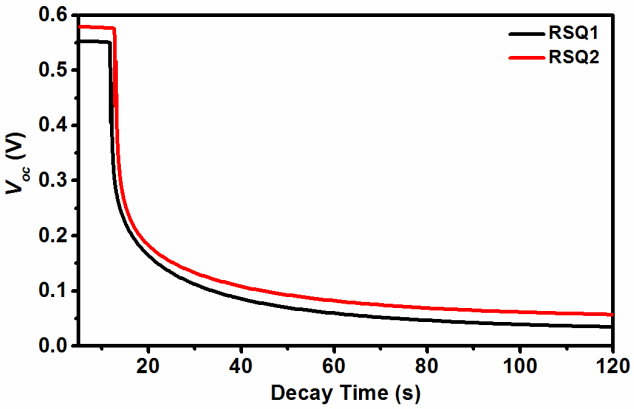

Figure 9. OCVD profiles of DSSCs based on **RSQ1-2** sensitizers and the experiments carried out under 1 sun intensity (100 mW cm^{-2}).

2.3. SUMMARY

In summary, squaraine-benzodithiophene (SQ-BDT) based dyes, **RSQ1, and RSQ2**, were synthesized in order to exploit the far red and NIR region of the solar spectrum for efficient DSSC. The direct heteroarylation method for C-C bond coupling was invoked to connect squaraine with BDT which helps to reduce the number of synthetic steps and chemical wastage. Both dyes exhibit good absorption in the NIR region and have favorable energy levels for efficient charge transfer. The UV-Vis absorption spectrum of dyes on thin TiO_2 films shows the formation of H-aggregates and **RSQ2** has smaller aggregate compared to **RSQ1** due to branched alkyl chains attached on BDT. DFT calculation showed delocalization of HOMO in central squaraine unit, and the LUMO is centered on BDT unit which predicts efficient electron transfer towards TiO_2 and also supports the photophysical and electrochemical observation. **RSQ2** sensitized DSSC gave the best photovoltaic performance with the PCE of 6.72%, without the addition of any co-adsorbents. The IPCE spectra exhibited a good response in the NIR region with onset at about 770 nm. The addition of CDCA led to significant reduction in dye loading on TiO_2 and proved to be harmful to the device performance which was more severe for the DSSC based on RSQ1. EIS analysis associates higher V_{OC} of **RSQ2** with higher electron transfer resistance at TiO_2/electrolyte interface. This is mainly due to the reduced aggregation and surface passivation by branched alkyl chain of **RSQ2** based DSSC. RSQ2 sensitized devices exhibited greater electron lifetime on TiO_2 which supports its higher V_{OC} in comparison to **RSQ1**.

2.4. EXPERIMENTAL

2.4.1. Materials and methods

All reagents and solvents were purchased from commercial sources unless otherwise noted. Solvents were dried and distilled by standard procedures immediately before use. The precursors, 5-Bromo-2,3,3-trimethyl-3H-indole (**5**)[44], 4,8-dimethoxybenzo[1,2-b:4,5-b']dithiophene[45] (**8a**) and 4,8-bis((2-ethylhexyl)oxy)benzo[1,2-b:4,5-b']dithiophene[46] (**8b**) were synthesized according to the procedures known in the literature. ^{1}H NMR and ^{13}C NMR were recorded in, $CDCl_3$, MeOH-d_4 or DMSO-d_6 on AV 200 MHz, AV 400 MHz and AV-500 MHz Bruker NMR spectrometers. High-resolution mass spectrometric measurements were carried out using the ESI method and an ion-trap mass analyzer. Absorption spectra were recorded at room temperature in quartz cuvette using SPECORD®210/ PLUS, Analytik Jena UV−Visible spectrophotometer. The cyclic voltammetry analysis (CV) was carried out

in anhydrous dichloromethane solvent by using 0.1 M tetrabutylammonium perchlorate as a supporting electrolyte and Fc/Fc^+ as an internal reference. The experiments were performed at room temperature in a nitrogen atmosphere with a three-electrode cell consisting of a platinum foil as a counter electrode, an Ag/Ag^+ reference electrode, and a platinum wire as a working electrode.

2.4.2. Solar cells Fabrication and Characterization

FTO (F-doped SnO_2 glass; 6 - 8 Ω /sq; Pilkington TEC 7) was cleaned with a diluted mucasol solution in water, deionized water, and ethanol, successively. To grow a TiO_2 blocking layer, the substrate was immersed in freshly prepared 50 mM aqueous $TiCl_4$ solution at 70 ºC for 30 min and washed with deionized water before drying at 125 ºC for 10 min. A paste of TiO_2 nanocrystal (< 20 nm, Ti-Nanoxide T/SP, Solaronix) was deposited on the $TiCl_4$ treated FTO substrate by the doctor-blade technique, to form a transparent layer of TiO_2. It was kept in air for 5 min and then annealed at 125 °C in air for 15 min which resulted in 6-8 μm thick mesoporous TiO_2 films. The annealed films were coated with scattering layer TiO_2 paste (WER2-O, Dyesol) and again annealed at 125 °C in air for 15 min. The films were then sintered at 325 °C for 5 min, 375 °C for 5 min, 450 °C for 15 min and 500 °C for 15 min with a heating rate of 5 °C per min in air. After reaching the furnace temperature at 50 °C, sintered films were immersed in freshly prepared 50 mM aqueous $TiCl_4$ solution at 70 ºC for 30 min. After sintering the $TiCl_4$-treated TiO_2 films again at 500 °C for 30 min, they were immediately immersed in 0.1 mM **RSQ** dye solution in dichloromethane for 5 h, washed and dried at 80 ºC. In case of CDCA added experiments, different ratio of CDCA added to 0.1 mM dye solution, and photoanode was dipped for 6 h. Sandwich type cell configuration was completed using platinum as a cathode, 0.5 M DMII, 0.1 M LiI, 0.1 M I_2 and 10 mM TBP in CH_3CN was used as an electrolyte and 25 μm spacer. *J-V* characteristics of the cells were measured using Keithley digital source meter (2420, Keithley, USA) controlled by a computer and standard AM 1.5 solar simulator (PET, CT200AAA, USA). To measure the photocurrent and voltage, an external bias of AM 1.5G light was applied using a xenon lamp (450 W, USHIO INC, Philippines) and *J-V* plot was recorded. The IPCE measurements were carried out with a Newport QE measurement kit by focussing a monochromatic beam of light from 300W Xe lamp onto the devices. Electrochemical impedance spectra (EIS) were measured on the Biologic potentiostat, equipped with a FRA2 module, with an applied potential of -0.45 V in the dark. The frequency range of 1Hz to 1MHz was explored with an

ac perturbation of 10 mV. The impedance spectra were analyzed using an equivalent circuit model of R1+R2/C2+R3/C3. The loading amount of the dyes was assessed by UV-Vis spectrophotometry as follows: Photoanodes were sensitized in the same dye solutions which were used for photovoltaic characterization. The photoanodes were taken out, and dyes were desorbed by dipping in a 2M solution of HCl in EtOH. The resultant dye solution was used to evaluate the dye concentration by UV-Vis study which allows the determination of the amount of dye adsorbed in terms of a number of moles per unit area of the TiO_2 film.

2.4.3. Synthetic Procedure and Characterization data

1-Hexyl-2,3,3-trimethyl-3H-indol-1-ium iodide (2). A mixture of 2,3,3- trimethylindolenine **1** (2 g, 12.56 mmol) and n-hexyl iodide (3.2 g,15.07 mmol) were stirred and heated at 100 ^oC for 12 h in a round bottom flask. The reaction mixture was cooled to room temperature after completion of the reaction. The contents were dissolved in minimum amount of dichloromethane and poured over 100 mL of diethyl ether and filtered under vacuum. The precipitate obtained was washed with diethyl ether (20 mL × 3) to give pure compound **2** (4.3 g, 92%) as brown solid. Mp 135-137 °C. ^{1}H NMR (200 MHz, $CDCl_3$) δ 7.71 – 7.49 (m, 4H), 4.76 – 4.54 (m, 2H), 3.10 (s, 3H), 2.04 – 1.82 (m, 2H), 1.64 (s, 6H), 1.51 – 1.18 (m, 6H), 0.86 (t, J = 6.9 Hz, 3H). ^{13}C NMR (101 MHz, MeOH-d_4) δ 197.6, 143.4, 142.5, 131.2, 130.5, 124.7, 116.6, 55.9, 49.5, 32.4, 28.9, 27.4, 23.5, 22.8, 14.3. HRMS (ESI) m/z: $[M]^+$ Calcd for $C_{17}H_{26}N^+$ 244.2060: Found 244.2053.

3-Butoxy-4-((1-hexyl-3,3-dimethylindolin-2-ylidene)methyl)cyclobut-3-ene-1,2-dione(3). To solution of compound **2** (3.5 g, 9.43 mmol) in 25 mL of n-butanol in a round bottom flask, 3,4-dibutoxycyclobut-3-ene-1,2-dione (2.13 g , 9.43 mmol) was added. To the stirring mixture triethylamine (1.34 g, 13.2 mmol) was added dropwise. The resultant mixture was stirred at room temperature for 12 h followed by heating at 70 ^oC for 1 h. Solvents were evaporated after the completion of the reaction, and the crude product was purified by column chromatography by silica gel to give compound **3** (2.9 g, 77%) as yellow solid. Mp 85-87 °C. ^{1}H NMR (400 MHz, $CDCl_3$) δ 7.31 – 7.24 (m, 2H), 7.12 – 7.00 (m, 1H), 6.88 (dd, *J* = 7.1, 1.4 Hz, 1H), 5.41 (s, 1H), 4.86 (t, *J* = 6.6 Hz, 2H), 3.87 – 3.75 (m, 2H), 1.93 – 1.80 (m, 2H), 1.74 (d, *J* = 7.4 Hz, 2H), 1.63 (d, *J* = 4.5 Hz, 6H), 1.52 (dd, *J* = 15.0, 7.5 Hz, 2H), 1.46 – 1.38 (m, 2H), 1.35 (ddd, *J* = 7.3, 4.5, 2.5 Hz, 4H), 1.01 (t, *J* = 7.4 Hz, 3H), 0.90 (t, *J* = 7.1 Hz, 3H). ^{13}C NMR (101 MHz, $CDCl_3$) δ 192.8, 187.7, 187.6, 173.7, 168.5, 142.8, 141.0,

127.8, 122.8, 122.1, 108.5, 81.4, 73.9, 48.1, 43.1, 32.3, 31.5, 27.1, 26.8, 26.4, 22.60, 18.9, 14.1, 13.8. HRMS (ESI) m/z: $[M+H]^+$ Calcd for $C_{25}H_{34}NO_3$ 396.2539; Found 396.2530.

3-((1-Hexyl-3,3-dimethylindolin-2-ylidene)methyl)-4-hydroxycyclobut-3-ene-1,2-dione(4). To a solution of compound **3** (2.45 g, 6.194 mmol) in 15 mL of acetone in a round bottom flask, 5 mL of 2N HCl was added. The resultant mixture was refluxed for 8 h, and solvents were removed under reduced pressure after completion of the reaction. The crude compound **1c** (1.98 g, 94%), obtained as dark yellow solid, was used further without purification. Mp 170-172 °C. ^{1}H NMR (400 MHz, $CDCl_3$) δ 10.01 (s, 1H), 7.31 (dd, J = 10.2, 7.9 Hz, 2H), 7.13 (t, J = 7.4 Hz, 1H), 6.96 (d, J = 7.8 Hz, 1H), 5.68 (s, 1H), 3.91 (t, J = 6.6 Hz, 2H), 1.82 – 1.74 (m, 2H), 1.67 (s, 6H), 1.43 (d, J = 6.1 Hz, 2H), 1.39 – 1.31 (m, 4H), 0.90 (t, J = 6.8 Hz, 3H). ^{13}C NMR (101 MHz, $CDCl_3$) δ 189.9, 187.6, 176.9, 170.7, 142.5, 141.4, 128.0, 123.6, 122.2, 109.2, 82.4, 48.7, 43.5, 31.5, 29.8, 27.0, 26.7, 26.6, 22.6, 14.0. HRMS (ESI) m/z: $[M+H]^+$ Calcd for $C_{21}H_{25}NO_3$ 340.1913; Found 340.1903.

5-Bromo-1-hexyl-2,3,3-trimethyl-3H-indol-1-ium iodide (6). A mixture of 5-bromo-2,3,3-trimethyl-3H-indole **5** (1 .7 g , 7.14 mmol) and n-hexyliodide (1.82 g , 8.56 mmol) was heated at 100^{o}C in a round bottom flask for 4 h. The reaction mixture was cooled to room temperature after completion of the reaction. The contents were dissolved in minimum amount of dichloromethane and precipitated by pouring in 100 mL of diethyl ether. The precipitate obtained was washed with diethyl ether (20 mL × 3) and dried under vacuum to give compound **6** (1.7g, 53%) as dark brown solid. Mp 208-210 °C. ^{1}H NMR (200 MHz, DMSO-d_6) δ 8.20 (s, 1H), 7.96 (d, *J* = 8.5 Hz, 1H), 7.85 (d, *J* = 8.7 Hz, 1H), 4.43 (t, *J* = 7.4 Hz, 2H), 2.84 (s, 3H), 1.80 (s, 2H), 1.55 (s, 6H), 1.30 (s, 6H), 0.86 (s, 3H). ^{13}C NMR (101 MHz, $CDCl_3$) δ 198.1, 145.5, 141.7, 133.7, 128.3, 128.2, 125.3, 118.3, 56.1, 49.8, 32.4, 28.8, 27.4, 23.5, 22.7, 14.3. HRMS (ESI) m/z: $[M]^+$ Calcd for $C_{17}H_{25}BrN^+$ 322.1165; Found 322.1160.

4-((5-Bromo-1-hexyl-3,3-dimethyl-3H-indol-1-ium-2-yl)methylene)-2-((1-hexyl-3,3-dimethylindolin-2-ylidene)methyl)-3-oxocyclobut-1-en-1-olate (7). A mixture of compound **6** (0.3 g, 0.88 mmol) and compound **4** (0.478 g, 1.06 mmol) in 16 mL of toluene / n-butanol (1:1) was refluxed in a two necked round bottom flask fitted with dean-stark apparatus for 24 h. After completion of the reaction, the solvent were removed under reduced

pressure and crude product was purified by column chromatography by silica gel using ethyl acetate/dichloromethane as eluent to yield compound **7** (0.32 g, 56%) as blue solid. Mp 172-173 °C. ^{1}H NMR (400 MHz, $CDCl_3$) δ 7.46 – 7.28 (m, 4H), 7.17 (t, *J* = 7.4 Hz, 1H), 7.01 (d, *J* = 7.9 Hz, 1H), 6.82, (dd, *J* = 13.3, 8.4 Hz, 1H), 6.06 – 5.83 (m, 2H), 4.01 (d, *J* = 7.1 Hz, 2H), 3.91 (s, 2H), 1.81 (s, 2H), 1.78 (d, *J* = 5.6 Hz, 12H), 1.72 (s, 2H), 1.45 – 1.28 (m, 12H), 0.89 (t, *J* = 6.5 Hz, 6H). ^{13}C NMR (101 MHz, $CDCl_3$) δ 181.1, 171.2, 168.6, 142.5, 130.8, 130.7, 128.0, 125.9, 125.8, 124.2, 122.5, 116.7, 116.2, 110.5, 109.8, 87.1, 86.9, 49.7, 49.2, 44.0, 31.6, 31.6, 29.8, 27.3, 27.2, 27.1, 27.0, 26.9, 26.8, 22.66, 22.65, 22.6, 14.1. HRMS (ESI) m/z: $[M+H]^+$ Calcd for $C_{38}H_{48}BrN_2O_2$ 643.2899; Found 643.2885.

4,8-Dimethoxybenzo[1,2-b:4,5-b']dithiophene-2-carbaldehyde (9a). In a two-necked round bottom flask fitted with reflux condenser, **8a** (1.2 g, 5.20 mmol) was taken. It was dissolved in 20 mL of 1,2-dichloroethane and N,N-dimethylformamide (8 mL, 104 mmol) was added to the mixture. The flask was cooled to 0 ^{o}C, and $POCl_3$ (9.5 mL, 104 mmol) was added to it dropwise and refluxed for 24 h. After completion of the reaction, the reaction mixture was poured into ice-cold solution of ammonium chloride and extracted with dichloromethane. The organic layer was dried over sodium sulfate, and solvents were removed under reduced pressure. The crude product was purified by column chromatography over silica gel with ethyl acetate/pet ether as eluent to afford **8a** (1.2 g, 80%) as light yellow solid. Mp 140-143 °C. ^{1}H NMR (200 MHz, $CDCl_3$) δ 10.10 (s, 1H), 8.23 (s, 1H), 7.52 (s, 2H), 4.22 (s, 3H), 4.13 (s, 3H). ^{13}C NMR (101 MHz, $CDCl_3$) δ 184.6, 148.0, 145.4, 143.0, 135.1, 131.6, 131.3, 130.1, 129.6, 128.9, 120.4, 61.5, 61.2. HRMS (ESI) m/z: $[M+H]^+$ Calcd for $C_{13}H_{11}O_3S_2$ 279.0150; Found 279.0140.

4,8-Bis((2-ethylhexyl)oxy)benzo[1,2-b:4,5-b']dithiophene-2-carbaldehyde (9b). In a two-necked round bottom flask fitted with reflux condenser, **8b** (2.8 g, 6.27 mmol) was taken. It was dissolved in 20 mL of 1,2-dichloroethane and N,N-dimethylformamide (9.76 mL, 125.4 mmol) was added to the mixture. The flask was cooled to 0 ^{o}C and $POCl_3$ (11.7 mL, 125.361 mmol) was added to it dropwise and refluxed for 48 h. After completion of reaction the reaction mixture was poured in ice-cold solution of ammonium chloride and extracted by dichloromethane. The organic layer was dried over sodium sulphate and solvents were removed under reduced pressure. The crude product was purified by column chromatography over silica gel with ethyl acetate/pet ether as eluent to afford **8a** ((2 g, 67%) as yellow

viscous oil. ^{1}H NMR (400 MHz, $CDCl_3$) δ 10.10 (s, 1H), 8.17 (s, 1H), 7.49 (s, 2H), 4.27 (d, J = 5.4 Hz, 2H), 4.18 – 4.15 (m, 2H), 1.82 (dd, J = 12.0, 6.0 Hz, 2H), 1.75 – 1.65 (m, 2H), 1.62 – 1.56 (m, 4H), 1.54 – 1.47 (m, 2H), 1.41 – 1.35 (m, 8H), 1.05 – 0.99 (m, 6H), 0.97 – 0.90 (m, 6H). ^{13}C NMR (101 MHz, $CDCl_3$) δ 184.7, 147.4, 144.7, 142.7, 135.3, 131.9, 131.5, 130.3, 129.9, 128.6, 120.6, 76.7, 76.4, 40.8, 30.5, 29.3, 24.0, 23.2, 14.3, 11.4. HRMS (ESI) m/z: $[M+H]^+$ Calcd for $C_{27}H_{39}O_3S_2$ 475.2341; Found 475.2333.

General synthetic procedure for direct arylation of squaraine and BDT.

In a Schlenk tube corresponding bromo-squaraine (**7)** and BDT aldehydes (**9a** and **9b**) were taken. The Shclenk tube is evacuated and refilled with nitrogen three times. $Pd(OAc)_2$ (5 mol%), PCy_3(10 mol%), PivOH (30 mol%) and K_2CO_3 (2.5 equiv) were added to it followed by 4 mL of anhydrous toluene. The mixture was stirred at 110 ºC for 24 h. After completion of the reaction, the mixture was poured into water and extracted with dichloromethane. The organic layer was then washed with brine, dried over sodium sulfate and concentrated under vacuum. The crude product was purified by column chromatography to give of pure compounds.

(**Z)-4-((5-(6-Formyl-4,8-dimethoxybenzo[1,2-b:4,5-b']dithiophen-2-yl)-1-hexyl-3,3-dimethyl-3H-indol-1-ium-2-yl)methylene)-2-(((Z)-1-hexyl-3,3-dimethylindolin-2-ylidene)methyl)-3-oxocyclobut-1-en-1-olate (10a).** From bromo-squaraine **7** (0.250 g, 0.388 mmol) and aldehyde **9a** (0.432 g, 1.55 mmol), the compound **10a** (0.2g, 61%) was obtained as green solid. Mp 251-253 °C. ^{1}H NMR (500 MHz, $CDCl_3$) δ 10.10 (s, 1H), 8.22 (s, 1H), 7.71 (d, *J* = 1.7 Hz, 1H), 7.69 (s, 1H), 7.69 (s, 1H), 7.39 (d, *J* = 7.3 Hz, 1H), 7.33 (td, *J* = 7.8, 0.9 Hz, 1H), 7.18 (t, *J* = 7.3 Hz, 1H), 7.02 (dd, *J* = 10.3, 8.5 Hz, 2H), 6.03 (s, 1H), 6.00 (s, 1H), 4.26 (s, 3H), 4.18 (s, 3H), 4.06 – 4.01 (m, 2H), 4.00 – 3.94 (m, 2H), 1.88 (s, 6H), 1.81 (s, 6H), 1.50 – 1.40 (m, 6H), 1.37 – 1.31 (m, 10H), 0.92 – 0.88 (m, 6H).^{13}C NMR (126 MHz, $CDCl_3$) δ 184.5, 181.3, 178.4, 171.4, 168.5, 147.6, 146.5, 145.0, 142.6, 142.4, 136.4, 131.8, 131.6, 130.2, 129.0, 128.5, 128.0, 126.9, 124.3, 122.5, 120.6, 114.8, 109.9, 109.5, 87.2, 61.4, 61.2, 49.8, 49.1, 44.1, 43.9, 31.63, 31.61, 29.8, 27.5, 27.33, 27.25, 27.13, 27.05, 26.9, 22.7, 14.1. HRMS (ESI) m/z: $[M+H]^+$ Calcd for $C_{51}H_{57}N_2O_5S_2$ 841.3709; Found 841.3701.

(Z)-4-((5-(4,8-Bis((2-ethylhexyl)oxy)-6-formylbenzo[1,2-b:4,5-b']dithiophen-2-yl)-1-hexyl-3,3-dimethyl-3H-indol-1-ium-2-yl)methylene)-2-(((Z)-1-hexyl-3,3-dimethylindolin-2-ylidene)methyl)-3-oxocyclobut-1-en-1-olate (10b). From bromo-squaraine **7** (0.200 g, 0.310 mmol) and aldehyde **9b** (0.589 g, 1.24 mmol), 0.150 g of compound **10b** (0.15 g, 46%) was obtained as green sticky gum. ^{1}H NMR (400 MHz, $CDCl_3$) δ 10.10 (s, 1H), 8.17 (s, 1H), 7.69 (d, *J* = 8.3 Hz, 1H), 7.66 (s, 1H), 7.63 (s, 1H), 7.39 (d, *J* = 7.3 Hz, 1H), 7.33 (t, *J* = 7.6 Hz, 1H), 7.18 (t, *J* = 7.4 Hz, 1H), 7.02 (dd, *J* = 7.5, 5.4 Hz, 2H), 6.03 (s, 1H), 6.00 (s, 1H), 4.32 (d, *J* = 5.4 Hz, 2H), 4.21 (d, *J* = 5.2 Hz, 2H), 4.06 – 3.95 (m, 4H), 1.87 (s, 6H), 1.81 (s, 6H), 1.73 – 1.53 (m, 10H), 1.47 – 1.39 (m, 14H), 1.36 – 1.25 (m, 10H), 1.05 (t, *J* = 7.3 Hz, 6H), 0.97 – 0.89 (m, 12H). ^{13}C NMR (101 MHz, $CDCl_3$) δ 184.6, 181.3, 178.5, 171.3, 168.5, 147.1, 146.1, 144.4, 142.4, 136.6, 132.0, 131.9, 130.3, 129.2, 128.7, 128.0, 126.8, 124.329, 122.5, 120.6, 115.0, 109.9, 87.2, 76.6, 76.3, 49.8, 49.1, 44.1, 40.8, 40.8, 31.6, 30.6, 30.5, 29.3, 27.4, 27.3, 27.13, 27.07, 26.9, 24.0, 23.3, 22.7, 14.3, 14.1, 11.5. HRMS (ESI) m/z: $[M+H]^+$ Calcd for $C_{65}H_{85}N_2O_5S_2$ 1037.5900; Found 1037.5876.

General procedure for Knoevenagel condensation of aldehyde to cyanoacetic acid: Corresponding aldehydes (**10a** and **10b**) were dissolved in 5 mL of chloroform and 5 mL of acetonitrile. To this 5 equiv cyanoacetic acid was added followed by 40 μL of piperidine. The resultant solution was stirred at 80 ^{o}C for 12 h. Solvents were removed under rotavap after completion of the reaction and dissolved in 50mL of dichloromethane. The organic layer was washed with water followed by brine and dried over sodium sulfate. The solvents were removed under reduced pressure and purified by column chromatography by silica gel using MeOH/$CHCl_3$ as an eluent.

4-((5-(6-(-2-Carboxy-2-cyanovinyl)-4,8-dimethoxybenzo[1,2-b:4,5-b']dithiophen-2-yl)-1-hexyl-3,3-dimethyl-3H-indol-1-ium-2-yl)methylene)-2-((-1-hexyl-3,3-dimethylindolin-2-ylidene)methyl)-3-oxocyclobut-1-en-1-olate (RSQ-1). From **10a** (0.15 g, 0.178 mmol) , pure compound **RSQ1** (0.1 g, 62%) was obtained as dark green solid. Mp 281-283 °C. ^{1}H NMR (400 MHz, DMSO-d_6 + $CDCl_3$) δ 8.30 (s, 1H), 7.95 (s, 1H), 7.67 (d, *J* = 9.7 Hz, 2H), 7.62 (d, *J* = 8.1 Hz, 1H), 7.33 (d, *J* = 7.3 Hz, 1H), 7.27 (t, *J* = 7.6 Hz, 1H), 7.11 (t, *J* = 7.4 Hz, 1H), 7.05 (t, *J* = 8.4 Hz, 2H), 5.88 (s, 1H), 5.84 (s, 1H), 4.12 (s, 3H), 4.07 (s, 3H), 4.04 – 3.89 (m, 4H), 1.75 (s, 6H), 1.69 (s, 6H), 1.40 – 1.16 (m, 16H), 0.81 (t, *J* = 6.5 Hz, 6H). ^{13}C NMR (101 MHz, DMSO-d_6 + $CDCl_3$) δ 181.3, 180.1, 170.2, 167.7, 145.6, 145.1, 143.8, 143.1,

142.8, 142.3, 141.7, 141.5, 135.7, 134.4, 130.7, 129.2, 128.9, 128.4, 127.9, 127.5, 126.3, 123.8, 121.8, 119.7, 117.6, 114.3, 109.6, 109.4, 86.3, 63.0, 60.7, 60.6, 48.9, 48.3, 43.1, 30.9, 29.0, 26.7, 26.5, 26.3, 26.0, 21.9, 13.5. HRMS (ESI) m/z: $[M]^+$ Calcd for $C_{54}H_{57}N_3O_6S_2$ 907.3689; Found 907.3683.

4-((5-(6-(-2-Carboxy-2-cyanovinyl)-4,8-bis((2-ethylhexyl)oxy)benzo[1,2-b:4,5-b']dithiophen-2-yl)-1-hexyl-3,3-dimethyl-3H-indol-1-ium-2-yl)methylene)-2-((-1-hexyl-3,3-dimethylindolin-2-ylidene)methyl)-3-oxocyclobut-1-en-1-olate (RSQ-2). From **10b** (0.1 g, 0.097 mmol), compound **RSQ2** (0.065, 61%) was obtained as dark green solid. Mp 242-243 °C. ^{1}H NMR (400 MHz, DMSO-d_6 + $CDCl_3$) δ 8.38 (s, 1H), 8.08 (s, 1H), 7.63 (d, *J* = 7.0 Hz, 2H), 7.58 (s, 1H), 7.35 (d, *J* = 7.3 Hz, 1H), 7.28 (t, *J* = 7.6 Hz, 1H), 7.11 (dd, *J* = 14.5, 7.6 Hz, 3H), 5.88 (s, 1H), 5.84 (s, 1H), 4.21 (d, *J* = 4.9 Hz, 2H), 4.13 (d, *J* = 4.2 Hz, 3H), 4.05 – 3.93 (m, 4H), 1.77 (s, 6H), 1.70 (s, 6H), 1.65 – 1.43 (m, 10H), 1.42 – 1.32 (m, 14H), 1.30 – 1.16 (m, 10H), 0.98 (dd, *J* = 16.7, 7.6 Hz, 6H), 0.91 – 0.87 (m, 6H), 0.83 (t, *J* = 6.2 Hz, 6H). ^{13}C NMR (101 MHz, $CDCl_3$) δ 181.1, 180.2, 177.4, 170.2, 167.5, 145.4, 145.3, 143.0, 142.9, 142.1, 141.7, 141.4, 135.1, 134.8, 131.3, 128.9, 128.3, 128.1, 127.5, 126.3, 123.7, 121.7, 119.5, 116.0, 115.9, 114.3, 109.7, 109.6, 86.5, 86.3, 78.2, 75.9, 75.4, 49.5, 48.9, 48.2, 43.2, 30.8, 29.9, 29.7, 28.6, 28.5, 26.6, 26.5, 26.3, 26.0, 23.2, 22.49, 22.46, 21.9, 13.7, 13.5, 10.9. HRMS (ESI) m/z: $[M+H]^+$ Calcd for $C_{68}H_{86}N_3O_6S_2$ 1104.5958; Found 1104.5946.

2.5. NMR Spectra

^{1}H and ^{13}C NMR spectra of 2

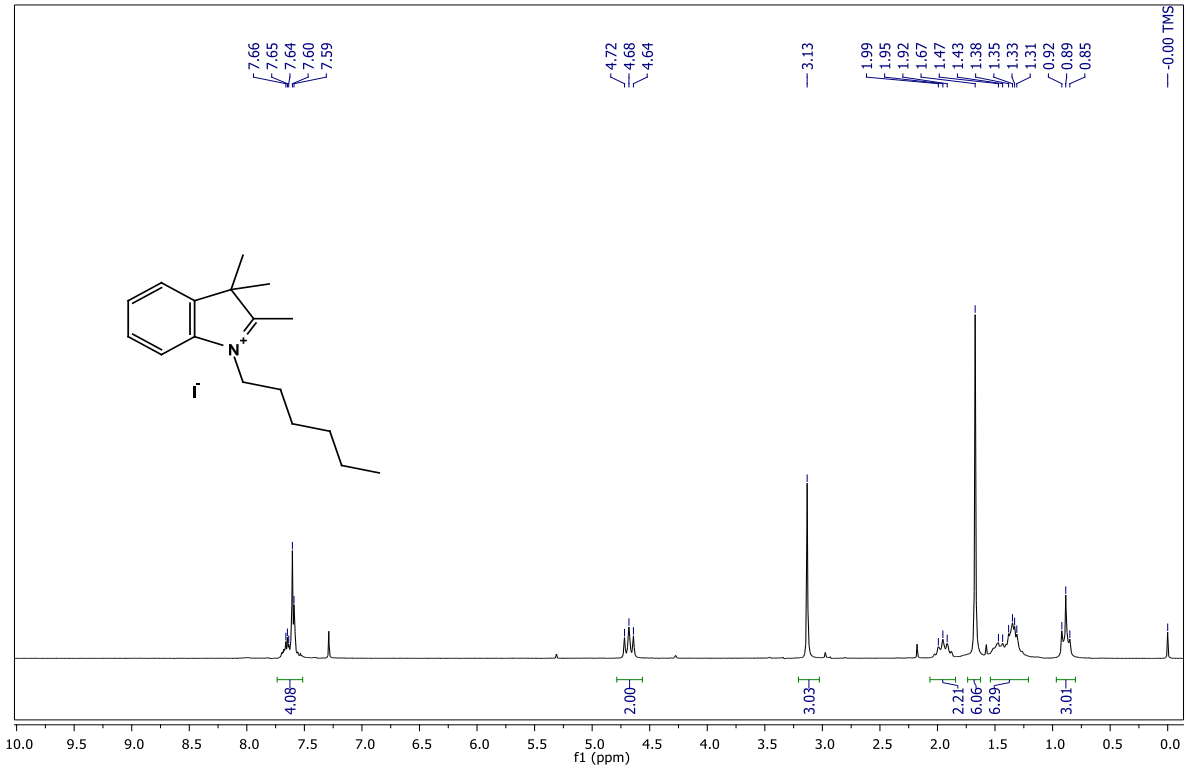

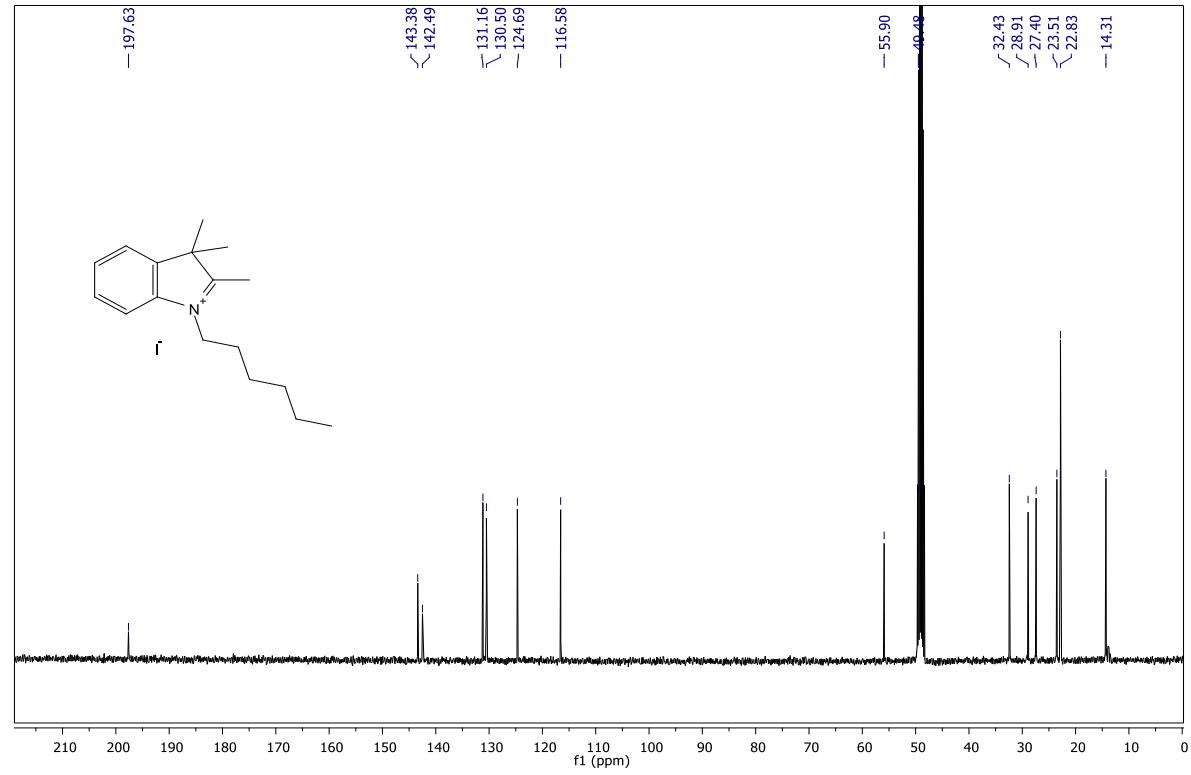

^{1}H and ^{13}C NMR spectra of 3

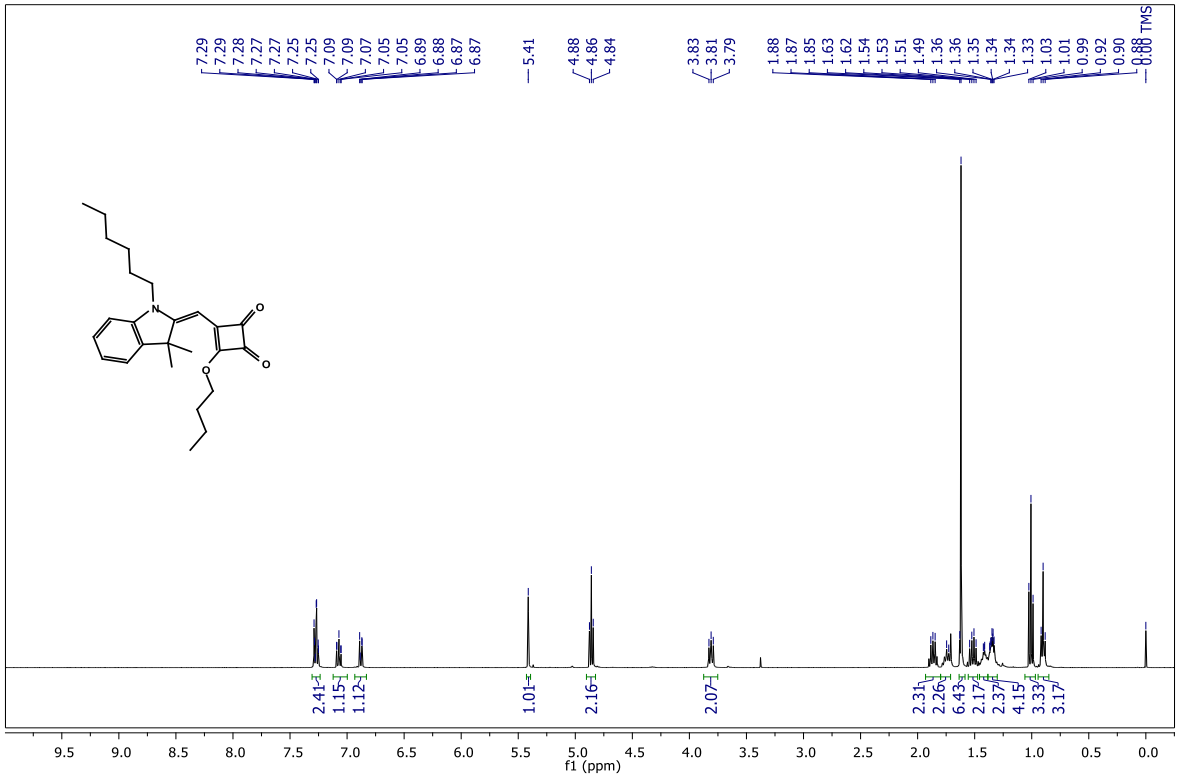

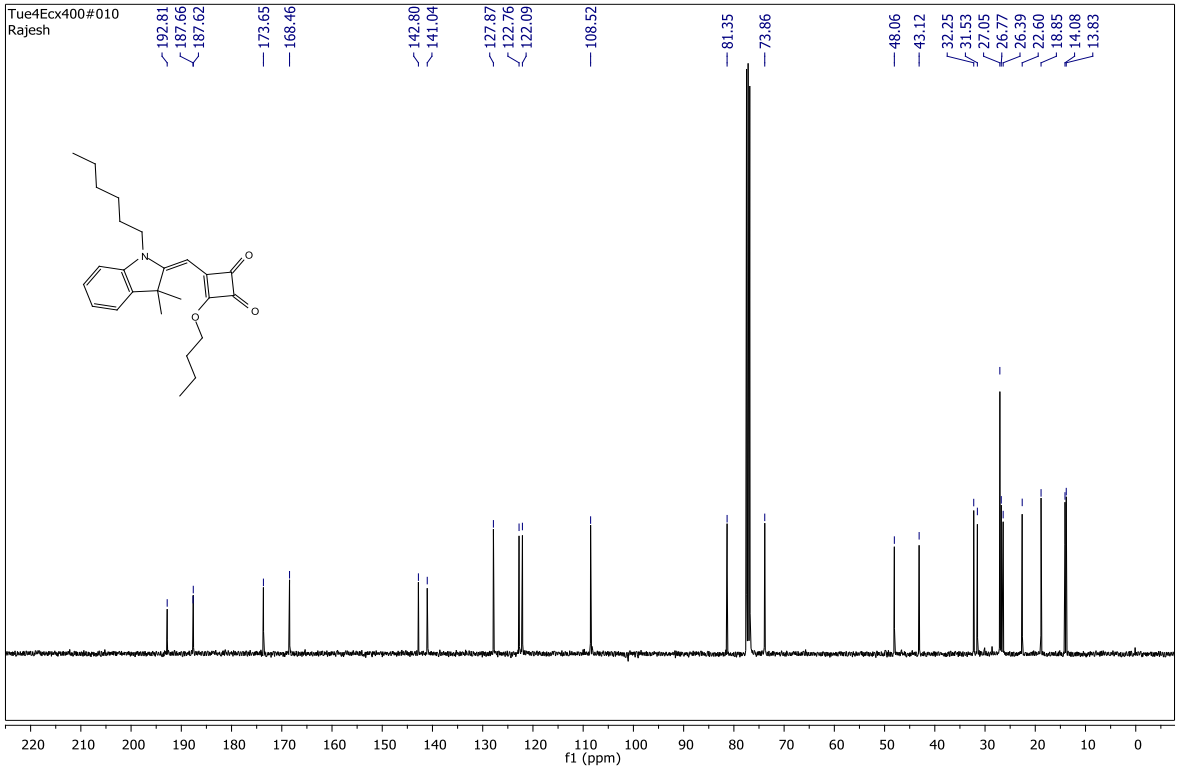

^{1}H and ^{13}C NMR spectra of 4

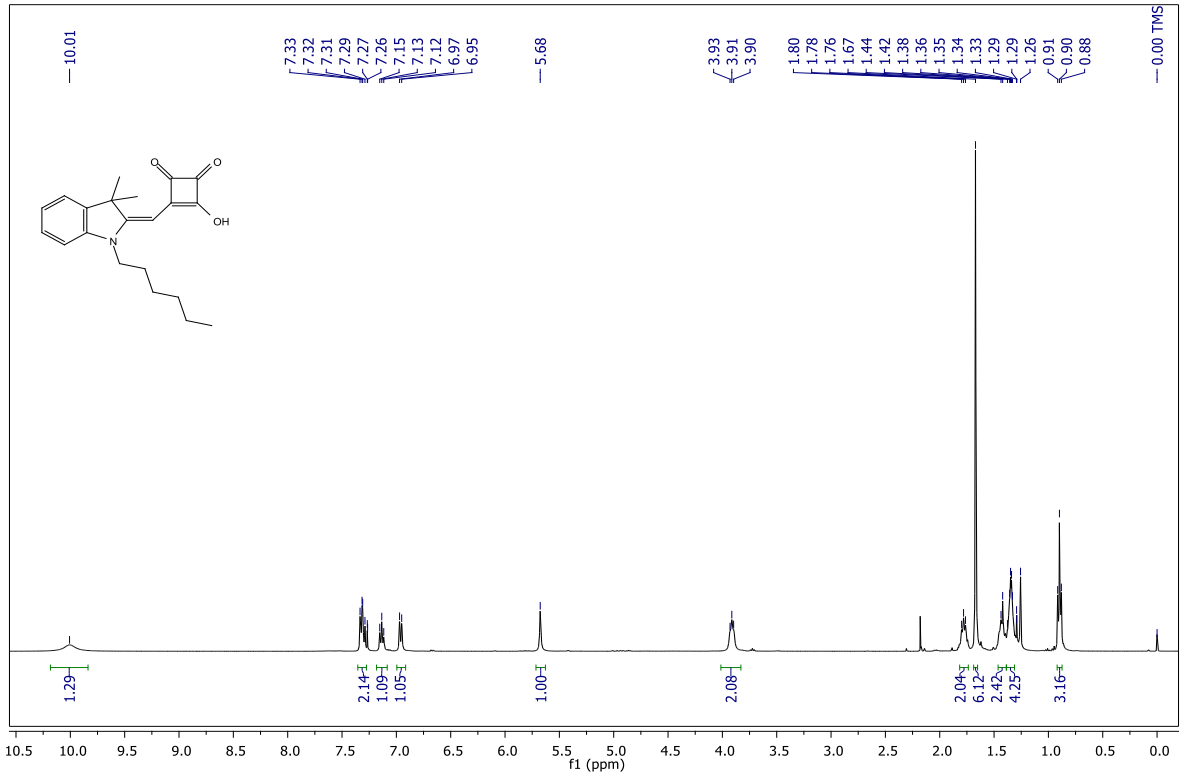

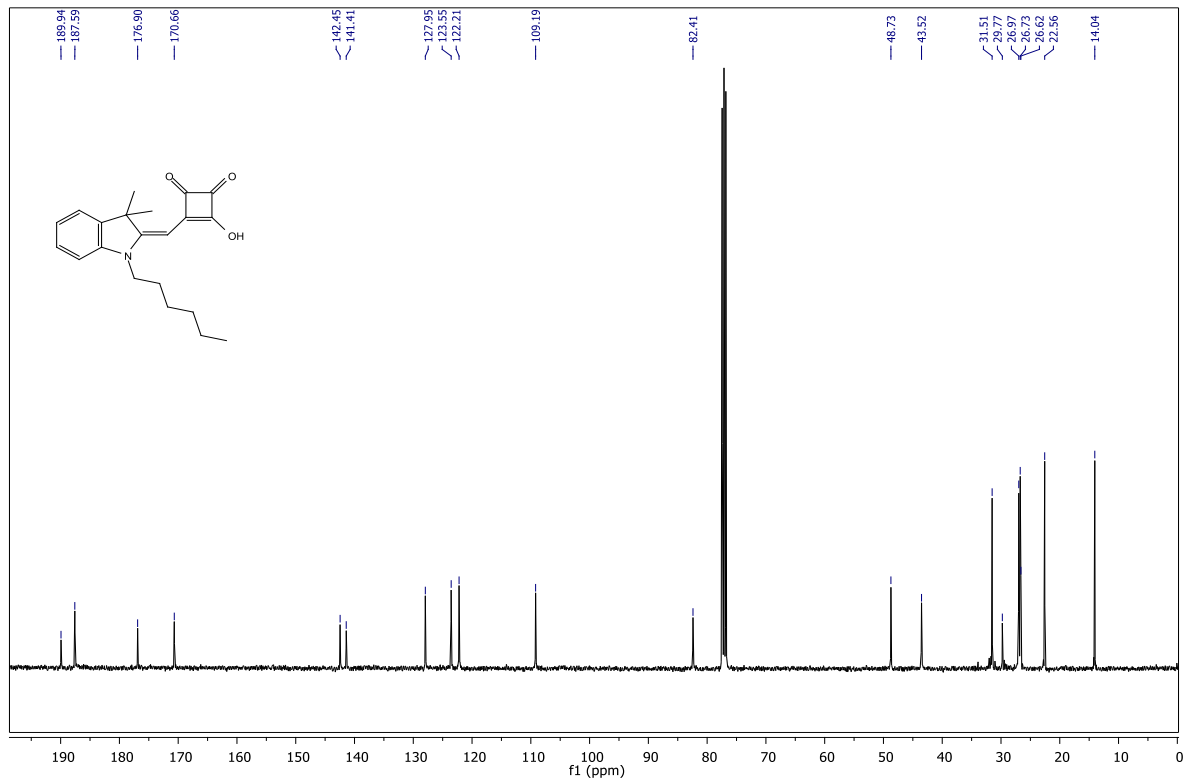

^{1}H and ^{13}C NMR spectra of 6

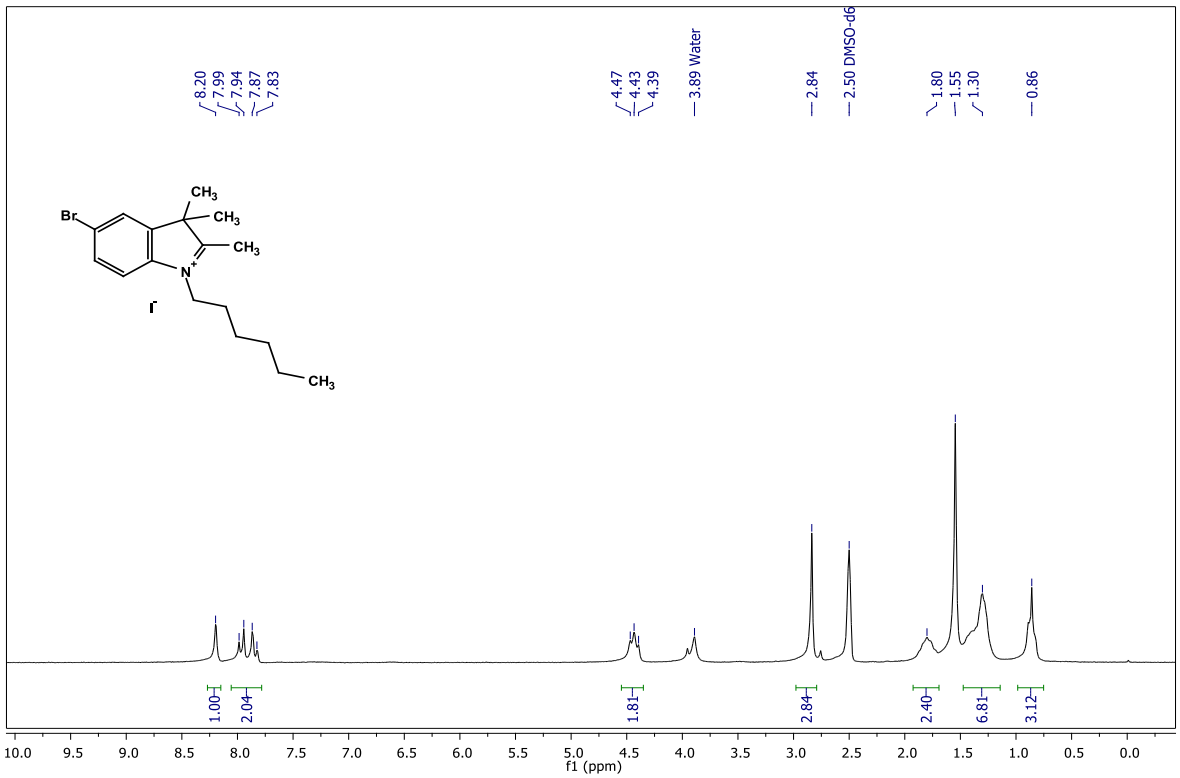

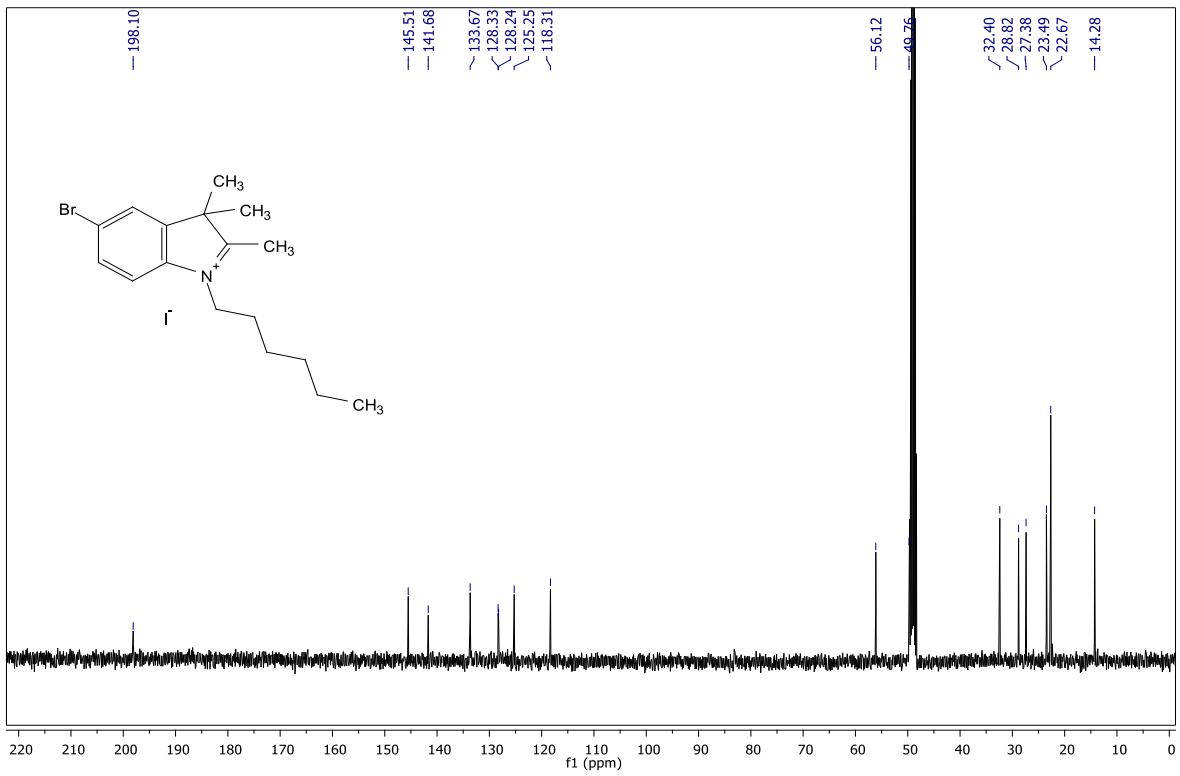

^{1}H and ^{13}C NMR spectra of 7

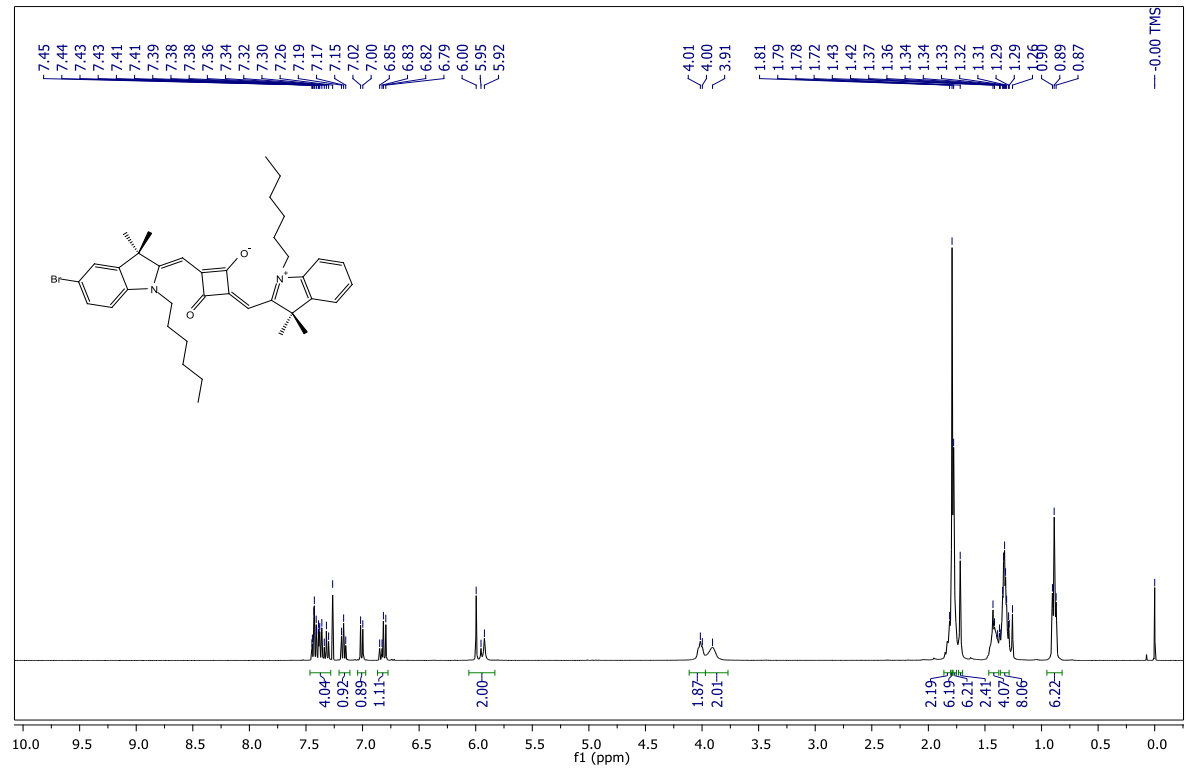

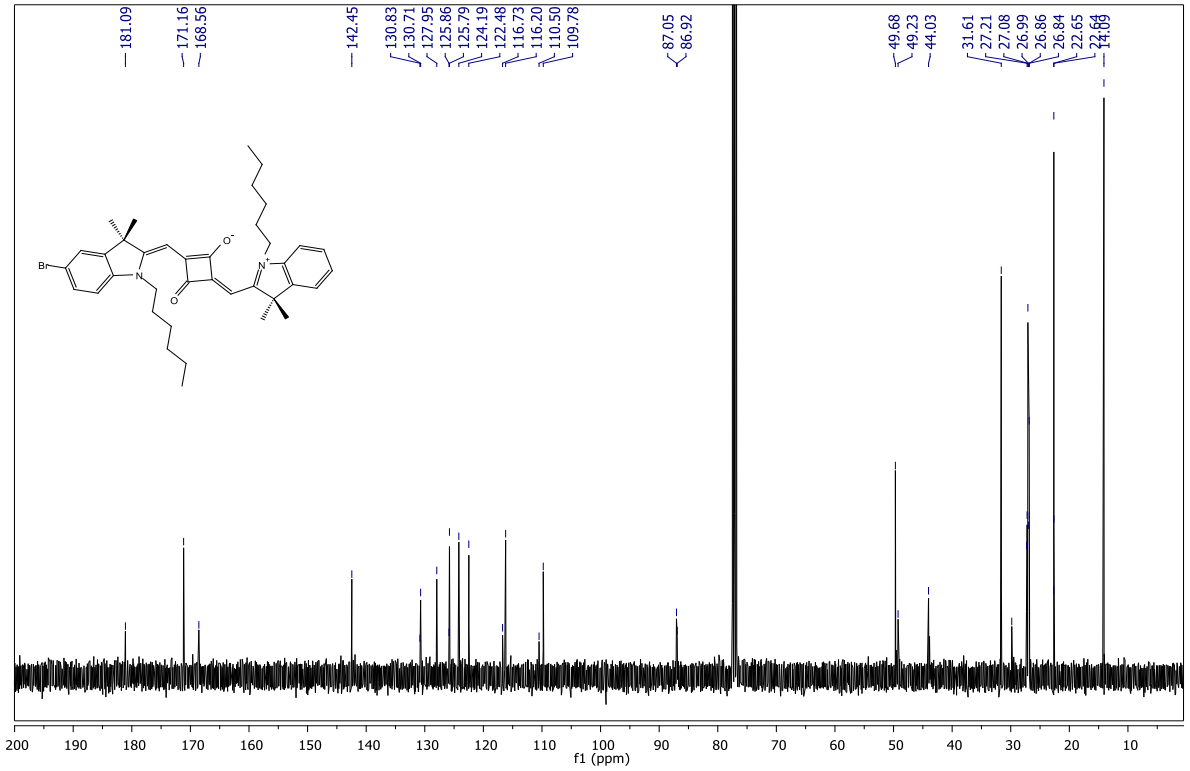

^{1}H and ^{13}C NMR spectra of 9a

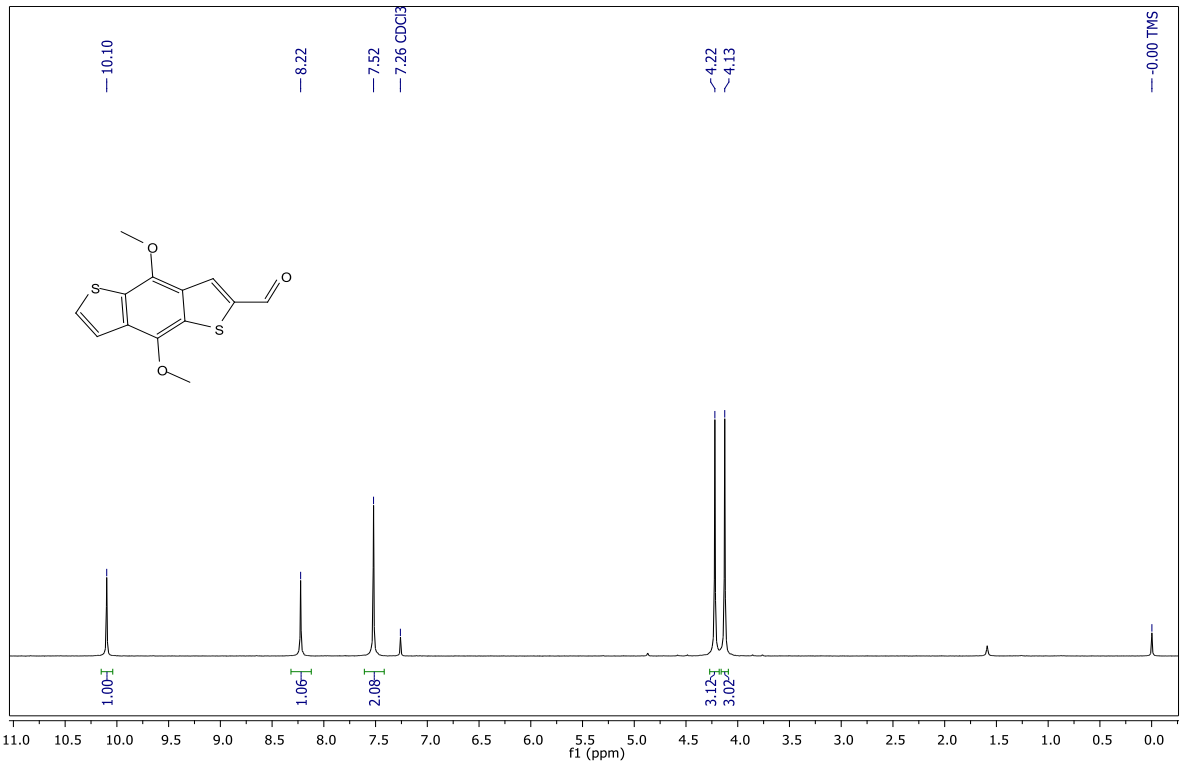

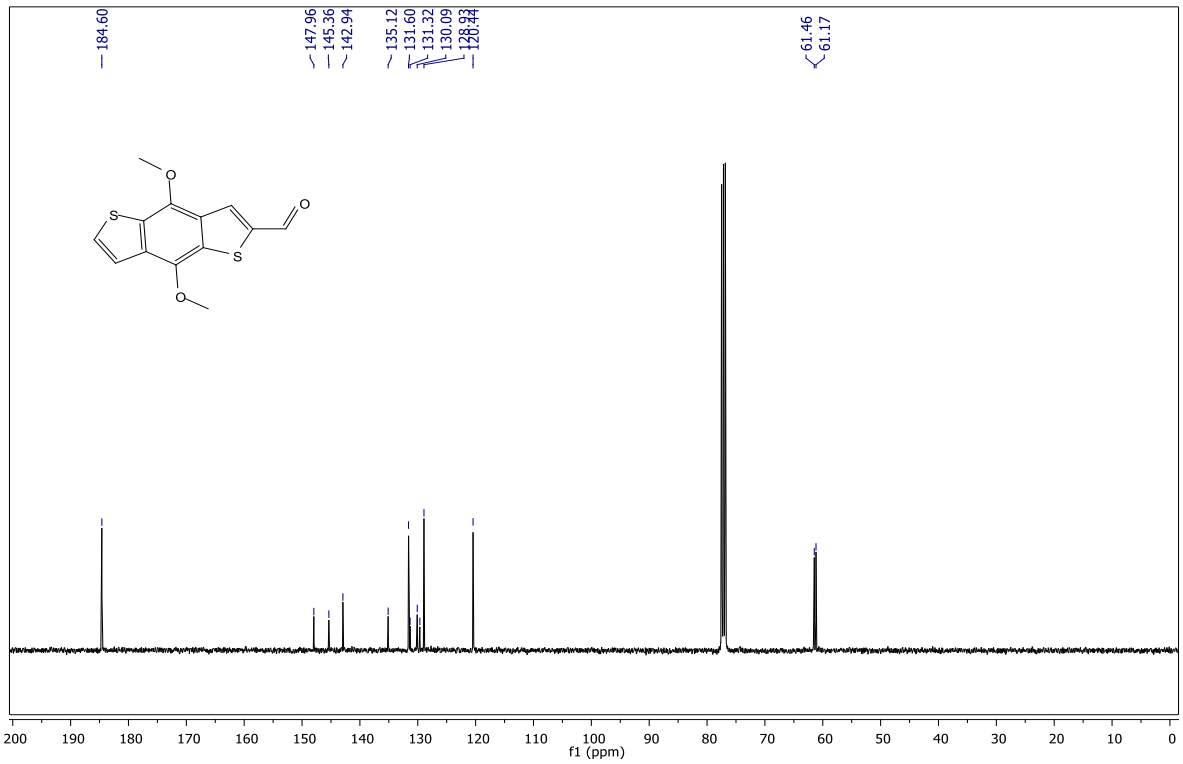

^{1}H and ^{13}C NMR spectra of 9b

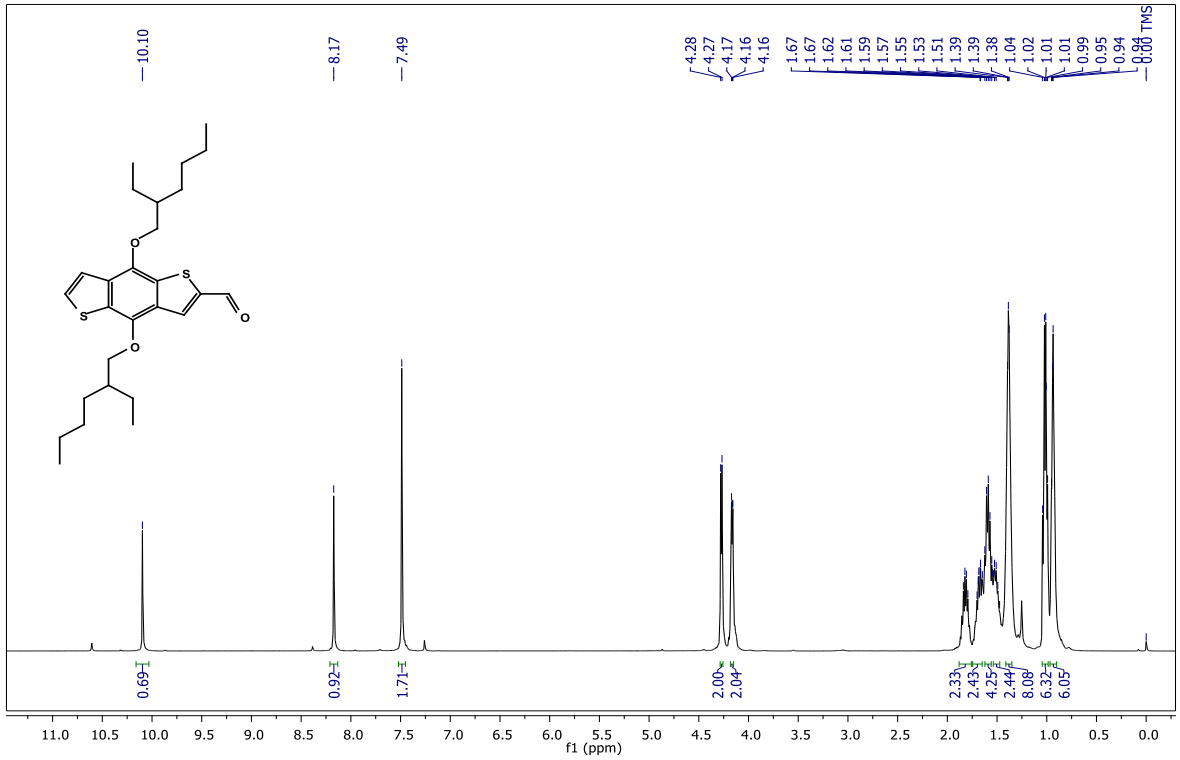

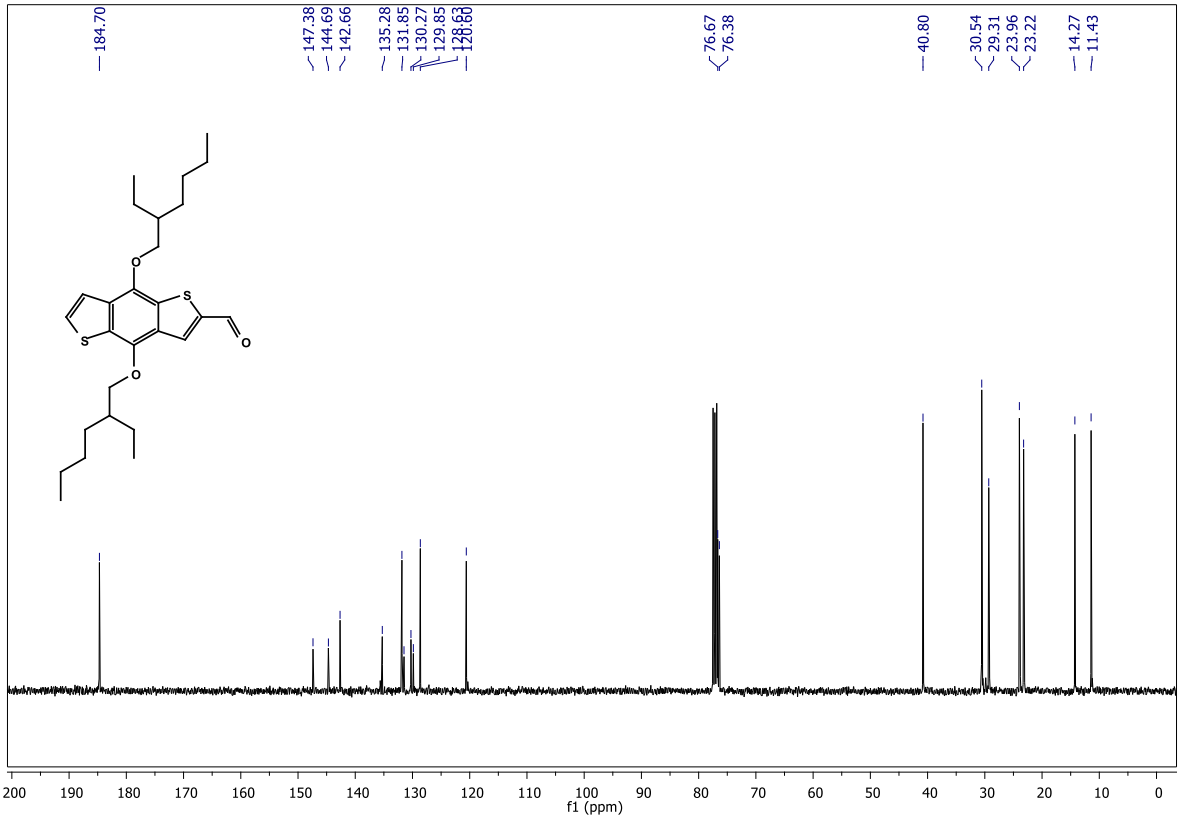

^{1}H and ^{13}C NMR spectra of 10a

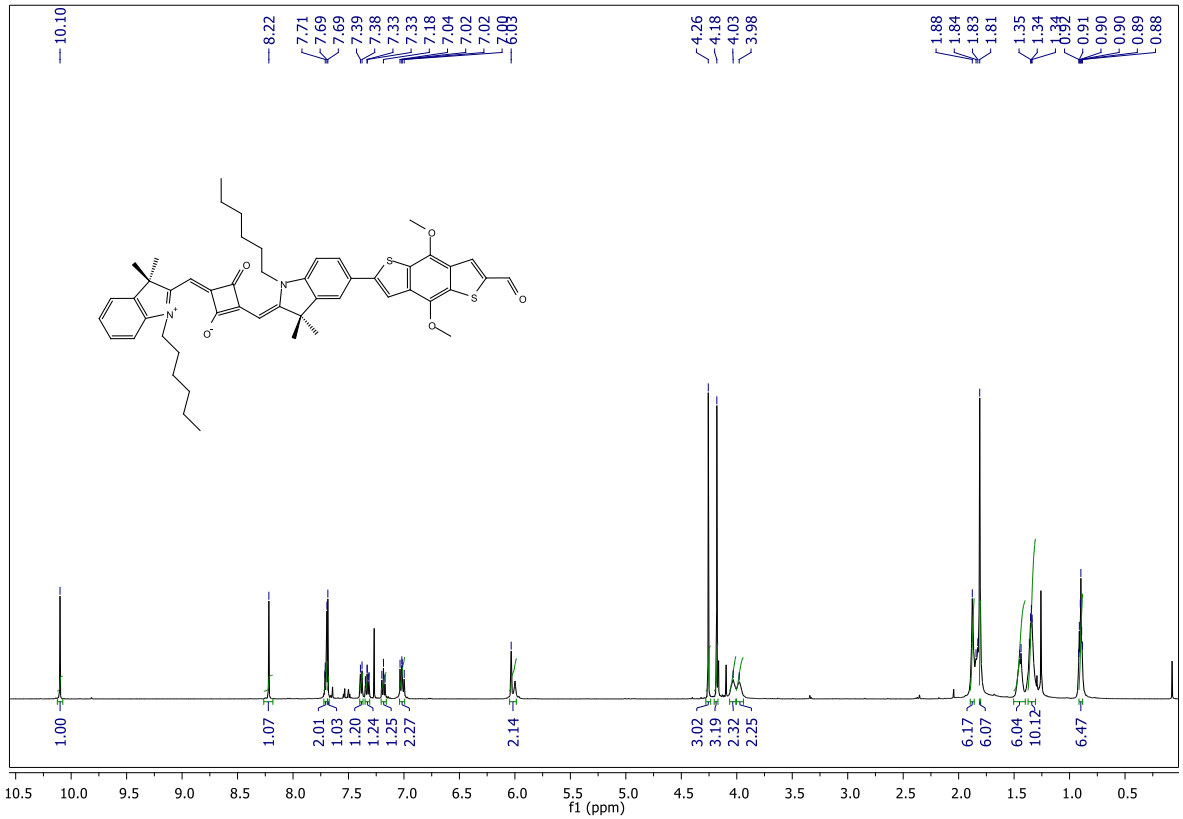

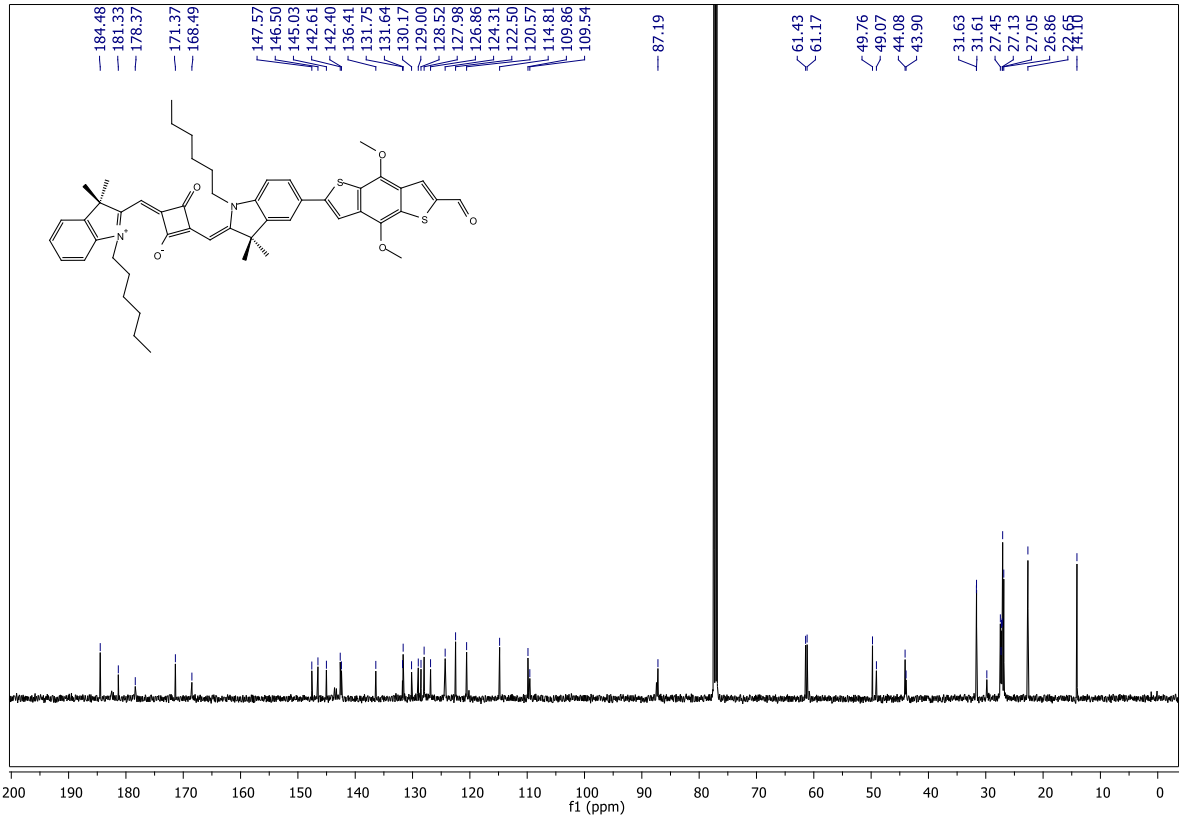

^{1}H and ^{13}C NMR spectra of 10b

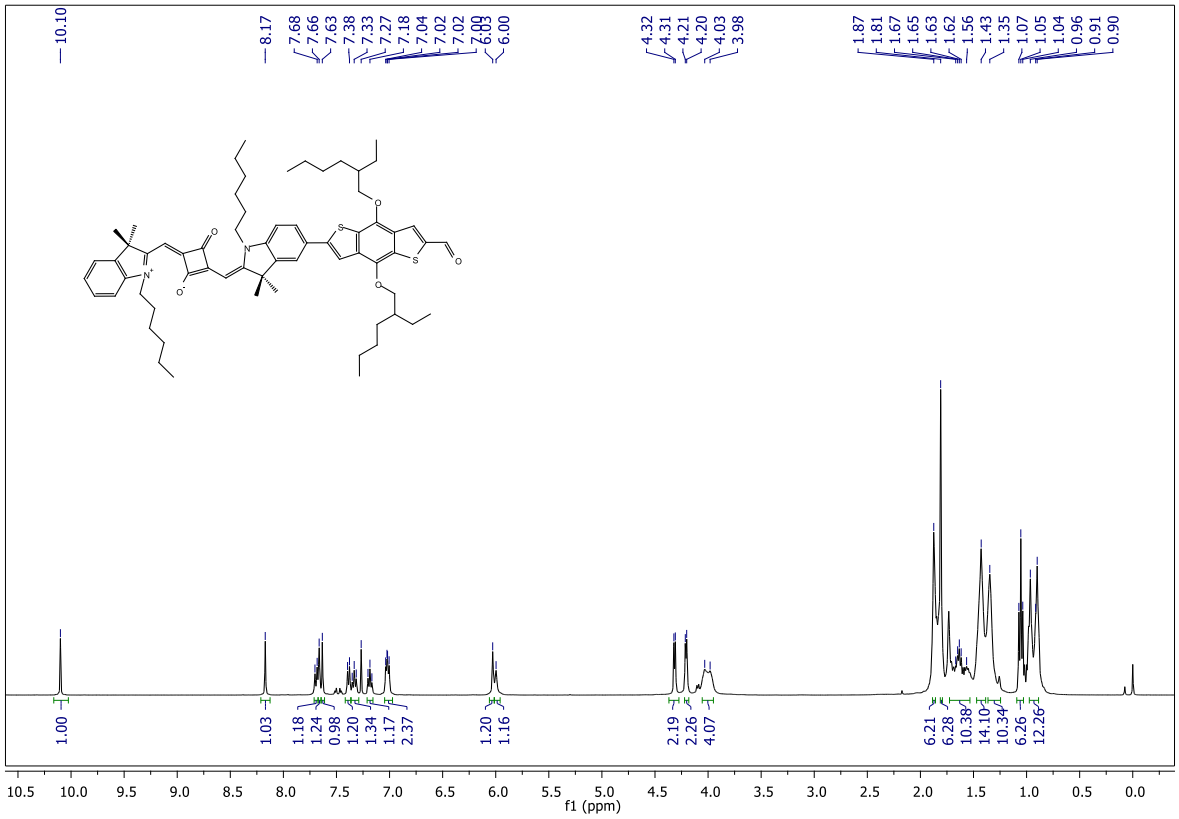

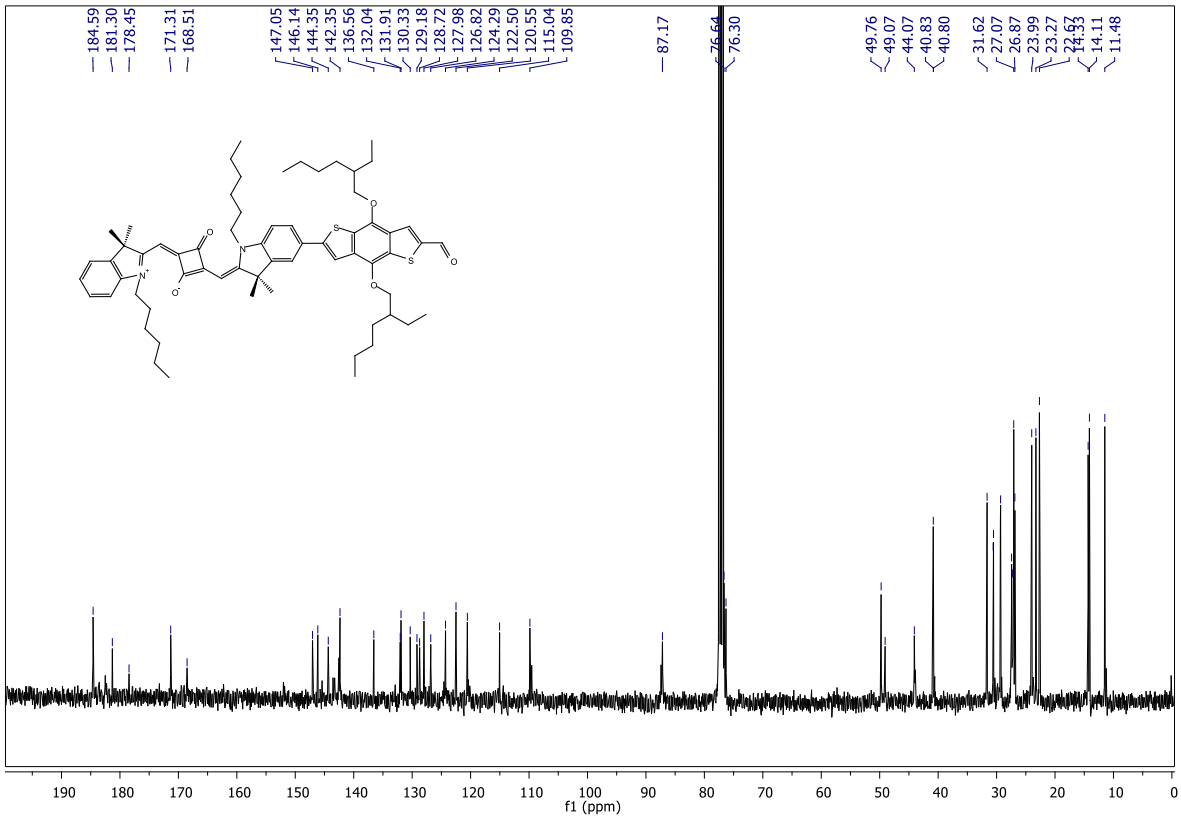

^{1}H and ^{13}C NMR spectra of RSQ1

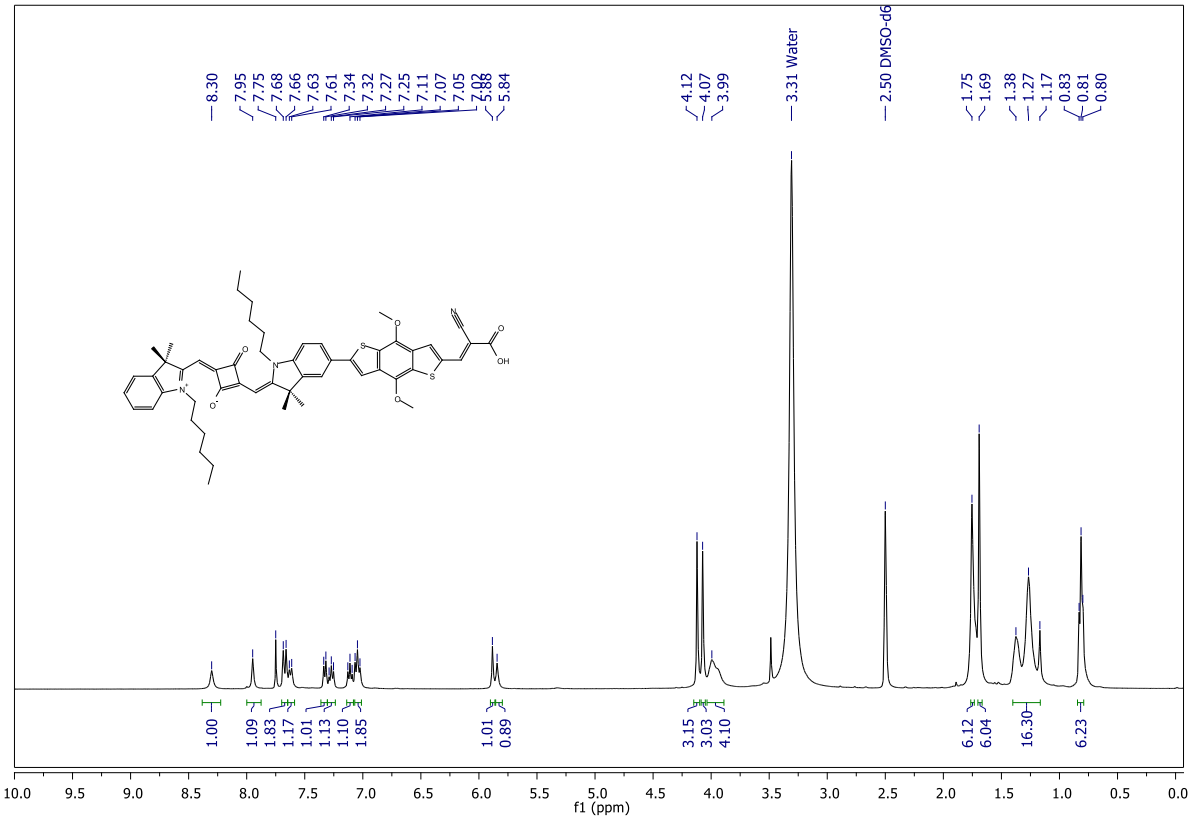

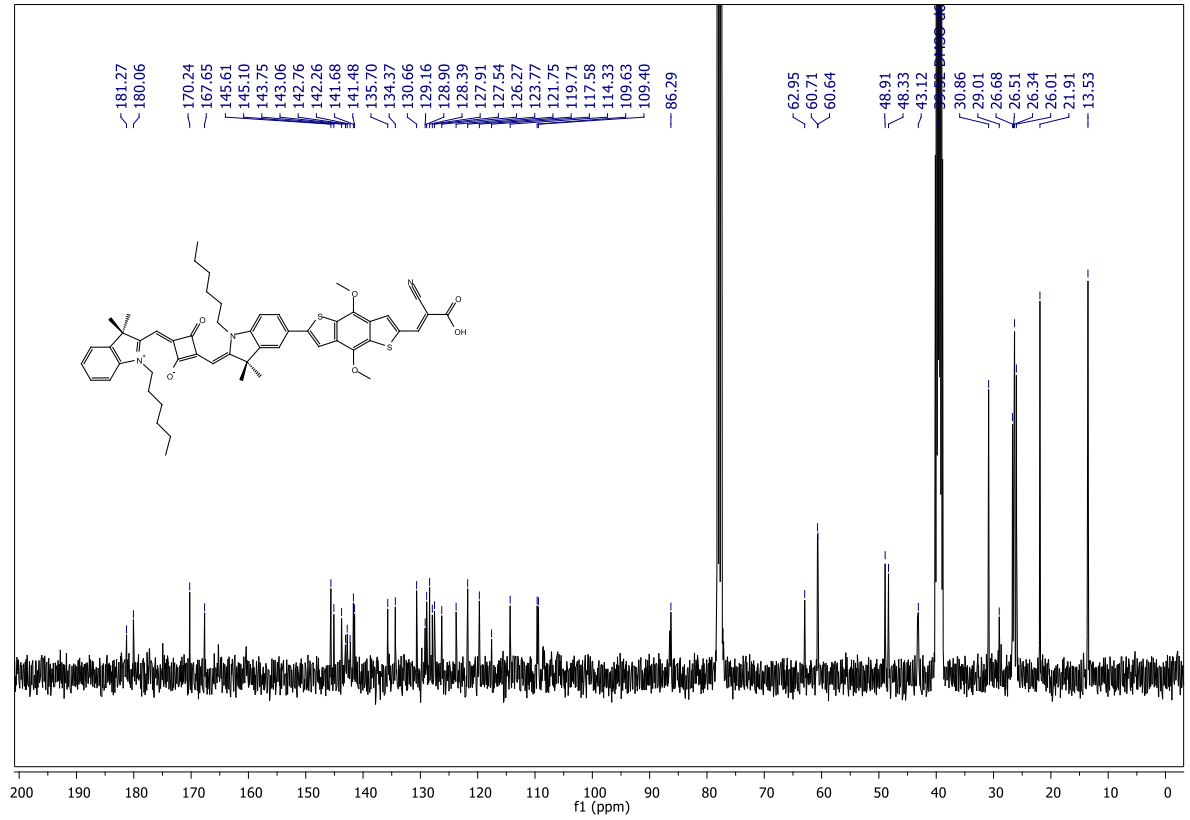

^{1}H and ^{13}C NMR spectra of RSQ2

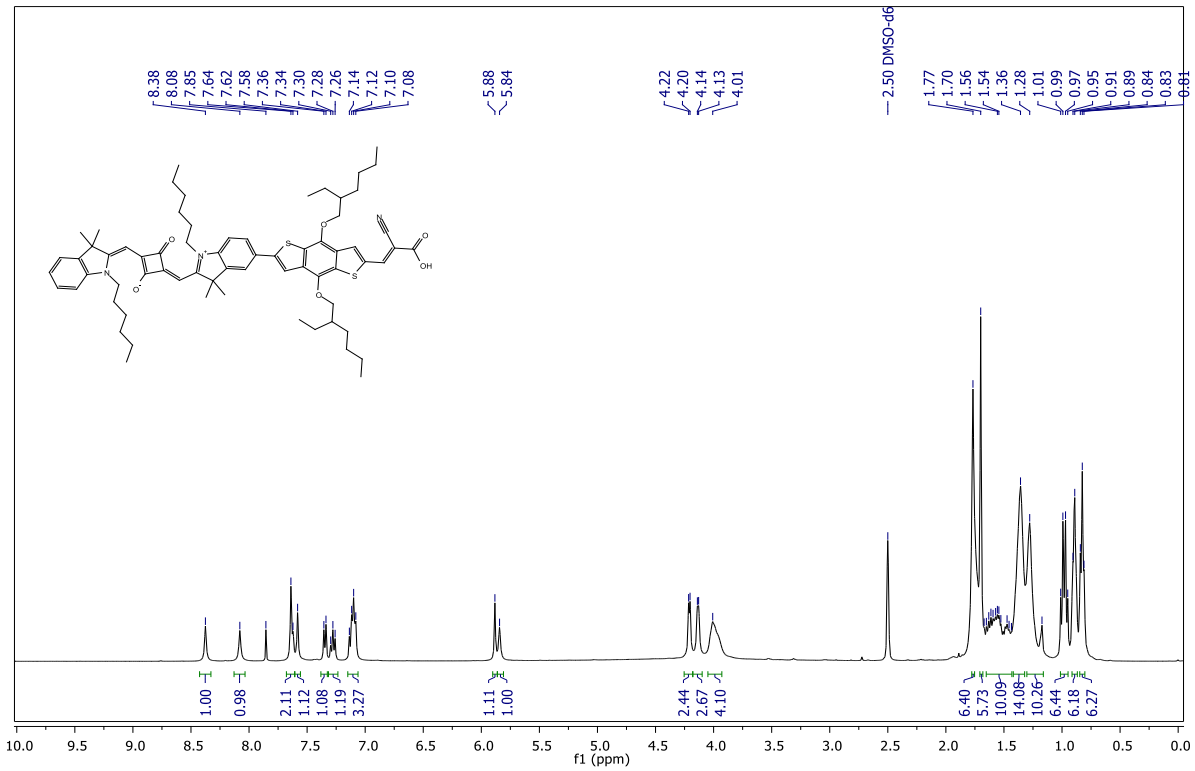

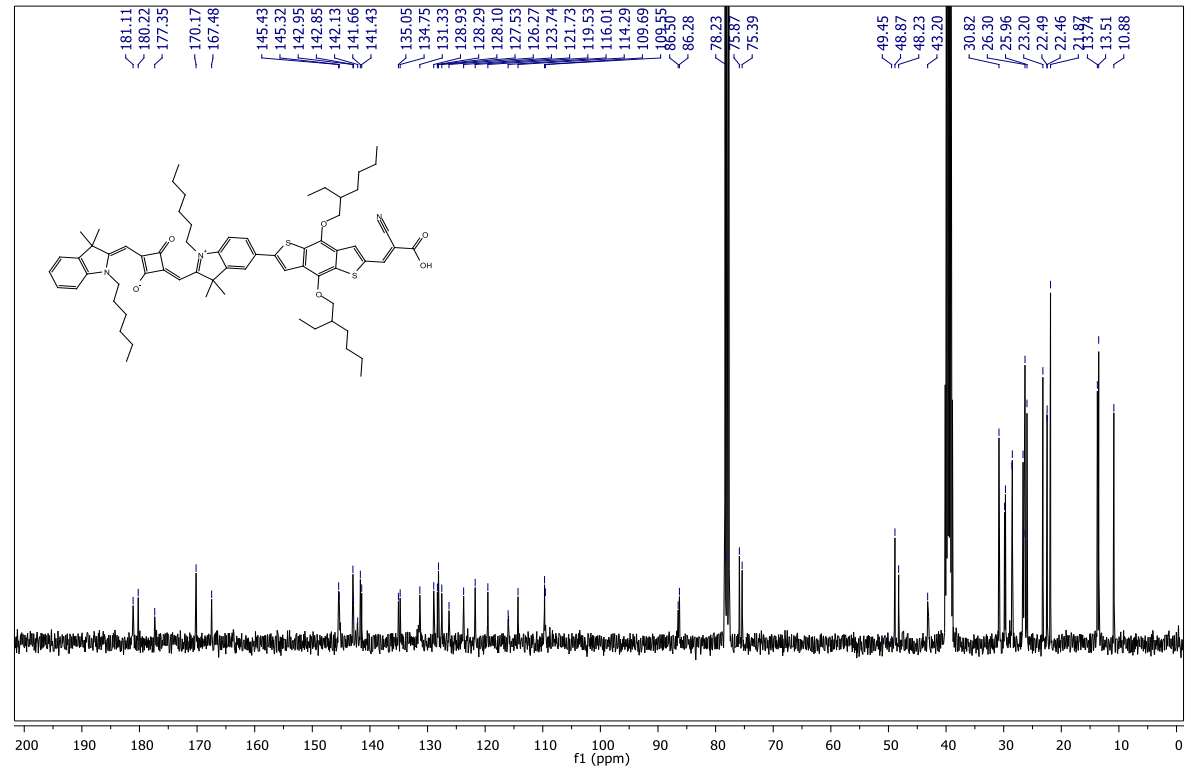

2.6. REFERENCES

(1) Hagfeldt, A.; Boschloo, G.; Sun, L.; Kloo, L.; Pettersson, H. *Chem. Rev.* **2010**, *110*, 6595–6663.

(2) Grätzel, M. *J. Photochem. Photobiol. C Photochem. Rev.* **2003**, *4*, 145–153.

(3) Chen, C.-Y.; Wang, M.; Li, J.-Y.; Pootrakulchote, N.; Alibabaei, L.; Ngoc-le, C.; Decoppet, J.-D.; Tsai, J.-H.; Grätzel, C.; Wu, C.-G.; Zakeeruddin, S. M.; Grätzel, M. *ACS Nano* **2009**, *3*, 3103–3109.

(4) Mathew, S.; Yella, A.; Gao, P.; Humphry-Baker, R.; Curchod, B. F. E.; Ashari-Astani, N.; Tavernelli, I.; Rothlisberger, U.; Nazeeruddin, M. K.; Grätzel, M. *Nat. Chem.* **2014**, *6*, 242–247.

(5) Zhou, N.; Prabakaran, K.; Lee, B.; Chang, S. H.; Harutyunyan, B.; Guo, P.; Butler, M. R.; Timalsina, A.; Bedzyk, M. J.; Ratner, M. A.; Vegiraju, S.; Yau, S.; Wu, C.-G.; Chang, R. P. H.; Facchetti, A.; Chen, M.-C.; Marks, T. J. *J. Am. Chem. Soc.* **2015**, *137*, 4414–4423.

(6) Yao, Z.; Zhang, M.; Wu, H.; Yang, L.; Li, R.; Wang, P. *J. Am. Chem. Soc.* **2015**, *137*, 3799–3802.

(7) Kakiage, K.; Aoyama, Y.; Yano, T.; Oya, K.; Fujisawa, J.; Hanaya, M. *Chem. Commun.* **2015**, *51*, 15894–15897.

(8) Alex, S.; Santhosh, U.; Das, S. *J. Photochem. Photobiol. Chem.* **2005**, *172*, 63–71.

(9) Otsuka, A.; Funabiki, K.; Sugiyama, N.; Yoshida, T.; Minoura, H.; Matsui, M. *Chem. Lett.* **2006**, *35*, 666–667.

(10) Kuster, S.; Sauvage, F.; Nazeeruddin, M. K.; Grätzel, M.; Nüesch, F. A.; Geiger, T. *Dyes Pigments* **2010**, *87*, 30–38.

(11) Pandey, S. S.; Inoue, T.; Fujikawa, N.; Yamaguchi, Y.; Hayase, S. *Thin Solid Films* **2010**, *519*, 1066–1071.

(12) de Miguel, G.; Ziółek, M.; Zitnan, M.; Organero, J. A.; Pandey, S. S.; Hayase, S.; Douhal, A. *J. Phys. Chem. C* **2012**, *116*, 9379–9389.

(13) Li, C.; Wang, W.; Wang, X.; Zhang, B.; Cao, Y. *Chem. Lett.* **2005**, *34*, 554–555.

(14) Mulhern, K. R.; Detty, M. R.; Watson, D. F. *J. Photochem. Photobiol. Chem.* **2013**, *264*, 18–25.

(15) Mann, J. R.; Gannon, M. K.; Fitzgibbons, T. C.; Detty, M. R.; Watson, D. F. *J. Phys. Chem. C* **2008**, *112*, 13057–13061.

(16) Yum, J.-H.; Walter, P.; Huber, S.; Rentsch, D.; Geiger, T.; Nüesch, F.; De Angelis, F.; Grätzel, M.; Nazeeruddin, M. K. *J. Am. Chem. Soc.* **2007**, *129*, 10320–10321.

(17) Shi, Y.; Hill, R. B. M.; Yum, J.-H.; Dualeh, A.; Barlow, S.; Grätzel, M.; Marder, S. R.; Nazeeruddin, M. K. *Angew. Chem. Int. Ed.* **2011**, *50*, 6619–6621.

(18) Delcamp, J. H.; Shi, Y.; Yum, J.-H.; Sajoto, T.; Dell'Orto, E.; Barlow, S.; Nazeeruddin, M. K.; Marder, S. R.; Grätzel, M. *Chem. – Eur. J.* **2013**, *19*, 1819–1827.

(19) Jradi, F. M.; Kang, X.; O'Neil, D.; Pajares, G.; Getmanenko, Y. A.; Szymanski, P.; Parker, T. C.; El-Sayed, M. A.; Marder, S. R. *Chem. Mater.* **2015**, *27*, 2480–2487.

(20) Bae, S. H.; Seo, K. D.; Kim, H. K. *Mol. Cryst. Liq. Cryst.* **2014**, *600*, 116–122.

(21) Bae, S. H.; Seo, K. D.; Choi, W. S.; Hong, J. Y.; Kim, H. K. *Dyes Pigments* **2015**, *113*, 18–26.

(22) Jradi, F. M.; O'Neil, D.; Kang, X.; Wong, J.; Szymanski, P.; Parker, T. C.; Anderson, H. L.; El-Sayed, M. A.; Marder, S. R. *Chem. Mater.* **2015**, *27*, 6305–6313.

(23) Yao, H.; Ye, L.; Zhang, H.; Li, S.; Zhang, S.; Hou, J. *Chem. Rev.* **2016**, *116*, 7397–7457.

(24) Pai, R. K.; N, A. T.; B, H. *RSC Adv.* **2016**, *6*, 23760–23774.

(25) Hao, X.; Liang, M.; Cheng, X.; Pian, X.; Sun, Z.; Xue, S. *Org. Lett.* **2011**, *13*, 5424–5427.

(26) Longhi, E.; Bossi, A.; Di Carlo, G.; Maiorana, S.; De Angelis, F.; Salvatori, P.; Petrozza, A.; Binda, M.; Roiati, V.; Mussini, P. R.; Baldoli, C.; Licandro, E. *Eur. J. Org. Chem.* **2013**, *2013*, 84–94.

(27) Chen, Y.-F.; Liu, J.-M.; Huang, J.-F.; Tan, L.-L.; Shen, Y.; Xiao, L.-M.; Kuang, D.-B.; Su, C.-Y. *J. Mater. Chem. A* **2015**, *3*, 8083–8090.

(28) Hao, X.; Liang, M.; Cheng, X.; Pian, X.; Sun, Z.; Xue, S. *Org. Lett.* **2011**, *13*, 5424–5427.

(29) Ackermann, L.; Vicente, R.; Kapdi, A. *Angew. Chem. Int. Ed.* **2009**, *48*, 9792–9826.

(30) Alberico, D.; Scott, M. E.; Lautens, M. *Chem. Rev.* **2007**, *107*, 174–238.

(31) Battace, A.; Lemhadri, M.; Zair, T.; Doucet, H.; Santelli, M. *Adv. Synth. Catal.* **2007**, *349*, 2507–2516.

(32) Urbani, M.; Medel, M.; Kumar, S. A.; Ince, M.; Bhaskarwar, A. N.; González-Rodríguez, D.; Grätzel, M.; Nazeeruddin, M. K.; Torres, T. *Chem. – Eur. J.* **2015**, n/a-n/a.

(33) Schipper, D. J.; Fagnou, K. *Chem. Mater.* **2011**, *23*, 1594–1600.

(34) Hara, K.; Wang, Z.-S.; Sato, T.; Furube, A.; Katoh, R.; Sugihara, H.; Dan-oh, Y.; Kasada, C.; Shinpo, A.; Suga, S. *J. Phys. Chem. B* **2005**, *109*, 15476–15482.

(35) Li, S.-L.; Jiang, K.-J.; Shao, K.-F.; Yang, L.-M. *Chem. Commun.* **2006**, *0*, 2792–2794.

(36) Geiger, T.; Kuster, S.; Yum, J.-H.; Moon, S.-J.; Nazeeruddin, M. K.; Grätzel, M.; Nüesch, F. *Adv. Funct. Mater.* **2009**, *19*, 2720–2727.

(37) Unger, E. L.; Morandeira, A.; Persson, M.; Zietz, B.; Ripaud, E.; Leriche, P.; Roncali, J.; Hagfeldt, A.; Boschloo, G. *Phys. Chem. Chem. Phys.* **2011**, *13*, 20172–20177.

(38) Yum, J.-H.; Baranoff, E.; Kessler, F.; Moehl, T.; Ahmad, S.; Bessho, T.; Marchioro, A.; Ghadiri, E.; Moser, J.-E.; Yi, C.; Nazeeruddin, M. K.; Grätzel, M. *Nat. Commun.* **2012**, *3*, 631.

(39) Hara, K.; Sato, T.; Katoh, R.; Furube, A.; Ohga, Y.; Shinpo, A.; Suga, S.; Sayama, K.; Sugihara, H.; Arakawa, H. *J. Phys. Chem. B* **2003**, *107*, 597–606.

(40) Wenger, S.; Bouit, P.-A.; Chen, Q.; Teuscher, J.; Censo, D. D.; Humphry-Baker, R.; Moser, J.-E.; Delgado, J. L.; Martín, N.; Zakeeruddin, S. M.; Grätzel, M. *J. Am. Chem. Soc.* **2010**, *132*, 5164–5169.

(41) Frisch, M. J.; Trucks, G. W.; Schlegel, H. B.; Scuseria, G. E.; Robb, M. A.; Cheeseman, J. R.; Scalmani, G.; Barone, V.; Mennucci, B.; Petersson, G. A.; Nakatsuji, H.; Caricato, M.; Fox, D. J.; et al. Gaussian, Inc.: Wallingford, CT, USA*Gaussian 09*, 2009.

(42) Wang, Q.; Moser, J.-E.; Grätzel, M. *J. Phys. Chem. B* **2005**, *109*, 14945–14953.

(43) Longo, C.; Nogueira, A. F.; De Paoli, M.-A.; Cachet, H. *J. Phys. Chem. B* **2002**, *106*, 5925–5930.

(44) Völker, S. F.; Renz, M.; Kaupp, M.; Lambert, C. *Chem. - Eur. J.* **2011**, *17*, 14147–14163.

(45) Mamada, M.; Kumaki, D.; Nishida, J.; Tokito, S.; Yamashita, Y. *ACS Appl. Mater. Interfaces* **2010**, *2*, 1303–1307.

(46) Mei, C.-Y.; Liang, L.; Zhao, F.-G.; Wang, J.-T.; Yu, L.-F.; Li, Y.-X.; Li, W.-S. *Macromolecules* **2013**, *46*, 7920–7931.

Chapter 3

Fluorenylindolenine based Unsymmetrical Squaraine Dyes for Dye-sensitized Solar Cells

3.1. INTRODUCTION

In DSSCs, the near-infrared (NIR) responsive organic dyes are critically needed as they are capable of generating high current density which can improve the performance of the cell.[1,2] Several efforts have been made to improve the efficiency of squaraine dyes by increasing the absorption in the NIR region. Some research groups have successfully enhanced the conjugation by attaching a π-spacer to squaraine dye to increase the length of the molecule which increased the absorption towards longer wavelength.[3–7] This approach was used in the previous chapter where we increased the absorption of squaraine dye by extending the conjugation towards anchoring group by using BDT based π-spacer. The branched alkyl chain on the **RSQ2** helped in controlling the aggregation which produced an efficiency of 6.72% without co-adsorbent. In another approach, the fused π-extended heterocyclic structures such as benz[e]indole,[8–10] benzo[*c,d*]indole,[11,12] and quinoline[13–15] have been used as strong donors in place of indole to shift the absorption to NIR through strong intramolecular charge transfer (ICT). These structures, however, could not convert the increased NIR absorption into better performance due to excessive aggregation. The increased planarity of the molecules due to π-extended moieties makes the aggregation more facile, and hence more exciton deactivation occurs.

The use of alkyl chains to counter aggregation is quite common in DSSCs. Due to their hydrophobic nature, the alkyl chains also help in suppressing recombination of electrons from TiO_2 to the electrolyte. According to its nature of linkage to the conjugated back bone, the alkyl chains can orient either in in-plane direction or out-of-plane direction. The latter can be achieved when two alkyl chains are originating from the same carbon which is a part of a rigid molecular structure. The geminal out-of-plane alkyl chains have been proved to be more successful than in-plane alkyl chains in controlling aggregation as it avoids close π-π stacking of molecules. Several dyes have been reported where geminal out-of-plane alkyl chains are installed on sp^3 carbon on the conjugated framework. The efficiency of 7.3% was obtained with the incorporation of cyclopentadithiophene (CPDT) as π-spacer in squaraine dye which utilized out-of-plane hexyl chains to control aggregation as well as enhance the absorption in NIR region through extended conjugation.[6] The result indicates that both electronic and steric factors are important in dye design and a certain modification in structural features of the dyes may lead to the significant improvement in cell efficiency. An unsymmetrical squaraine

dye **DTS-CA**, which has a squaraine unit linked with silolodithiophene (DTS) π–spacer possessing out-of-the plane ethylhexyl chains, exhibits an efficiency of 8.9%.[3] Based on these findings we investigated the possibility of increasing the conjugation in squaraine dye while maintaining the planarity of the molecule to enhance the absorption towards the NIR region, and also include out-of-plane branched alkyl chains to control aggregation on TiO_2 surface. To this end, we explored a strategy to fuse fluorene moiety with indolenine, which can provide an opportunity to incorporate two sets of germinal out-of-plane alkyl chains on squaraine dye.

Fluorene is an aromatic biphenyl compound, fused together in a rigid structure which makes it planar and increases aromaticity. The fluorene has active methylene CH_2 center which can be functionalized easily with geminal alkyl chains using a strong base. Fluorene moiety with out-of-plane alkyl chains have frequently been used in DSSC as well as in other fields of organic electronics.[16–21] Apart from fluorene, the indolenine unit of squaraine dye itself provides the opportunity of attaching out-of-plane alkyl chains as it also possesses sp3-C center. However, the protocol to include the out-of-plane chain on indolenine is quite different from fluorene. Recently, squaraine dyes based on indolenine unit having out-of-plane C-8 and C-10 alkyl chain on the sp^3-C were reported by our group. The dyes helped effectively in reducing aggregation and enhancing surface passivation which gave the efficiency up to 9.1%.[22] Similar indolenine unit was used in core-unsymmetrical, heterotraingulene squaraine dyes which helped to obtain the efficiency of 6.73% without coadsorbent.[23] In this chapter, we report the synthesis of a fused donor for squaraine dyes where fluorene moiety is fused with indolenine to give fluorenylindolenine donor. This donor provides two sets of out-of-plane alkyl chains, one centered on fluorene and other on indolenine, which extends in opposite directions. The fused structure also provides π-extension which helps to increase conjugation in the molecule. Hence, utilizing this donor in squaraine dye can help to avoid to aggregation as well as extend the conjugation in NIR region. A series of four dyes, **XSQ1-4**, were synthesized using this donor. **XSQ1** and **XSQ2** contained indole units towards anchoring side with N-methylated and N-hexylated fluorenylindolenine donor, respectively. **XSQ3** and **XSQ4** contain benz[e]indole unit towards anchoring side with N-methylated and N-hexylated donor, respectively to systematically investigate their effect on various electronic properties of dyes and DSSC parameters.

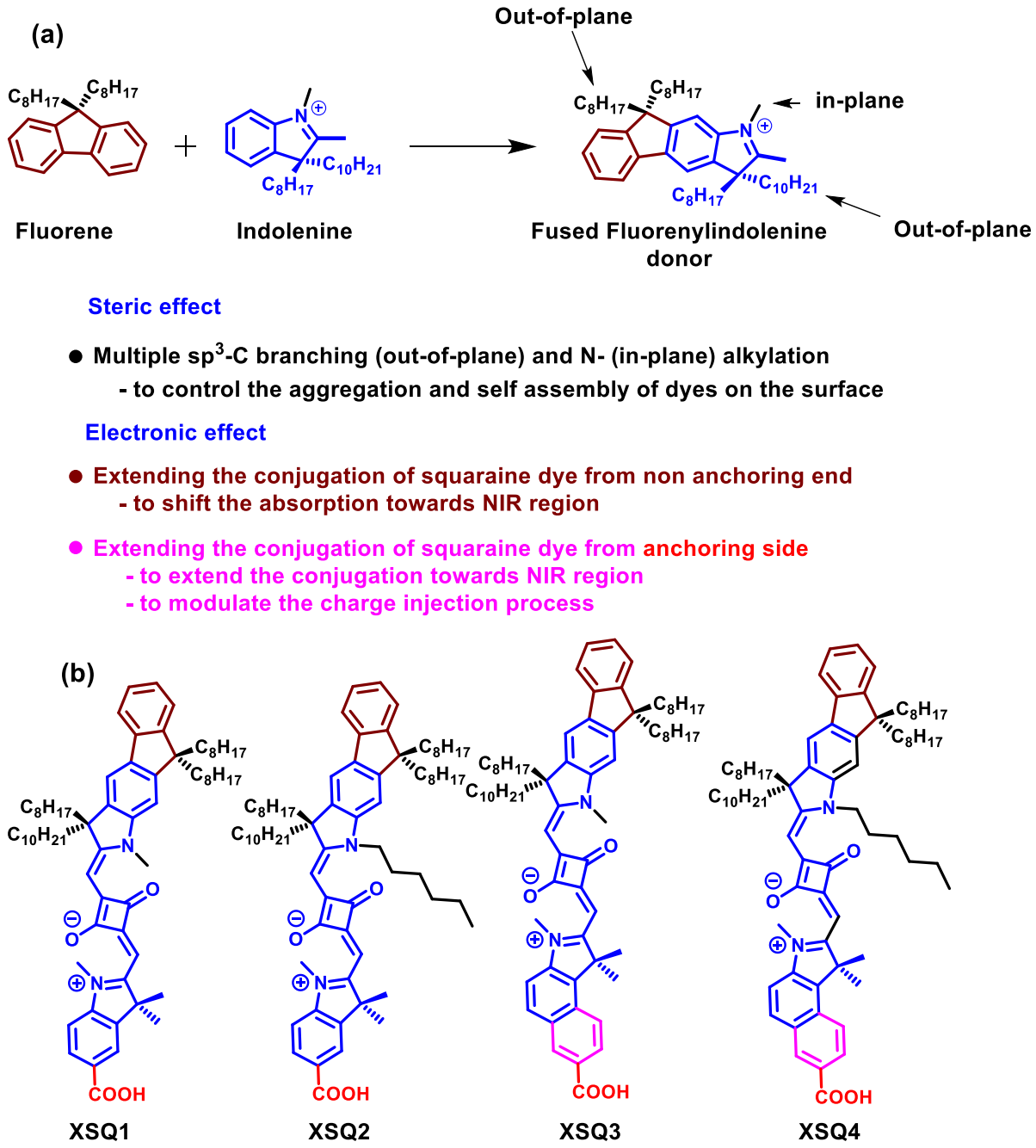

Figure 1. (a) Design of fused fluorenylindolenine based donor and (b) Unsymmetrical squaraine dyes **XSQ1-4**.

3.2. RESULTS AND DISCUSSION

3.2.1. Synthesis

The synthesis of the dyes **XSQ1-4** is illustrated in **Scheme 1** and **2**.

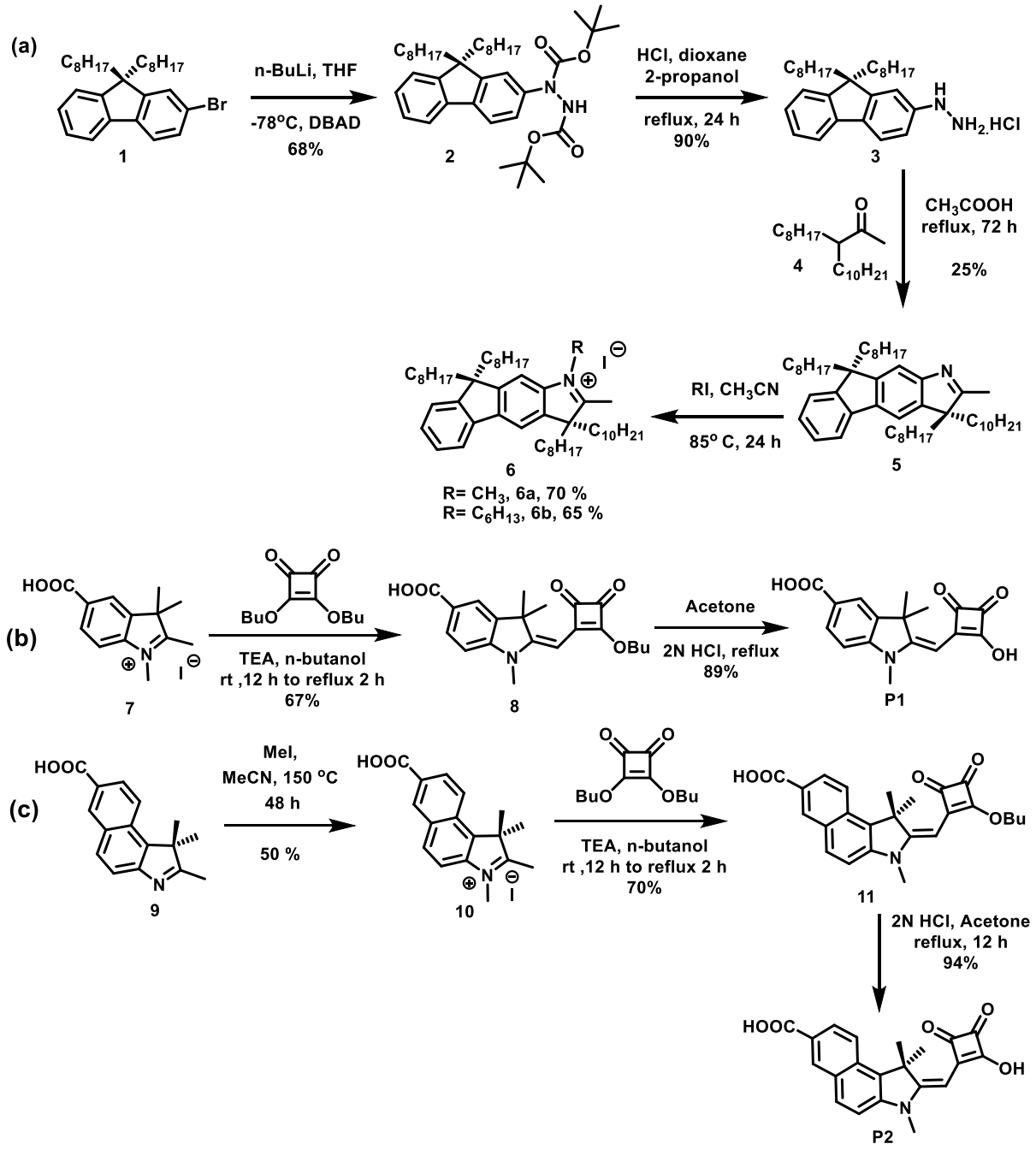

Scheme 1. (a) Synthesis of fluorenylindolium salts **6a** and **6b**, (b) semi-squaric acid **P1,** (c) semi-squaric acid **P2**.

The precursor **1** was treated with *n*-butyllithium in anhydrous THF at -78 ºC followed by addition of dibutylazadicarboxylate (DBAD) which gave *tert*-BOC protected hydrazine derivative **2**. The treatment of **2** with hydrochloric acid in dioxane and isopropanol mixture afforded the deprotected hydrazine derivative **3** in good yield. The compound **3** was refluxed with branched methyl ketone **4** in acetic acid to give fluorenylindolenine **5** in moderate yield

which was heated with methyl iodide and hexyl iodide in a sealed tube to afford the corresponding fluorenylindolium salts **6a** and **6b**, respectively. N-methylated carboxy[e]indolium iodide, **7** was treated with 3,4-dibutoxy-3-cyclobutene-1,2-dione in the presence of Et_3N at room temperature overnight followed by reflux for 2 h to yield semisquarate **8**. The compound **8** was refluxed with 2N HCl in acetone to provide semisquaric acid (**P1)** in quantitative yields. The carboxybenz[e]indole **9** was reacted with methyl iodide to give N-methylated carboxybenz[e] indolium salt **10** which gave the semisquaric acid **P2** in the same fashion as described above. In the final step, the semi-squaric acid **P1** was refluxed with **6a** in n-butanol/toluene mixture under azeotropic distillation of water employing Dean−Stark apparatus to give squaraine dyes **XSQ1**, whereas the dye **XSQ2** was obtained by reacting **P1** with **6b**. Similarly, the dyes **XSQ3** and **XSQ4** were obtained by treating semisquaric acid **P2** with **6a** and **6b**, respectively. All the dye were thoroughly characterized by ^{1}H-NMR, ^{13}C-NMR, and mass spectrometric techniques.

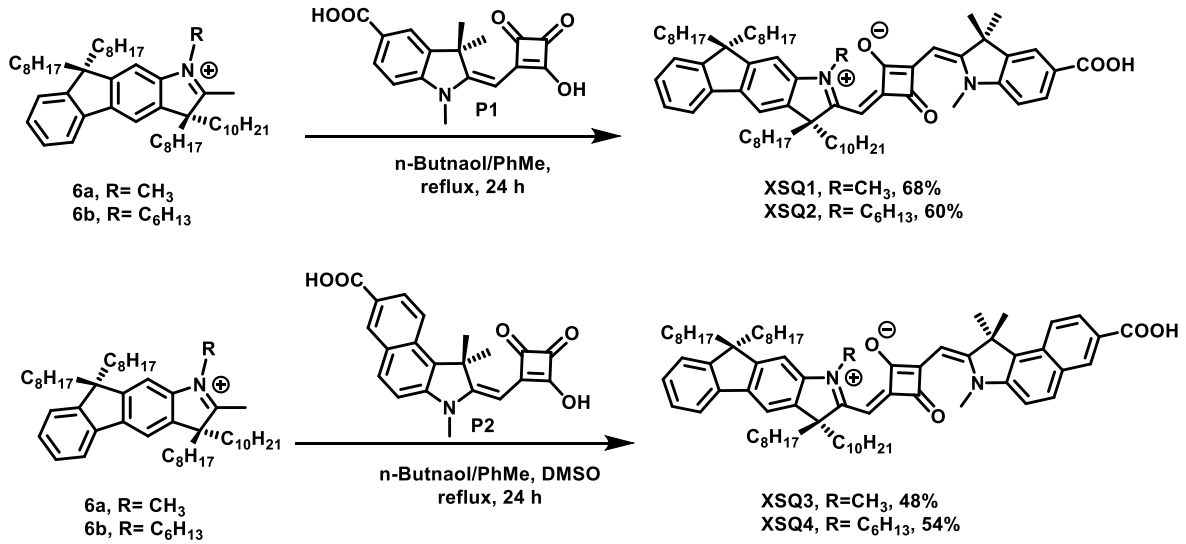

Scheme 2. Synthetic route to unsymmetrical squaraine dyes **(XSQ1-4)**.

3.2.2. Optical and Electrochemical Properties

The UV-Vis absorption and emission spectra of **XSQ1-4** in CH_2Cl_2 solution are shown in **Figure 2a** and **2b.** All the dyes displayed intense absorption ($\varepsilon \geq 10^5$ $M^{-1}cm^{-1}$) towards the far-red region in solution due to efficient ICT. **XSQ1-2** exhibited the absorption spectra ranging from 545 to 698 nm with maxima (λ_{max}) at 665 and 666 nm for **XSQ1** and **XSQ2** respectively. **XSQ3** and **XSQ4** absorb majorly between 553 to 711 nm and showed λ_{max} at

679 and 681 nm respectively which is red-shifted by ca.15 nm in comparison to **XSQ1-2**. A small shoulder peak due to vibronic coupling is also observed for each dye in their absorption spectrum.

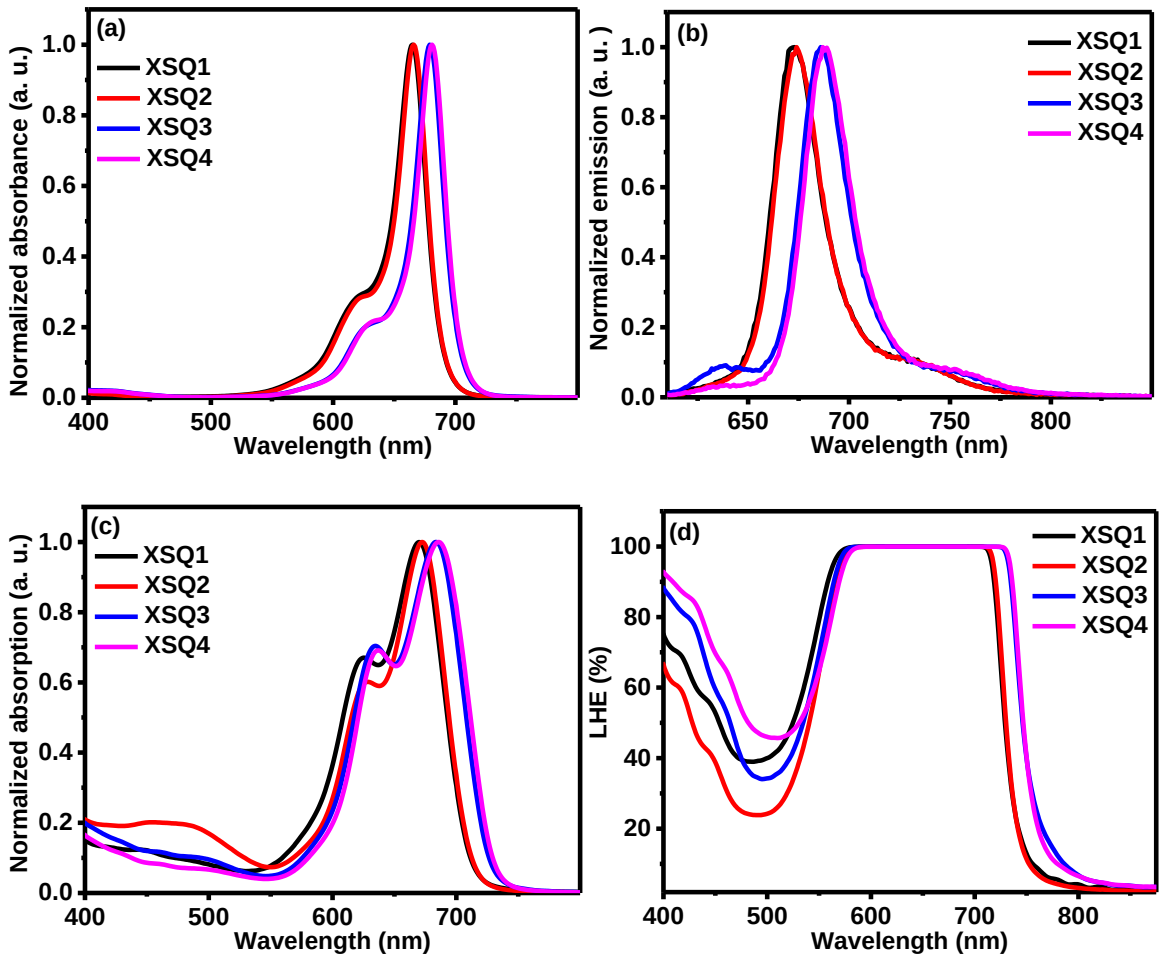

Figure 2. (a) Normalized absorption spectra, (b) Normalized emission spectra excited at 600 nm, (c) Normalized absorption spectra on TiO_2, and (d) Light harvesting efficiency of **XSQ** dyes.

In comparison to its parent squaraine dye **SQ1** (λ_{max} = 640 nm),[22] the red shift of 25 nm was observed for **XSQ1-2** due to the extended conjugation by fused fluorenylindolenine. In case of **XSQ3-4**, this shift increased to 40 nm due to the additional extension of conjugation by benz[e]indole moiety. To understand the assembly of **XSQ1-4** dyes on TiO_2, the bare TiO_2 electrodes were dipped for 15 minutes into the CH_2Cl_2 solutions (0.1 mM) of the dyes, and UV-Vis spectra were recorded (**Figure 2c**). The absorption spectra of dyes on TiO_2 film showed peak broadening due to aggregation and interaction between TiO_2 and carboxylic

group of the dyes. **XSQ1-2** showed extended absorption on TiO_2 ranging between 550 nm to 715 nm whereas **XSQ3-4** covered the spectral range from 550 nm to 730 nm. The λ_{max} on the TiO_2 film is slightly red-shifted to about 5 nm compared to the solution, and an additional peak at shorter wavelength appeared probably due to H-type aggregation on TiO_2 which leads to dimer formation.

Table 1. Optical and electrochemical data of **XSQ** dyes

Dyes	$^{Abs}\lambda_{max}$ (nm)[a]	$^{Emi}\lambda_{max}$ (nm)[b]	λ_{max}/ TiO_2 (nm)[c]	$^{dimer}A/^{mono}A$	$\varepsilon \times 10^5$ ($M^{-1}cm^{-1}$)[d]	$E_{g/DFT}$ (eV)[e]	E_{HOMO} (V vs NHE)[f]	$E_{0\text{-}0}$ (eV)[g]	E_{LUMO} (V vs NHE)[h]
XSQ1	665	673	625, 670	0.67	2.2	2.19	0.78V	1.85	-1.09
XSQ2	666	674	628, 672	0.60	3.0	2.19	0.75	1.85	-1.10
XSQ3	679	686	635, 684	0.70	2.4	2.18	0.67	1.82	-1.15
XSQ4	681	687	637, 686	0.69	3.5	2.17	0.66	1.81	-1.15

[a]UV−Vis absorption in CH_2Cl_2. [b]Emission studies in CH_2Cl_2 (excited at 600 nm). [c]On thin film of TiO_2, thickness = 6 μm, dipping time = 15 min, and [XSQ] = 0.1 mM in EtOH. [d]Molar extinction coefficient ε. [e]Band gap calculated by DFT. [f]E_{HOMO} of XSQ1−4 in CH_2Cl_2, Fc/Fc^+ was used as the external standard and potential measured vs. Fc/Fc^+ (eV) was converted to NHE (V) by addition of 0.63 V. [g]$E_{0\text{-}0}$ was deduced at the intersection of absorption and emission spectra using equation $E_{0\text{-}0}$ (eV) = $1240/\lambda_{0\text{-}0}$. [h]$E_{LUMO}$ levels were measured by subtracting E_{HOMO} from $E_{0\text{-}0}$.

The ratio of the optical density of the monomer to the dimer ($^{dimer}A/^{monomer}A$) is given in **Table 1,** and it helped in concluding the extent of aggregation for each dye on the TiO_2 surface, which revealed that **XSQ2** is the least aggregated in comparison to other dyes. Apart from the peaks at low energy region, there is low-intensity absorption of high energy (400-550 nm) which suggests a good coupling of higher excited state orbitals with TiO_2. The light harvesting efficiency (LHE = $1\text{-}10^{-A}$) was calculated by measuring absorption in transmittance mode of dye adsorbed film which was obtained by immersing the TiO_2 film in

the dye solution for an extended period of 6 h. LHE expresses the ability of sensitizers to absorb photons on the TiO_2 thin film across the visible-NIR spectrum of solar irradiation (**Figure 2d**). All the dyes showed more than 90% LHE between 560 nm to 730 nm, and **XSQ3-4** showed 20 nm red-shifted onset compared to **XSQ1-2**. The LHE onset was found at ca. 750 nm for **XSQ1**-2 and 775 nm for **XSQ3**-4 which shows that dyes have potential to give a response in NIR region. The mixed LHE response was observed in the visible region between 400 to 550 nm where **XSQ4** showed maximum intensity.

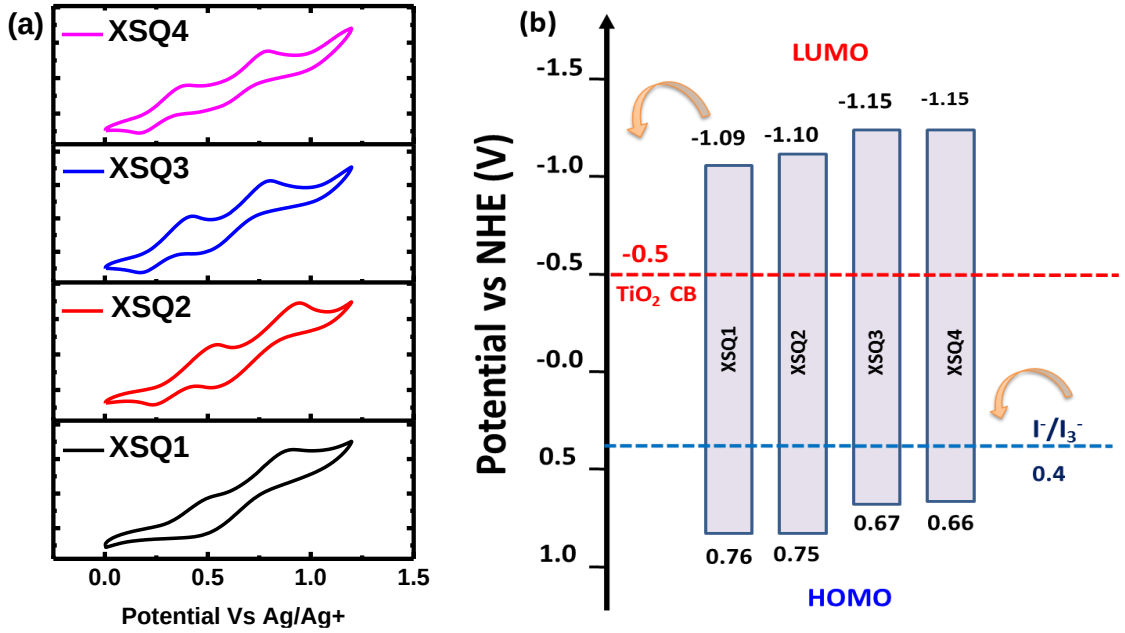

Figure 3. (a) Cyclic Voltammogram of **XSQ** dyes measured in CH_2Cl_2 (b) Energy level diagram for **XSQ** dyes with DSSC device components.

In order to examine the feasibility of electron transfer at TiO_2/dye/electrolyte interfaces, the redox potentials of **XSQ** dyes were measured by cyclic voltammetry (CV) in a CH_2Cl_2 solution with tetrabutylammonium perchlorate ($TBAClO_4$) as electrolyte and ferrocene as an external reference. The cyclic voltammograms of **XSQ** dyes exhibit two-electron oxidation peaks, which are characteristic of squaraine dyes (**Figure 3a**). The HOMO energy levels (E_{HOMO}) of the dyes were calculated from the oxidation onset on the CV curve and found to be at 0.76 V (**XSQ1**), 0.75 V (**XSQ2**), 0.67 V (**XSQ3**) and 0.66 V (**XSQ4**) vs. NHE, which lie well below the electrochemical potential of I^-/I_3^- (0.4 V vs. NHE) to provide enough driving force ($-\Delta G_{reg} > 0.15$ eV)[24] for dye regeneration (**Table 1**). The HOMO energy levels of **XSQ3-4** were 90 mV above the **XSQ1-2**, which could be attributed to the

stronger electron releasing effect of carboxybenz[e]indole unit present on anchoring end of the **XSQ3-4**. The LUMO energy levels (E_{LUMO}) were calculated by subtracting $E_{0\text{-}0}$ from E_{HOMO} and are found at -1.09 V (**XSQ1**), -1.10 V (**XSQ2**),-1.15 V (**XSQ3**),-1.15 V (**XSQ4**). These values lie well above the conduction band edge of TiO_2 (0.5 V vs. NHE) which predicts efficient charge injection ($-\Delta G_{inj} > 0.2$ eV) into TiO_2.[25]

3.2.3. Computational Studies

To deeply understand the structural, electronic, and optical properties of **XSQ** dyes, quantum mechanical calculation were carried out using density functional theory (DFT) at B3LYP/6-31G (d,p) level in Gaussian 09.[26] The optimized geometry of **XSQ2** and **XSQ4** dye are shown in **Figure 4**. The distance between the lower branched chain and the terminal atom of the anchoring group (-COOH) was calculated to be at 14.7 and 16 Å for **XSQ2** and **XSQ4** respectively. Since the dimension of CDCA molecule (14.2 Å) is slightly lesser than the distance between the lower branched chain and anchoring groups, there is a possibility that CDCA molecules can occupy the space under the dye molecules when co-adsorbed on TiO_2, which may help to passivate the TiO_2 surface more efficiently. The top view of these molecules shows that the alkyl chains are stretched up to 18 and 20 Å in out of the plane direction towards opposite side, effectively covering the π-surface which can help in controlling aggregation of dyes on the TiO_2 surface.

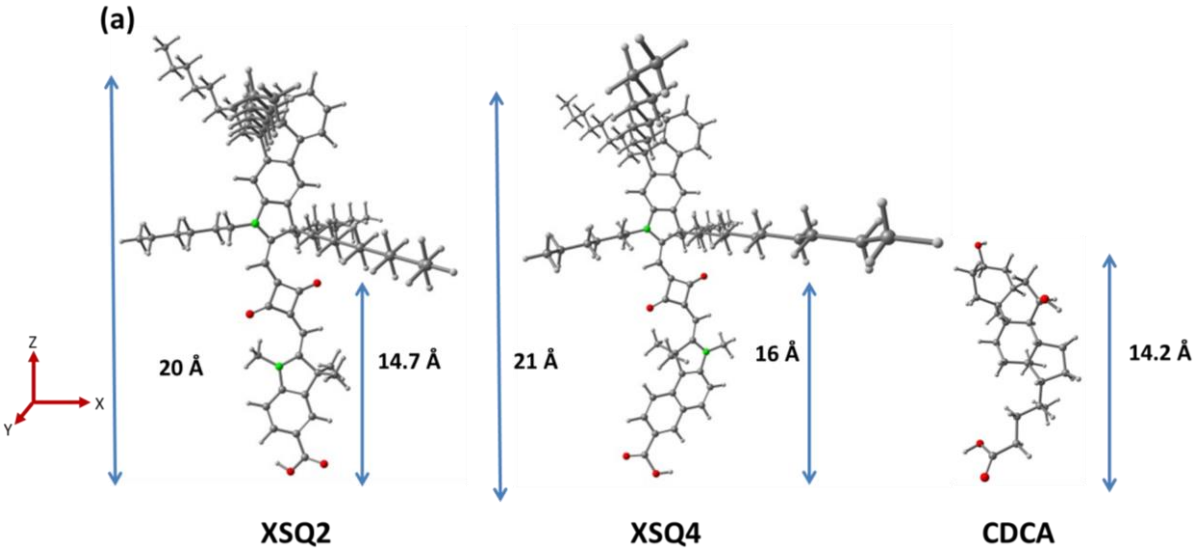

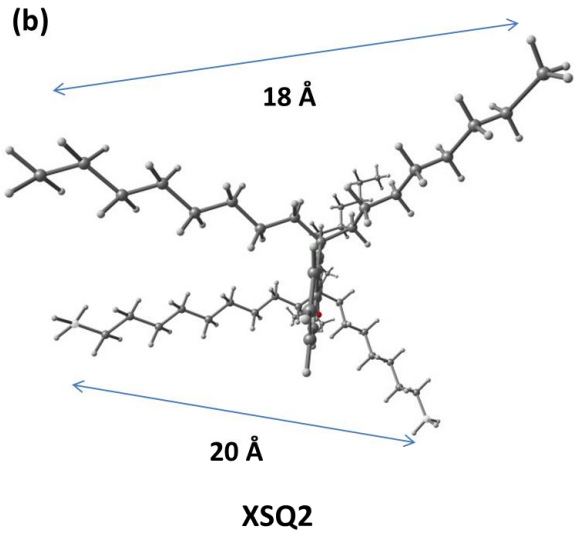

Figure 4. Optimized geometry structure of **XSQ2** and **XSQ4** and CDCA a) lateral view b) top view.

The suitable spatial distributions of the frontier molecular orbitals (FMO) are crucial for facilitating the electron-transfer processes. Ideally, the highest occupied molecular orbitals (HOMO) should be away from the TiO_2, and lowest unoccupied molecular orbitals (LUMO) should be as close as possible to the TiO_2 for efficient electron injection. The electron density distribution in the frontier molecular orbitals (HOMO and LUMO) of the dyes under investigation is shown by isodensity plots in **Figure 5**.

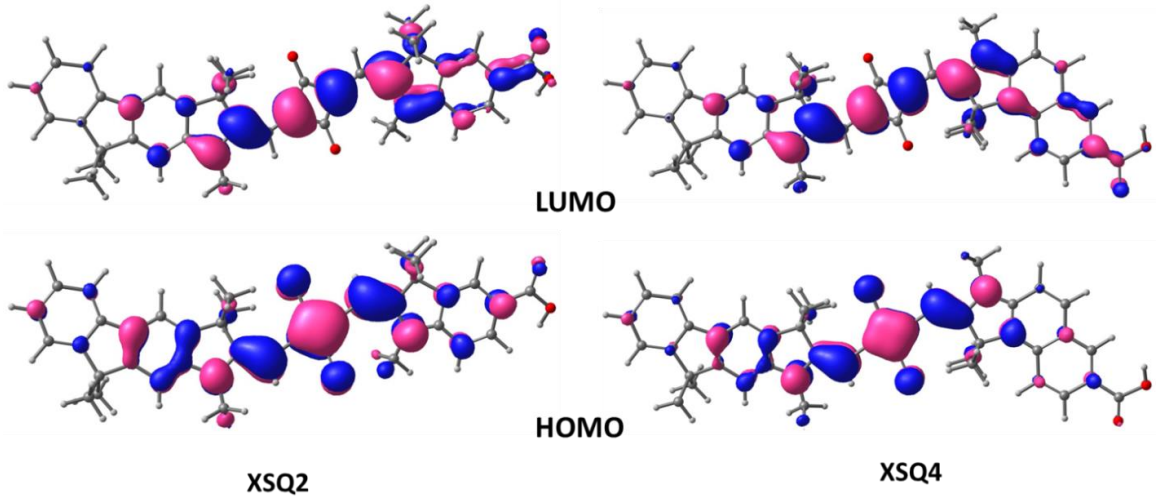

Figure 5. Isodensity plots of **XSQ2** and **XSQ4** (alkyl chains are removed for clarity).

The HOMO of both indole (**XSQ1** and **XSQ2**) and benzindole dyes (**XSQ3** and **XSQ4**) is predominantly delocalized over central squaraine unit with a slight spread in fluorenylindolenine unit. The LUMO shows an apparent shift in the electron density from the fluorenylindolenine unit towards anchoring group for both the dyes which is significant for the facile charge transfer. It also ensures the good electronic coupling between the excited state dye and TiO_2 due to the presence of sufficient electron density on the anchoring group which is important for the efficient injection of electrons from the excited dye molecule into the conduction band of the TiO_2. However, looking at the optimized structure, it can be observed that benzindole based dyes (**XSQ2**-4) have more bent structure compared to **XSQ1-2**. We suspect that this bending may lead to non-directionality in molecular dipole which was confirmed by comparing the calculated dipole moments of **XSQ1** (10.0 D) and **XSQ2** (10.6 D) with **XSQ2** (7.4 D) and **XSQ4** (7.3 D) (**Table 2**).

Table 2. Calculated dipole moments of the XSQ dyes[a]

Dye	**Dipole components (Debye)**			
	μ_x	μ_y	μ_z	Total
XSQ1	-4.7	-2.0	8.7	10.0
XSQ2	-4.3	-3.0	9.2	10.6
XSQ3	5.6	0.3	4.7	7.4
XSQ4	5.4	-0.2	4.9	7.3

[a]The *z*-axis corresponds to the TiO_2 surface normal

3.2.4. Photovoltaic Performance

The photovoltaic measurements of the DSSCs fabricated using **XSQ1**-4 dyes were done under irradiance of 100 mW cm^{-2} simulated AM 1.5G sunlight. The current density-voltage (*J-V*) plots are shown in **Figure 6,** and the data are summarized in **Table 3**. In the absence of coadsorbent, all the dyes gave moderate DSSC performance, with **XSQ2** dye exhibiting the maximum PCE of 4.12% with J_{SC} of 9.22 mA cm^{-2} and V_{OC} of 0.636 V whereas **XSQ3** showed the minimum efficiency of 2.36% with J_{SC} of 5.51 mA cm^{-2}, V_{OC} of 0.618 V and *ff* of 69.23%. **XSQ1** and **XSQ4** showed the efficiency of 3.34% and 3.98% respectively.

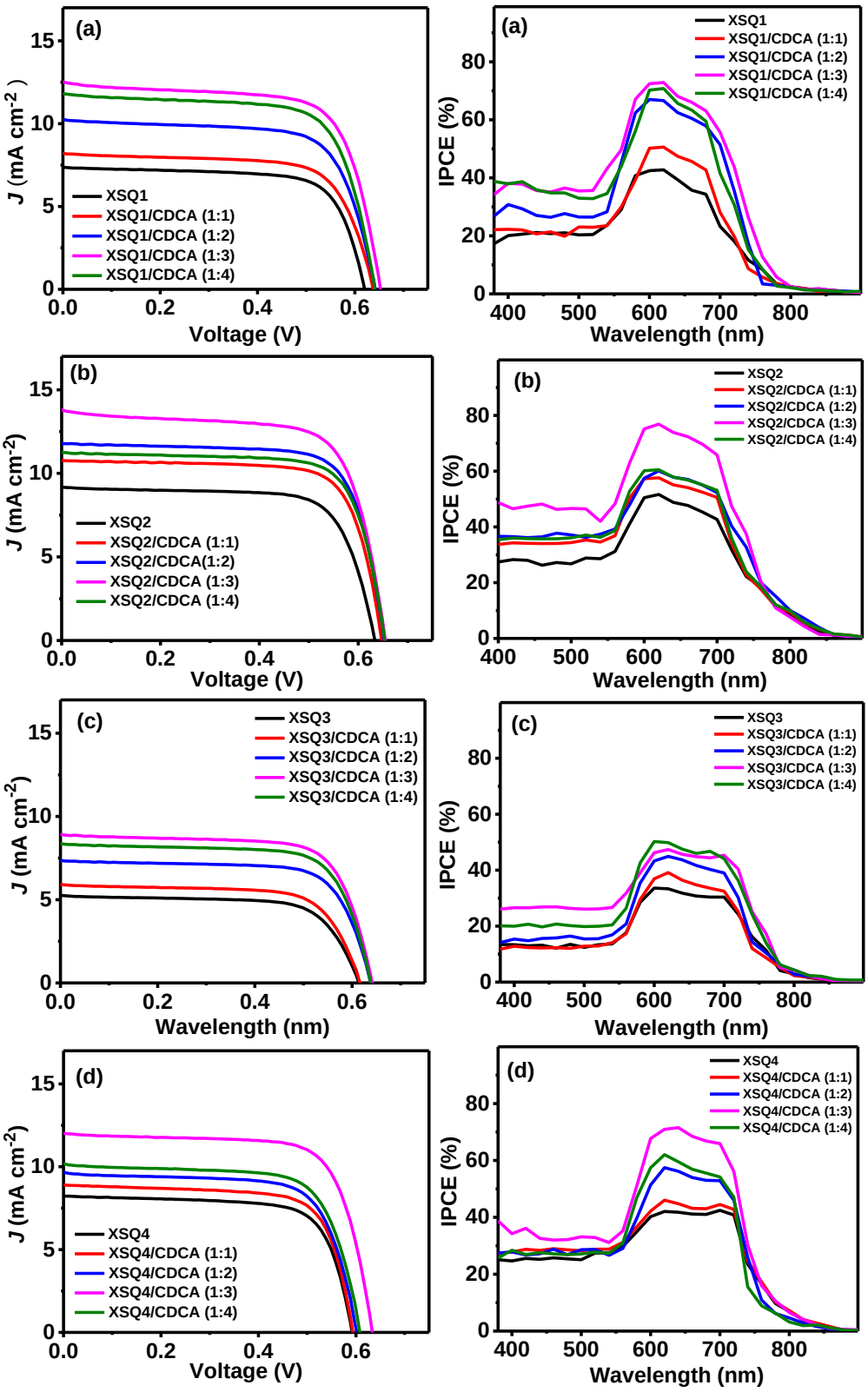

Figure 6. *J-V* plots and IPCE curve of a) **XSQ1**, b**) XSQ2**, c) **XSQ3** and d) **XSQ4** sensitized cells with varying CDCA equivalents. (Dipping time = 12 h, TiO_2 active area = 0.22 cm^2).

Though the V_{OC} of these cells varies slightly, the significant variation in the performance of the dyes comes from the difference in their J_{SC}. The gradual increase in the amount of co-adsorbent (CDCA) improved the performance of the cells, and all the **XSQ** dyes gave their best photovoltaic properties at 3 equiv CDCA. **XSQ2** showed the highest efficiency among all the dyes with PCE of 6.57% mostly due to ca. 50% increment in J_{SC} (13.99 mA cm^{-2}) after addition of 3 equiv of the CDCA. The trends of J_{SC} can be correlated to IPCE spectra of the cells **(Figure 6,** left**)**. The IPCE spectra of the **XSQ** dyes showed a good response in the region of 550 nm to 700 nm with onset up to ca. 800 nm. IPCE spectra also shows a moderate response in the visible region between 400 to 550 nm. It was observed that, by increasing the concentration of CDCA up to 3 equiv, J_{SC} was increased significantly without affecting the distribution of IPCE response from the aggregated state. This indicated that the formation of the larger aggregates was decreased and the smaller aggregates could effectively participate in the charge injection process. A moderate decrease in V_{OC} and J_{SC} upon further increasing the CDCA concentration indicated depletion of dye amount on the TiO_2 surface.

Table 3. Photovoltaic performance of **XSQ** dyes with and without CDCA (the results of best five devices for each dye with a deviation are summarized)[a]

Dye	V_{OC} (V)	J_{SC} (mA cm^{-2})	*ff* (%)	η (%)	Dye loading (mol cm^{-2})[c]
XSQ1	0.621 ± 0.003	7.20 ± 0.11	70.1 ± 0.13	3.21± 0.13	8.68×10^{-8}
XSQ1/CDCA (1:1)	0.638 ± 0.002	8.21 ± 0.14	70.1± 0.6	3.67 ± 0.11	-
XSQ1/CDCA (1:2)	0.64 1 ± 0.002	10.30 ± 0.15	70.3 ± 0.2	4.63± 0.1	-
XSQ1/CDCA (1:3)	0.652 ± 0.003	12.60 ± 0.13	70.0 ± 0.4	5.75 ± 0.15	8.06×10^{-8}
XSQ1/CDCA (1:4)	0.641 ± 0.002	11.88 ± 0.11	70.5 ± 0.5	5.36 ± 0.13	-
XSQ2	0.634 ± 0.002	9.21 ± 0.20	71.1± 0.2	4.12± 0.12	7.81×10^{-8}
XSQ2/CDCA (1:1)	0.647 ± 0.003	10.70 ± 0.21	71.2± 0.3	4.92 ± 0.11	-
XSQ2/CDCA (1:2)	0.653 ± 0.002	11.20 ± 0.18	71.6 ± 0.2	5.23 ± 0.16	-

XSQ2/CDCA (1:3)	0.657 ± 0.002	13.80 ± 0.19	71.2 ± 0.3	6.42 ± 0.15	7.11×10^{-8}
XSQ2/CDCA (1:4)	0.653 ± 0.003	11.11 ± 0.2	71.3± 0.4	5.17 ± 0.14	-
XSQ3	0.616 ± 0.002	5.30 ± 0.21	69.1 ± 0.13	2.25 ± 0.11	1.36×10^{-7}
XSQ3/CDCA (1:1)	0.618± 0.002	5.95 ± 0.15	70.0± 0.23	2.57 ± 0.12	-
XSQ3/CDCA (1:2)	0.639± 0.003	7.38 ± 0.16	70.1 ± 0.3	3.31± 0.11	-
XSQ3/CDCA (1:3)	0.643 ± 0.002	8.98 ± 0.20	70.2 ± 0.2	4.05 ± 0.14	1.10×10^{-7}
XSQ3/CDCA (1:4)	0.641± 0.003	8.38 ± 0.23	69.8 ± 0.5	3.75 ± 0.15	-
XSQ4	0.591 ± 0.002	8.30 ± 0.21	68.9± 0.4	3.38± 0.16	6.27×10^{-8}
XSQ4/CDCA (1:1)	0.594± 0.002	8.91 ± 0.25	69.2± 0.2	3.66 ± 0.17	-
XSQ4/CDCA (1:2)	0.602± 0.003	9.7 1 ± 0.17	68.7 ± 0.3	4.01 ± 0.12	-
XSQ4/CDCA (1:3)	0.633 ± 0.002	12.1 ± 0.18	70.1 ± 0.4	5.37 ± 0.13	6.22×10^{-8}
XSQ4/CDCA (1:4)	0.608± 0.002	10.21 ± 0.21	69.4± 0.5	4.31 ± 0.14	-

[a]Photovoltaic performance of XSQ cells, the thickness of electrode: 8 + 4 μm (transparent + scattering) layer of TiO_2, Electrolyte: iodolyte Z-50 from Solaronix. [Dye] = 0.1 mM in EtOH, dipping time = 12 h, Active area of 0.22 cm^2 and measurements were carried out under 1 sun intensity (100 mW cm^{-2}). [c]Dye loading was calculated for cells without CDCA and with CDCA (3 equiv).

Since all the dyes gave their best performance in the presence of 3 equiv CDCA, *J-V* and IPCE of these devices were studied in detail to explain the effect of CDCA on dye assembly (**Figure 8**). The dye loading amount was also calculated for all the devices, without CDCA, and with 3 equiv CDCA.

In the presence of 3 equiv CDCA, **XSQ2** exhibited the best IPCE profile with 76% IPCE at 620 nm and ca. 40% IPCE between 400-500 nm. **XSQ1** and **XSQ4** displayed similar IPCE trace, the result of which could be observed in their similar J_{SC} values of 12.73 and 12.28 mA cm^{-2} respectively.

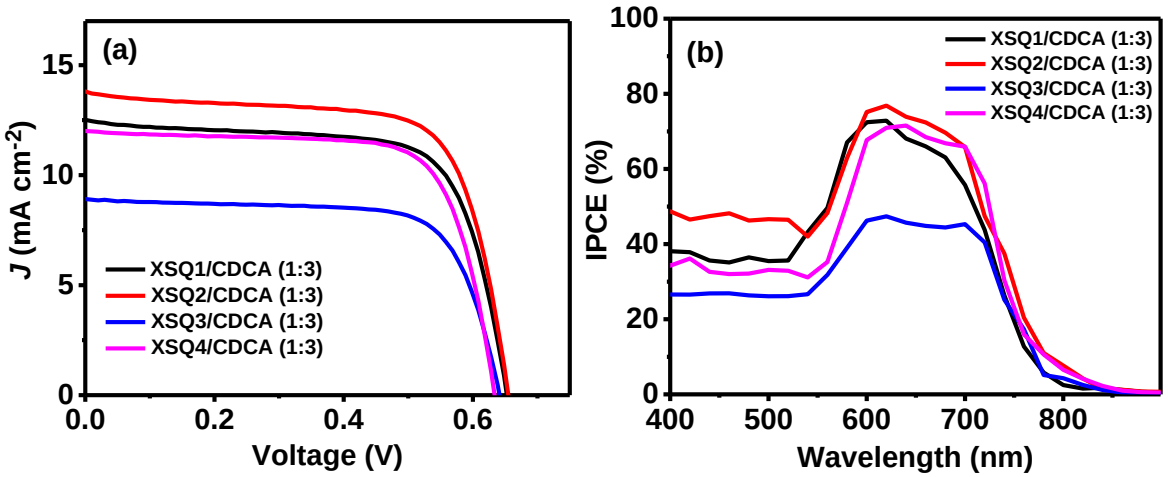

Figure 8. (a) *J*−*V* curve and (b) IPCE spectrum of **XSQ1-4** sensitized cells with 3 equiv CDCA.

Due to greater IPCE in the region of 400 to 550 nm the **XSQ2** surpassed other dyes and produced J_{SC} of 13.99 mA cm^{-2}. **XSQ3** revealed the poorest response managing up to 40% IPCE only at between 600 to 720 nm and around 22% between 400-550 nm. It is interesting to note that the decrease in the amount of adsorbed dyes after addition of 3 equiv CDCA is very low, ca. 8-19%, whereas the increase in J_{SC} is significantly high, 44-74%.For example, in case of **XSQ2**, the decrease in dye loading is only 8.9% after addition of 3 equiv CDCA whereas the increase in J_{SC} is ca. 48%. Similarly, **XSQ2** observed 74% increase in J_{SC} in the presence of 3 equiv CDCA. It shows that CDCA is able to control aggregation without reducing the dye amount significantly. These observations can be explained if we take into the account the possibility that instead of replacing the dye, CDCA is taking up the void spaces between the dyes. The DFT calculations also support this observation which shows that the branched alkyl chains are stretching up to 20 Å in out-of-the plane direction and may create enough gap for CDCA molecule to anchor between dyes. The distance between the lower branch chain and the terminal oxygen atom of carboxylic acid (14.7 Å and 16 Å for **XSQ2** and **XSQ4** respectively) is also greater than the length of CDCA (14.2 Å). Hence, it is conceivable that CDCA molecule might just anchor between the dyes and the dye amount basically remains the same. Such preferential self-assembled monolayers of dyes act as a hydrophobic barrier layer, due to the presence of out-of-plane alkyl groups at sp^3-C atoms and alkyl chains at N-atom, which avoids the charge recombination of electrons from TiO_2 to the oxidized electrolyte. It is also noted that dyes with N-hexyl alkyl chains showed better efficiency than N-methylated dyes as **XSQ1** showed the η of 5.90%, which is lower

compared to **XSQ2**. A similar trend was observed for benz[e]indole based dye where **XSQ3** showed η of 4.19% which is lower than the efficiency of **XSQ4** (η = 5.5%) based cell. This observation suggests that N-hexyl chain could help the dyes assemble favorably on to the TiO_2 surfaces besides passivating the surface. Additionally, the V_{OC} values of indole based **XSQ1-2** are slightly higher than **XSQ3-4** ($\Delta V_{OC} \approx 10$ mV) which can be attributed to the upshift in conduction band (CB) edge due to greater dipole moments of **XSQ1-2** in the direction normal to the TiO_2.[27,28]

3.2.5. Electrochemical Impedance Spectroscopy (EIS)

To understand the charge transfer process and recombination dynamics inside the DSSCs, electrochemical impedance spectroscopy (EIS) was carried out in the dark at various applied potentials viz. -0.38, -0.41, -0.47 and -0.50 V (**Figure 9**).

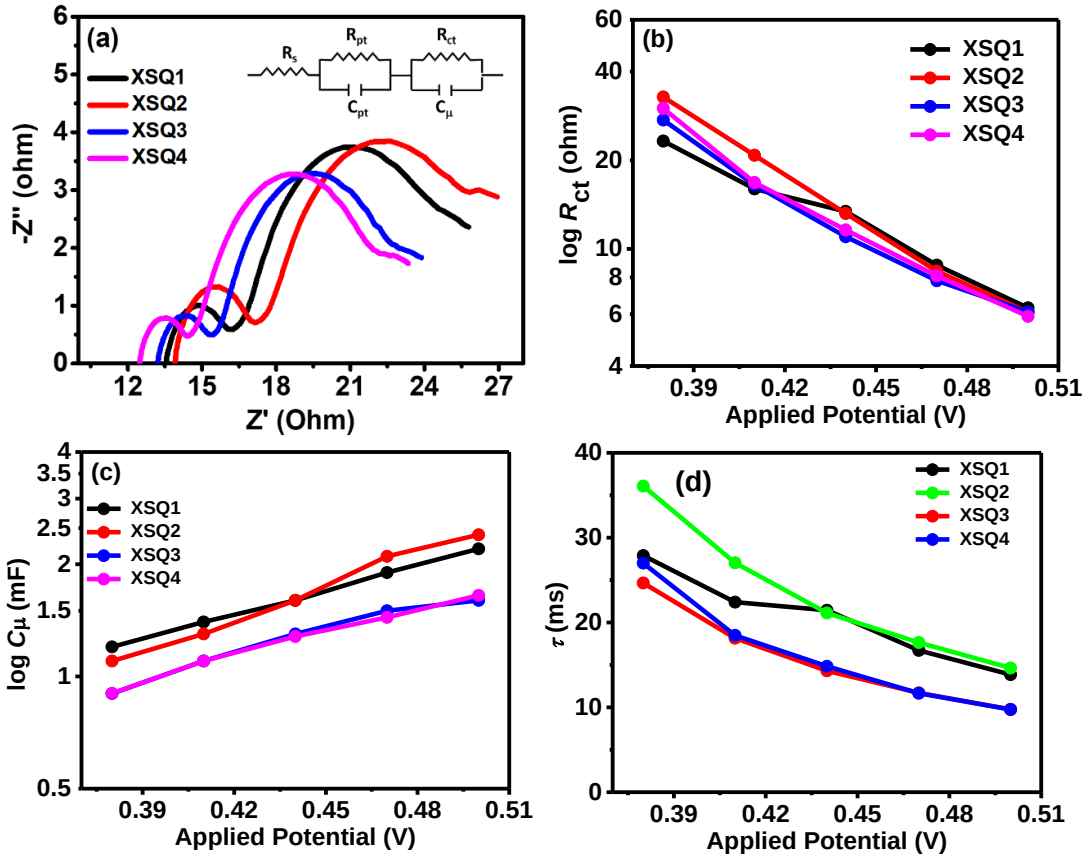

Figure 9. Impedance analysis of XSQ dyes. (a) The Nyquist plot at an applied bias of -0.5 V (the inset shows the equivalent circuit), (b) log R_{ct} vs. applied potential, (c) log C_{μ} vs. applied potential, and d) log τ vs. applied potential.

As the device architecture and electrolytes, including fabrication conditions, are similar for all the cells, any characteristic feature obtained in EIS is mainly due to the effect of dye interactions inside the cell. The Nyquist plots at an applied bias of 0.50 V are shown in **Figure 9a.** The smaller semicircle in the high-frequency region is ascribed to the charge transfer processes at the interface of Pt electrode and electrolyte. This semicircle provides the value of charge transfer resistance at counter electrode (R_{Pt}), equivalent capacitance (C_{Pt}) and series resistance (R_S). The larger semicircle in intermediate frequency region gives the information regarding charge recombination dynamics between dye-sensitized TiO_2 and electrolyte. The radius of the semicircle gives the recombination resistance (R_{ct}), and the peak value provides chemical capacitance (C_μ) at this interface and hence sheds light on the effect of dyes on charge transfer dynamics inside the cell. The R_{ct} values of XSQ sensitized cells do not vary significantly, and they have the approximately same R_{ct} value at -0.50 V applied bias which could be expected as all the dyes have similar crowded branched chains resulting in equal surface passivation to TiO_2 (**Table 4**).

Table 4. EIS Parameters of **XSQ** dye cells at an applied potential of −0.5 V in the dark

XSQ Dyes	R_s (ohm)	R_{ct} (ohm)	C_μ (mF)	μ (ms)
XSQ1	13.6	6.3	2.2	13.9
XSQ2	13.9	6.1	2.4	14.6
XSQ3	12.4	6.1	1.6	9.8
XSQ4	13.1	5.9	1.7	10.0

The trend in chemical capacitance (C_μ) is slightly different, and **XSQ1-2** have the higher C_μ compared to **XSQ3-4** which ultimately results in the longer lifetime ($\tau = R_{ct} \times C_\mu$) for **XSQ1-2** dyes than **XSQ2-4**. Generally, the electron lifetime on TiO_2 affects open circuit voltage of DSSC, and the τ values of **XSQ** dye based cell (without CDCA) follows the same trend as $V_{OC,}$ i.e., **XSQ3** (9.8 ms) < **XSQ4** (10.0 ms) < **XSQ1** (13.9 ms) < **XSQ2** (14.6 ms). The dyes **XSQ1** and **XSQ2** have higher dipole moments which may bring the conduction band slightly upward, allowing a higher concentration of electrons on TiO_2 in comparison to **XSQ2** and **XSQ4** dyes which leads to greater electron lifetime in **XSQ1-2** based DSSC.[27,28]

3.3. SUMMARY

The electronic and steric factors in the molecular structure of dyes play a significant role in the performance of DSSCs. We have designed and synthesized a series of four donor-acceptor-donor (D-A-D) unsymmetrical squaraine dyes, **XSQ1-4**, with the fused fluorenylindolenine based donor. The fused structure of fluorenylindolenine helped in extending the absorption in the far-red region, and the two sp^3-C centers available on this donor were utilized to incorporate out-of-the plane alkyl chains in opposite directions to control the aggregation of dyes on the TiO_2 surface. All the dyes showed good absorption in the far-red spectral region with the absorption of benz[e]indole based dyes, **XSQ3-4,** more red-shifted than indole-based **XSQ1-2**. Their HOMO and LUMO energy levels are suitably placed for efficient charge injection and dye regeneration processes. Due to extensive coverage of branched out-of-the plane alkyl chains on both side of the molecular plane aggregation was effectively controlled in all the dyes. DFT based calculations predicted efficient electron transfer towards TiO_2 and showed higher dipole moments for **XSQ1-2** in comparison to **XSQ3-4**. Owing to the higher short-circuit current density, **XSQ2** showed the best photovoltaic performance with the PCE of 6.57% in the presence of 3 equiv CDCA. EIS analysis indicated higher electron lifetime on TiO_2 for **XSQ2** sensitized solar cell which explains its slightly greater V_{OC}.

3.4. EXPERIMENTAL

3.4.1. Materials and Methods

All reagents for dye synthesis and device fabrication were purchased from commercial sources and used without purification unless otherwise noted. Tetrahydrofuran and toluene were purified by standard procedures immediately before use. The precursors 9,9-di-n-octyl-2-bromofluorene[29](**1)**, 5-carboxy-1,2,3,3-tetramethyl-3H-indol-1-ium[23] (**7**) 1,1,2-trimethyl-1H-benzo[e]indole-7-carboxylic acid[10] (**10)**, and 3-octyltridecan-2-one[23] **(4)** were synthesized according to the procedures known in the literature.The synthesized compounds were purified by column chromatography over silica get (230-400 mesh) unless otherwise noted. ^{1}H NMR and ^{13}C NMR were recorded in, $CDCl_3$, MeOH-d_4 or DMSO-d_6 on 200, 400 and 500 MHz NMR spectrometers. High-resolution mass spectrometric measurements were carried out using the ESI method and an ion-trap mass analyzer. Matrix-assisted laser desorption

ionization time-of-flight mass spectrometry (MALDI-TOF MS) were recorded and ABSciex 5800 MALDI-TOF mass spectrometer, Absorption spectra were recorded at room temperature in quartz cuvette using a UV−Visible spectrophotometer. The cyclic voltammetry (CV) analysis was carried out in anhydrous dichloromethane solvent by using 0.1 M tetrabutylammonium perchlorate as supporting electrolyte and Fc/Fc^+ as an internal reference. The experiments were performed at room temperature in a nitrogen atmosphere with a three-electrode cell consisting of a platinum foil as a counter electrode, an Ag/Ag^+ reference electrode, and a platinum wire as the working electrode. *J-V* characteristics of the cells were measured using Keithley digital source meter (2420, Keithley, USA) controlled by a computer and standard AM 1.5 solar simulator (PET, CT200AAA, USA). To measure the photocurrent and voltage, an external bias of AM 1.5G light was applied using a xenon lamp (450 W, USHIO INC, Philippines) and *J-V* plot was recorded. The IPCE measurements were carried out with a Newport QE measurement kit by focussing a monochromatic beam of light from 300W Xe lamp onto the devices. Electrochemical impedance spectra (EIS) were measured on the Biologic potentiostat, equipped with a FRA2 module, with an applied potential of -0.38, -0.41, -0.47 and -0.50 V in the dark. The frequency range was explored from 1Hz to 1MHz with an ac perturbation of 10 mV. The impedance spectra were analyzed using an equivalent circuit model of R1+R2/C2+R3/C3.

3.4.2. Device Fabrication Procedure

The preparation of TiO_2 electrodes and fabrication of the cells for photovoltaic measurements were carried out according to the previously reported procedures by our group.[22,30] FTO (F-doped SnO_2 glass;6-8 Ω/sq) was cleaned sequentially by mucasol (2% in water), deionized water, and isopropanol using an ultra-sonication for 15 min. To grow a blocking layer of TiO_2, the cleaned FTO substrates was dipped in freshly prepared aqueous 0.05 M $TiCl_4$ solution at 70° C for 30 min, and washed immediately with deionized water, and followed by annealing in air at 125° C for 10 min. The mesoscopic transparent thin layer (6-8 μm thickness) of TiO_2 was coated onto $TiCl_4$ treated FTO using TiO_2 paste (< 20 nm, Ti-Nanoxide T/SP) by using doctorblade technique. The film was kept in air for 5 min and annealed at 125 °C in air for 15 min before coating scattering layer on it. Dyesol, WER2-O paste was used to coat a 4-6 μm thick scattering layer of TiO_2, kept in air for 5 min and annealed at 125 °C in air for 15 min. The resulting 0.22 cm^2 active area films were sintered at 325 °C for 5 min, 375 °C for 5 min, 450 °C for 15 min and 500 °C for 15 min with heating

rate of 5 °C per min in air. After reaching the furnace temperature at 50 °C, the sintered films were treated in $TiCl_4$ solution as described before and again sintered at 500 °C for 30 min. The films were allowed to cool down to 50 ° C and immediately immersed in 0.1 mM **XSQ** dye solutions (with and without CDCA) in EtOH and kept for 12 h at rt. The dye loaded electrodes are washed thoroughly with EtOH, to remove physisorbed molecules. Finally the dye cell was assembled by joining the electrolyte (Iodolyte Z50) filled photoanode and platinum cathode using a 25 μm thick spacer.

3.4.3. Synthetic Procedure and Characterization data

Di-*tert*-Butyl 1-(9,9-dioctyl-9H-fluoren-2-yl)hydrazine-1,2-dicarboxylate (2). *n*-Butyllithium (1.6 M, 4.8 mL, 7.7 mmol) was added slowly to a stirred solution of 9,9-di-n-octyl-2-bromofluorene (3.0 g, 6.4 mmol) in anhydrous THF (35 mL) at -78 ºC, under nitrogen. After stirring for 30 min, di-*tert*-butylazodicarboxylate (3.2 g, 14.1 mmol) dissolved in anhydrous THF (35 mL) was added to the reaction mixture. After stirring at -78 ºC for 2 h, the mixture was allowed to warm to room temperature and stirred further for 18 h. Glacial acetic acid (1.5 mL) was added slowly and the mixture stirred further for 4 h at room temperature. Ether (50 mL) and water (50 mL) were added. The aqueous layer was separated and extracted with ether (2 × 60 mL). The combined organic extracts were then washed with brine (60 mL), dried over sodium sulphate, filtered and the solvent completely removed. The crude material was purified by column chromatography over silica (CH_2Cl_2/pet ether as) to give 4 as sticky gum (2.72 g, 68%). ^{1}H NMR (200 MHz, $CDCl_3$) δ 7.72 – 7.53 (m, 2H), 7.42 – 7.25 (m, 5H), 1.93 (t, *J* = 8.0 Hz, 4H), 1.50 (s, 18H), 1.08 (d, *J* = 19.7 Hz, 20H), 0.81 (t, *J* = 6.7 Hz, 6H), 0.73 – 0.47 (m, 4H). ^{13}C NMR (100 MHz, $CDCl_3$) δ 155.7, 154.0, 153.9, 151.0, 141.6, 140.7, 138.9, 126.9, 126.9, 122.9, 119.7, 119.6, 82.2, 81.6, 55.2, 40.5, 31.9, 30.2, 29.4, 28.3, 23.9, 22.7, 14.2. HRMS (ESI) m/z $[M + H]^+$ Calcd for $C_{39}H_{61}O_4N_2$ 621.4626, found 621.4628.

2-(9,9-Dioctyl-9H-fluoren-2-yl)hydrazin-1-ium chloride (3). A solution of concentrated hydrochloric acid (4.1 mL) in 1,4- dioxane (12 mL) was added to a solution of **2** (2.8 g, 4.5 mmol) in 2-propanol (25 mL). The reaction mixture was heated at 85 ºC for 1 h. After cooling to room temperature, the solvent was completely removed to give **3** as pink sticky gum (1.85 g, 90%), which was used directly to next step without purification.

3-Decyl-2-methyl-3,9,9-trioctyl-3,9-dihydroindeno[1,2-f]indole (5). The compound **3** (1.5 g, 3.3 mmol) and 3-octyltridecan-2-one **4**[23] (2.0 g, 6.6 mmol) were taken with 30 mL acetic acid in round bottom flask. The resultant mixture was heated for 3 day at 90 ºC. After completion of the reaction, the solvents were removed under reduced pressure. The residue was dissolved in dichloromethane and washed with 5% KOH solution. The organic layer was collected and dried over sodium sulfate and purified by column chromatography (CH_2Cl_2/Pet ether) to give **5** as dark yellow oil (0.570 g, 25%). ^{1}H NMR (200 MHz, $CDCl_3$) δ 7.68 (d, *J* = 7.6 Hz, 1H), 7.47 (s, 1H), 7.45 (s, 1H), 7.38 – 7.27 (m, 3H), 2.23 (s, 3H), 2.03 – 1.92 (m, 4H), 1.75 (d, *J* = 35.2 Hz, 4H), 1.13 (dd, *J* = 30.5, 17.4 Hz, 46H), 0.80 (t, *J* = 6.6 Hz, 12H), 0.61 (s, 6H). ^{13}C NMR (100 MHz, $CDCl_3$) δ 186.6, 155.2, 151.3, 151.0, 141.6, 141.4, 138.4, 126.7, 126.6, 122.9, 119.3, 114.3, 112.9, 62.5, 55., 40.7, 37.4, 32.0, 31.9, 30.2, 30.0, 29.9, 29.7, 29.6, 29.4, 29.4, 29.3, 23.9, 23.8, 22.8, 22.7, 16.4, 14.2. MALDI-TOF (m/z) $[M+H]^+$ calcd for $C_{50}H_{82}N$: 696.6447; found: 696.4977.

3-Decyl-1,2-dimethyl-3,9,9-trioctyl-3,9-dihydroindeno[1,2-f]indol-1-ium iodide (6a). A mixture of **5** (0.150 g, 0.22mmol) and iodomethane (0.125 g, 0.86 mmol) in acetonitrile (5 mL) was heated under nitrogen at 85 ºC for 24 h in a sealed pressure tube. The reaction mixture was cooled to room temperature and the solvent and excess iodomethane were completely removed under vacuum to give compound **6a** (70%, 0.130 g) which was used further without purification.

3-Decyl-1-hexyl-2-methyl-3,9,9-trioctyl-3,9-dihydroindeno[1,2-f]indol-1-ium iodide (6b). A mixture of **5** (0.150 mg, 0.22 mmol) and iodohexane (0.183 g, 0.86 mmol) in acetonitrile (5 mL) was heated under nitrogen at 85 ºC for 24 h in a sealed pressure tube. The reaction mixture was cooled to room temperature before the solvent and excess iodomethane were completely removed under vacuum to give compound **6b** (65%, 0.130 g) which was used further without purification.

(E)-2-((2-Butoxy-3,4-dioxocyclobut-1-en-1-yl)methylene)-1,3,3-trimethylindoline-5-carboxylic acid (8). In a 50 mL round bottom flask, compounds **7** (1 g, 2.89 mmol) and 3, 4-Dibutoxy-3-cyclobutene-1,2-dione (0.79 g, 3.47 mmol, 1.2 equiv) were dissolved in *n*-butanol (15 mL). Anhydrous triethylamine (2 mL) was added to the reaction mixture and stirred for 24 hrs at room temperature, then refluxed at 70 ºC for 1 h. The solvent was removed under reduced pressure and the crude product was purified by column

chromatography (EtOAc/pet ether) to afford compound **8** (0.72 g, 67%). ^{1}H NMR (400 MHz, DMSO-d_6) δ 12.72 (s, 1H), 7.93 (s, 1H), 7.90 (d, *J* = 8.5 Hz, 1H), 7.25 (d, *J* = 8.4 Hz, 1H), 5.39 (s, 1H), 4.80 (t, *J* = 6.5 Hz, 2H), 3.41 (s, 3H), 1.79 (dd, *J* = 14.5, 6.9 Hz, 2H), 1.57 (s, 6H), 1.44 (dd, *J* = 15.0, 7.5 Hz, 2H), 0.94 (t, *J* = 7.4 Hz, 3H). ^{13}C NMR (101 MHz, DMSO-D6) δ 192.00, 188.94, 187.47, 172.40, 167.99, 167.16, 146.89, 140.25, 130.30, 124.42, 122.86, 108.58, 82.45, 73.62, 46.79, 39.52, 31.48, 30.05, 26.42, 18.17, 13.53. HRMS (ESI): m/z Calcd for $C_{21}H_{23}NO_5Na$ $[M+ Na]^+$ 392.1468. Found: 392.1465.

(E)-2-((2-Hydroxy-3,4-dioxocyclobut-1-en-1-yl)methylene)-1,3,3-trimethylindoline-5-carboxylic acid (P1). In a 50 ml round bottom flask, compound **8** (1 mmol) was dissolved in acetone (15 mL). 2N HCl (2 mL) was added to the mixture and refluxed for 8 h. The solvent was removed under reduced pressure to afford product **P1** and used without any further purification (0.28 g, 89%). ^{1}H NMR (500 MHz, DMSO-d_6) δ 7.81-7.93 (m, 2H), 7.16 (d, J = 8.77 Hz, 1H), 5.53 (s, 1H), 3.36 (s, 3H), 1.57 (s, 6H). ^{13}C NMR (100 MHz, DMSO-d_6) δ 192.6, 174.0, 167.3, 165.4, 147.3, 140.1, 130.3, 123.6, 122.8, 107.9, 83.5, 46.3, 29.8, 26.7. HRMS (ESI): m/z Calcd for $C_{17}H_{16}NO_5$ $[M + H]^+$ 314.1023. Found: 314.1012.

7-Carboxy-1,1,2,3-tetramethyl-1H-benzo[e]indol-3-ium iodide (10). The compound **9** (1 g, 3.95 mmol), Iodomethane (2.8 g, 19.75 mmol) and 8 mL acetonitrile were taken in a sealed tube and heated at 150 ºC for 48 h. After completion of the reaction the contents were poured into 50 mL of diethyl ether and the precipitate obtained was filtered. The residue was washed with diethyl ether (3×20 mL) and dried under vacuum to give compound **11** (0.78 g , 50%). ^{1}H NMR (200 MHz, DMSO-d_6) δ 8.87 (s, 1H), 8.52 (d, *J* = 6.3 Hz, 1H), 8.47 (d, *J* = 6.1 Hz, 1H), 8.26 – 8.13 (m, 2H), 4.11 (s, 3H), 2.90 (s, 3H), 1.76 (s, 6H). ^{13}C NMR (100 MHz, DMSO-d_6) δ 197.3, 167.1, 141.3, 136.5, 132.4, 132.3, 132.2, 129.1, 129.0, 127.5, 124.0, 114.9, 55.5, 35.3, 21.3, 14.2. HRMS (ESI) m/z $[M]^+$ Calcd for $C_{17}H_{18}NO_2^+$: 268.1332, found 268.1325.

(E)-2-((2-Butoxy-3,4-dioxocyclobut-1-en-1-yl)methylene)-1,1,3-trimethyl-2,3-dihydro-1H-benzo[e]indole-7-carboxylic acid (11). To a mixture of compound **9** (0.5 g, 1.26 mmol) in 20 mL of *n*-butanol, 3,4-dibutoxycyclobut-3-ene-1,2-dione (0.72 g , 3.16 mmol) was added. To the stirring mixture, triethylamine (0.38 g, 3.78 mmol) was added dropwise. The resultant mixture was stirred at room temperature for 12 h followed by heating at 70 ºC for 3 h. Solvents were evaporated after the completion of reaction and crude product was purified

by column chromatography ($MeOH/CH_2Cl_2$) to give compound **11** (0.37 g, 70%). ^1H NMR (200 MHz, DMSO) δ 8.63 (s, 1H), 8.23 (d, *J* = 9.1 Hz, 1H), 8.17 (d, *J* = 9.1 Hz, 1H), 8.00 (dd, *J* = 8.9, 1.6 Hz, 1H), 7.69 (d, *J* = 8.9 Hz, 1H), 5.39 (s, 1H), 4.82 (t, *J* = 6.6 Hz, 2H), 3.52 (s, 3H), 1.95 – 1.70 (m, 8H), 1.46 (dq, *J* = 14.4, 7.2 Hz, 2H), 0.96 (t, *J* = 7.3 Hz, 3H). ^{13}C NMR (125 MHz, DMSO) δ 192.3, 188.1, 186.9, 172.1, 170.0, 167.4, 142.6, 132.5, 131.5, 131.3, 129.8, 129.4, 126.6, 125.3, 122.3, 111.7, 81.4, 73.6, 48.9, 31.6, 30.3, 26.2, 18.2, 13.6. HRMS (ESI) m/z $[M + H]^+$ Calcd for $C_{25}H_{26}O_5N$ 420.1805, found 420.1794.

(E)-2-((2-Hydroxy-3,4-dioxocyclobut-1-en-1-yl)methylene)-1,1,3-trimethyl-2,3-dihydro-1H-benzo[e]indole-7-carboxylic acid (P2). To a solution of compound **11** (0.35 g, 0.834 mmol) in 10 mL of acetone, 1 mL of 2N HCl was added. The resultant mixture was refluxed for 8 h, and solvents were removed under reduced pressure after the completion of reaction. The crude compound **P2** (0.286 g, 94%) was used further without purification. ^1H NMR (200 MHz, DMSO) δ 8.60 (s, 1H), 8.21 (d, *J* = 8.8 Hz, 1H), 8.12 (d, *J* = 8.9 Hz, 1H), 7.97 (d, *J* = 8.5 Hz, 1H), 7.62 (d, *J* = 8.8 Hz, 1H), 5.56 (s, 1H), 3.47 (s, 3H), 1.83 (s, 6H). ^{13}C NMR (100 MHz, $CDCl_3$) δ 192.7, 192.1, 191.6, 173.6, 167.7, 167.4, 142.9, 132.5, 131.3, 130.7, 129.9, 129.0, 126.4, 124.9, 122.1, 111.4, 82.3, 48.4, 30.0, 26.3. HRMS (ESI) m/z $[M + H]^+$ Calcd for $C_{21}H_{18}O_5N$ 364.1179, found 364.1170.

(E)-2-(((E)-5-Carboxy-1,3,3-trimethylindolin-2-ylidene)methyl)-4-((3-decyl-1-methyl-3,9,9-trioctyl-3,9-dihydroindeno[1,2-f]indol-1-ium-2-yl)methylene)-3-oxocyclobut-1-en-1-olate (XSQ1). Compound **6a** (0.200 g, 0.240 mmol) and **P1** (0.156 g, 0.480 mmol) were taken in flask fitted with dean stark apparatus. 20 mL of *n*-butanol/toluene (1:1) was added and the contents were refluxed for 24 hours. After completion of the reaction, solvents were removed under reduced pressure and residue was purified by column chromatography ($MeOH/CH_2Cl_2$) to give pure compound **XSQ1** (0.165 g, 68%). ^1H NMR (500 MHz, $CDCl_3$) δ 8.12 (d, *J* = 8.3 Hz, 1H), 8.06 (s, 1H), 7.73 (d, *J* = 7.4 Hz, 1H), 7.58 (s, 1H), 7.38 – 7.28 (m, 3H), 7.03 – 6.92 (m, 2H), 6.18 (s, 1H), 5.99 (s, 1H), 3.71 (s, 3H), 3.52 (s, 3H), 2.09 – 2.00 (m, 4H), 1.98 – 1.92 (m, 2H), 1.85 (s, 6H), 1.21 – 1.16 (m, 6H), 1.14 – 1.01 (m, 40H), 0.83 – 0.74 (m, 14H), 0.63 – 0.51 (m, 6H). ^{13}C NMR (125 MHz, $CDCl_3$) δ 170.6, 151.9, 150.7, 147.7, 144.1, 142.0, 140.6, 139.1, 138.8, 131.3, 127.1, 124.1, 123.0, 119.7, 113.8, 108.0, 88.3, 59.3, 55.4, 48.2, 40.7, 32.0, 31.9, 30.6, 30.1, 29.7, 29.6, 29.39, 29.35, 29.3, 29.2, 27.5,

24.2, 23.8, 22.7, 22.7, 14.2. HRMS (ESI) m/z: [M + H]+ calcd for $C_{68}H_{97}N_2O_4$: 1005.7448; found:1005.7446.

(E)-2-(((E)-5-Carboxy-1,3,3-trimethylindolin-2-ylidene)methyl)-4-((3-decyl-1-hexyl-3,9,9-trioctyl-3,9-dihydroindeno[1,2-f]indol-1-ium-2-yl)methylene)-3-oxocyclobut-1-en-1-olate (XSQ2). Compound **6b** (0.200 g, 0.220 mmol) and **P1** (0.104 g, 0.330 mmol) were taken in flask fitted with dean stark apparatus. 20 mL of *n*-butanol/toluene (1:1) was added and the contents were refluxed for 24 hours. After completion of reaction, solvents were removed under reduced pressure and residue was purified by column chromatography (MeOH/ CH_2Cl_2) to give pure compound **XSQ2** (0.150g, 60%). ^{1}H NMR (500 MHz, $CDCl_3$) δ 8.13 (d, *J* = 8.4 Hz, 1H), 8.07 (s, 1H), 7.73 (d, *J* = 7.4 Hz, 1H), 7.59 (s, 1H), 7.34 (td, *J* = 14.5, 7.1 Hz, 3H), 6.96 (d, *J* = 7.7 Hz, 2H), 6.22 (s, 1H), 6.00 (s, 1H), 4.19 (s, 2H), 3.52 (s, 3H), 3.11 (s, 2H), 2.04 (dd, *J* = 17.7, 9.7 Hz, 4H), 1.99 – 1.91 (m, 2H), 1.86 (s, 6H), 1.47 – 1.38 (m, 2H), 1.35 – 1.24 (m, 6H), 1.20 – 1.15 (m, 6H), 1.12 – 1.01 (m, 37H), 0.86 (t, *J* = 7.0 Hz, 3H), 0.83 – 0.74 (m, 15H), 0.70 – 0.45 (m, 8H). ^{13}C NMR (125 MHz, $CDCl_3$) δ 171.3, 170.7, 168.0, 151.6, 150.7, 147.8, 143.8, 141.9, 140.6, 138.7, 131.3, 127.1, 124.1, 122.9, 119.7, 113.8, 108.0, 104.7, 88.2, 59.3, 55.3, 48.2, 40.7, 40.4, 32.0, 31.93, 31.90, 31.7, 30.5, 30.1, 29.7, 29.6, 29.4, 29.3, 29.2, 27.8, 27.5, 27.1, 24.2, 23.9, 22.7, 22.67, 22.65, 14.2, 14.1. HRMS (ESI) m/z: [M+H]+ calcd for $C_{73}H_{107}N_2O_4$: 1075.8231; found: 1075.8220.

(E)-2-((E)-(7-Carboxy-1,1,3-trimethyl-1,3-dihydro-2H-benzo[e]indol-2-ylidene)methyl)-4-((3-decyl-1-methyl-3,9,9-trioctyl-3,9-dihydroindeno[1,2-f]indol-1-ium-2-yl)methylene)-3-oxocyclobut-1-en-1-olate (XSQ3). Compound **6a** (0.180 g, 0.22 mmol) and **P2** (0.156 g, 0.43 mmol) were taken in flask fitted with dean stark apparatus. 20 mL of *n*-butanol/toluene (1:1) and 2mL of DMSO were added to solubilize the mixture. The contents were refluxed for 24 hours. After completion of reaction, solvents were removed under reduced pressure and residue was purified by column chromatography (MeOH/CH_2Cl_2) to give pure compound **XSQ3** (0.110 g, 48%). ^{1}H NMR (500 MHz, $CDCl_3$) δ 8.74 (s, 1H), 8.36 – 8.12 (m, 2H), 7.99 (s, 1H), 7.72 (d, *J* = 7.3 Hz, 1H), 7.57 (s, 1H), 7.39 – 7.27 (m, 4H), 6.95 (s, 1H), 6.19 (s, 1H), 6.05 (s, 1H), 3.64 (s, 5H), 3.11 (s, 1H), 2.09 (d, *J* = 24.8 Hz, 6H), 2.06 – 1.89 (m, 6H), 1.24 – 0.99 (m, 46H), 0.87 – 0.71 (m, 14H), 0.67 – 0.51 (m, 6H). ^{13}C NMR (125 MHz, $CDCl_3$) δ 170.8, 170.3, 151.7, 150.6, 144.2, 142.6, 140.8, 138.2, 133.7, 131.7, 131.1, 130.1, 127.1, 126.9, 125.2, 122.9, 122.7, 119.5, 113.7, 110.8, 103.9, 88.6, 87.5, 58.9,

55.3, 50.7, 40.7, 40.4, 32.0, 31.9, 30.1, 29.8, 29.74, 29.70, 29.6, 29.42, 29.39, 29.35, 29.3, 29.2, 27.1, 24.3, 23.8, 22.7, 22.69, 14.2. HRMS (ESI) m/z: [M+H]+ calcd for $C_{72}H_{99}N_2O_4$: 1055.7605; found: 1055.7596.

(E)-2-((E)-(7-Carboxy-1,1,3-trimethyl-1,3-dihydro-2H-benzo[e]indol-2-ylidene)methyl)-4-((3-decyl-1-hexyl-3,9,9-trioctyl-3,9-dihydroindeno[1,2-f]indol-1-ium-2-yl)methylene)-3-oxocyclobut-1-en-1-olate (XSQ4). Compound **6b** (0.180 g, 0.22 mmol) and **P2** (0.156 g, 0.43 mmol) were taken in flask fitted with dean stark apparatus. 20 mL of n-butanol/toluene (1:1) and 2mL of DMSO were added to solubilize the mixture. The contents were refluxed for 24 hours. After completion of reaction, solvents were removed under reduced pressure and residue was purified by column chromatography (MeOH/CH_2Cl_2) to give pure compound (0.100 g, 54%). ^{1}H NMR (500 MHz, $CDCl_3$) δ 8.77 (s, 1H), 8.35 – 8.15 (m, 2H), 8.01 (d, *J* = 6.1 Hz, 1H), 7.75 (d, *J* = 7.4 Hz, 1H), 7.60 (s, 1H), 7.40 – 7.29 (m, 4H), 6.96 (s, 1H), 6.24 (s, 1H), 6.07 (s, 1H), 4.17 (s, 2H), 3.66 (s, 3H), 3.16 (s, 2H), 2.14 (s, 6H), 2.10 – 2.01 (m, 4H), 2.01 – 1.94 (m, 2H), 1.92 – 1.85 (m, 2H), 1.49 – 1.43 (m, 2H), 1.36 – 1.27 (m, 4H), 1.23 – 1.18 (m, 6H), 1.16 – 1.05 (m, 37H), 0.88 (t, *J* = 7.0 Hz, 3H), 0.85 – 0.75 (m, 15H), 0.72 – 0.48 (m, 8H). ^{13}C NMR (125 MHz, $CDCl_3$) δ 170.5, 170.1, 151.5, 150.6, 144.0, 142.6, 140.8, 139.0, 138.2, 135.4, 133.8, 131.6, 131.1, 130.1, 127.1, 126.9, 125.2, 122.9, 122.7, 119.6, 113.7, 110.7, 104.4, 88.5, 87.3, 58.9, 55.2, 50.6, 40.7, 32.0, 31.96, 31.9, 31.8, 30.1, 29.7, 29.6, 29.5, 29.4, 29.3, 29.2, 27.7, 27.2, 24.3, 23.9, 22.7, 22.7, 22.4, 14.2, 14.1. HRMS (ESI) m/z: [M +H]+ calcd for $C_{77}H_{109}N_2O_4$: 1125.8387; found: 1125.8378.

3.5. NMR Spectra

^{1}H and ^{13}C NMR spectra of 2

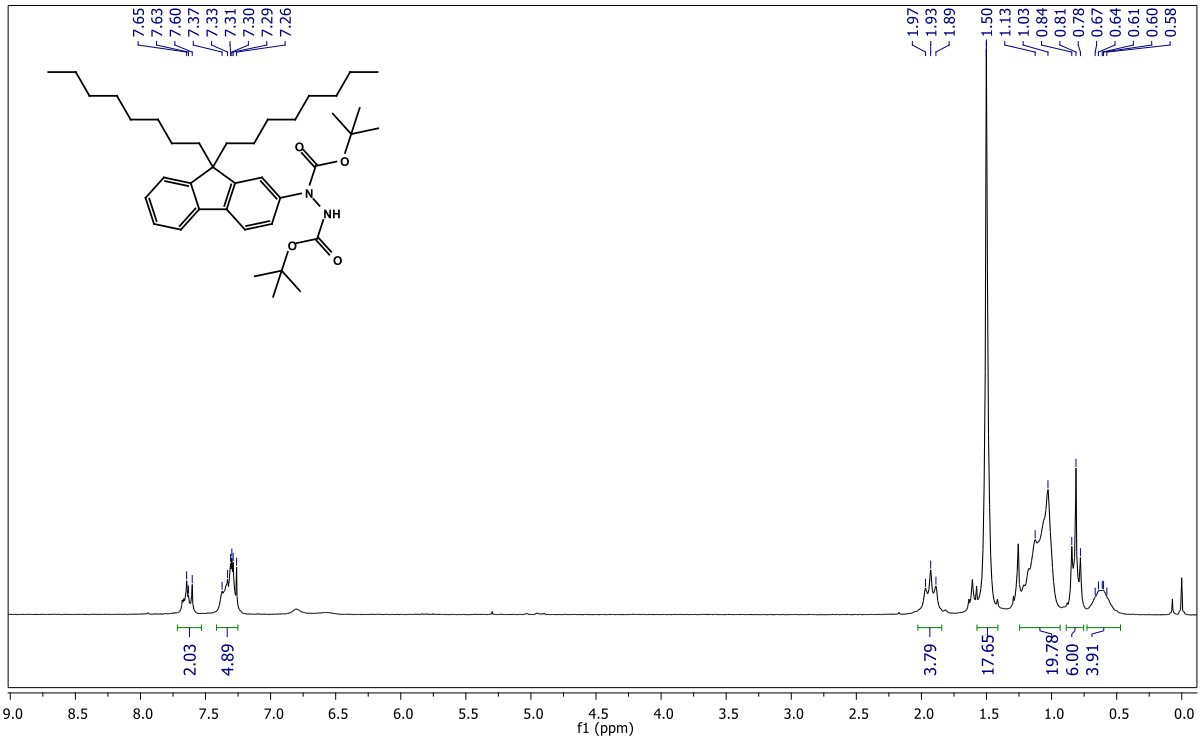

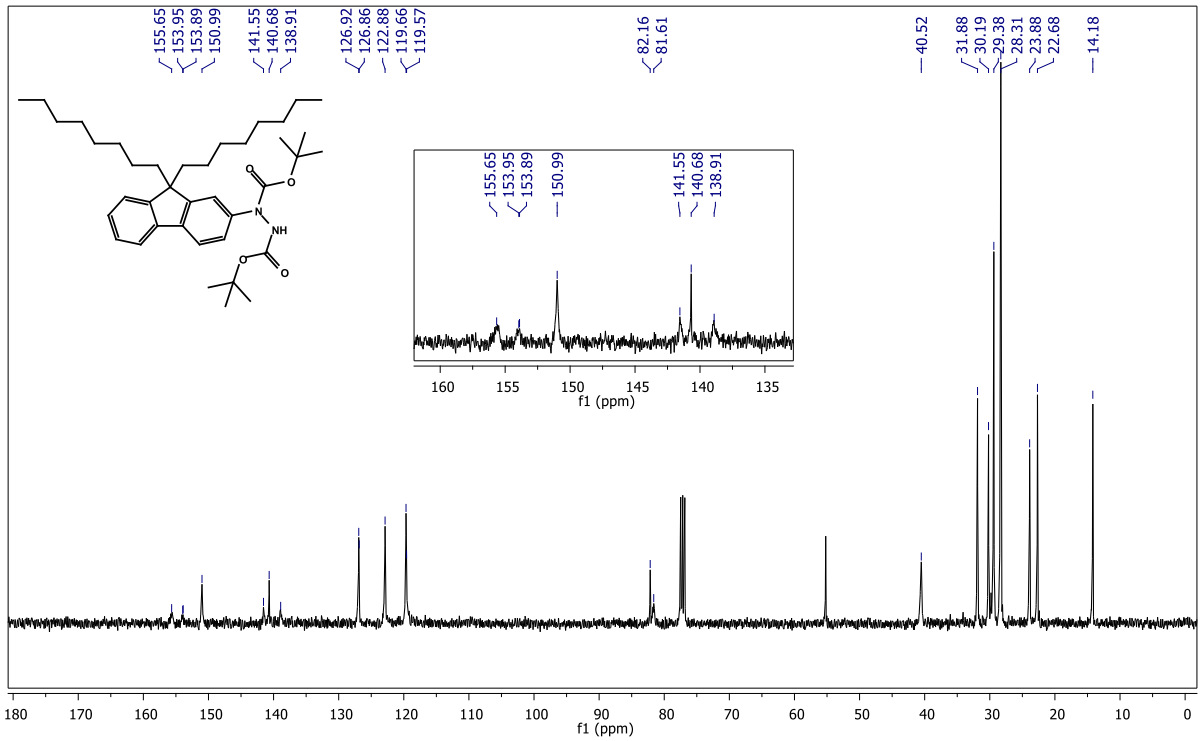

^{1}H and ^{13}C NMR spectra of 5

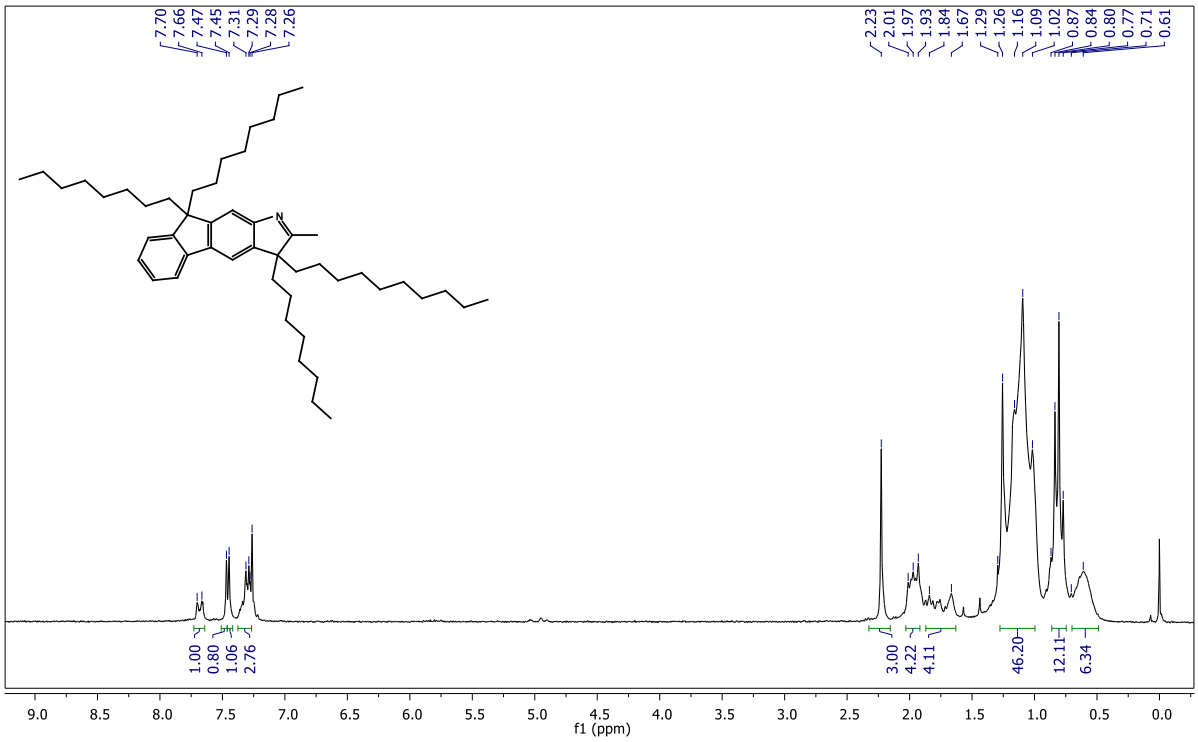

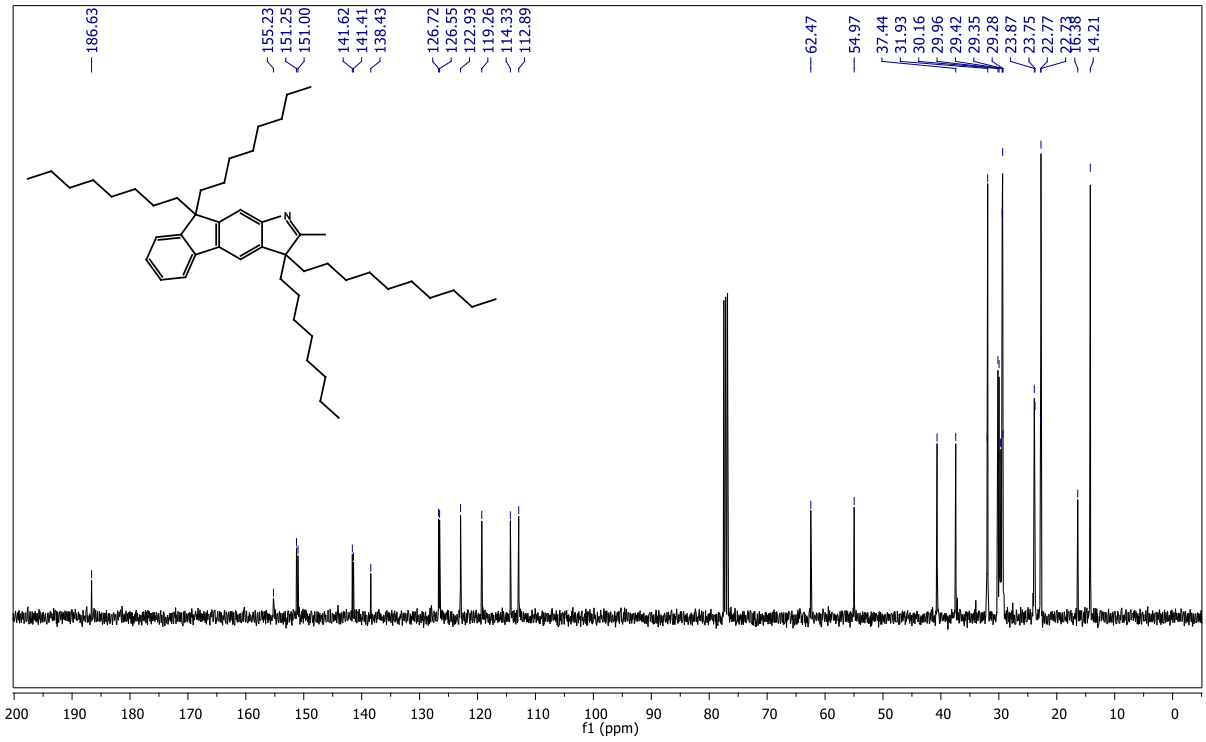

^{1}H and ^{13}C NMR spectra of 8

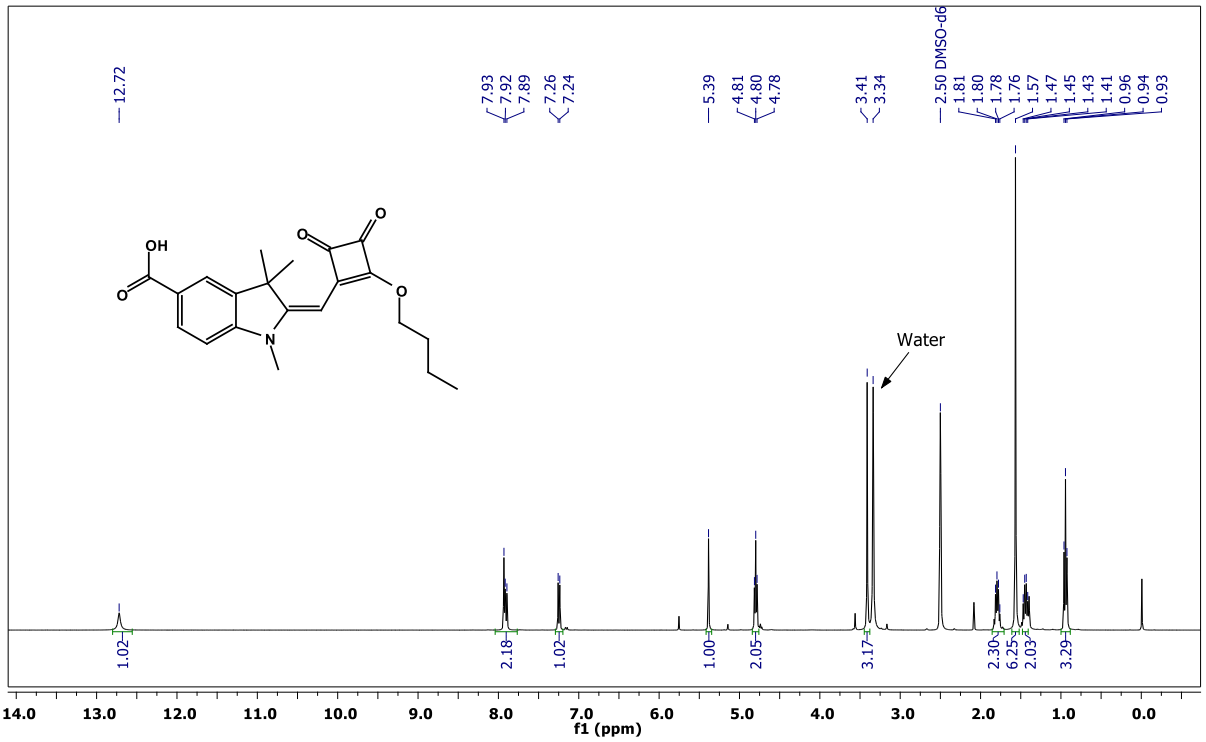

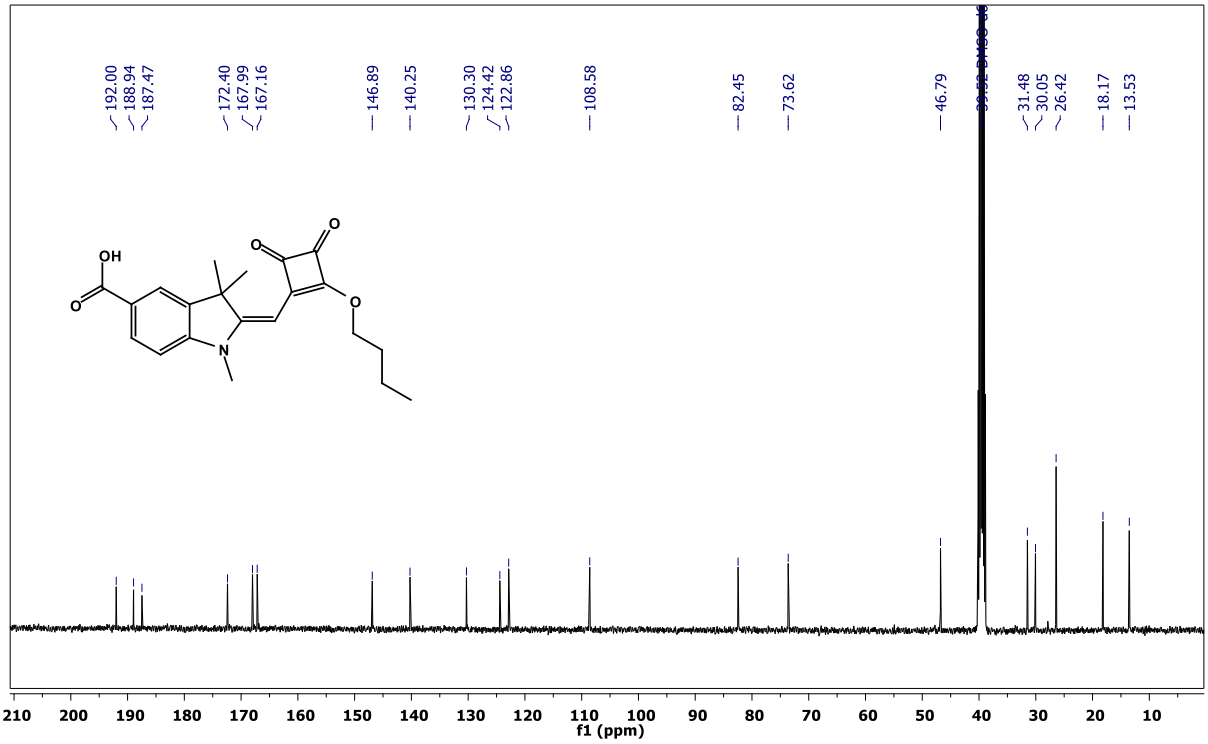

^{1}H and ^{13}C NMR spectra of 9

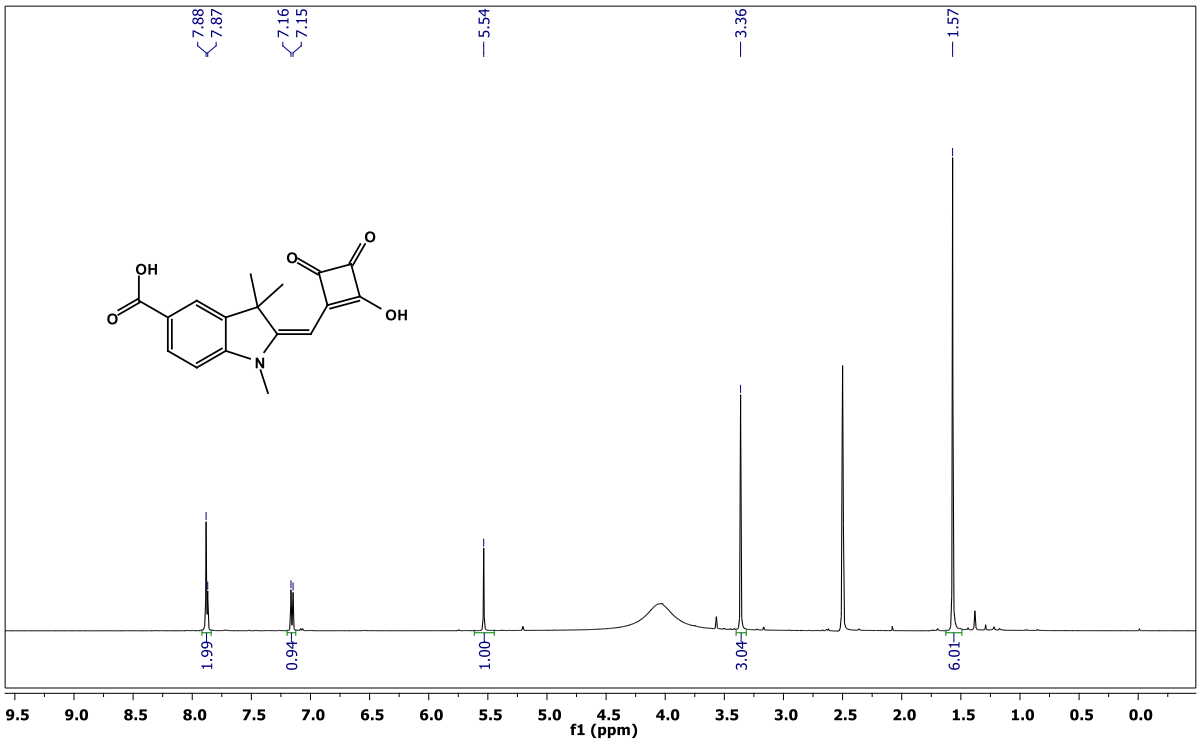

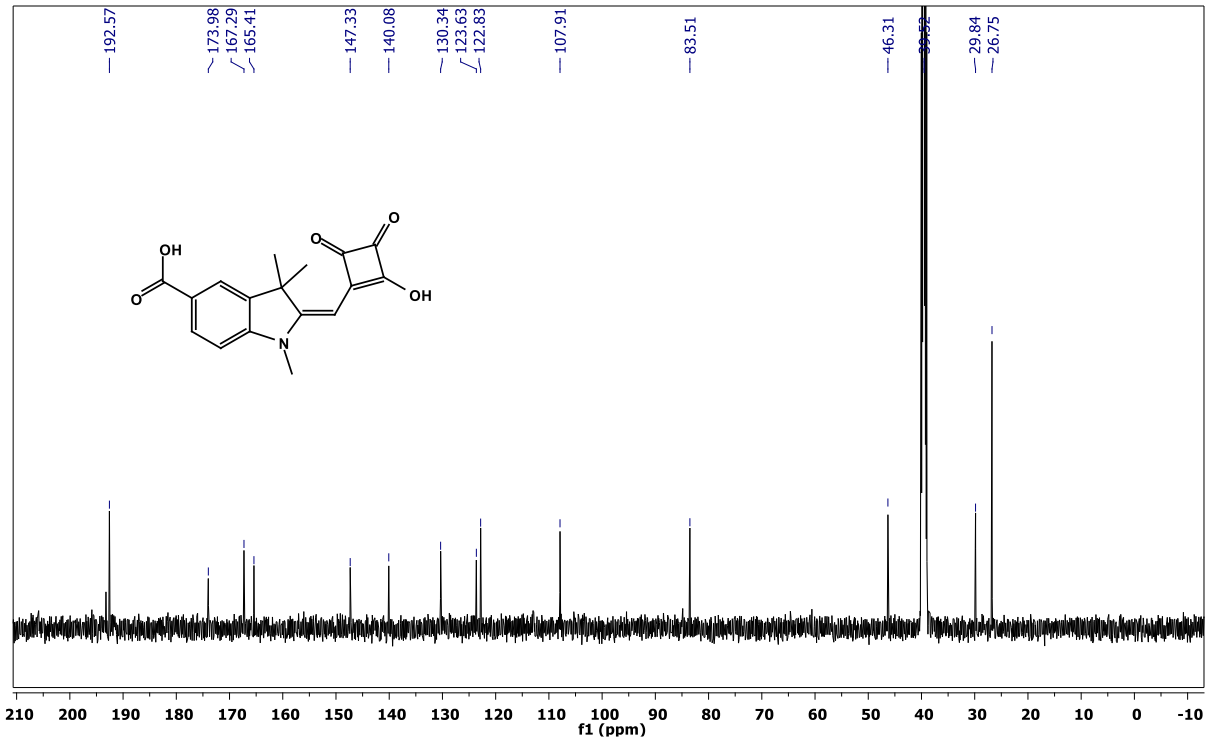

^{1}H and ^{13}C NMR spectra of 8.

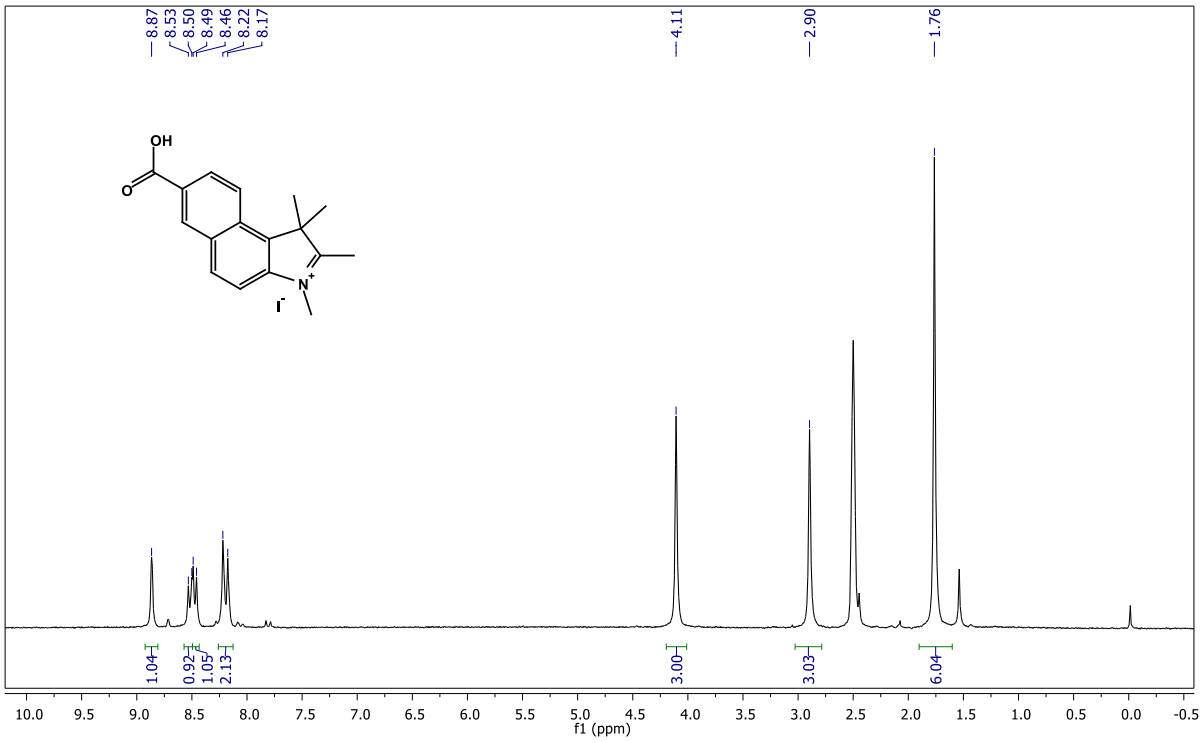

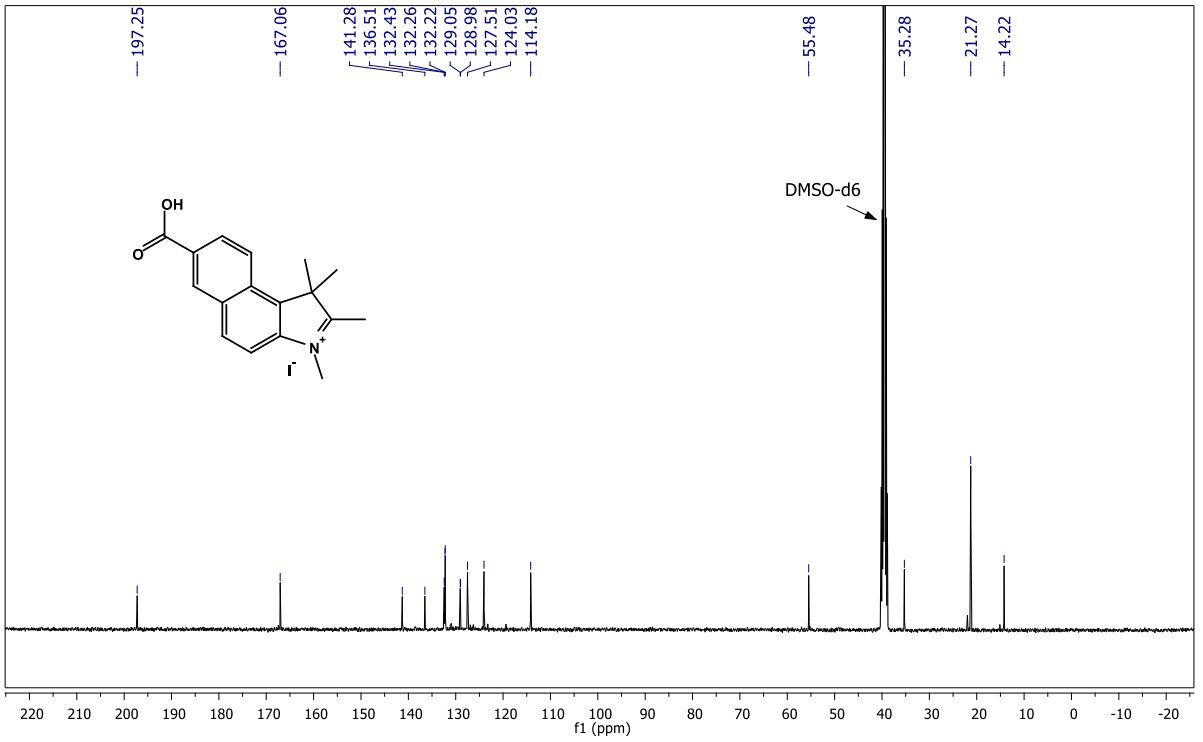

^{1}H and ^{13}C NMR spectra of **9**

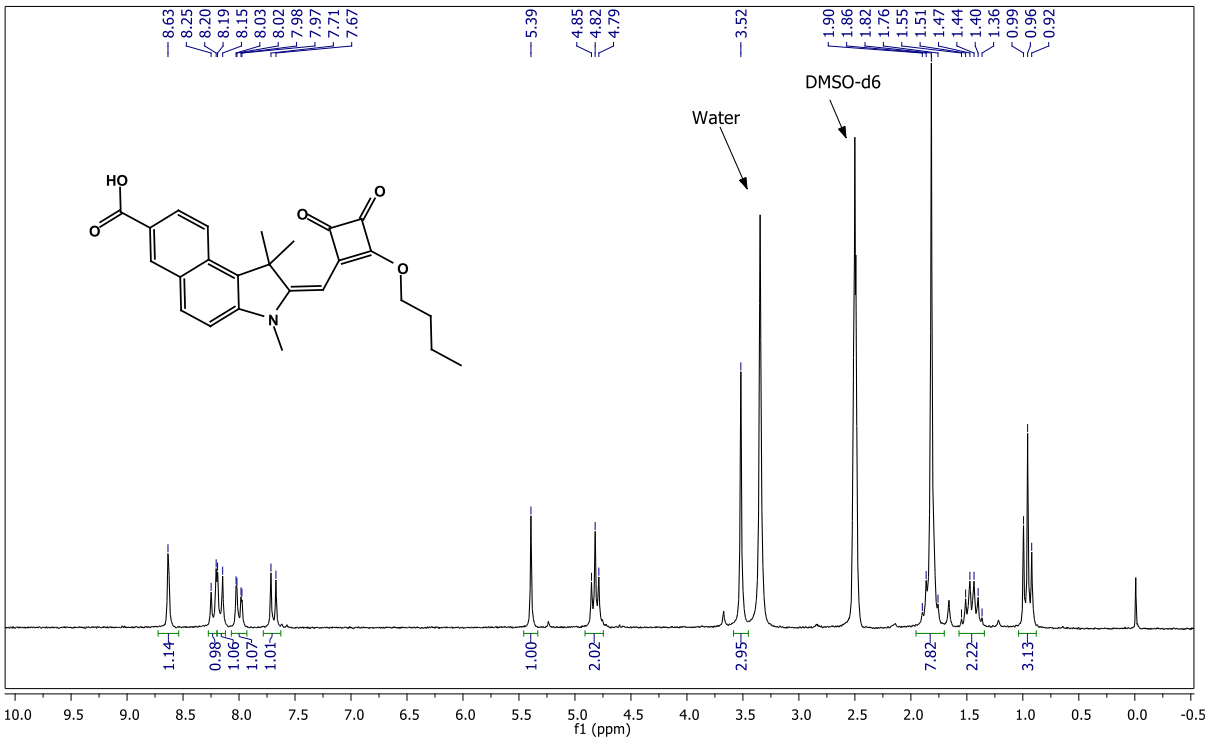

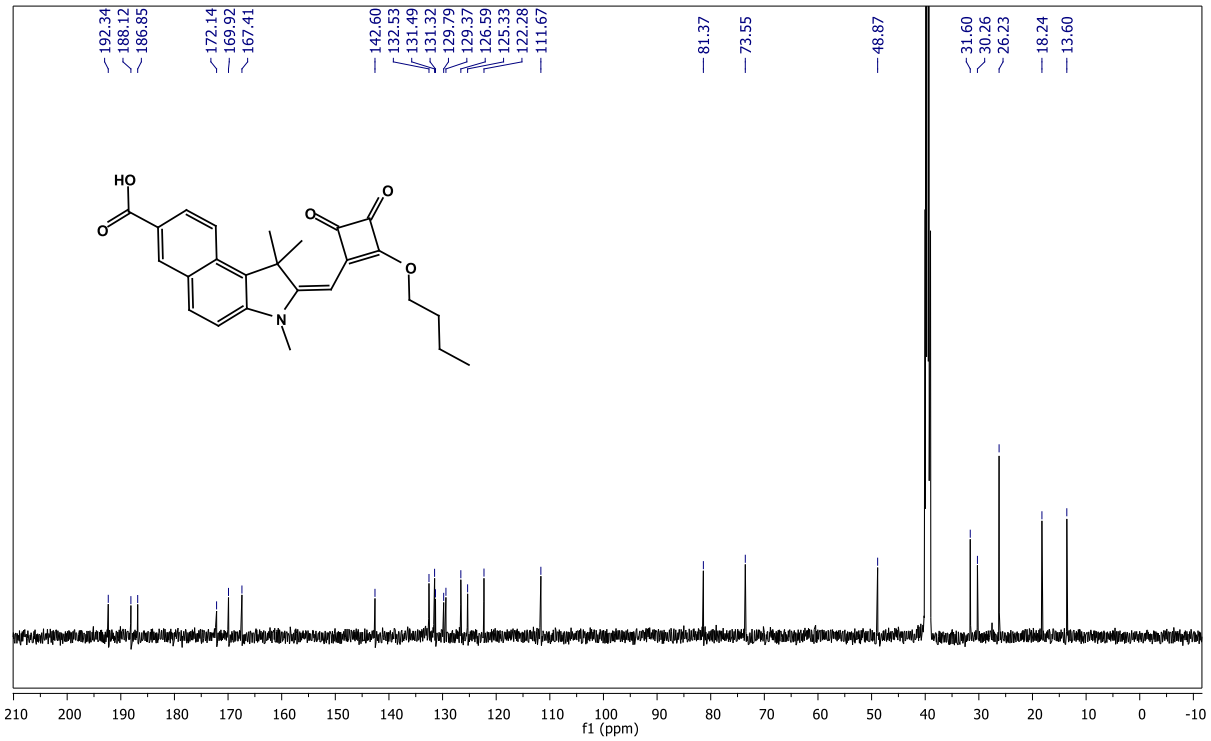

^{1}H and ^{13}C NMR spectra of **10**

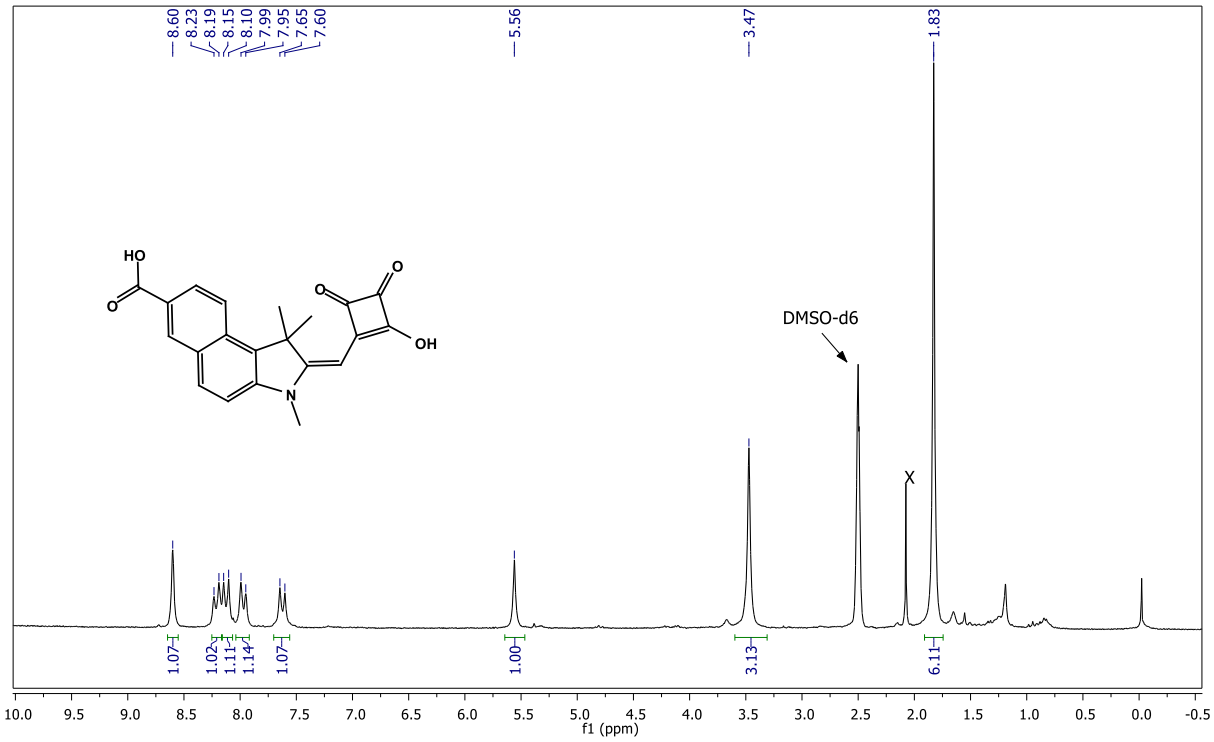

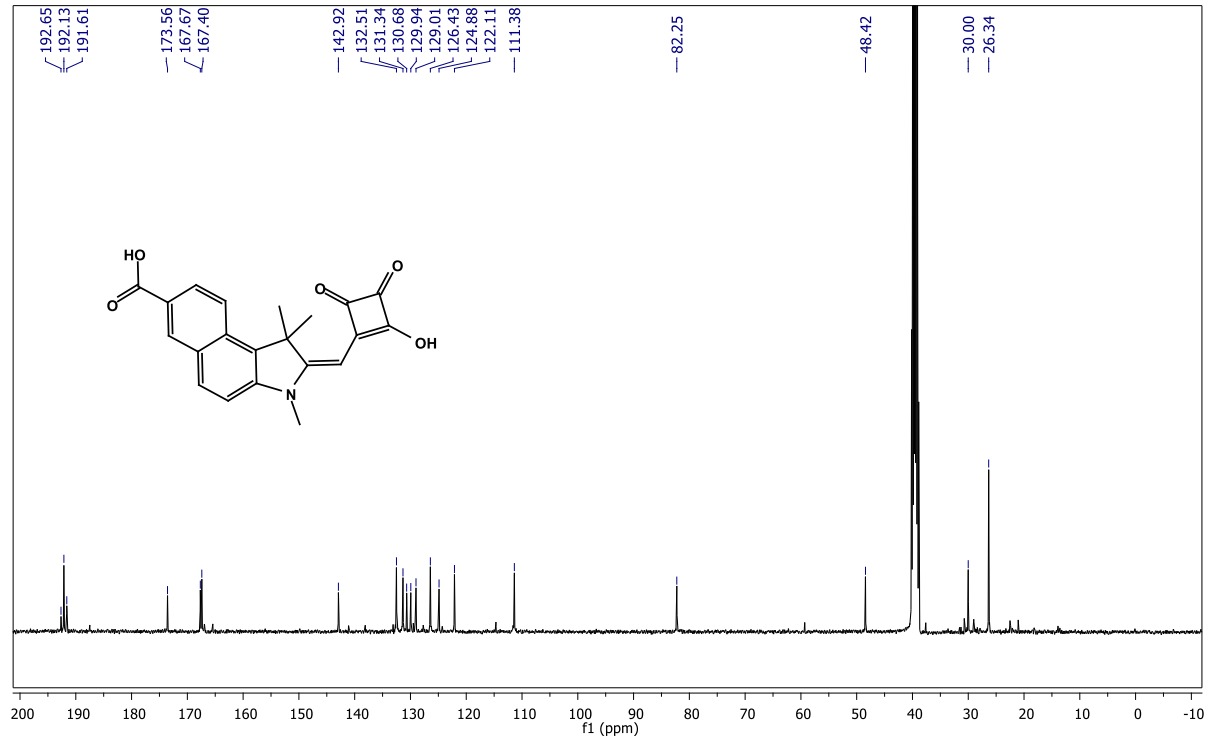

^{1}H and ^{13}C NMR spectra of XSQ1

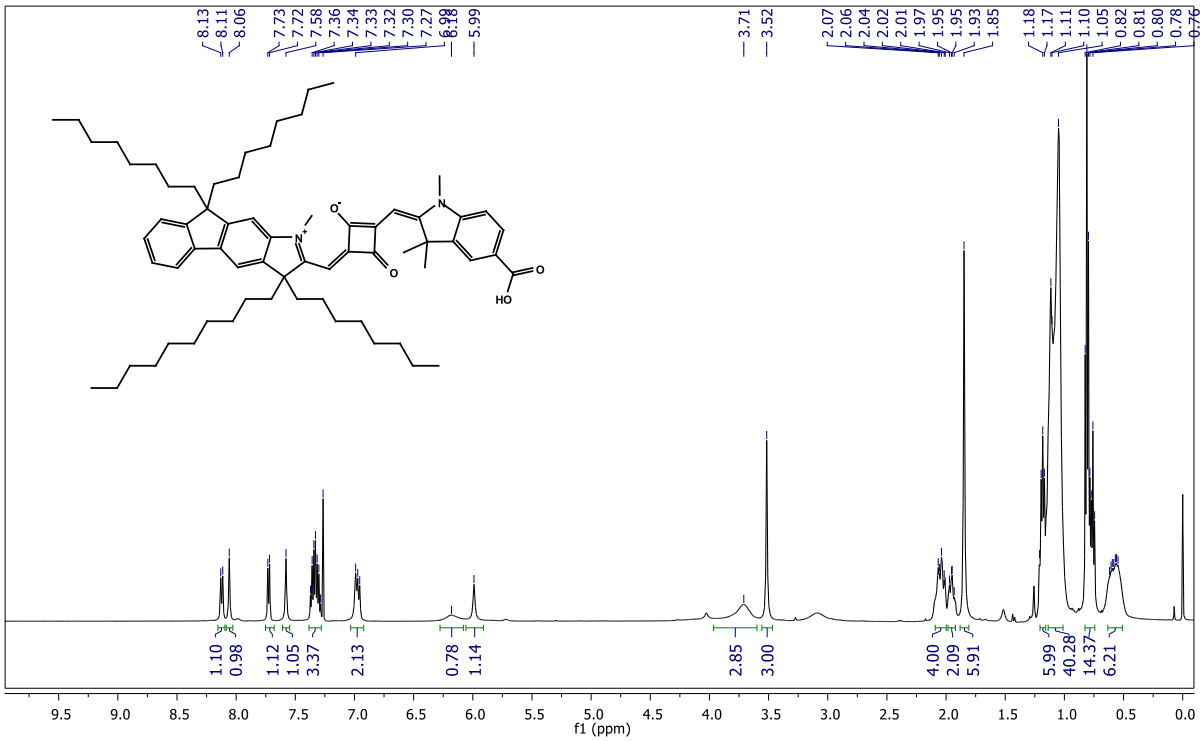

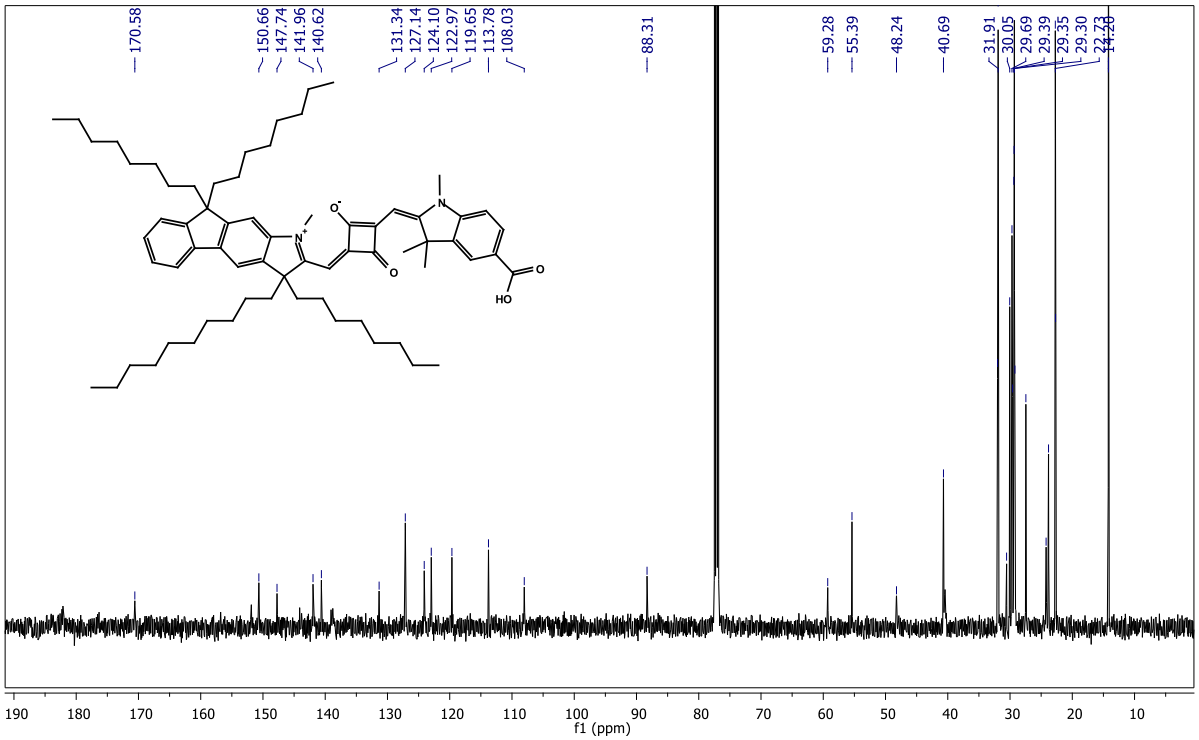

^{1}H and ^{13}C NMR spectra of XSQ2

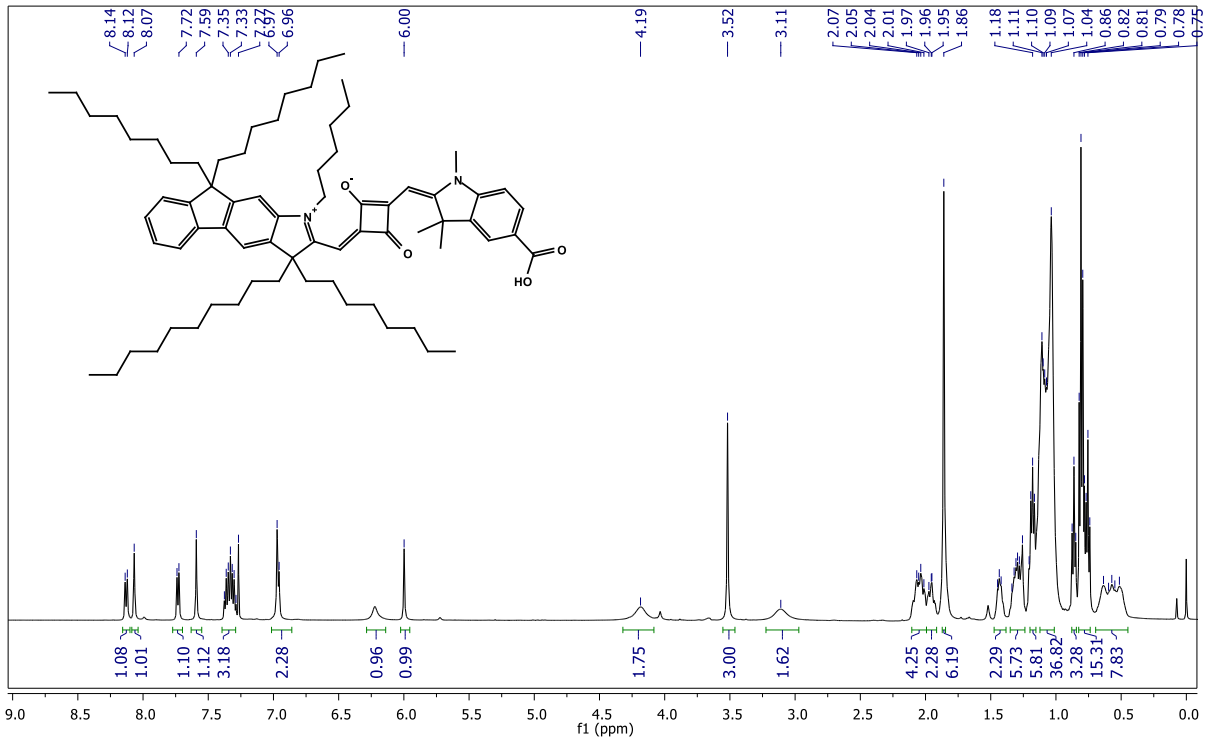

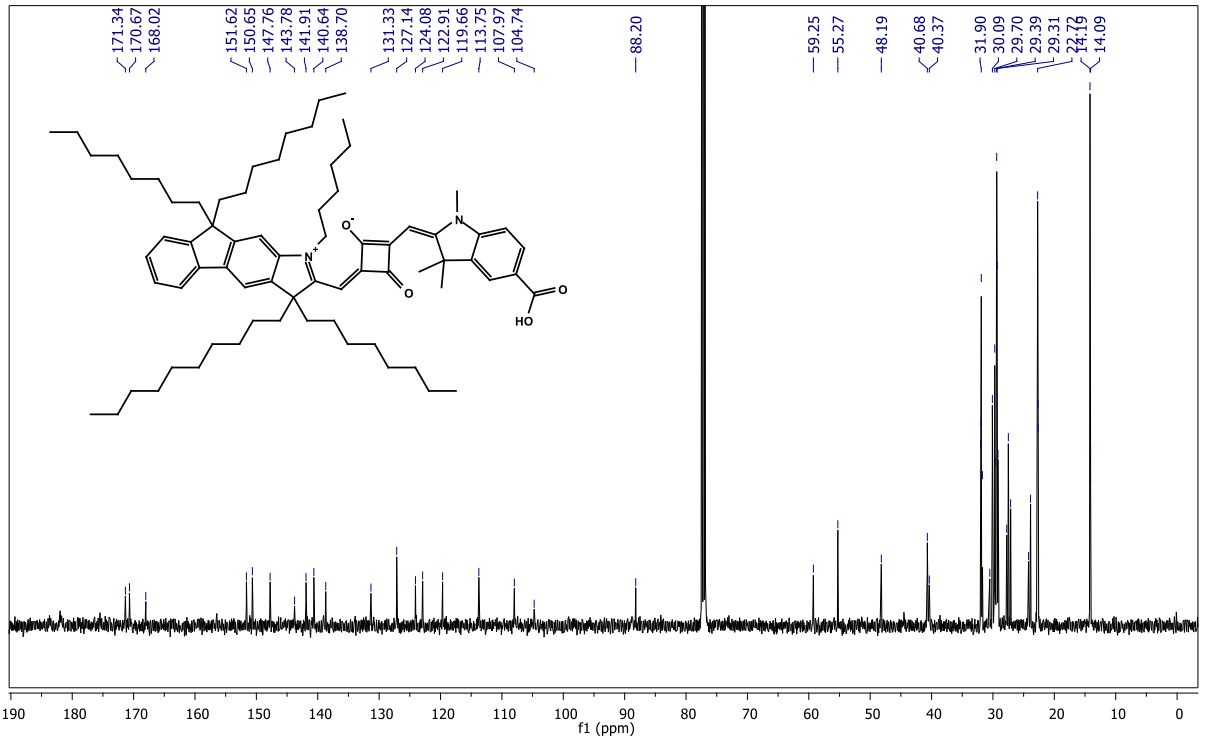

^{1}H and ^{13}C NMR spectra of XSQ3

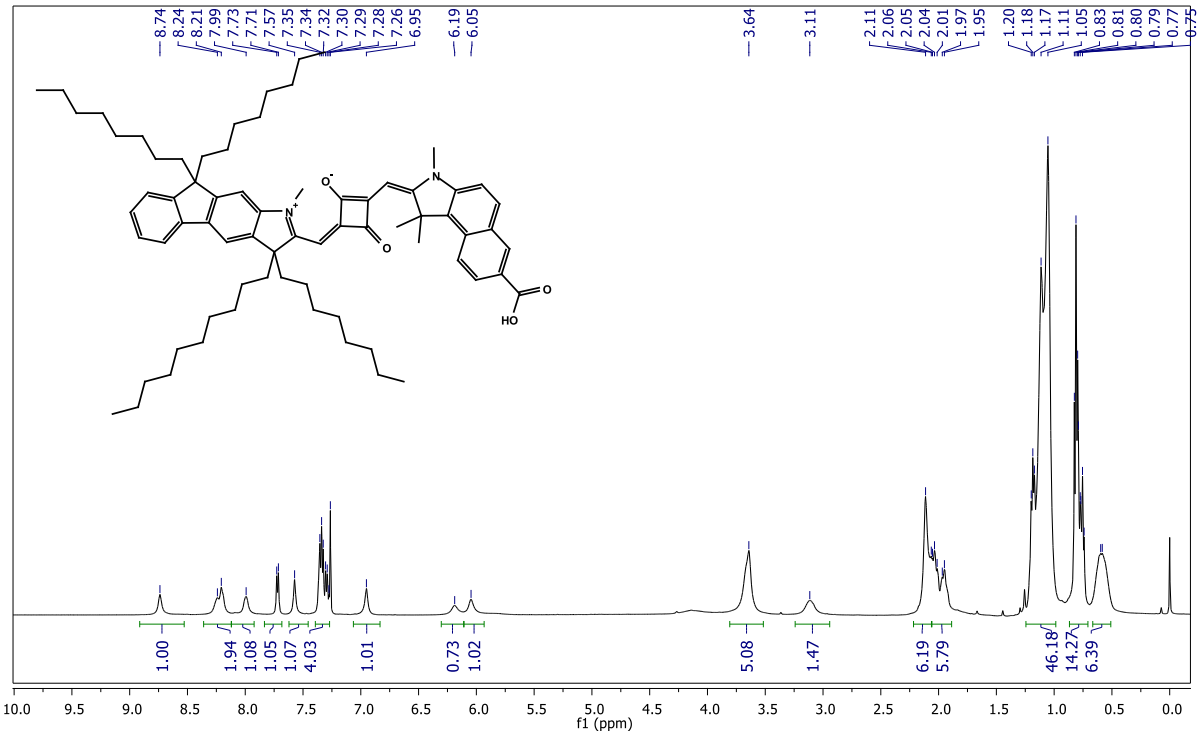

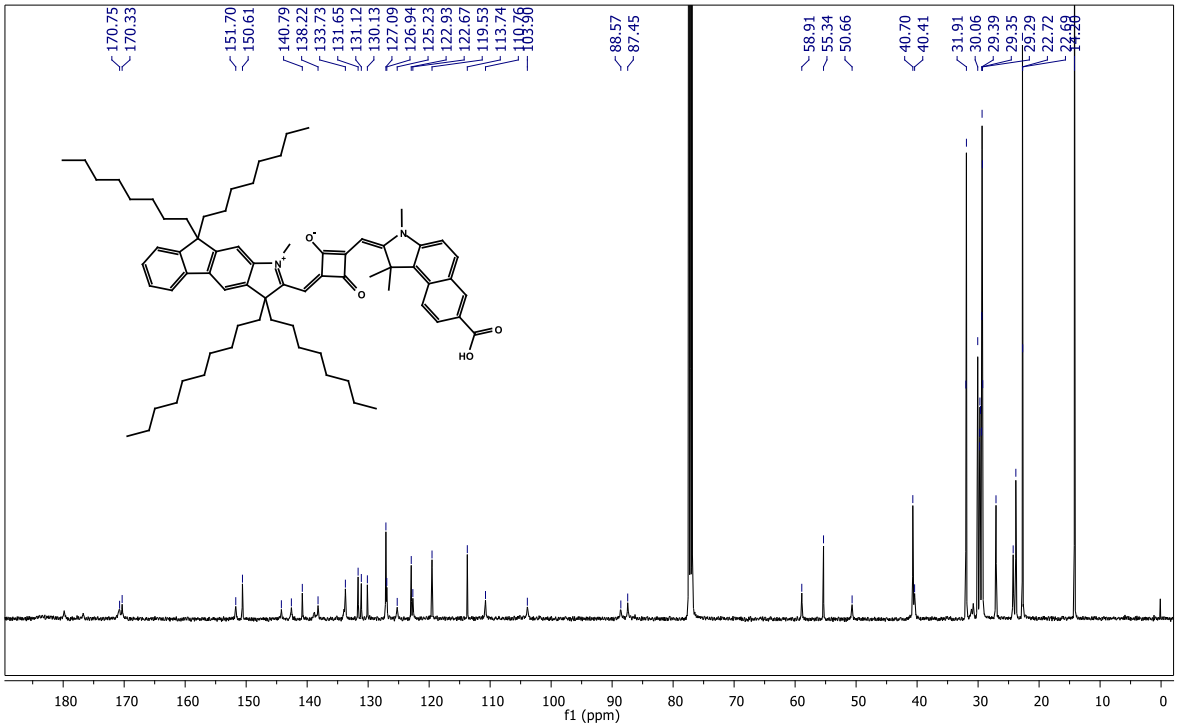

^{1}H and ^{13}C NMR spectra of XSQ4.

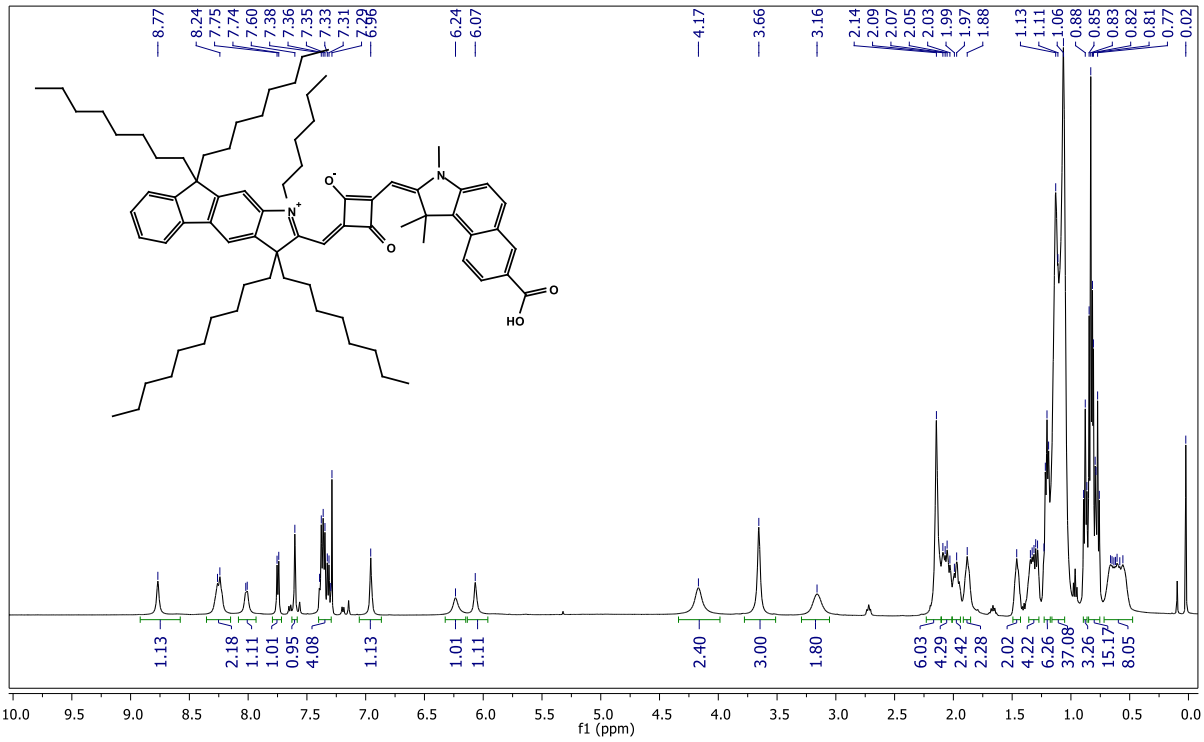

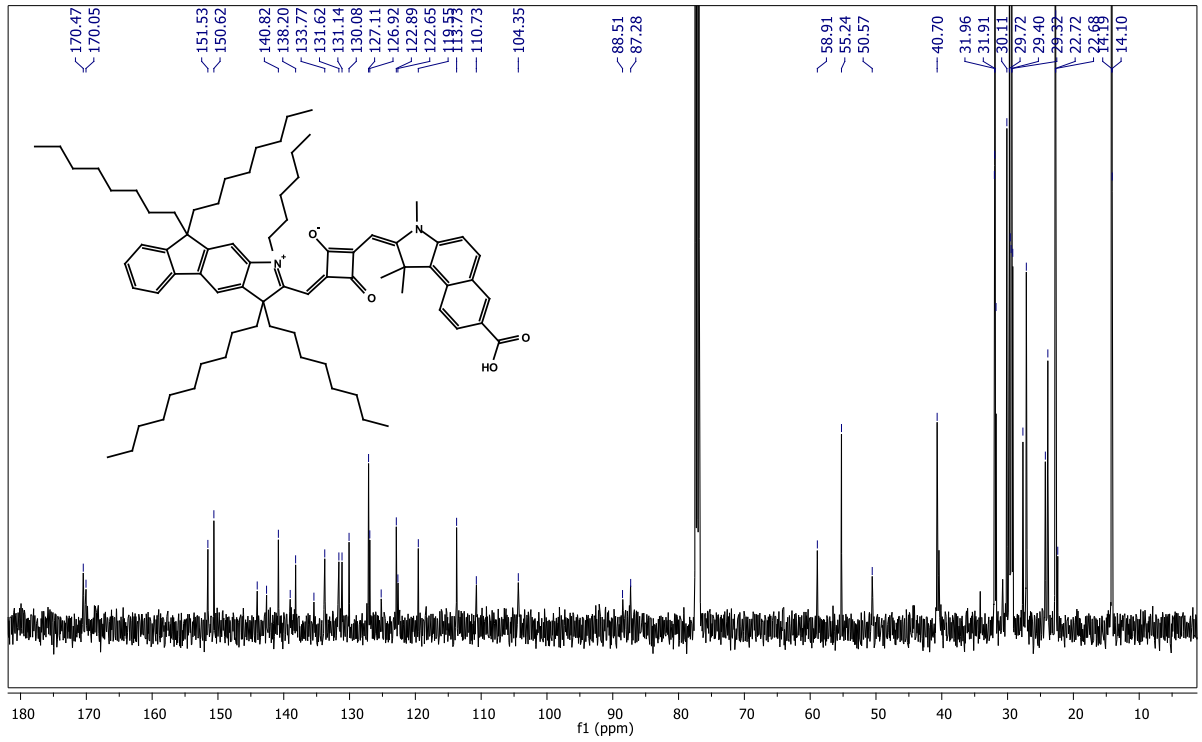

3.6. REFERENCES

(1) Zhang, S.; Yang, X.; Numata, Y.; Han, L. *Energy Environ. Sci.* **2013**, *6*, 1443.

(2) Brogdon, P.; Cheema, H.; Delcamp, J. H. *ChemSusChem* **2018**, *11*, 86–103.

(3) Jradi, F. M.; Kang, X.; O'Neil, D.; Pajares, G.; Getmanenko, Y. A.; Szymanski, P.; Parker, T. C.; El-Sayed, M. A.; Marder, S. R. *Chem. Mater.* **2015**, *27*, 2480–2487.

(4) Jradi, F. M.; O'Neil, D.; Kang, X.; Wong, J.; Szymanski, P.; Parker, T. C.; Anderson, H. L.; El-Sayed, M. A.; Marder, S. R. *Chem. Mater.* **2015**, *27*, 6305–6313.

(5) Shi, Y.; Hill, R. B. M.; Yum, J.-H.; Dualeh, A.; Barlow, S.; Grätzel, M.; Marder, S. R.; Nazeeruddin, M. K. *Angew. Chem. Int. Ed.* **2011**, *50*, 6619–6621.

(6) Delcamp, J. H.; Shi, Y.; Yum, J.-H.; Sajoto, T.; Dell'Orto, E.; Barlow, S.; Nazeeruddin, M. K.; Marder, S. R.; Grätzel, M. *Chem. – Eur. J.* **2013**, *19*, 1819–1827.

(7) Bae, S. H.; Seo, K. D.; Choi, W. S.; Hong, J. Y.; Kim, H. K. *Dyes Pigments* **2015**, *113*, 18–26.

(8) Hanumantha Rao, G.; Venkateswararao, A.; Giribabu, L.; Prakash Singh, S. *Photochem. Photobiol. Sci.* **2016**, *15*, 287–296.

(9) Geiger, T.; Kuster, S.; Yum, J.-H.; Moon, S.-J.; Nazeeruddin, M. K.; Grätzel, M.; Nüesch, F. *Adv. Funct. Mater.* **2009**, *19*, 2720–2727.

(10) Park, J.; Barbero, N.; Yoon, J.; Dell'Orto, E.; Galliano, S.; Borrelli, R.; Yum, J.-H.; Censo, D. D.; Grätzel, M.; K. Nazeeruddin, M.; Barolo, C.; Viscardi, G. *Phys. Chem. Chem. Phys.* **2014**, *16*, 24173–24177.

(11) Maeda, T.; Nitta, S.; Sano, Y.; Tanaka, S.; Yagi, S.; Nakazumi, H. *Dyes Pigments* **2015**, *122*, 160–167.

(12) Maeda, T.; Shima, N.; Tsukamoto, T.; Yagi, S.; Nakazumi, H. *Synth. Met.* **2011**, *161*, 2481–2487.

(13) Pandey, S. S.; Watanabe, R.; Fujikawa, N.; Shivashimpi, G. M.; Ogomi, Y.; Yamaguchi, Y.; Hayase, S. *Tetrahedron* **2013**, *69*, 2633–2639.

(14) Yan, Z.; Guang, S.; Su, X.; Xu, H. *J. Phys. Chem. C* **2012**, *116*, 8894–8900.

(15) Li, J.-Y.; Chen, C.-Y.; Ho, W.-C.; Chen, S.-H.; Wu, C.-G. *Org. Lett.* **2012**, *14*, 5420–5423.

(16) Kumar, D.; Justin Thomas, K. R.; Lee, C.-P.; Ho, K.-C. *J. Org. Chem.* **2014**, *79*, 3159–3172.

(17) Singh, P.; Baheti, A.; Thomas, K. R. J.; Lee, C.-P.; Ho, K.-C. *Dyes Pigments* **2012**, *95*, 523–533.

(18) Thomas, K. R. J.; Lin, J. T.; Hsu, Y.-C.; Ho, K.-C. *Chem. Commun.* **2005**, *0*, 4098–4100.

(19) Yella, A.; Humphry-Baker, R.; Curchod, B. F. E.; Ashari Astani, N.; Teuscher, J.; Polander, L. E.; Mathew, S.; Moser, J.-E.; Tavernelli, I.; Rothlisberger, U.; Grätzel, M.; Nazeeruddin, M. K.; Frey, J. *Chem. Mater.* **2013**, *25*, 2733–2739.

(20) Wu, C.-H.; Pan, T.-Y.; Hong, S.-H.; Wang, C.-L.; Kuo, H.-H.; Chu, Y.-Y.; Diau, E. W.-G.; Lin, C.-Y. *Chem. Commun.* **2012**, *48*, 4329–4331.

(21) Choi, H.; Kim, J.-J.; Song, K.; Ko, J.; Nazeeruddin, M. K.; Grätzel, M. *J. Mater. Chem.* **2010**, *20*, 3280–3286.

(22) Alagumalai, A.; M. K., M. F.; Vellimalai, P.; Sil, M. C.; Nithyanandhan, J. *ACS Appl. Mater. Interfaces* **2016**, *8*, 35353–35367.

(23) Karjule, N.; MK, M. F.; Nithyanandhan, J. *J. Mater. Chem. A* **2016**, *4*, 18910–18921.

(24) Wenger, S.; Bouit, P.-A.; Chen, Q.; Teuscher, J.; Censo, D. D.; Humphry-Baker, R.; Moser, J.-E.; Delgado, J. L.; Martín, N.; Zakeeruddin, S. M.; Grätzel, M. *J. Am. Chem. Soc.* **2010**, *132*, 5164–5169.

(25) Hara, K.; Sato, T.; Katoh, R.; Furube, A.; Ohga, Y.; Shinpo, A.; Suga, S.; Sayama, K.; Sugihara, H.; Arakawa, H. *J. Phys. Chem. B* **2003**, *107*, 597–606.

(26) Frisch, M. J.; Trucks, G. W.; Schlegel, H. B.; Scuseria, G. E.; Robb, M. A.; Cheeseman, J. R.; Scalmani, G.; Barone, V.; Mennucci, B.; Petersson, G. A.; Nakatsuji, H.; Caricato, M.; Fox, D. J.; et al. Gaussian, Inc.: Wallingford, CT, USA*Gaussian 09*, 2009.

(27) Buhbut, S.; Clifford, J. N.; Kosa, M.; Anderson, A. Y.; Shalom, M.; Major, D. T.; Palomares, E.; Zaban, A. *Energy Environ. Sci.* **2013**, *6*, 3046.

(28) Liang, Y.; Cheng, F.; Liang, J.; Chen, J. *J. Phys. Chem. C* **2010**, *114*, 15842–15848.

(29) Liu, S.-J.; Zhao, Q.; Deng, Y.; Xia, Y.-J.; Lin, J.; Fan, Q.-L.; Wang, L.-H.; Huang, W. *J. Phys. Chem. C* **2007**, *111*, 1166–1175.

(30) Bisht, R.; M. K., M. F.; Singh, A. K.; Nithyanandhan, J. *J. Org. Chem.* **2017**, *82*, 1920–1930.

Chapter 4

Indenoquinaldine based Unsymmetrical Squaraine Dyes for Near-Infrared Responsive Dye-sensitized Solar Cells

4.1. INTRODUCTION

Several sensitizers have been synthesized for DSSCs, and continuous exploration in their structure-property relationship has improved the efficiency up to 13%. Many of these dyes have very good IPCE (80-90%) in the visible light region (ca. 350– 600 nm) which helps them generate high photocurrent. However, most of these dyes lack absorption in NIR region, and a significant portion of incident photon remains uncollected. To utilize the low energy photons of the solar spectrum, it is necessary to develop NIR responsive dyes for DSSC. Among the NIR sensitizers, squaraine dyes are considered as one of the promising candidates because of their intense absorption, high photostability, and their ability to extend absorption to longer wavelengths.

In the previous chapter, we fused fluorene with indolenine to enhance the absorption of squaraine dyes towards longer wavelengths and incorporated out-of-plane alkyl chains to avoid aggregation. The out-of-plane alkyl chain facilitated immensely in controlling aggregation which helped the **XSQ3** to obtain 6.4% efficiency. However, the IPCE response could not be increased beyond 800 nm. To improve the photoresponse of squaraine dyes further into NIR region we explored the possibility of fusing fluorene unit with more π-extended heterocyclic moieties instead of indolenine. Several fused π-extended heterocyclic structures have been incorporated in squaraine dyes as they can induce strong intramolecular charge transfer (ICT) as well as maintain planarity of the molecule. Benz[e]indole[1,2] have been used as donor instead of indole to influence its absorption, and Park et al. managed to attain IPCE onset of ca. 750 nm with response up to ca 80% from 650 to 710 nm leading to efficiency over 6%.[3] In order to further push the absorption beyond 750 nm, Li et al. used carboxylated quinoline unit towards anchoring group and triphenylamine towards non-anchoring side to give the NIR-absorbing dye with IPCE onset up to 1050 nm[4]. Pyrylium and Thiopyrylium components were also explored in squaraine dyes, and IPCE onset at 800 nm was obtained. The best IPCE response of ca.45% was obtained at 700 nm which led to the best PCE of 2.63% for pyrylium based dye.[5] Benzo[c,d]indolenine based squaraine dye by Maeda et al gave the IPCE onset at 1000 nm but with very weak response (max IPCE of 3%) which lead to PCE of only 0.32%.[6] In another approach, dimeric squaraine dye BSQ01[7] was synthesized by Kuster et al. which showed IPCE onset at 800nm with the response of 18% leading to PCE of 1.3%. Maeda et al. improved upon this dimeric structure by modifying the donor at one end which improved the IPCE onset to 900nm with PCE of 2.26%.[8] In their later

work, Maeda et al. extended the IPCE onset to ca. 1000 nm by synthesizing trimeric squaraine dyes but PCE (η = 2.13%) could not be improved due to low IPCE response and poor V_{oc}. [9] Despite the strong NIR absorption, the squaraine dyes based on fused π–extended heterocyclic structures have low efficiency (~ 1-3%) which is due to either dye aggregation on TiO_2 or mismatched HOMO-LUMO levels. Thus, controlling the aggregation while maintaining good efficiency has been a major challenge in NIR absorbing dyes. In an attempt to overcome this shortcoming, we have designed and synthesized a series of unsymmetrical squaraine dyes (**ISQ1-3**) for DSSC consisting of a fused fluorene-quinaldine (Indenoquinaldine) based donor which can help in increasing the absorption in NIR region and also accommodates long alkyl chains at its sp^3-C center to control dye aggregation on TiO_2 surface. Quinaldine is chosen to fuse with fluorene as it has the ability to provide good absorption in NIR region in squaraine dyes.[10,11] While all the dyes retained indenoquinaldine as a donor, carboxyindolenine (**ISQ1**), carboxybenz[e]indoleine (**ISQ2**) and carboxyquinaldine (**ISQ3**) were used towards anchoring group to systematically investigate their effect on various electronic properties of dyes and DSSC parameters.

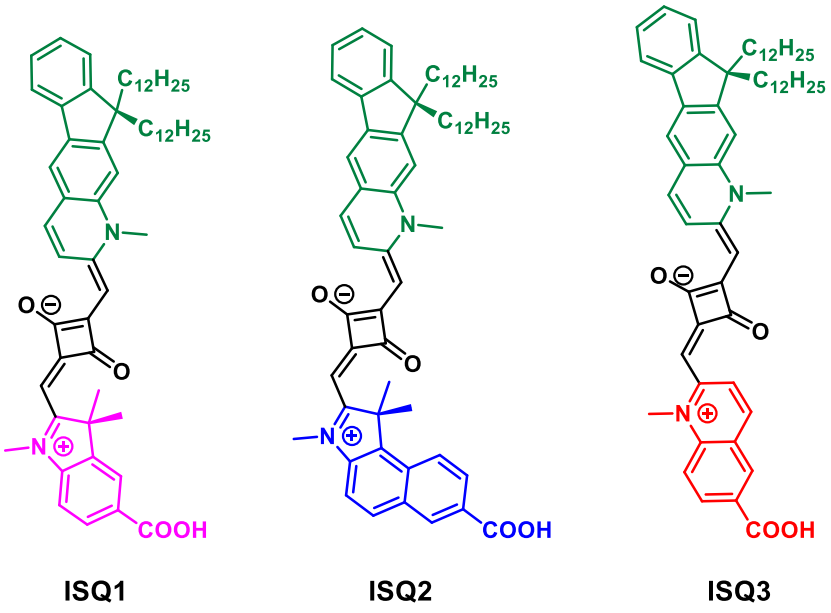

Figure 1. The molecular structures of **ISQ** dyes.

4.2. RESULTS AND DISCUSSION

4.2.1. Synthesis

The synthetic route for the dyes **ISQ1-3** is demonstrated in **scheme 1** and **2**. The key steps are the synthesis of indenoquinaldinium salt **5** and semi-squaric acid derivatives of carboxyindole **P1**, carboxybenz[e]indole **P2** and carboxyquinoline **P3**. Precursors, **P1** and **P2**, were synthesized according to the procedure described in the previous chapter (**Chapter 3**). To synthesize indenoquinaldinium salt **5**, 2-nitrofluorene (**1**) was functionalized with 12 carbon long chains by heating with dodecyliodide in aqueous NaOH and toluene. The resultant compound **2** was reduced to 2-amino-9,9-didodecylfluorene (**3**) by hydrazine hydrate in the presence of catalyst Pd/C.

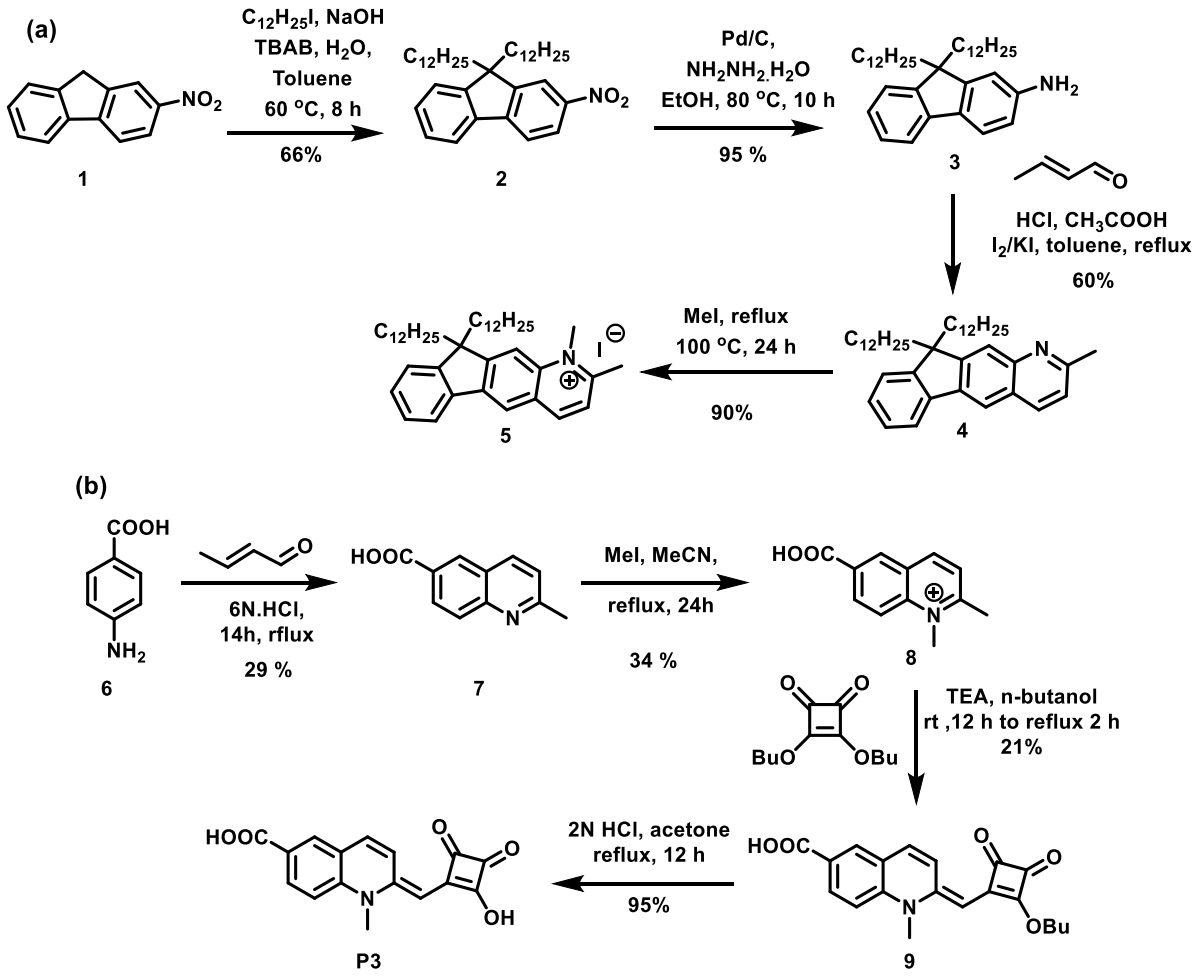

Scheme 1. Synthesis of compound a) indenoquinaldinium iodide 5, d) semi-squaric acid **P3.**

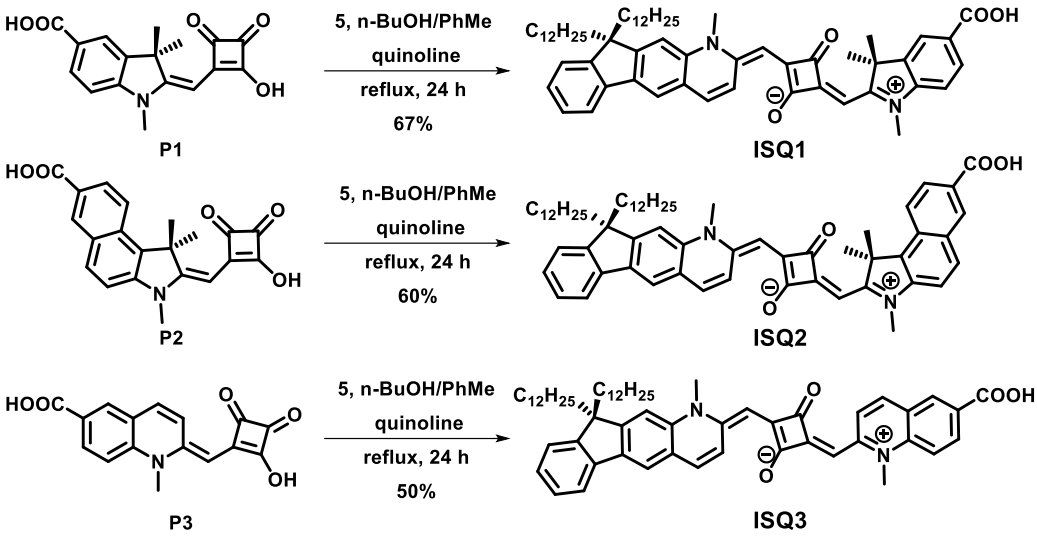

Scheme 2. Synthesis of indenoquinaldine donor based squaraine dyes (**ISQ1-3**).

The amine derivative **3** was treated with crotonaldehyde in the presence of HCl and acetic acid under Skraup-Doebner-Von Miller reaction condition to afford indenoquinaldine **4**. The compound **4** was subsequently heated with methyl iodide in a sealed tube to give N-methyl indenoquinaldinium salt **5**. To obtain precursor **P3**, we synthesized carboxyquinalidine **7** by refluxing 4-aminobenzoic acid with crotonaldehyde in 6N HCl. The product was treated with methyliodide to give methylated carboxyquinaldinium iodide **8**. This salt was treated with 3,4-dibutoxy-3-cyclobutene-1,2-dione in n-butanol in the presence of triethylamine to give compound **9**. The treatment of compound **9** with HCl in acetone afforded semi-squaraic acid **P3** in good yield. In the final step, the semi-squaric acid derivative **P1** was refluxed with indenoquinaldinium salt **5** in n-BuOH/PhMe mixture under azeotropic distillation of water employing Dean−Stark apparatus to give squaraine dyes **ISQ1**. Similarly, the dyes **ISQ2** and **ISQ3** were obtained by treating **5** with **P2** and **P3** respectively. All the dyes were carefully characterized by ^{1}H-NMR, ^{13}C-NMR spectroscopy, and high resolution mass spectrometric (HRMS) techniques.

4.2.2. Optical and Electrochemical Properties

The optical properties of **ISQ1-3** dyes were investigated by UV-vis absorption and emission spectroscopy in $CHCl_3$ solutions (**Figure 2** and data are summarized in **Table 1**). **ISQ** dyes exhibited intense absorption band in the far-red region with high extinction coefficient ($\geq 10^5$ M^{-1} cm^{-1}) due to strong intramolecular charge transfer (ICT) process. Due to the strong donating effect of the indenoquinaldine unit, **ISQ1** showed the absorption maximum (λ_{max}) at

692 nm with onset at 734 nm. The red-shifted λ_{max} at 715 nm with onset at 760 nm was observed for **ISQ2** due to extended conjugation by carboxybenz[e]indole unit towards anchoring group.

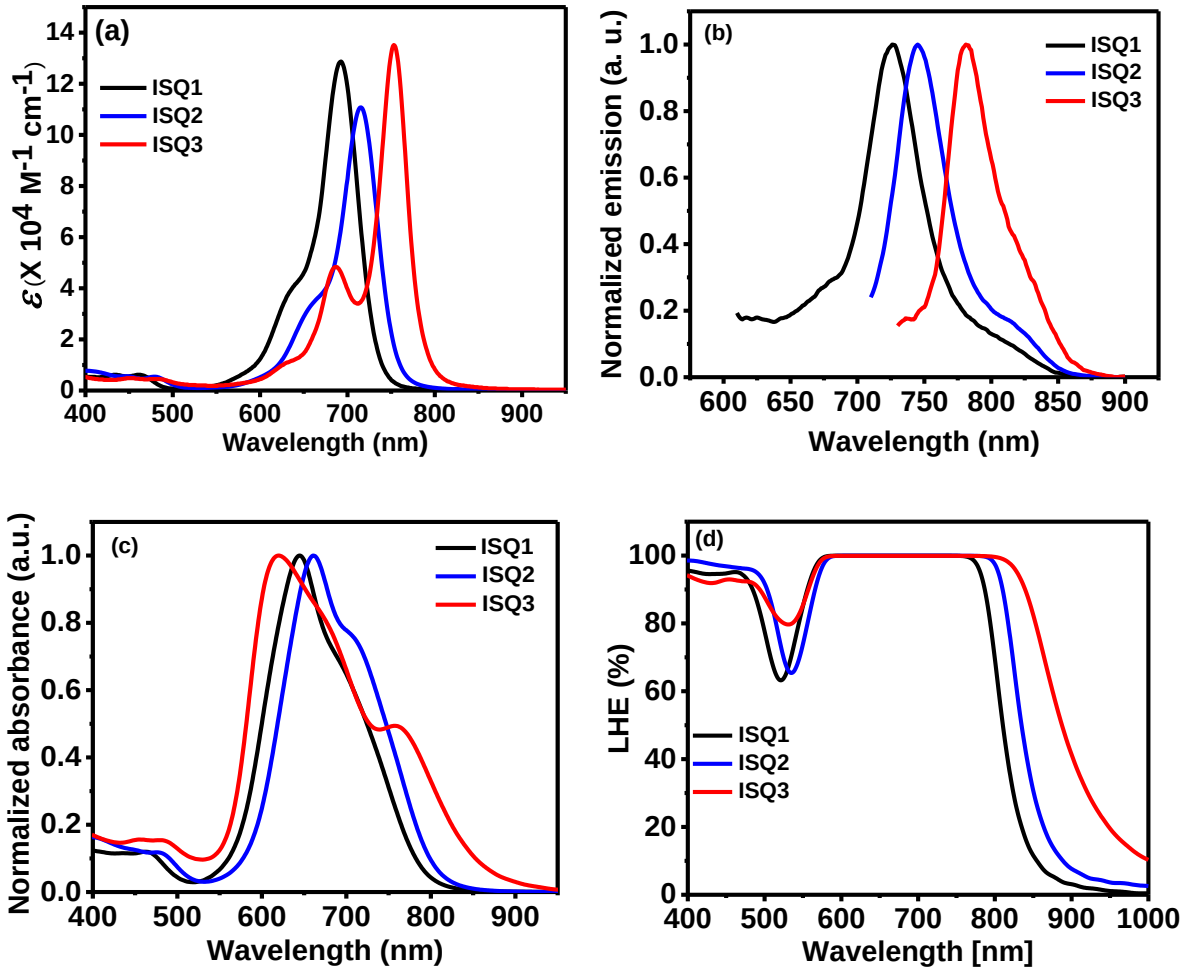

Figure 2. (a) The absorption spectra of **ISQ1-3** in $CHCl_3$ ([dye] = 6 µM), (b) Normalized emission spectra ([dye] = 6 µM in $CHCl_3$), λ_{exc} = 600nm (**ISQ1**), 700 nm (**ISQ2**) and 720 nm (**ISQ3**) , (c) Normalized absorption spectra of **ISQ** dyes immobilized on TiO_2, and (d) Light harvesting efficiency of the **ISQ** dyes.

The presence of quinaldine on both ends of central squaraine unit caused the maximum bathochromic shift for **ISQ3** and λ_{max} was determined at 754 nm with onset at 800 nm. The same trend was observed in emission spectra of the dyes which displayed emission maxima at 726 nm, 745 nm and 781 nm for **ISQ1**, **ISQ2** and **ISQ3** respectively (**Figure 2b**). Apart from the intense absorption in NIR region, a weak absorption ($\varepsilon \approx 10^3$ $M^{-1}cm^{-1}$) in the visible

region was observed between 400 to 500 nm for **ISQ1-3** which can be beneficial to absorb the high energy photons as well.

The titania coated glass was immersed in 0.1 mM dye solution for 15 minutes, and the absorption spectra of dye anchored on TiO_2 film were recorded to understand the interaction of dyes on TiO_2 film. The spectra displayed peak broadening compared to the spectra in solution due to strong coupling of anchoring group (-COOH) with TiO_2. and the formation of H-type (blue-shifted) aggregates prominently (**Figure 2c**). **ISQ3** exhibited maximum broadening with high-intensity absorption ranging from 550 nm to 900 nm. Light harvesting efficiency (LHE = 1- 10^{-A}) of dyes anchored on TiO_2 represents the capacity of dyes to absorb the photons of various energy across the solar spectrum. LHE profiles show that all the dyes are able to harvest the photons from visible as well as NIR region with LHE ≥ 90% in 400-500 nm and 550-850 nm range which makes these sensitizers suitable candidates for panchromatic absorption. The dyes **ISQ1**, **ISQ2,** and **ISQ3** showed LHE onset at 850 nm, 880 nm, and 1000 nm respectively which lie well in the NIR region.

Cyclic voltammetry was carried out in CH_2Cl_2 solutions to determine their redox potentials as well as to calculate the electron-injection ($-\Delta G_{inj}$) and dye regeneration ($-\Delta G_{reg}$) driving forces (**Figure 3**). HOMO levels of the dyes **ISQ1-3** were obtained from the first oxidation onset and calculated to be at 0.62 V, 0.55V, and 0.47 V respectively (Vs. NHE) (**Table 1**). The upward shift of HOMO in case of **ISQ2** and **ISQ3** can be attributed to the stronger donating effect of benz[e]indole and quinoline respectively compared to indole. **ISQ1** shows high potential offset ($-\Delta G_{reg}$ = 220 meV) with respect to redox level of I^-/I_3^- (0.4 V) which provides large driving force for effective dye regeneration whereas **ISQ2** ($-\Delta G_{reg}$ = 150 meV) and **ISQ3** ($-\Delta G_{reg}$ = 70 meV) shows moderate driving force (**Figure 3b**). The LUMO levels were calculated by subtracting E_{0-0} from E_{HOMO} and found to be at -1.13 V, -1.15 V and -1.15 V (vs. NHE) for **ISQ1**, **ISQ2**, and **ISQ3** respectively which gives enough energy offset ($-\Delta G_{inject} \approx$ 700 meV) for charge injection into the conduction band (CB) of TiO_2 (-0.5 V). While the HOMO levels varied significantly, the LUMO levels were essentially the same for all the dyes. The band gap ($E_{0\text{-}0}$) was calculated from the intersection of absorption and emission curve and found to be at 1.75 eV, 1.70 eV and 1.62 eV for **ISQ1**, **ISQ2,** and **ISQ3** respectively.

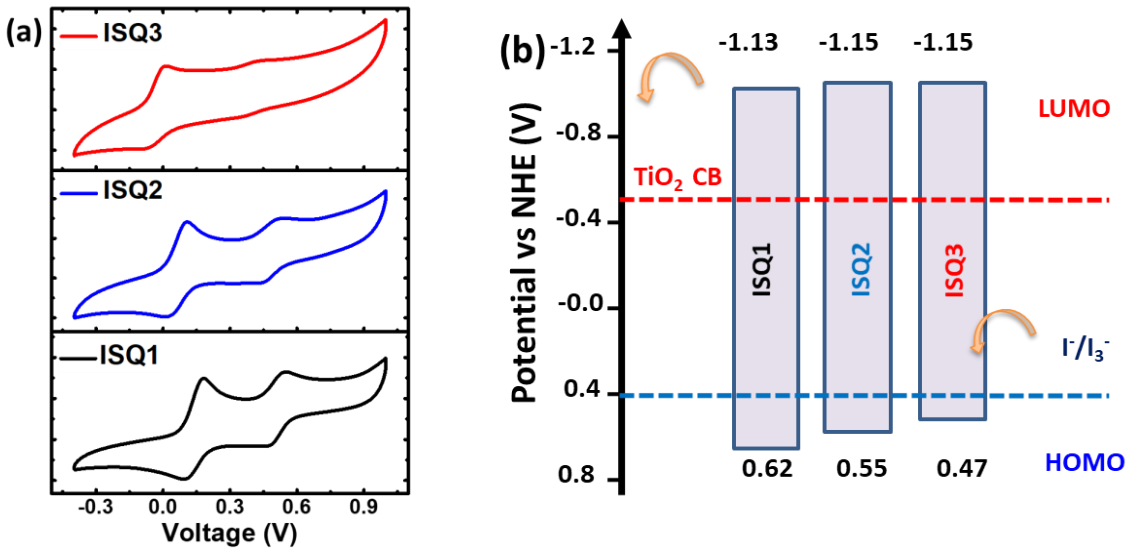

Figure 3. (a) Cyclic voltammogram of **ISQ** dyes measured in CH_2Cl_2 (b) Energy level diagram for **ISQ** dyes with DSSC device components.

Table 1. Optical and electrochemical data of **ISQ** dyes

Dyes	$^{Abs}\lambda_{max}$ /CH_2Cl_2 (nm)[a]	$^{Emi}\lambda_{max/}$ CH_2Cl_2 (nm)[b]	$^{abs}\lambda_{max}$/ TiO_2 (nm)[c]	$\varepsilon \times 10^4$ ($M^{-1}cm^{-1}$)[d]	$E_{g/DFT}$ (eV)[e]	E_{HOMO} (V vs NHE)[f]	$E_{0\text{-}0}$ (eV)[g]	E_{LUMO} (V vs NHE)[h]
ISQ1	462, 692	726	645, 690	0.62, 12.9	2.09	0.62	1.75	-1.13
ISQ2	480, 715	745	661, 714	0.56, 11.1	1.97	0.55	1.70	-1.15
ISQ3	487, 754	781	620, 753	0.43, 13.5	1.77	0.47	1.62	-1.15

[a]UV−Vis absorption in $CHCl_3$. [b]Emission studies. [c]On thin film of TiO_2, thickness = 6 μm, dipping time = 15 min, and [**ISQ**] = 0.1 mM in CH_2Cl_2. [d]Molar extinction coefficient ε. [e]Band gap calculated by DFT. [f]E_{HOMO} of **ISQ1−3** in CH_2Cl_2, Fc^+/Fc was used as the external standard, and potential measured vs. Fc/Fc+ (eV) was converted to NHE (V) by addition of 0.7 V. [g]$E_{0\text{-}0}$ was deduced at the intersection of absorption and emission spectra using equation $E_{0\text{-}0}$ (eV) = $1240/\lambda_{0\text{-}0}$. [h]$E_{LUMO}$ levels were measured by subtracting E_{HOMO} from $E_{0\text{-}0}$.

4.2.3. Computational Studies

To gain the additional insights into the structural properties, and the nature of excited states of **ISQ** dyes, quantum mechanical calculation were carried out using density functional theory (DFT) and time-dependent DFT (TD-DFT) at B3LYP/6-31G (d,p) level in Gaussian 09[12]. Electron density distribution after structural optimization in the HOMOs and LUMOs of the dyes under investigation is shown in Figure 4. Isodensity surface plots of **ISQ1-3** dyes show that HOMO are predominantly confined to central squaraine unit (**Figure 4)**. The HOMO and LUMO overlap for the most part of **ISQ1-3** dyes, however, there is slight delocalization of LUMO towards the anchoring group in case of **ISQ3**. This shift of electron density from the HOMO to LUMO level beneficial for the spontaneous charge transfer and the presence of electron density on the anchoring group also ensure the good electronic coupling between the excited state dye and TiO_2. LUMO+1 and LUMO+2 are prominently delocalized towards anchoring group for the **ISQ3** dye which suggests that it can exhibit better charge injection compared to **ISQ1-2** and can counterbalance the effect of low driving force for dye regeneration.

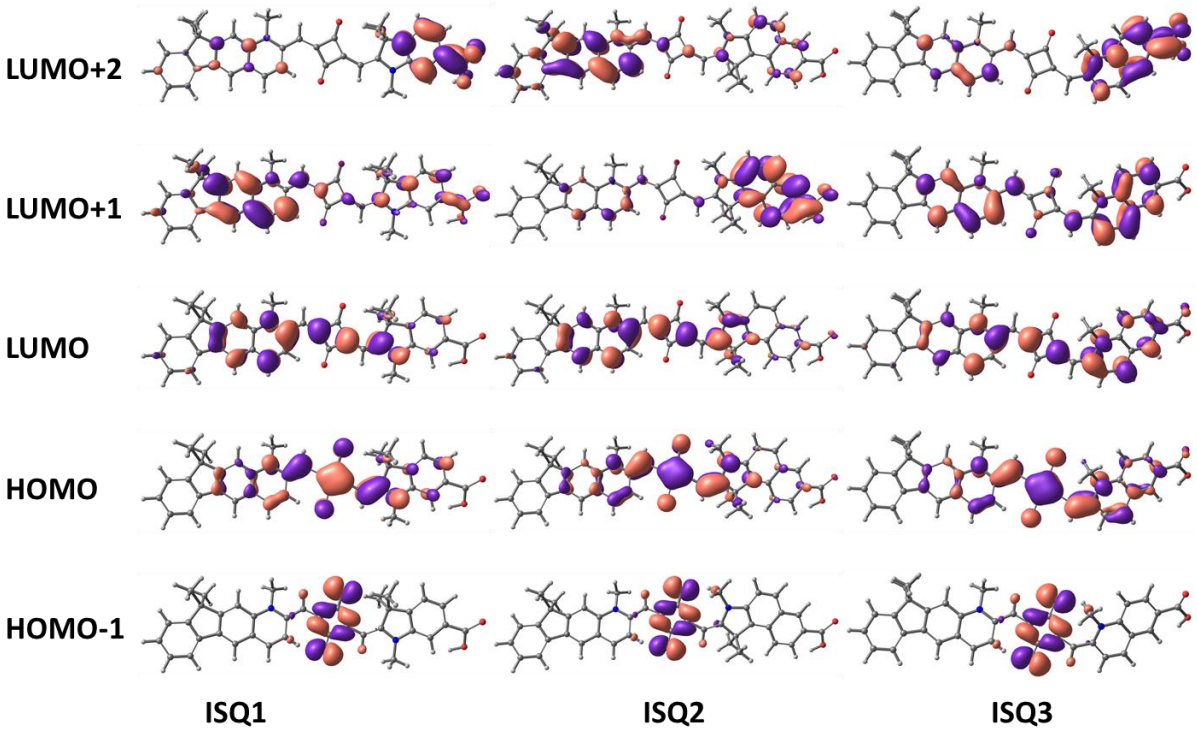

Figure 4. Isodensity surface plots of **ISQ1-3** dyes (alkyl chains are removed for clarity)

The simulated absorption spectra were plotted using TD-DFT to understand the excited state nature of **ISQ** dyes (**Figure 5**).

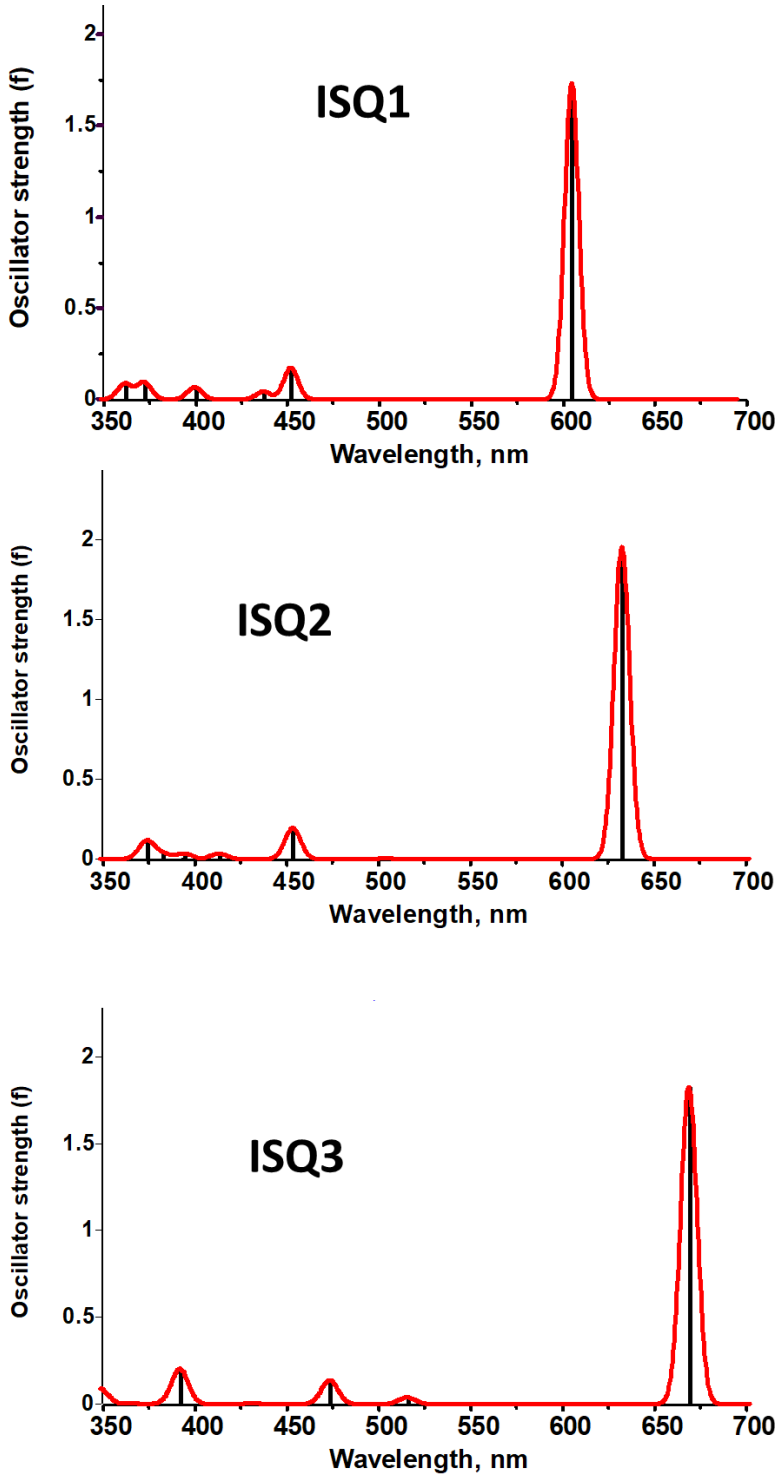

Figure 5. The simulated absorption spectra of **ISQ** dyes calculated by TD-DFT using B3LYP functional and 6-31G (d,p) basis set.

The simulated spectra were found to be consistent with the experimental ones, and by comparing the two spectra it can be predicted that the peaks of high oscillator strength (f ≈ 1.7-1.9) at longer wavelength originates exclusively from HOMO-LUMO vertical energy transition (> 99% contribution) in all the dyes. In addition, the high energy peaks with low oscillator strength (f ≈ 0.1 – 0.2) between 350 and 500 nm were also observed which are associated with the transition to higher excited states, i.e. LUMO+1, LUMO+2 (**Table 2**).

Table 2. Computed wavelengths and oscillator strengths (f) of the electronic transitions for **ISQ** dyes (H: HOMO, L: LUMO)

Dye	Computed λ_{abs} (nm)	Oscillator strength (f)	Composition
ISQ1	604.59 nm	1.71	H → L+1 (99%)
	451.64 nm	0.17	H → L+1 (93%)
	436.75 nm	0.04	H → L+2 (97%)
	371.75 nm	0.09	H-2 → L (53%), H-3→ L (23%)
ISQ2	632.41 nm	1.94	H → L (99%)
	453.14 nm	0.19	H → L+2 (96%)
	373.72 nm	0.11	H-3 → L (70%), H→ L+4 (11%)
ISQ3	668.56 nm	1.82	H → L (100%)
	515.27 nm	0.04	H → L+1 (84%)
	473.12 nm	0.14	H → L+2 (80%)
	391.62 nm	0.20	H-2 → L (68%), H-4 → L (20%)

4.2.4. Photovoltaic Performance

The photovoltaic measurements of the DSSCs fabricated using **ISQ1-3** dyes were done under irradiance of 100 mW cm^{-2} simulated AM 1.5G sunlight. The current density-voltage (J-V) plot and IPCE spectra of the best cells are shown in **Figure 6** and data are summarized in **Table 3**.

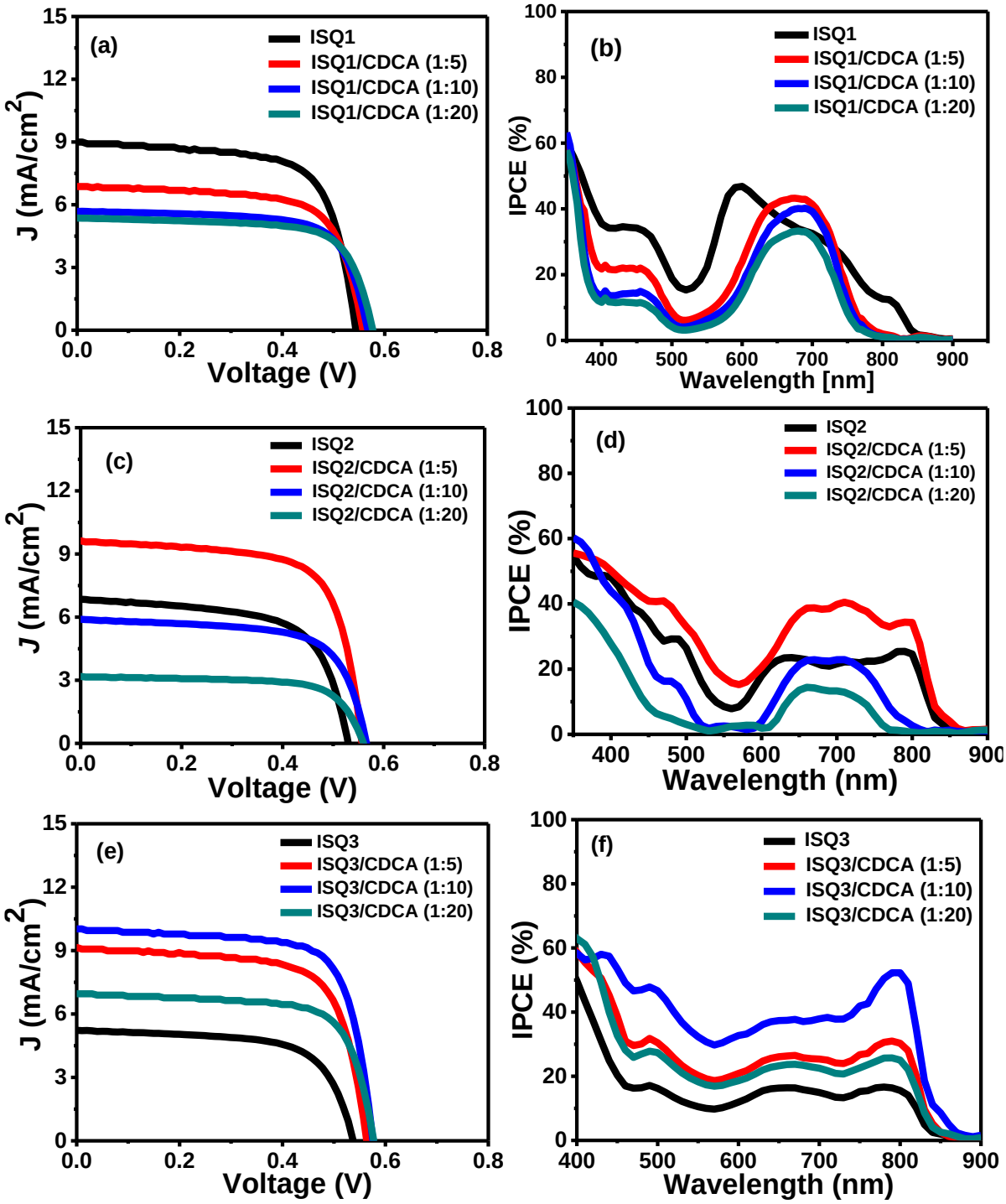

Figure 6. *J*−*V* and IPCE curve of **ISQ** sensitized dyes with varying CDCA concentration in dye solution in CH_2Cl_2. (dipping time = 12 h, TiO_2 active area = 0.22 cm^2).

Table 3. Photovoltaic parameters for **ISQ1-3** sensitized DSSCs employing the I^-/I_3^- electrolyte under the optimized conditions[a]

Dyes	J_{SC} (mA cm^{-2})	V_{OC} (V)	*ff* (%)	η (%)	Dye loading (mol cm^{-2})[b]
ISQ1	8.99	0.544	68.4	3.34	2.33×10^{-7}
ISQ1/CDCA (1:5)	6.86	0.558	68.9	2.63	7.56×10^{-8}
ISQ1CDCA (1:10).	5.68	0.568	70.7	2.28	-
ISQ1/CDCA (1:20)	5.36	0.578	70.7	2.19	-
ISQ2	6.85	0.537	64.1	2.35	2.82×10^{-7}
ISQ2/CDCA (1:5)	9.62	0.558	68.7	3.68	1.22×10^{-7}
ISQ2CDCA (1:10)	5.89	0.562	69.0	2.28	-
ISQ2/CDCA (1:20)	3.18	0.570	69.7	1.26	-
ISQ3	5.23	0.538	65.7	1.85	2.54×10^{-7}
ISQ3/CDCA (1:5)	9.15	0.564	69.2	3.57	-
ISQ3CDCA (1:10)	10.02	0.576	72.0	4.15	1.05×10^{-7}
ISQ3/CDCA (1:20)	6.95	0.578	70.9	2.84	-

[a]Photovoltaic performance of **ISQ** cells, thickness of electrode: 8 + 4 μm (transparent + scattering) layer of TiO_2, Electrolyte: iodolyte Z-50 from Solaronix. [Dye] = 0.1 mM in CH_2Cl_2, dipping time = 12 h, Active area of 0.22 cm^2 and measurements were carried out under 1 sun intensity (100 mW cm^{-2}). [b]Dye loading was calculated spectrophotometrically by desorbing dye-sensitized photoanode in 2M HCl in EtOH and CH_2Cl_2 (1:1).

The DSSC based on **ISQ1** gave the PCE of 3.24% whereas **ISQ2** and **ISQ3** showed PCE of 2.35% and 1.85% without using any co-adsorbent. The major difference in their cell performance comes from the variation in the short circuit current density (J_{SC}) which is highest for **ISQ1** (8.99 mA cm^{-2}), followed by **ISQ2** (6.85 mA cm^{-2}) and **ISQ3** (5.23 mA cm^{-2}). The low short circuit current density could be ascribed to the reduced charge injection due to the strong aggregation of dye on TiO_2 which is maximum in case of **ISQ3**.

To minimize the negative effect of aggregation, the dyes were co-adsorbed in the presence of CDCA. All the **ISQ** dyes showed different response with the addition of CDCA (**Figure 6** and **Table 3**). The efficiency of **ISQ1** dyes reduced to 2.63% mainly due to a reduction in J_{SC} (6.86 mA cm^{-2}), even though the slight improvement in V_{OC} was observed (0.558 V). In contrast, the performance of **ISQ2** and **ISQ3** sensitized cells improved when co-adsorbed with CDCA. **ISQ2** achieved the maximum efficiency of 3.68% on addition of 5 equiv CDCA with V_{OC} of 0.558 V and J_{SC} of 9.62 mA cm^{-2}. **ISQ3** achieved the best efficiency of 4.15% with J_{SC} of 10.02 mA cm^{-2}, V_{OC} of 0.576 V, and *ff* of 72%, in presence 10 equiv of CDCA. Further addition of CDCA led to a reduction in device efficiency of all the dyes, primarily due to substantial loss of J_{SC}. It was suspected that the decrease in efficiency of **ISQ1** on the addition of CDCA could be due to reduced adsorption of dyes on the TiO_2 surface resulting from the competitive binding of CDCA. To validate our premise, the dye loading was calculated by desorption of dye-sensitized photo-anodes in the presence of 2M ethanolic HCl followed by spectrophotometric measurement of dye concentration. In case of **ISQ1**, the addition of CDCA as low as 5 equiv led to the drastic decrease of 68% in dye content. The dye loading of **ISQ2** with 5 equiv CDCA (1.22×10^{-7} mol cm^{-2}) was significantly higher than the dye content of **ISQ1** devices with 5 equiv. CDCA (7.56×10^{-8} mol cm^{-2}). **ISQ3** sensitized cells, even in the presence of 10 equiv CDCA, showed higher dye content (1.05×10^{-7} mol cm^{-2}) compared to **ISQ1** (5 equiv CDCA). It demonstrates that dye-dye interaction is poor in case of **ISQ1** compared to other dyes, and it can be replaced by CDCA on TiO_2 rather easily (**Figure 7**). Thus, the variable effect of CDCA on the performance of DSSC could be ascribed to competitive binding of **ISQ1-3** dyes and CDCA on TiO_2. On the one hand, CDCA helps in improving J_{SC} and V_{OC} by reducing exciton quenching induced by aggregation on TiO_2 surface, on the other hand, it may replace the dye molecules to reduce the effective dye content on the photo-anode leading to poor performance.[13]

The variation in J_{SC} can be further explained through a detailed investigation of incident photon-to-current conversion efficiency (IPCE) spectra (**Figure 6b**, **6d**, and **6f**)). **ISQ1** showed best IPCE response with a maximum of 46% at 600 nm without CDCA, which is primarily contributed by the H-type aggregates. There is also a peak of low IPCE (12%) at 810 nm which can be attributed to current generation from J-aggregates.

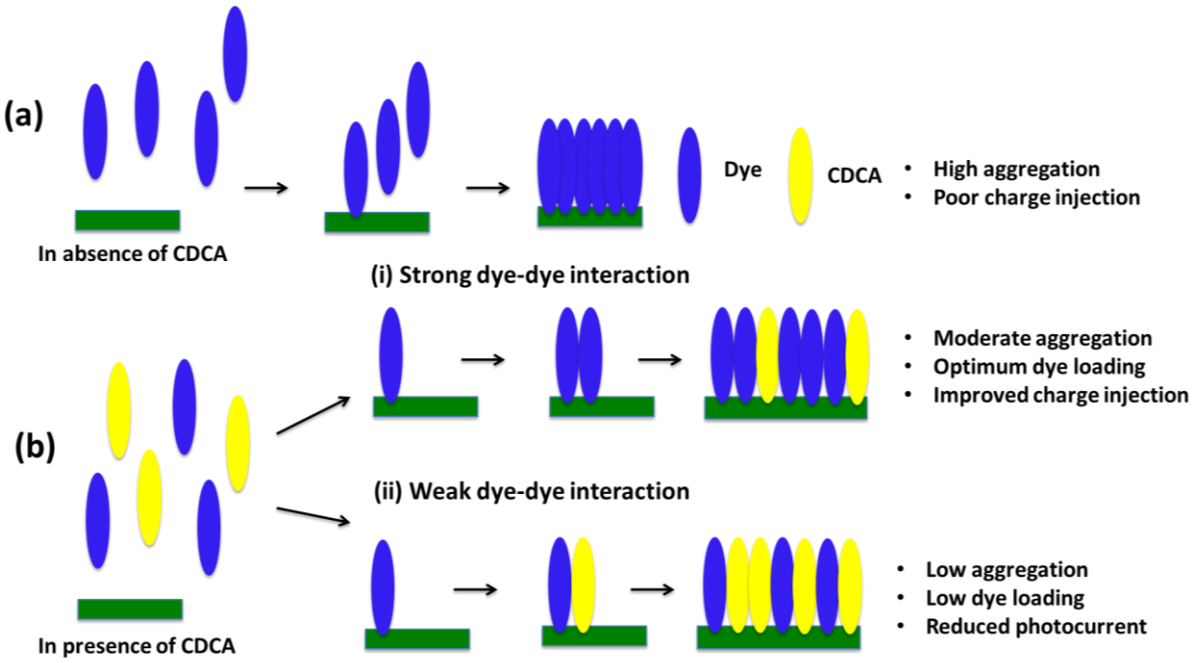

Figure 7. Cartoon representation of the formation of dye aggregate and variation in dye loading in the (a) absence of CDCA and the (b) presence of CDCA.

When CDCA is added, the aggregation was reduced effectively which can be observed as the disappearance of the peaks at 600 nm and 810 nm. The reduction in aggregation, though improved the V_{OC} from 0.544V to 0.558 V in **ISQ1** based cell, the severe decrease in dye amount led to low IPCE which in turn led to reduced $J_{SC.}$ In the case of **ISQ2**, the H-aggregates (23% at 640 nm) and J-aggregates (25% at 790 nm) contributed almost equally to IPCE, however, the overall response was much lower compared to **ISQ1**. Similarly, for **ISQ3**, the IPCE response was very low with equal contribution from H- (16% at 660 nm) and J- aggregates (16% at 780 nm). The reason behind the low IPCE for **ISQ2** and **ISQ3** in the absence of CDCA could be the formation of tightly stacked large-sized aggregates which could not inject electrons into the TiO_2. The extended π-surface of **ISQ2** and **ISQ3** due to benz[e]indole and quinoline moieties respectively, may induce such close intermolecular packing. The absence of two out-of-plane methyl group on carboxyquinoline group may

cause the **ISQ3** to aggregate excessively. When CDCA was added, both **ISQ2** and **ISQ3** showed improved IPCE response (**Figure 8b**).

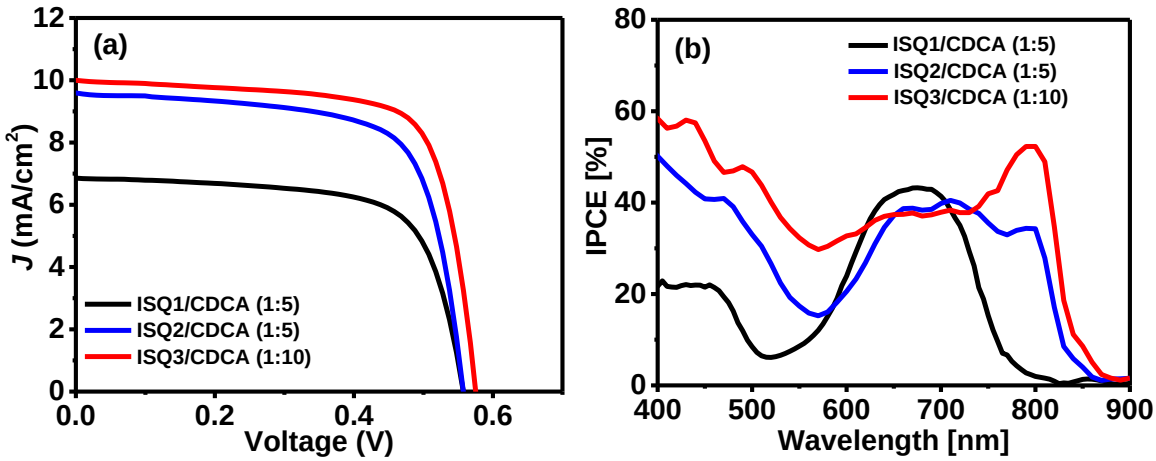

Figure 8. *J*−*V* and IPCE curves of the best device for **ISQ1-3** in the presence of CDCA.

ISQ2, with 5 equiv CDCA, showed IPCE of over 30% in between 650 to 800 nm with three distinct humps on the curve which are contributed by the H-type aggregates (39% at 650 nm), monomer (40% at 710 nm) and J-type aggregates (34% at 800 nm). In the case of **ISQ3** with 10 equiv CDCA), the contribution by J- aggregates was more prominent with IPCE over 50% at 800 nm whereas IPCE of 30-40% was obtained in the range of 600-750 nm which was contributed mainly by the monomer and H-type dye aggregates on the TiO_2 surface. The results indicate that for **ISQ2** and **ISQ3**, the addition of CDCA facilitated the formation of smaller aggregates in a controlled fashion which helped to inject electron more efficiently while maintaining the broad spectrum in comparison to the devices without CDCA. Remarkably, a substantial IPCE response of over 40% in the visible region (400-550 nm) was also observed in case of **ISQ3**. The origin of this response can be traced to the high concentration of electron density on anchoring group in higher excited states (LUMO, LUMO+1, and LUMO+2) which led to strong electronic coupling and good charge injection into the TiO_2 despite low oscillator strength. Hence, with the help of panchromatic IPCE, **ISQ3** attained better J_{SC} compared to other dyes and eventually higher efficiency.

4.2.5. Electrochemical Impedance Spectroscopy (EIS)

To explain the slight difference in V_{OC} values of **ISQ** sensitized cell electrochemical impedance spectroscopy (EIS) was carried out under dark conditions. Referring to the energy band diagram and the carrier transfer processes in **Figure 3**, the V_{OC} is calculated from the potential difference between the quasi-Fermi level of TiO_2 (E_F) and the chemical potential of redox species (E_{redox}) in the electrolyte (eq1).[14]

$$V_{OC} = E_{redox} - E_F \qquad (1)$$

$$E_F = E_{CB} + k_B T \ln\left(\frac{n_c}{N_c}\right) \qquad (2)$$

According to eq 2 the variation in E_F is linked to the number of electrons on the TiO_2 (n_c) and conduction band (E_{CB}) of TiO_2, where k_B is Boltzmann constant, and N_c is the effective density of state, T is the absolute temperature (293 K). Thus, V_{OC} is intimately susceptible to shift in the TiO_2 conduction band edge (E_{CB}), which can be deduced from the chemical capacitance (C_μ) and fluctuation of electron density, which is associated to the electron lifetime(s) determined by the charge recombination rate.[15,16] Typical EIS Nyquist plots for DSSCs based on the **ISQ1-3** dyes were measured in the dark under applied bias −0.5, −0.47, −0.44 and −0.41 V are fitted using $R_S + R_{Pt}/C_{Pt} + R_{ct}/C_\mu$ circuit model. The larger semicircle at lower frequencies in Nyquist plots represents the interfacial charge-transfer resistance (R_{ct}) at the TiO_2-dye/electrolyte interface (**Figure 9a**).

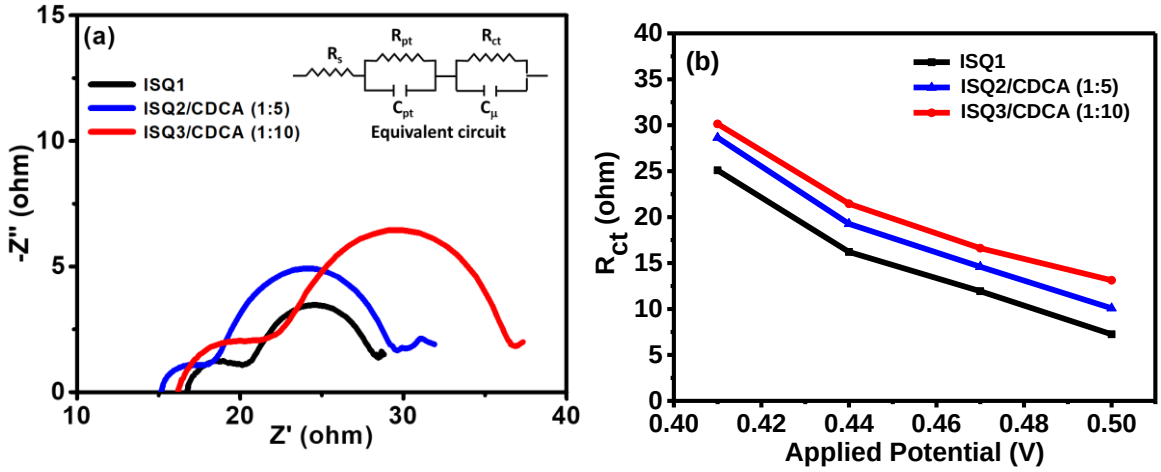

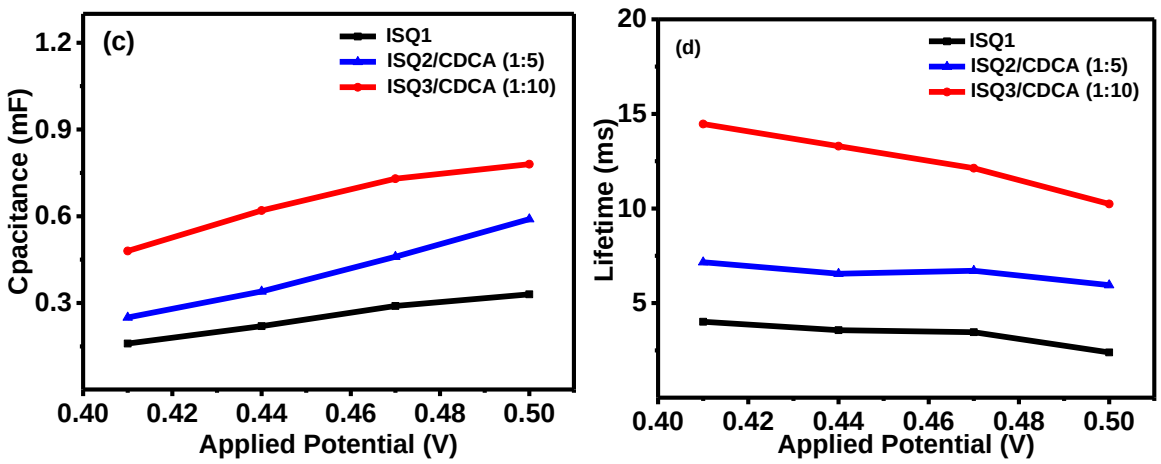

Figure 9. (a) The Nyquist plot at an applied bias of 0.5 V(the inset shows the equivalent circuit), (b) R_{ct} vs. applied potential, (c) C_{μ} vs. applied potential, and d) τ vs. applied potential.

The fitted recombination resistance (R_{ct}) value of **ISQ** sensitized devices (under an applied bias of -0.5 V) increases in the order of **ISQ1** (7.25 Ω) < **ISQ2** (10.08 Ω) < **ISQ3** (13.13 Ω), which is consistent with the sequence of V_{OC} values (**Figure 9b** and **Table 5**). Larger the R_{ct} values, slower is the recombination of electrons from the conduction band of TiO_2 to the oxidized I_3^- species in the electrolyte. The capacitance values also followed the same trend (**ISQ1** (0.33 mF) < **ISQ2** (0.59 mF) < **ISQ3** (0.78 mF)) which indicates the effect of dye on the conduction band shift. The electron lifetime(s) on TiO_2 were calculated from R_{CT} and chemical capacitance C_{μ} using $\tau = R_{ct} \times C_{\mu}$. The longer electron lifetime in **ISQ3** sensitized cell further supports the higher V_{OC} for **ISQ3** (10.24 ms) compared to **ISQ1**(2.39 ms) and **ISQ2** (5.94 ms) based cells (**Figure 5d** and **Table 4**).

Table 4. EIS parameters of **ISQ** dye cells at an applied potential of −0.5 V in the dark

Dyes	R_S (ohm)	R_{ct} (ohm)	C_{μ} (mF)	τ (ms)
ISQ1	15.80	7.25	0.33	2.39
ISQ2/CDCA (1:5)	14.56	10.08	0.59	5.94
ISQ3/CDCA (1:10)	14.41	13.13	0.78	10.24

4.3. SUMMARY

A series of NIR responsive unsymmetrical squaraine dyes (**ISQ1-3**) featuring a fused fluorenylquinoline as a π-extended donor have been successfully designed and synthesized. The sp^3-C center available on the fluorene unit was employed to incorporate twelve carbon long out-of-plane alkyl chains to control dye aggregation on titanium dioxide (TiO_2) surface. Indole (**ISQ1**), benz[e]indole (**ISQ2**) and quinoline (**ISQ3**) moieties were included towards anchoring group to increase the absorption in NIR region and systematically study the effect of the electronic modification on DSSC performance. All the dyes exhibit intense absorption ($\varepsilon \geq 10^5$ M^{-1} cm^{-1}) in the NIR region with onset at 820 nm for **ISQ3** and spectra broadened after absorption on TiO_2 surface which extends up to 1000 nm. The variable photovoltaic response was observed after addition of CDCA where the efficiency of **ISQ1** dyes decreased in contrast to improvement in efficiency of **ISQ2** and **ISQ3** due to competitive binding of CDCA against the dye. The incident photon to current efficiency (IPCE) spectrum of the **ISQ3** based device showed panchromatic response which ranges from 400 nm to 880 nm with IPCE up to 50% at 800 nm. The efficient electron injection by both H-type and J-type aggregates along with the monomers was observed. DFT and TDFT suggested the delocalization of LUMO+1 and LUMO+2 towards anchoring group which facilitated charge injection by high energy excitations as well especially for **ISQ3** which results in IPCE response in the visible region. As a result, **ISQ3** displayed the best photovoltaic properties among the dyes in the presence of 10 equiv CDCA with J_{SC} of 10.02 mA cm^{-2}, V_{OC} of 0.58 V and *ff* of 72% which led to the PCE of 4.15%. Electrochemical impedance spectroscopy (EIS) analysis revealed attenuated charge recombination for **ISQ3** based DSSC which attributes to its higher V_{oc} in comparison to other dyes. The results present a useful approach for developing efficient and NIR responsive sensitizers for DSSC application.

4.4. EXPERIMENTAL SECTION.

4.4.1. Materials and Methods

All reagents for dye synthesis and device fabrication were purchased from commercial sources and used without purification unless otherwise noted. ^1H NMR and ^{13}C NMR were recorded in, $CDCl_3$, MeOH-d_4 or DMSO-d_6 on 200, 400 and 500 MHz NMR spectrometers. High-resolution mass spectrometric measurements were carried out using the

ESI method and an ion-trap mass analyzer. Matrix-assisted laser desorption ionization time-of-flight mass spectrometry (MALDI-TOF MS) were recorded and ABSciex 5800 MALDI-TOF mass spectrometer, Absorption spectra were recorded at room temperature in quartz cuvette using a UV−visible spectrophotometer. The cyclic voltammetry (CV) analysis was carried out in anhydrous dichloromethane (CH_2Cl_2) using 0.1 M tetrabutylammonium perchlorate (0.1) M) as supporting electrolyte and Fc/Fc^+ as an internal reference. The experiments were performed at room temperature in a nitrogen atmosphere with a three-electrode cell consisting of a platinum foil as a counter electrode, a non-aqueous Ag/Ag^+ (0.01 M) reference electrode, and a platinum wire as the working electrode at the scan rate of 50 mVs^{-1}. The energy level of HOMO of **ISQ1-3** was calculated from oxidation onset and converted to NHE (V) by addition of 0.70 V[17] using the equation E_{HOMO} (V vs. NHE) = [{ $E_{ox/onset} - E_{1/2}$ (Fc/Fc^+)} + 0.7] V vs. NHE. LUMO was calculating by subtracting $E_{0\text{-}0}$ from E_{HOMO}. All the quantum mechanical calculations were conducted using the Gaussian 09 software. The optimization of the ground-state geometry was carried out at the Density Functional Theory (DFT) level, using the B3LYP hybrid functional and the 6- 31G(d,p) atomic basis set. The computation of the 10 lowest excited states with time-dependent density functional theory (TD-DFT) was carried out using the same atomic basis set. *J-V* characteristics of the solar cells were measured using Keithley digital source meter (2420, Keithley, USA) controlled by a computer and standard AM 1.5 solar simulator (PET, CT200AAA, USA). To measure the photocurrent and voltage, an external bias of AM 1.5G light was applied using a xenon lamp (450 W, USHIO INC, Philippines) and *J-V* plot was recorded. The IPCE measurements were carried out with a Newport QE measurement kit by focussing a monochromatic beam of light from 300W Xe lamp onto the devices. Electrochemical impedance spectra (EIS) were measured on the Biologic potentiostat, equipped with a FRA2 module, with an applied potentials of −0.5, −0.47, −0.44 and −0.41 V in the dark. The frequency range explored was 1Hz to 1MHz with an ac perturbation of 10 mV. The impedance spectra were analyzed using an equivalent circuit model of R1+R2/C2+R3/C3.

4.4.2. DSSC Fabrication Procedure

The preparation of TiO_2 electrodes and fabrication of the cells for photovoltaic measurements were carried out according to the previously reported procedures from our group[13,18]. FTO (F-doped SnO_2 glass; 6-8 Ω/sq) was cleaned sequentially by mucasol (2% in

water), deionized water, and isopropanol using an ultra-sonication for 15 min. To grow a blocking layer of TiO_2, the cleaned FTO substrates were dipped in freshly prepared aqueous 0.05 M $TiCl_4$ solution at 70 ºC for 30 min, and washed immediately with deionized water, and followed by annealing in air at 125º C for 10 min. The mesoscopic transparent thin layer (6-8 μm thickness) of TiO_2 was coated onto modified FTO using TiO_2 paste (< 20 nm, Ti-Nanoxide T/SP) by the doctorblade technique, then kept in air for 5 min and annealed at 125 ºC in the air for 15 min. Dyesol, WER2-O paste was used to coat a 4-6 μm thick TiO_2 scattering layer, kept in air for 5 min and annealed at 125 ºC in the air for 15 min. The resulting 0.22 cm^2 active area films were sintered at 325 ºC for 5 min, 375 ºC for 5 min, 450 ºC for 15 min and 500 ºC for 15 min with a heating rate of 5 °C per min in air. After cooling the furnace temperature to 50 ºC, sintered films were again treated in $TiCl_4$ solution as described before. The treated film was sintered again at 500 ºC for 30 min, allowed to cool to 50 ºC, and immediately immersed in 0.1 mM **ISQ** dye solution (with and without CDCA) in CH_2Cl_2 at room temperature for 12 h. The dye-loaded electrodes are washed thoroughly with CH_2Cl_2, to remove physisorbed molecules. Finally, the dye cell was assembled by joining the electrolyte (Iodolyte Z50) filled photoanode and platinum cathode using a 25 μm thick spacer.

4.4.3. Synthetic Procedure and Characterization Data

9,9-Didodecyl-2-nitro-9H-fluorene (2). 2-nitrofluorene (3.0 g, 14.20 mmol), 1-iodododecane (12.6 g, 42.61 mmol) and tetrabutyl ammonium bromide (0.3 g, 0.710 mmol) were taken in 70 mL toluene in two-necked flask. 23 mL of 50% (in weight) aqueous solution of NaOH was added to the mixture rapidly with constant stirring. The resultant mixture was stirred at 60 ºC for 8 h under argon atmosphere. The reaction mixture was cooled to room temperature, and 1 M HCl (100 mL) was added to it followed by addition of 100 mL of water. The reaction mixture was extracted with ethyl acetate, washed with brine and dried over anhydrous sodium sulfate. Solvents were removed under reduced pressure, and the residue was purified by column chromatography (EtOAc-pet ether) to afford pure compound 2 as pale yellow oil (5.13 g, 66%). ^{1}H NMR (500 MHz, $CDCl_3$) δ 8.26 (dd, J = 8.3, 2.0 Hz, 1H), 8.20 (d, J = 2.0 Hz, 1H), 7.83 – 7.75 (m, 2H), 7.45 – 7.36 (m, 3H), 2.08 – 1.96 (m, 4H), 1.27 – 1.12 (m, 24H), 1.08 – 1.00 (m, 12H), 0.86 (t, J = 7.0 Hz, 6H), 0.68 – 0.46 (m, 4H). ^{13}C NMR (125 MHz, $CDCl_3$) δ 152.5, 152.1, 147.8, 147.3, 138.9, 129.4, 127.5, 123.4, 123.436, 121.32, 119.90, 118.38, 77.16, 55.82, 40.19, 32.03, 30.00, 29.72, 29.65, 29.63, 29.45, 29.35,

23.88, 22.81, 14.25. HRMS (ESI) m/z: $[M+H]^+$ Calcd for $C_{37}H_{58}NO_2$ 548.4468, found 548.4456

2-Amino-9,9-didodecylfluorene (3). To a mixture of compound **2** (2.0 g, 3.65 mmol) in 30 mL EtOH, 0.2 g of 10% Pd/C was added. The resultant mixture was stirred at room temperature under argon atmosphere for 15 minutes. Then hydrazine monohydrate (1 mL) was added dropwise over 15 min. The reaction mixture was stirred at 80 ºC for 10 h. The reaction mixture was cooled to the room temperature after the completion and filtered over celite to collect the filtrate. The solvents were removed to give the desired compound as white solid (1.8 g, 95%). Mp 55-57 ºC. ^{1}H NMR (400 MHz, $CDCl_3$) δ 7.54 (d, J = 7.5 Hz, 1H), 7.47 (d, J = 8.4 Hz, 1H), 7.27 – 7.22 (m, 2H), 7.18 (d, J = 7.2 Hz, 1H), 6.69 – 6.62 (m, 2H), 1.97 – 1.79 (m, 4H), 1.28 – 1.14 (m, 24H), 1.10 – 1.01 (m, 12H), 0.87 (t, J = 6.8 Hz, 6H), 0.69 – 0.55 (m, 4H). ^{13}C NMR (100 MHz, $CDCl_3$) δ 152.8, 149.9, 146.0, 141.7, 132.7, 126.7, 125.5, 122.7, 120.6, 118.4, 114.1, 110.0, 77.2, 54.9, 40.8, 32.1, 30.3, 29.8, 29.5, 23.9, 22.8, 14.3. HRMS (ESI) m/z: $[M+H]^+$ Calcd for $C_{37}H_{60}N$ 518.4726, found 518.4718.

10,10-Didodecyl-2-methyl-10H-indeno[1,2-g]quinoline (4). In a two-necked round bottom flask, compound **3** (1.9 g, 3.60 mmol), acetic acid (0.2 mL, 3.6 mmol) and 20 mL HCl (6 M) was added. The mixture was refluxed at 100 ºC for 1 h, followed by addition of iodine (42 mg, 0.18 mmol), potassium iodide (60 mg, 0.36 mmol) and 4 mL toluene to it. Then crotonaldehyde (0.6 mL, 7.2 mmol) dissolved in 2 mL of toluene was added to the reaction flask dropwise over 30 min. The resulting mixture was refluxed for another 6 h and cooled to the room temperature after completion of the reaction. The ammonia solution 10 mL was added to neutralize the reaction. 50 mL water was added to the reaction mixture, extracted by ethyl acetate and the organic phase was dried over sodium sulfate. The solvents were removed under reduced pressure, and the residue was purified by column chromatography (EtOAc-Pet ether) to afford pure compound **4** as a dark brown oil (1.23 g, 60%). ^{1}H NMR (400 MHz, $CDCl_3$) δ 8.11 (d, J = 8.4 Hz, 1H), 8.01 (s, 1H), 7.95 (s, 1H), 7.82 (d, J = 4.5 Hz, 1H), 7.41 – 7.33 (m, 3H), 7.27 (d, J = 8.5 Hz, 1H), 2.76 (s, 3H), 2.13 – 1.97 (m, 4H), 1.25 – 1.07 (m, 23H), 1.07 – 0.98 (m, 12H), 0.85 (t, J = 6.9 Hz, 6H), 0.68 – 0.58 (m, 4H). ^{13}C NMR (100 MHz, $CDCl_3$) δ 158.3, 153.4, 151.4, 148.2, 140.2, 140.0, 136.5, 128.3, 127.2, 126.3, 123.3, 122.2, 121.5, 120.5, 117.0, 55.2, 41.4, 32.0, 30.2, 29.8, 29.7, 29.7, 29.4, 29.4, 25.5, 24.1, 22.8, 14.3. HRMS (ESI) m/z: $[M+H]^+$ Calcd for $C_{41}H_{62}N$ 568.4882, found 568.4877.

10,10-Didodecyl-1,2-dimethyl-10H-indeno[1,2-g]quinolin-1-ium iodide (5). The compound **4** (0.68 g, 1.2 mmol), Iodomethane (0.85g, 6 mmol) and 2 mL acetonitrile were taken in a sealed tube and heated at 100 ºC for 48 h. After completion of the reaction the solvents were removed to give compound **5** as yellow gum which was used without further purification (0.767 g, 90%). ^{1}H NMR (200 MHz, $CDCl_3$) δ 8.87 (d, *J* = 8.5 Hz, 1H), 8.39 (s, 1H), 8.22 (s, 1H), 8.01 – 7.87 (m, 2H), 7.52 – 7.40 (m, 3H), 4.77 (s, 3H), 3.33 (s, 3H), 2.25 – 2.07 (m, 4H), 1.22 – 1.02 (m, 35H), 0.85 (t, *J* = 6.4 Hz, 6H), 0.63 – 0.44 (m, 4H). ^{13}C NMR (101 MHz, $CDCl_3$) δ 161.65, 159.06, 151.30, 145.43, 143.87, 140.06, 137.42, 130.58, 128.78, 128.06, 124.78, 123.60, 121.84, 119.39, 112.11, 57.01, 54.45, 41.58, 41.12, 32.01, 29.97, 29.71, 29.65, 29.43, 24.69, 24.16, 22.79, 14.24. HRMS (ESI) m/z: $[M]^+$ Calcd for $C_{42}H_{64}N^+$ 582.5033, found 582.5031.

2-Methylquinoline-6-carboxylic acid (7). 4-aminobenzoic acid (**6**) (5 g, 36.46 mmol) was taken in 6N HCl (35 ml) and refluxed for 2 h. Crotonaldehyde (5.1 g, 72.92 mmol) was added dropwise over 40 min. It was refluxed, and then once again crotonaldehyde was added and refluxed for further 24 h. The reaction mixture was cooled to room temperature after completion of the reaction. 50 mL of water was added and extracted with ethyl acetate. Aqueous ammonia solution was added to the aqueous layer to adjust the pH 7 and again extracted with ethyl acetate. The organic layers were combined, and the solvents were removed under reduced pressure. The residue was purified by column chromatography (ethyl acetate-pet ether) to give light brown solid (2.0 g, 29%). Mp 210-212 ºC. ^{1}H NMR (400 MHz, DMSO) δ 8.59 (s, 1H), 8.41 (d, J = 8.4 Hz, 1H), 8.17 (d, J = 8.7 Hz, 1H), 7.96 (d, J = 8.7 Hz, 1H), 7.49 (d, J = 8.4 Hz, 1H), 2.68 (s, 3H). ^{13}C NMR (125 MHz, DMSO) δ 167.12, 161.35, 149.07, 137.45, 130.62, 128.79, 128.52, 127.82, 125.47, 122.97, 25.07. HRMS (ESI) m/z: $[M+H]^+$ Calcd for $C_{11}H_{10}NO_2$ 188.0712, found 188.0701.

6-Carboxy-1,2-dimethylquinolin-1-ium iodide (8). Compound **7** (1g, 5.34 mmol) and 1-iodomethene (2.5g, 17.63 mmol) were taken with 5 mL acetonitrile in a sealed tube and heated at 150 ºC for 24 h. The reaction mixture was cooled to room temperature and the solvents were removed under reduced pressure. The precipitate was washed with ether (4×20 mL) to afford the required compound as a green powder (0.6 g, 34%). Mp 265-267 ºC. ^{1}H NMR (200 MHz, DMSO-d_6) δ 9.26 (d, J = 8.6 Hz, 1H), 9.00 (d, J = 1.8 Hz, 1H), 8.69 (d, J = 9.4 Hz, 1H), 8.55 (dd, J = 9.3, 1.9 Hz, 1H), 8.22 (d, J = 8.6 Hz, 1H), 4.47 (s, 3H), 3.11 (s, 3H). ^{13}C NMR (100 MHz, $CDCl_3$) δ 165.76, 163.26, 146.46, 141.01, 133.89, 132.21, 130.67,

127.56, 126.07, 119.92, 40.16, 23.46. HRMS (ESI) m/z: $[M]^+$ Calcd for $C_{12}H_{12}NO_2^+$ 202.0863, found 202.0857.

2-((2-Butoxy-3,4-dioxocyclobut-1-en-1-yl)methylene)-1-methyl-1,2-dihydroquinoline-6-carboxylic acid (9). To a mixture of compound **8** (1g, 3.04 mmol) and 3, 4-dibutoxycyclobut-3-ene-1,2-dione (0.69 g, 3.04 mmol) in 10 mL *n*-butanol, 0.5 mL (0.37 g, 3.65 mmol) triethylamine was added. The reaction mixture was stirred at room temperature for 12 h under nitrogen atmosphere. After completion of the reaction, solvents were removed under reduced pressure. The residue were dissolved in 100 mL of DCM, washed with 100 mL of 2N HCl and the organic layer was dried over sodium sulfate. The solvents were removed under reduced pressure and crude product was purified by column chromatography (MeOH-CH_2Cl_2) to afford the required compound as an orange solid (0.22 g, 21%). Mp 170-172 ºC. ^{1}H NMR (200 MHz, DMSO-d_6) δ 8.36 (d, J = 9.5 Hz, 1H), 8.18 (s, 1H), 8.06 (d, J = 9.1 Hz, 1H), 7.72 (t, J = 9.7 Hz, 2H), 5.33 (s, 1H), 4.75 (t, J = 6.4 Hz, 2H), 3.70 (s, 3H), 1.89 – 1.67 (m, 2H), 1.43 (dd, J = 15.4, 7.6 Hz, 2H), 0.94 (t, J = 7.2 Hz, 3H). HRMS (ESI) m/z: $[M+H]^+$ Calcd for $C_{20}H_{20}NO_5$ 354.1341, found 354.1328. (^{13}C NMR could not be obtained due to poor solubility.)

2-((2-Hydroxy-3,4-dioxocyclobut-1-en-1-yl)methylene)-1-methyl-1,2-dihydroquinoline-6-carboxylic acid (P3). Compound **9** (0.2 g, 0.57mmol) was dissolved in 10 mL acetone and refluxed for 15 min followed by addition of 1 mL 2N HCl. The resultant mixture was again refluxed for 12 h under nitrogen. The reaction mixture was cooled to room temperature after completion of the reaction and solvents were removed under reduced pressure to afford desired compound **P3** as orange solid which was used without further purification (0. 161 g, 95%). Mp 291-293 ºC. ^{1}H NMR (200 MHz, DMSO) δ 8.42 (d, J = 9.6 Hz, 1H), 8.07 (d, J = 1.6 Hz, 1H), 7.98 (dd, J = 9.0, 1.7 Hz, 1H), 7.58 (d, J = 4.4 Hz, 1H), 7.53 (d, J = 5.5 Hz, 1H), 5.48 (s, 1H), 3.59 (s, 3H). ^{13}C NMR (125 MHz, DMSO) δ 192.1, 174.6, 166.6, 148.9, 143.2, 131.6, 131.4, 129.6, 124.3, 124.2, 122.6, 114.8, 88.5, 35.6. HRMS (ESI) m/z: $[M+H]^+$ Calcd for $C_{16}H_{12}NO_5$ 298.0715, found 298.0702

2-(((E)-5-Carboxy-1,3,3-trimethylindolin-2-ylidene)methyl)-4-((10,10-didodecyl-1-methyl-10H-indeno[1,2-g]quinolin-1-ium-2-yl)methylene)-3-oxocyclobut-1-en-1-olate (ISQ1). Compound 5 (0.2 g, 0.28 mmol) and **P1** (0.105 g, 0.34 mmol) were dissolved in 10 mL of *n*-butanol/dry toluene (1:1) mixture in a two-necked round bottom flask and charged

with Dean-Stark apparatus. 1 mL of quinoline was added to the reaction mixture and refluxed for 24 h under inert atmosphere. The reaction mixture was cooled to room temperature and the solvents were removed under reduced pressure. The residue was purified by column chromatography (MeOH-CH_2Cl_2) to afford the required dye as dark green solid (0.165 g, 67%). Mp. 200-202 ºC. ^{1}H NMR (400 MHz, $CDCl_3$) δ 9.57 (d, J = 9.3 Hz, 1H), 8.09 (d, J = 8.4 Hz, 1H), 8.03 (s, 1H), 7.98 – 7.87 (m, 2H), 7.85 – 7.72 (m, 1H), 7.54 (s, 1H), 7.44 – 7.34 (m, 3H), 6.87 (d, J = 8.4 Hz, 1H), 6.30 (s, 1H), 5.84 (s, 1H), 4.13 (s, 3H), 3.44 (s, 3H), 2.15 – 1.96 (m, 4H), 1.83 (s, 6H), 1.24 – 1.02 (m, 36H), 0.84 (t, J = 6.9 Hz, 6H), 0.65 – 0.49 (m, 4H). ^{13}C NMR (100 MHz, $CDCl_3$) δ 184.7, 181.8, 180.8, 170.5, 168.1, 165.4, 156.9, 153.7, 150.6, 148.1, 141.6, 139.8, 138.9, 136.8, 131.3, 128.8, 127.6, 125.7, 125.6, 124.0, 123.3, 123.2, 120.7, 119.2, 109.7, 107.3, 96.0, 87.8, 56.2, 47.5, 41.1, 37.8, 32.00, 30.4, 30.1, 29.7, 29.6 29.4, 29.4, 27.6, 24.0, 22.8, 14.2. HRMS (ESI) m/z: $[M]^+$ Calcd for $C_{59}H_{76}N2O_4$ 876.5805, found 876.5793.

2-((E)-(7-Carboxy-1,1,3-trimethyl-1,3-dihydro-2H-benzo[e]indol-2-ylidene)methyl)-4-((10,10-didodecyl-1-methyl-10H-indeno[1,2-g]quinolin-1-ium-2-yl)methylene)-3-oxocyclobut-1-en-1-olate (ISQ2). Compound **5** (0.2 g, 0.28 mmol) and **P2** (0.101 g, 0.34 mmol) were dissolved in 10 mL *n*-butanol/dry toluene (1:1) mixture in a two-necked round bottom flask equipped with Dean-Stark apparatus. 1 mL of quinoline was added to the reaction mixture and refluxed for 24 h under inert atmosphere. The reaction mixture was cooled to room temperature and the solvents were removed under reduced pressure. The contents were purified by column chromatography (MeOH-CH_2Cl_2) to afford the required dye as dark green solid (0.121 g, 50%). Mp. 180-182 ºC. ^{1}H NMR (500 MHz, $CDCl_3$) δ 9.54 (d, J = 9.1 Hz, 1H), 8.70 (s, 1H), 8.19 (d, J = 11.0 Hz, 2H), 7.93 (d, J = 8.0 Hz, 1H), 7.87 (d, J = 12.9 Hz, 2H), 7.77 (d, J = 4.4 Hz, 1H), 7.49 (s, 1H), 7.38 (d, J = 6.1 Hz, 3H), 7.27 (s, 1H), 6.25 (s, 1H), 5.89 (s, 1H), 4.08 (s, 3H), 3.55 (s, 3H), 2.10 (s, 6H), 2.06 – 1.97 (m, 4H), 1.23 – 1.11 (m, 24H), 1.06 – 1.01 (m, 12H), 0.84 (t, J = 7.1 Hz, 6H), 0.64 – 0.55 (m, 4H). ^{13}C NMR (126 MHz, $CDCl_3$) δ 184.92, 181.91, 179.01, 168.78, 168.06, 156.57, 153.20, 150.61, 139.94, 139.38, 139.02, 136.06, 133.68, 133.06, 131.44, 131.18, 129.68, 128.57, 127.58, 126.97, 125.70, 125.41, 124.92, 123.17, 122.44, 120.56, 119.11, 110.51, 109.51, 95.40, 86.82, 56.14, 49.88, 41.08, 37.57, 32.00, 30.53, 30.06, 29.70, 29.65, 29.42, 29.36, 27.14, 23.97, 22.78, 14.23.. HRMS (ESI) m/z: $[M]^+$ Calcd for $C_{63}H_{78}N_2O_4$ 926.5962, found 926.5956.

(E)-2-(((E)-6-Carboxy-1-methylquinolin-2(1H)-ylidene)methyl)-4-((10,10-didodecyl-1-methyl-10H-indeno[1,2-g]quinolin-1-ium-2-yl)methylene)-3-oxocyclobut-1-en-1-olate (ISQ3). Compound 5 (0.2 g, 0.28 mmol) and **P3** (0.124 g, 0.34 mmol) were dissolved in 10 mL *n*-butanol/dry toluene (1:1) mixture in a two-necked round bottom flask equipped with Dean-Stark apparatus. 1 mL of quinoline was added to the reaction mixture and refluxed for 24 h under inert atmosphere. The reaction mixture was cooled to room temperature and the solvents were removed under reduced pressure. The contents were purified by column chromatography (MeOH-CH_2Cl_2) to afford the required dye as dark green solid (0.156 g, 60%). Mp 142-144 ºC. ^{1}H NMR (400 MHz, DMSO-d_6 /$CDCl_3$ (1:1)) δ 9.29 (d, J = 9.3 Hz, 1H), 9.05 (d, J = 9.5 Hz, 1H), 8.01 (s, 1H), 7.97 (s, 2H), 7.82 (d, J = 9.4 Hz, 1H), 7.75 (d, J = 4.5 Hz, 1H), 7.69 (s, 1H), 7.41 (d, J = 8.9 Hz, 1H), 7.37 – 7.33 (m, 2H), 7.32 – 7.29 (m, 2H), 5.84 (s, 1H), 5.57 (s, 1H), 3.97 (s, 3H), 3.64 (s, 3H), 2.08 – 1.96 (m, 4H), 1.17 – 1.05 (m, 24H), 1.00 – 0.95 (m, 12H), 0.79 (t, J = 6.8 Hz, 6H), 0.52 – 0.45 (m, 4H). ^{13}C NMR (100 MHz, DMSO-d_6 /$CDCl_3$ (1:1)) δ 176.51, 170.77, 170.24, 156.07, 151.83, 150.50, 149.08, 143.60, 140.18, 139.22, 138.53, 135.19, 132.00, 131.28, 129.85, 129.45, 128.28, 127.46, 126.71, 125.00, 124.01, 123.12, 120.51, 119.09, 114.66, 110.30, 98.92, 94.50, 93.74, 79.15, 55.97, 37.51, 36.11, 31.75, 29.72, 29.45, 29.37, 29.16, 29.08, 23.75, 22.55, 14.27. HRMS (ESI) m/z: $[M]^+$ Calcd for $C_{58}H_{72}N_2O_4$ 860.5492, found 860.5474.

4.5. NMR Spectra

^{1}H and ^{13}C NMR spectra of 2

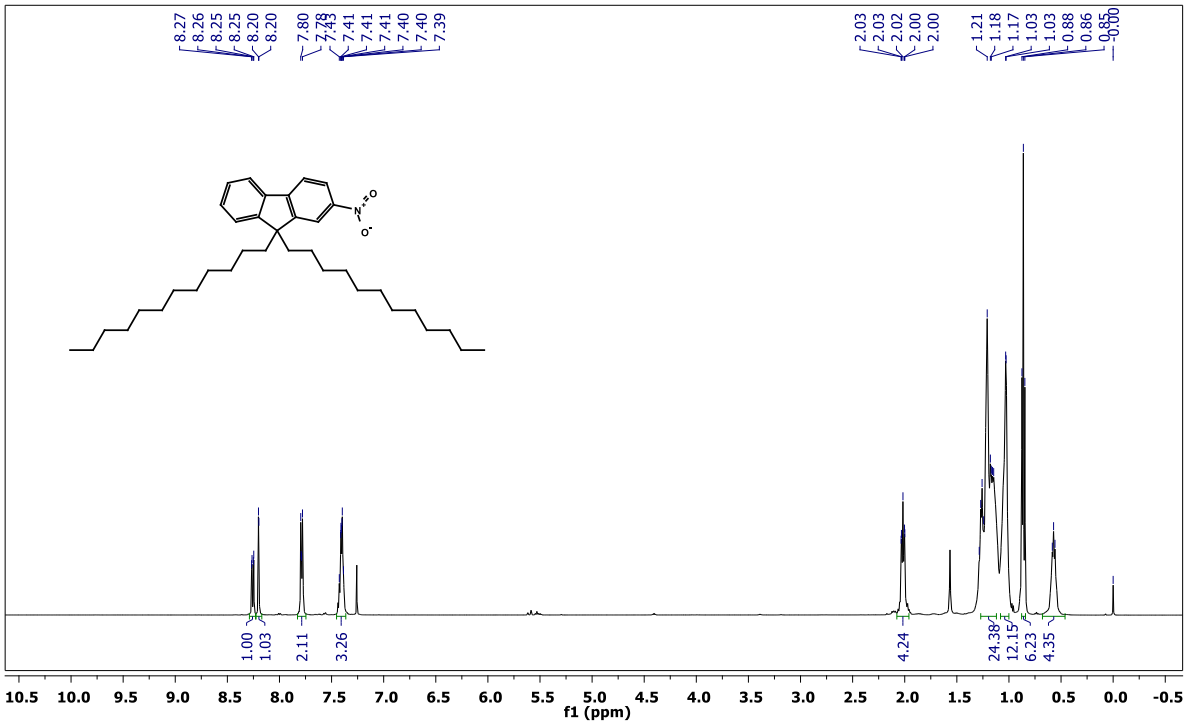

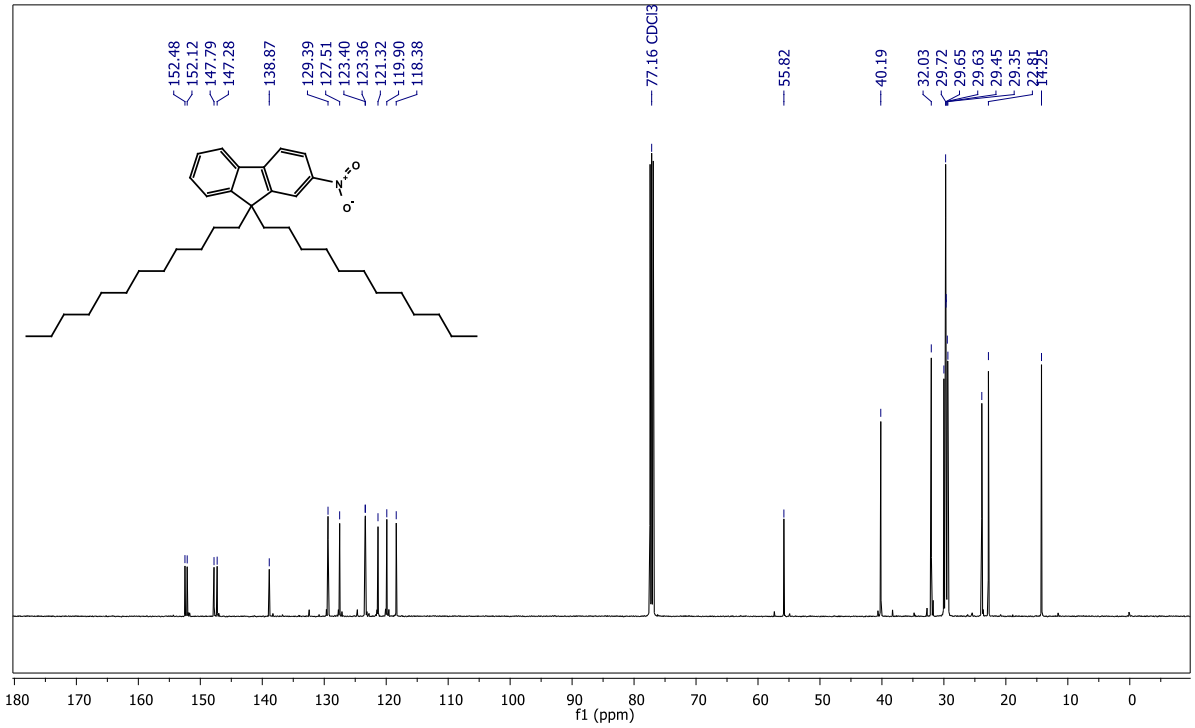

H and ^{13}C NMR spectra of 3

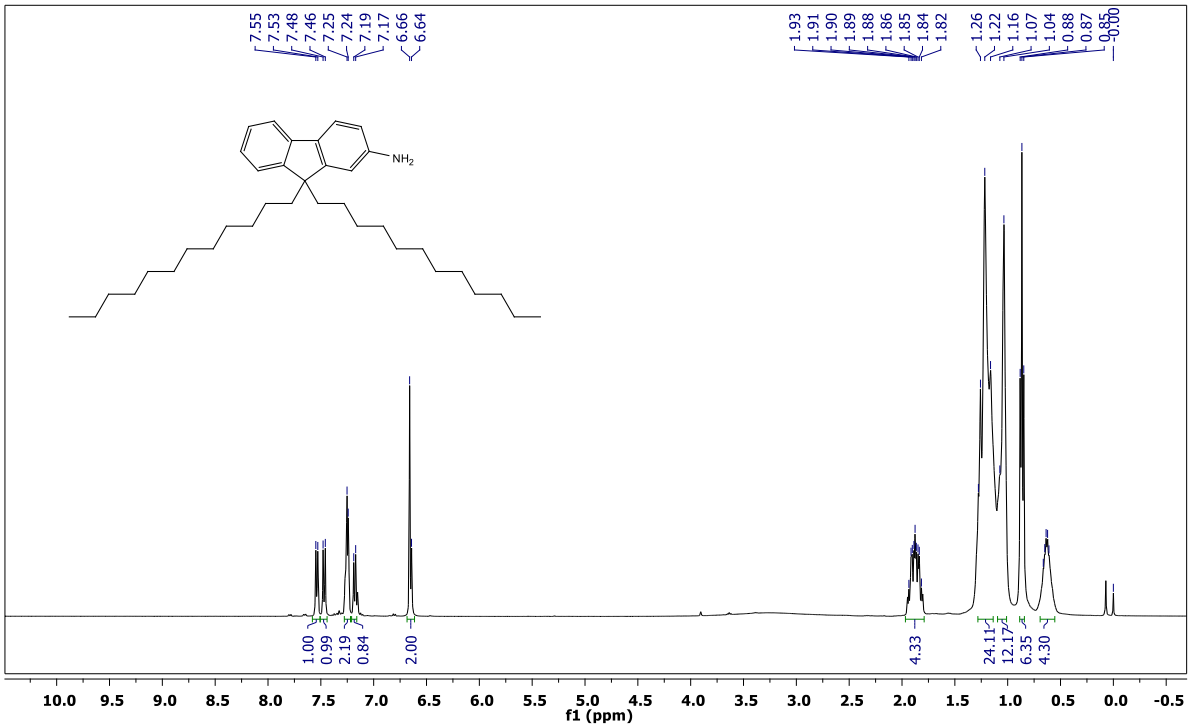

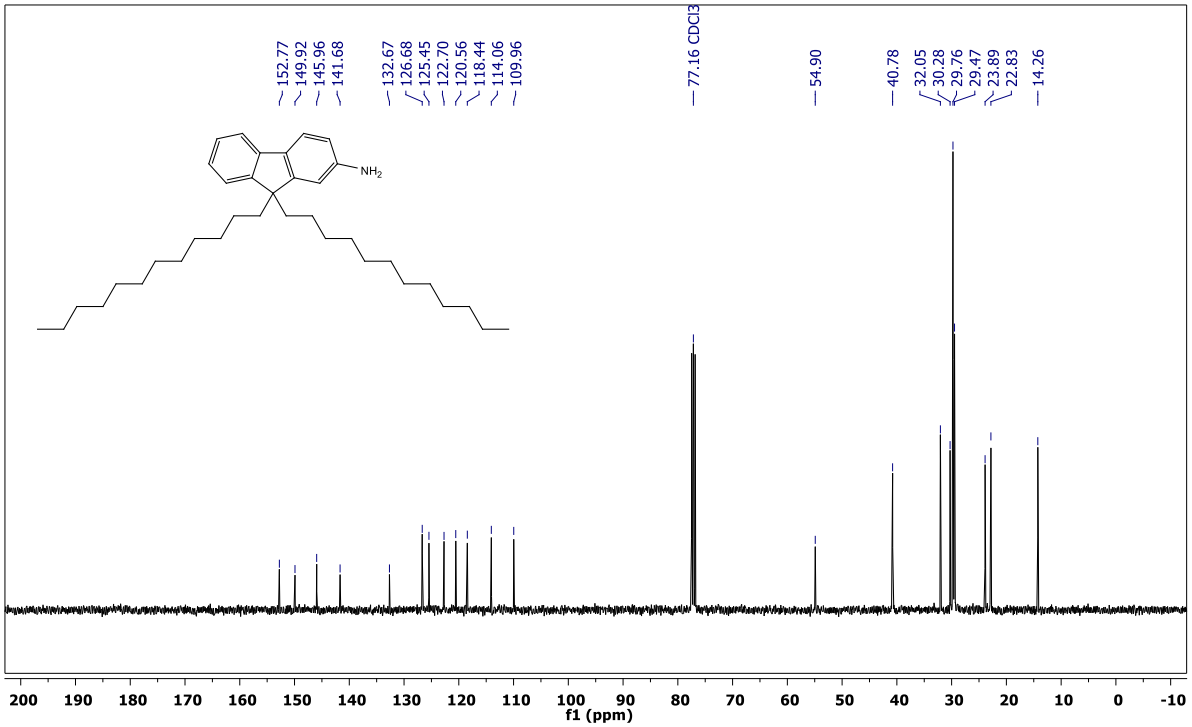

^{1}H and ^{13}C NMR spectra of 4

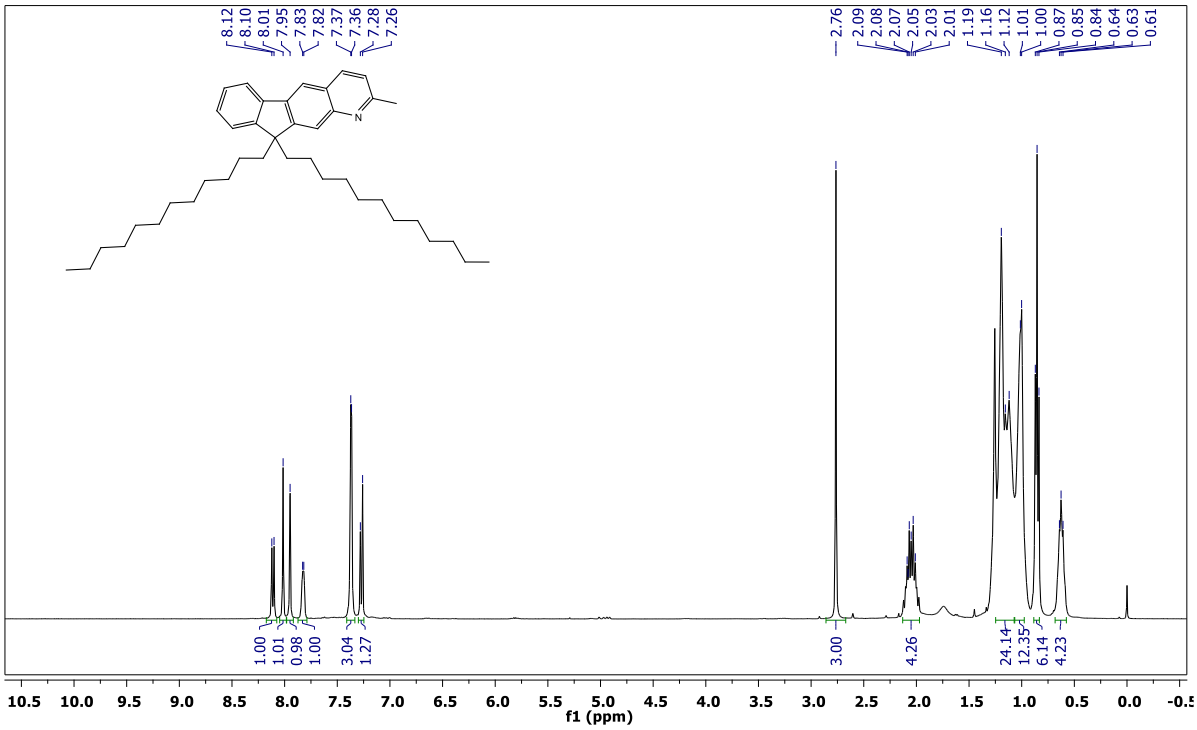

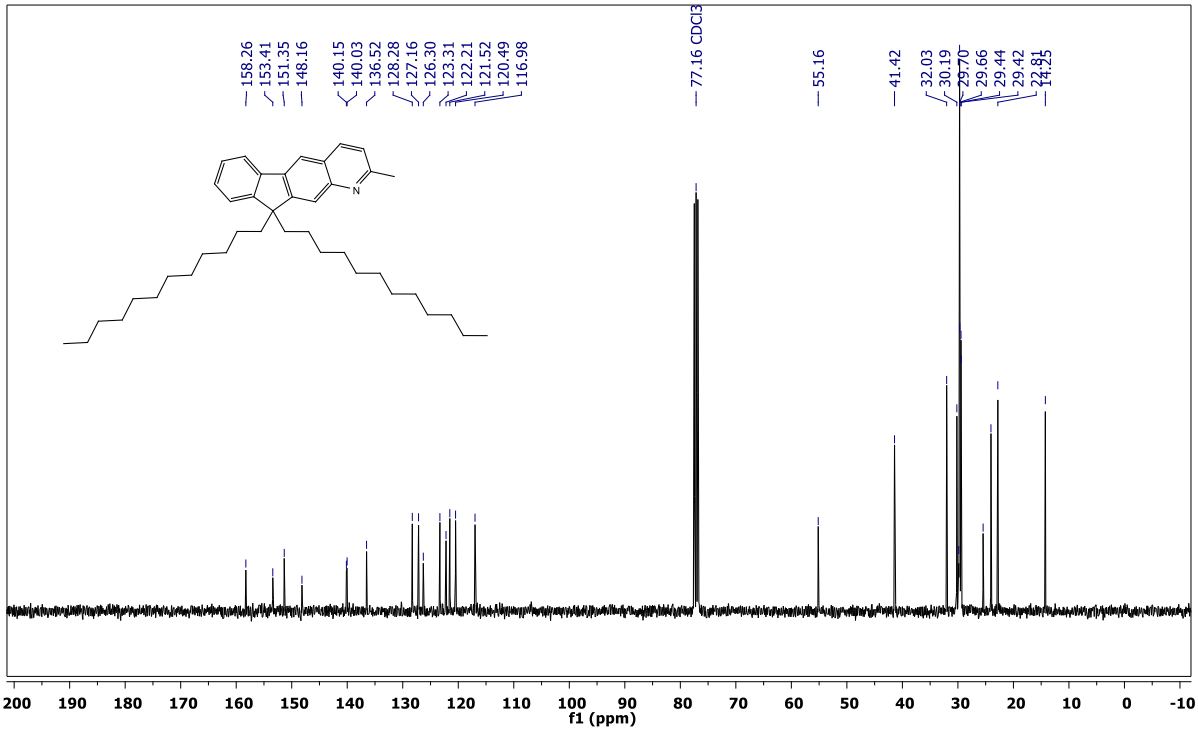

^{1}H and ^{13}C NMR spectra of 5

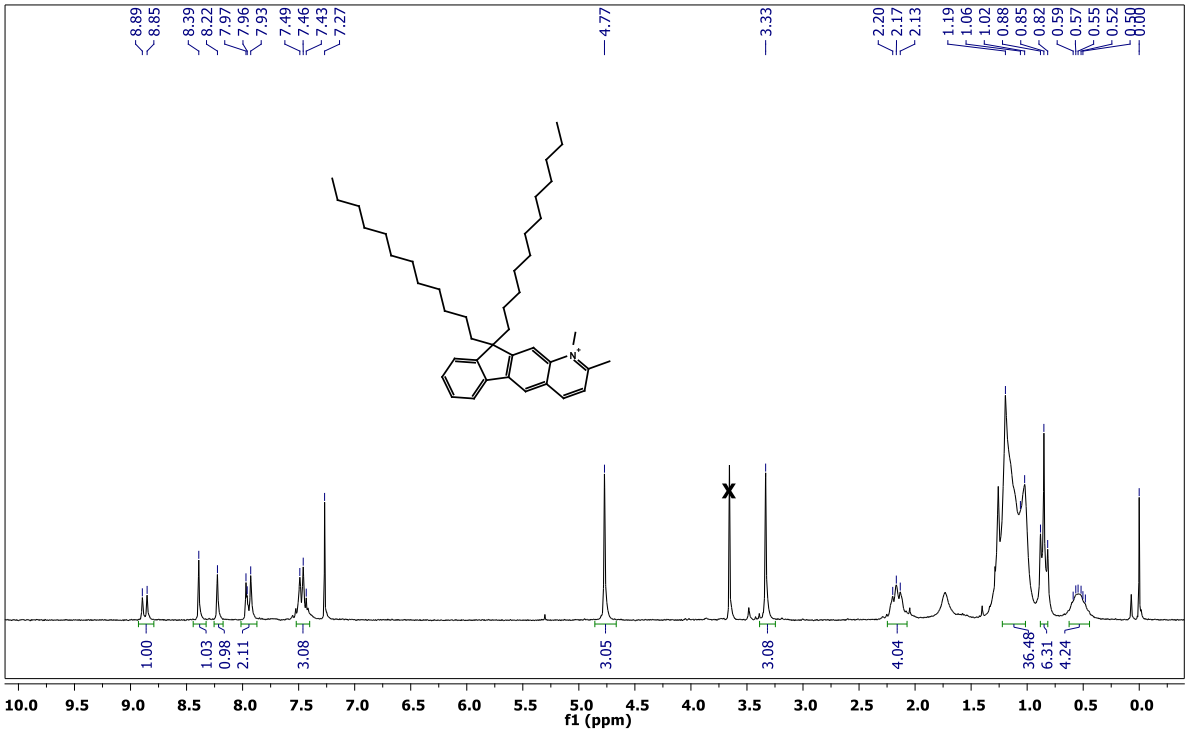

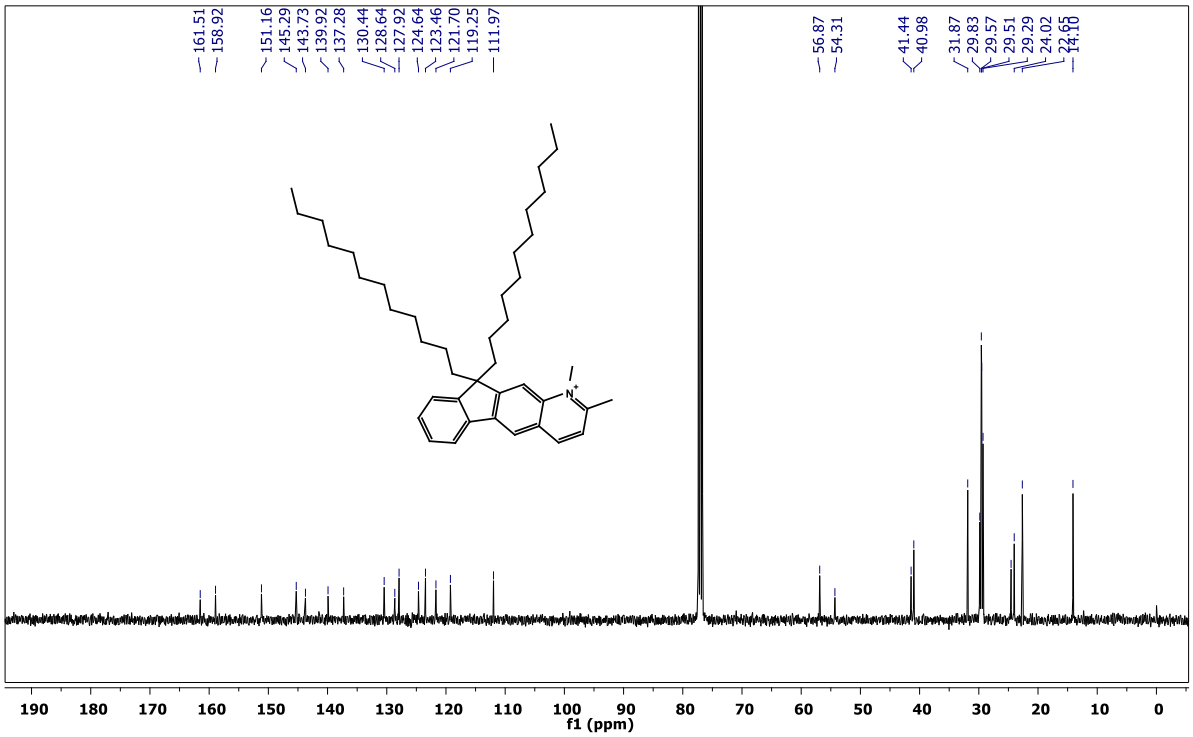

^{1}H and ^{13}C NMR spectra of 7

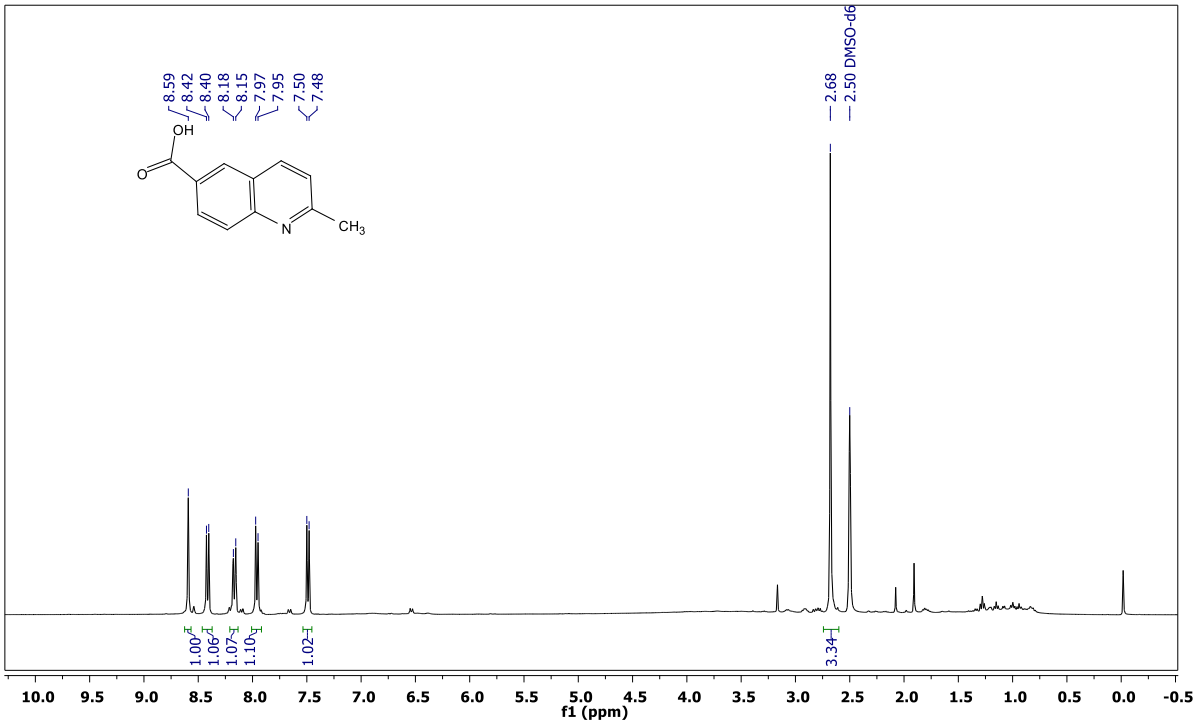

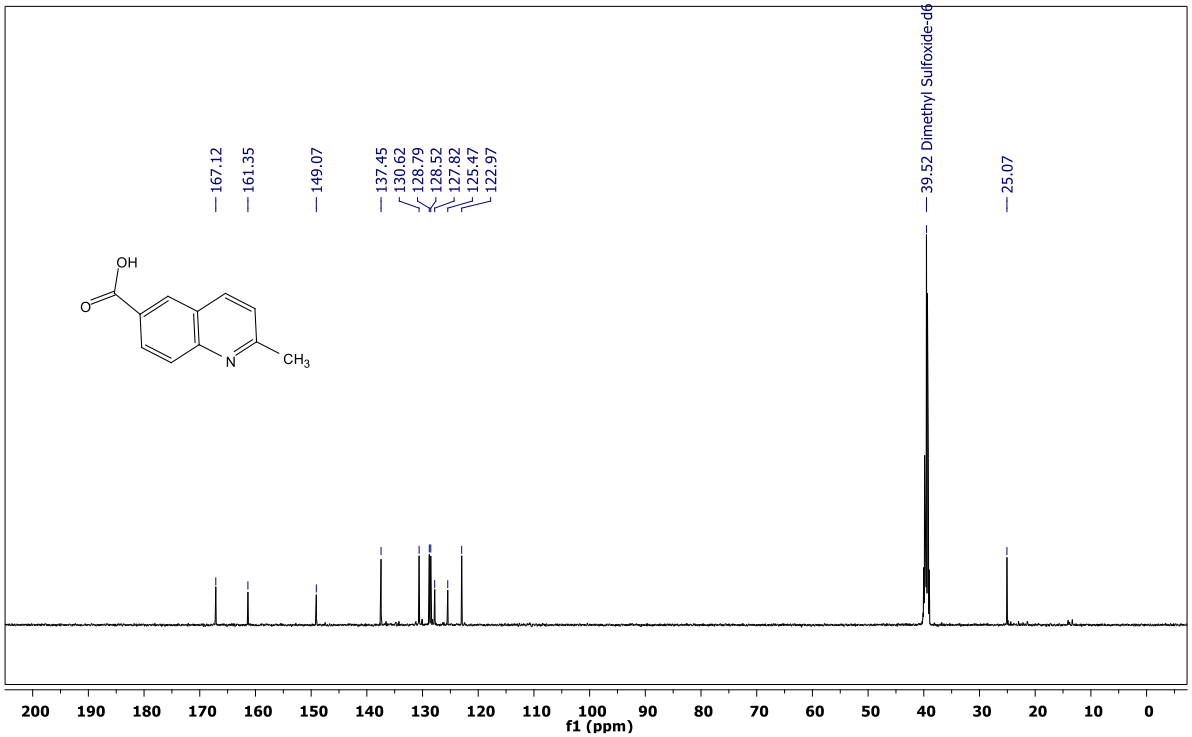

^{1}H and ^{13}C NMR spectra of 8

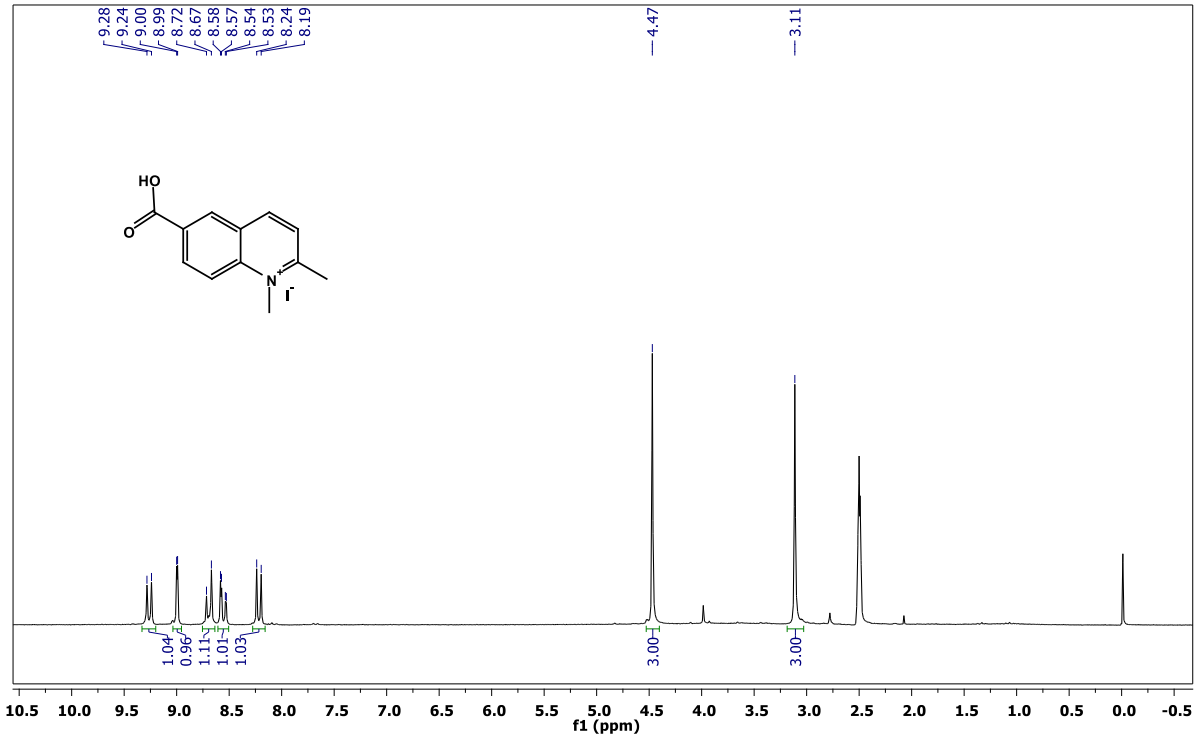

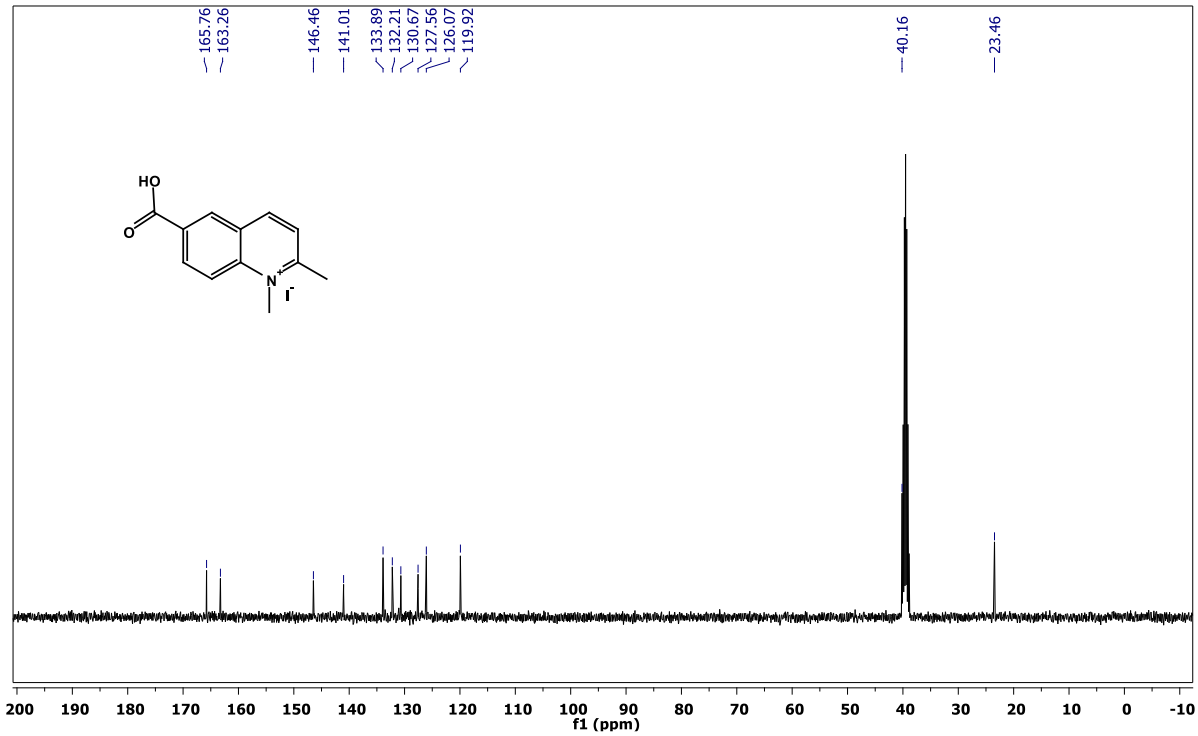

^{1}H NMR spectra of 9.

{^{13}C NMR spectrum could not be obtained due to poor solubility}

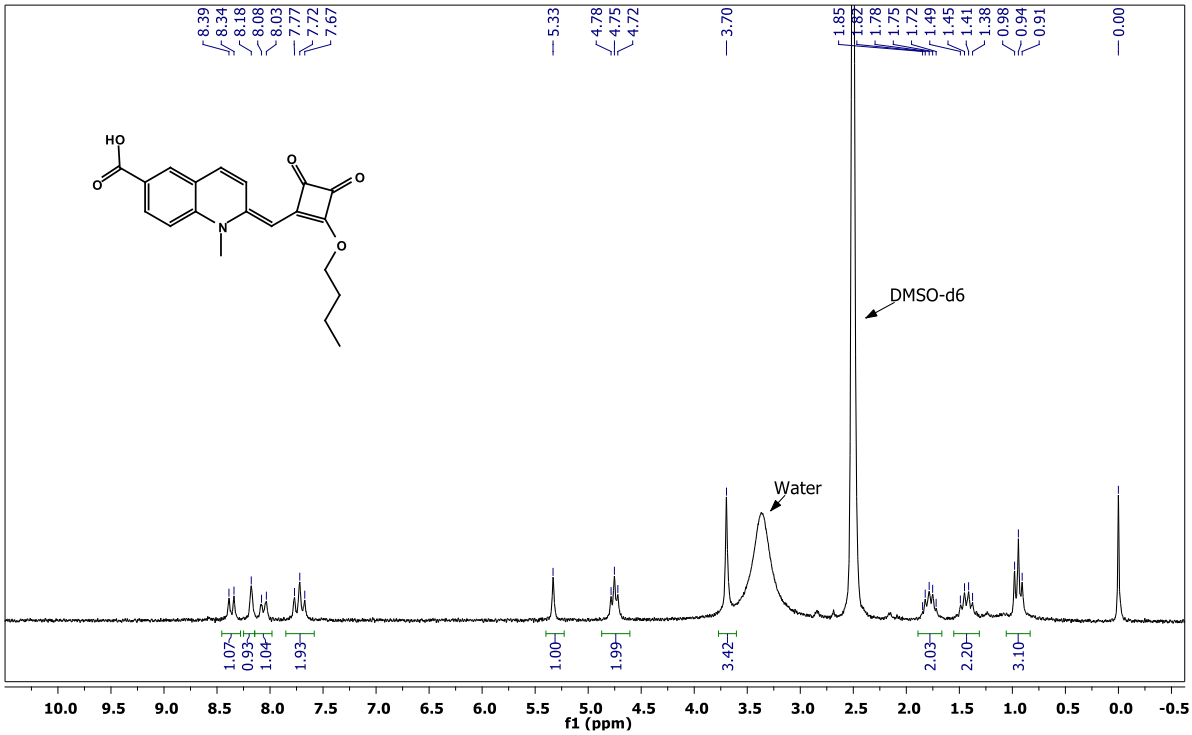

^{1}H and ^{13}C NMR spectra of P3.

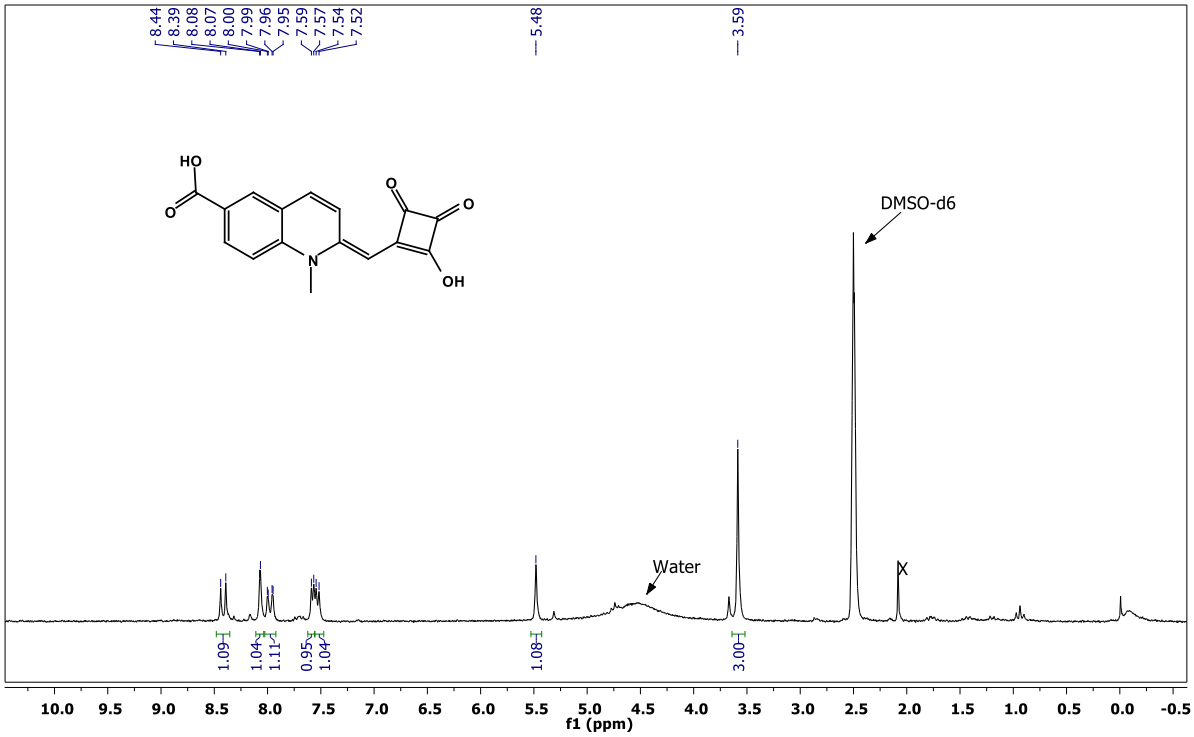

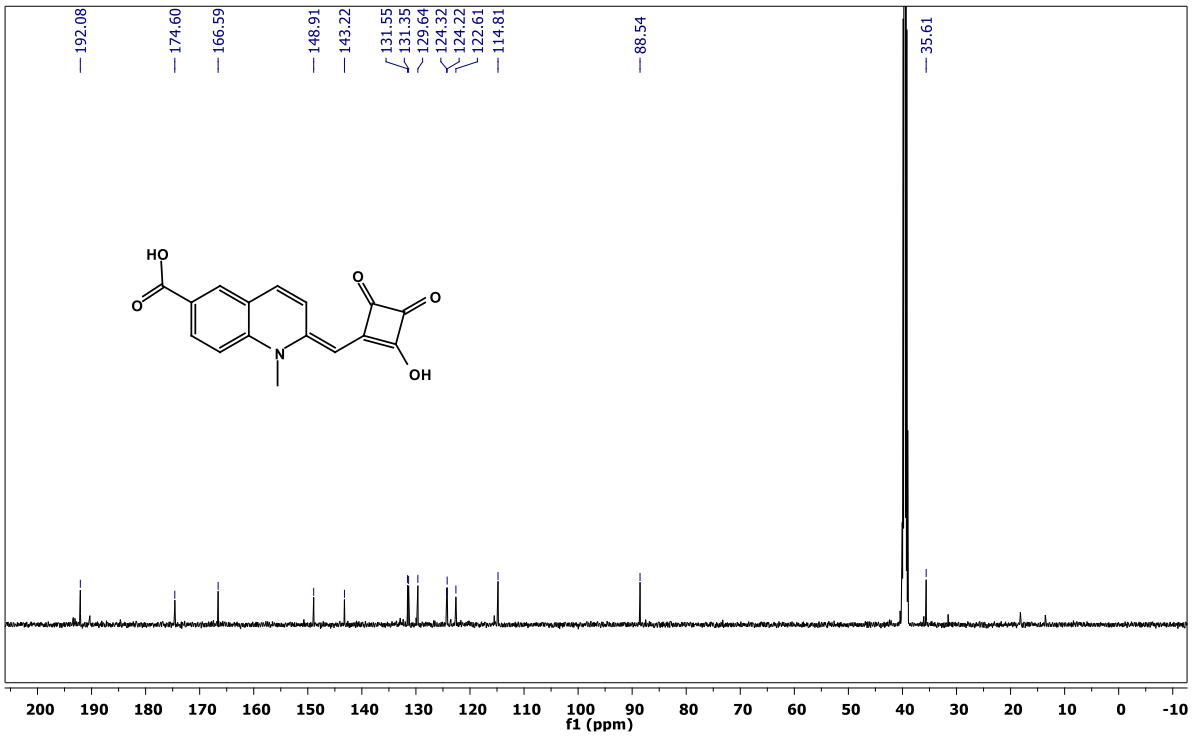

^{1}H and ^{13}C NMR spectra of ISQ1

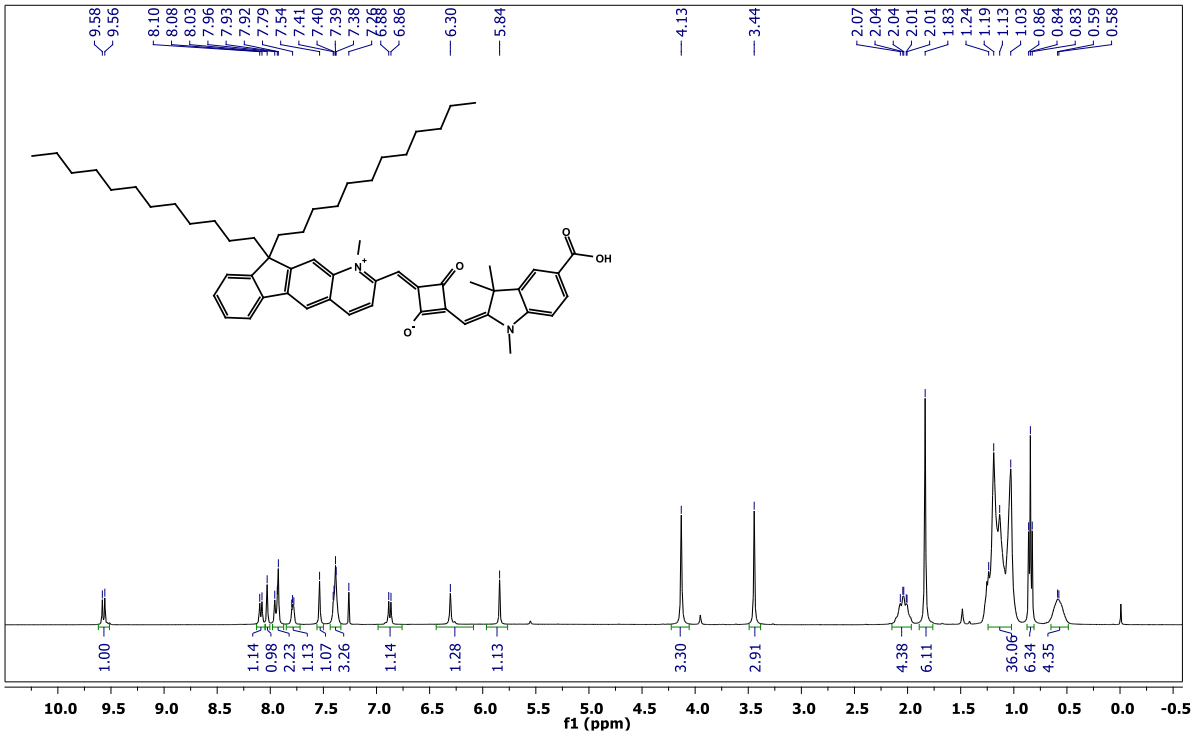

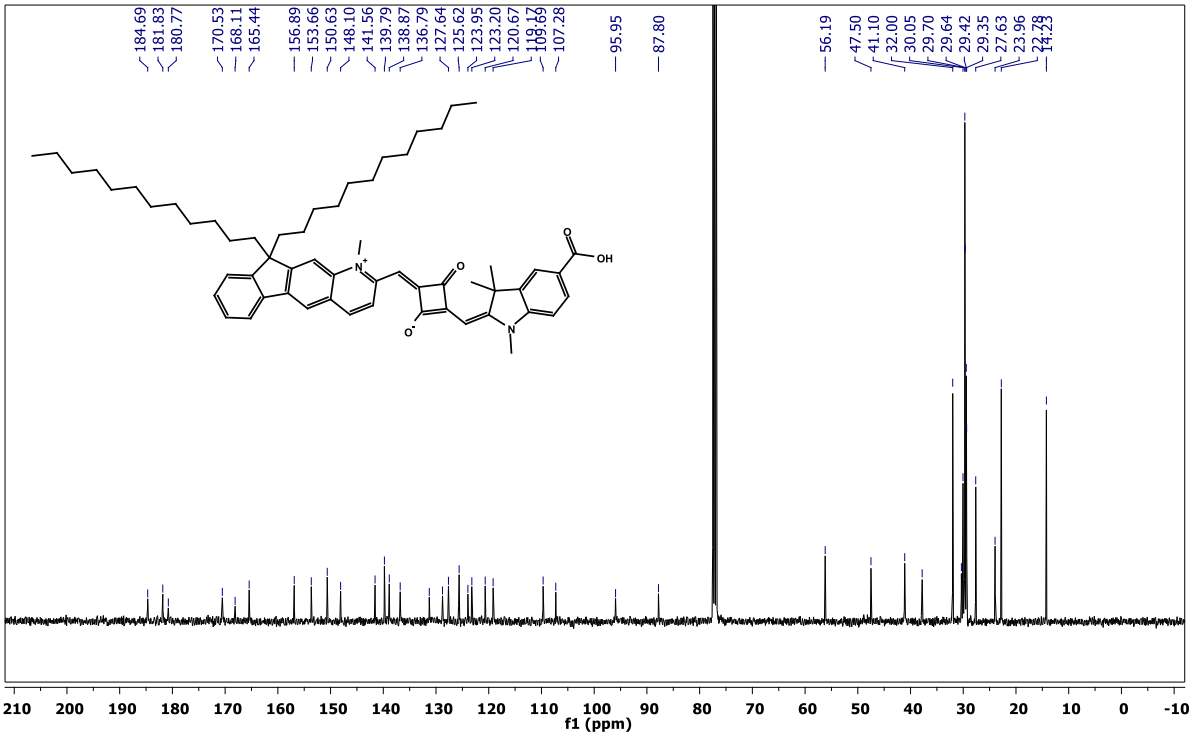

^{1}H and ^{13}C NMR spectra of ISQ2

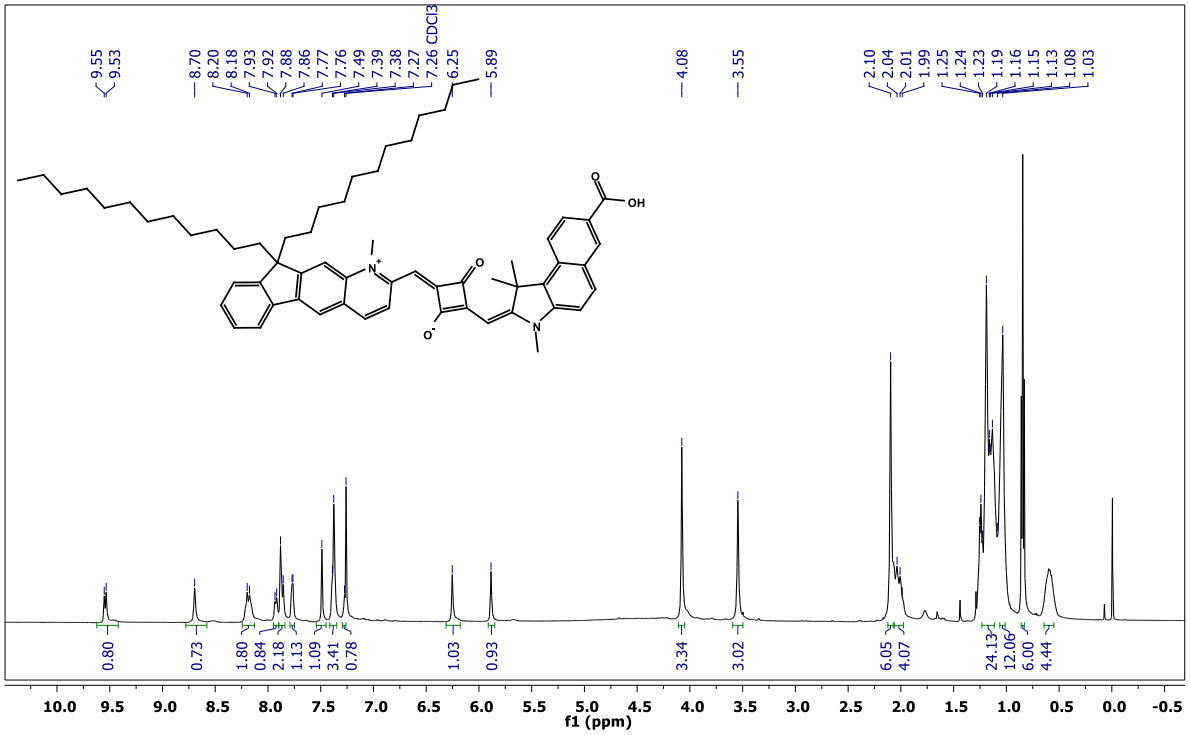

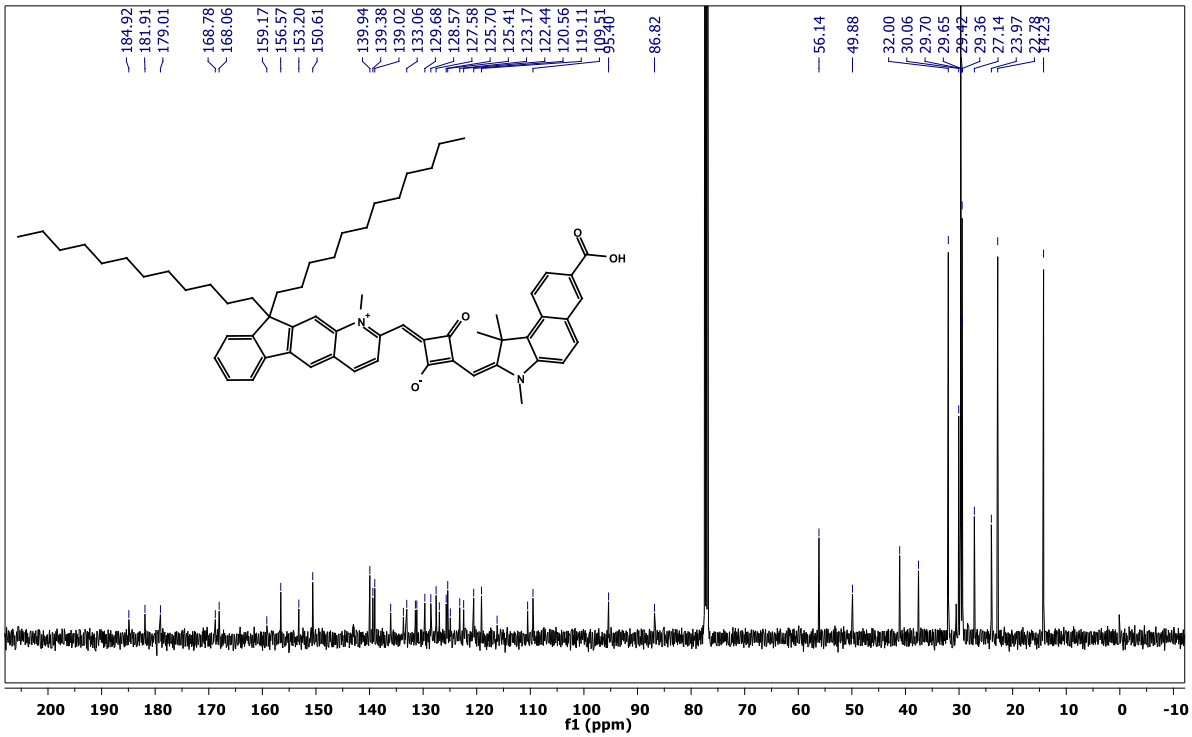

^{1}H and ^{13}C NMR spectra ($CDCl_3$ + DMSO-d_6) of ISQ3

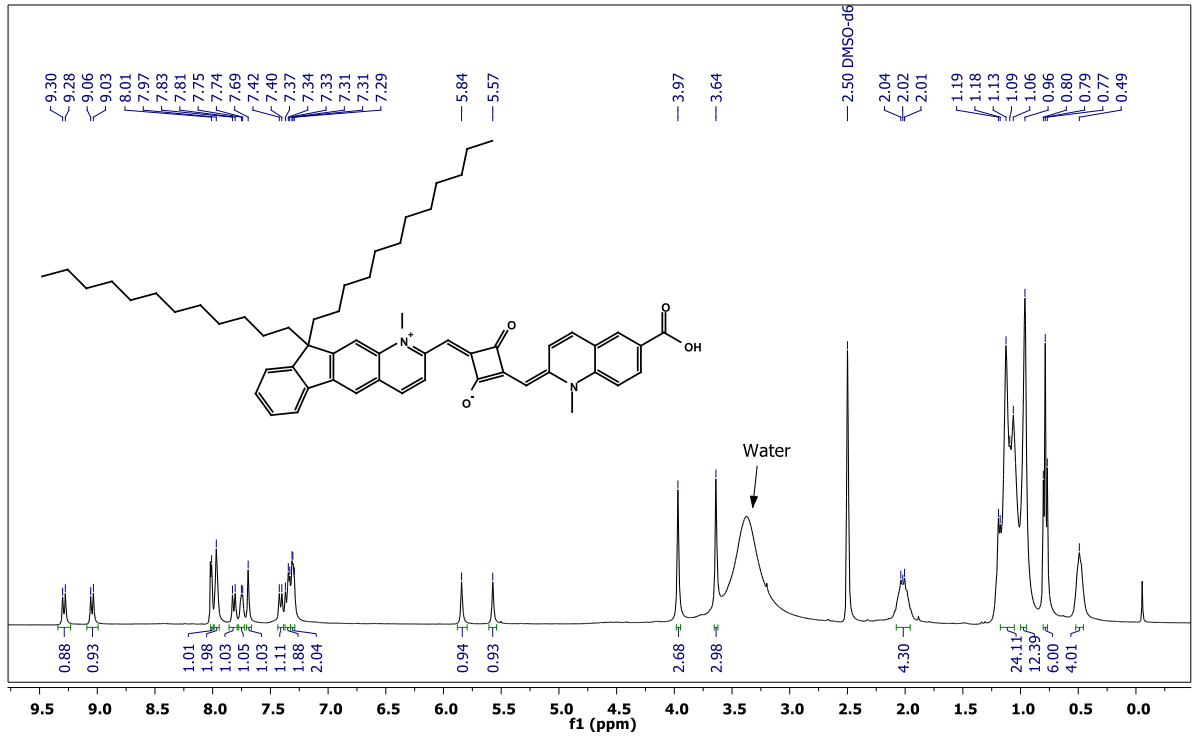

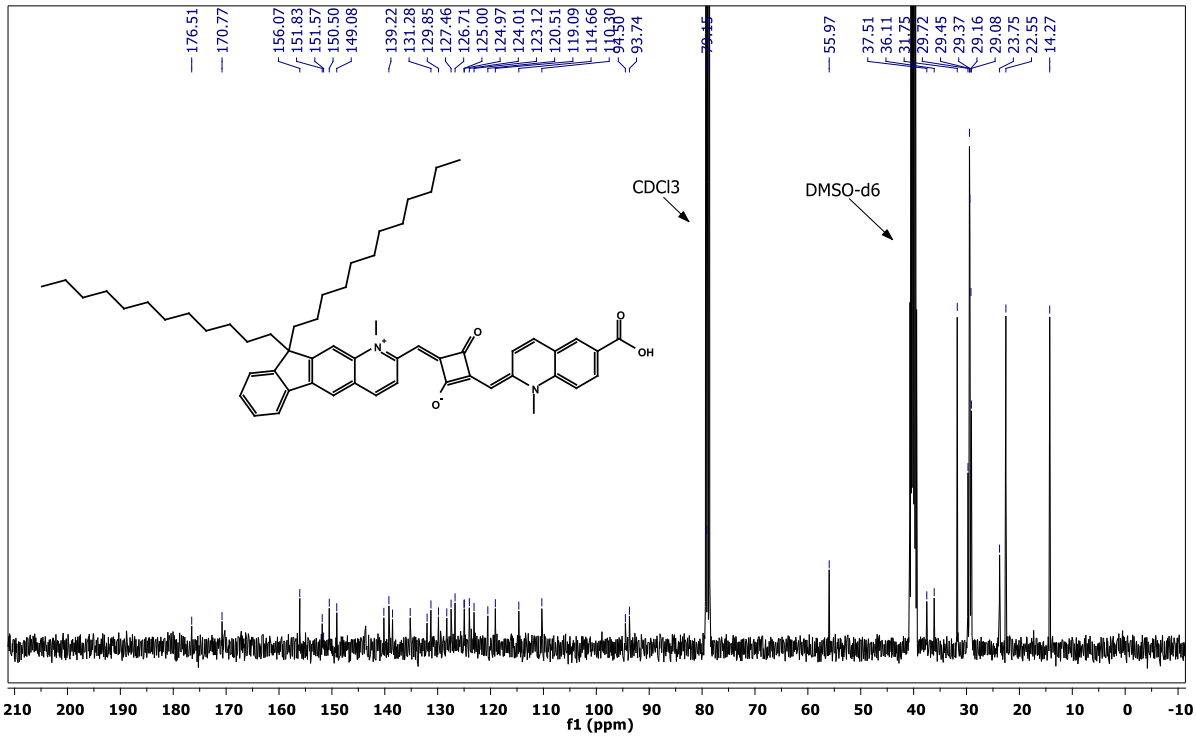

4.6. REFERENCES

(1) Hanumantha Rao, G.; Venkateswararao, A.; Giribabu, L.; Prakash Singh, S. *Photochem. Photobiol. Sci.* **2016**, *15*, 287–296.

(2) Geiger, T.; Kuster, S.; Yum, J.-H.; Moon, S.-J.; Nazeeruddin, M. K.; Grätzel, M.; Nüesch, F. *Adv. Funct. Mater.* **2009**, *19*, 2720–2727.

(3) Park, J.; Barbero, N.; Yoon, J.; Dell'Orto, E.; Galliano, S.; Borrelli, R.; Yum, J.-H.; Censo, D. D.; Grätzel, M.; K. Nazeeruddin, M.; Barolo, C.; Viscardi, G. *Phys. Chem. Chem. Phys.* **2014**, *16*, 24173–24177.

(4) Li, J.-Y.; Chen, C.-Y.; Ho, W.-C.; Chen, S.-H.; Wu, C.-G. *Org. Lett.* **2012**, *14*, 5420–5423.

(5) Maeda, T.; Nitta, S.; Nakao, H.; Yagi, S.; Nakazumi, H. *J. Phys. Chem. C* **2014**, *118*, 16618–16625.

(6) Maeda, T.; Nitta, S.; Sano, Y.; Tanaka, S.; Yagi, S.; Nakazumi, H. *Dyes Pigments* **2015**, *122*, 160–167.

(7) Kuster, S.; Sauvage, F.; Nazeeruddin, M. K.; Grätzel, M.; Nüesch, F. A.; Geiger, T. *Dyes Pigments* **2010**, *87*, 30–38.

(8) Maeda, T.; Hamamura, Y.; Miyanaga, K.; Shima, N.; Yagi, S.; Nakazumi, H. *Org. Lett.* **2011**, *13*, 5994–5997.

(9) Maeda, T.; Arikawa, S.; Nakao, H.; Yagi, S.; Nakazumi, H. *New J. Chem.* **2013**, *37*, 701–708.

(10) Yan, Z.; Guang, S.; Su, X.; Xu, H. *J. Phys. Chem. C* **2012**, *116*, 8894–8900.

(11) Jyothish, K.; Arun, K. T.; Ramaiah, D. *Org. Lett.* **2004**, *6*, 3965–3968.

(12) Frisch, M. J.; Trucks, G. W.; Schlegel, H. B.; Scuseria, G. E.; Robb, M. A.; Cheeseman, J. R.; Scalmani, G.; Barone, V.; Mennucci, B.; Petersson, G. A.; Nakatsuji, H.; Caricato, M.; Fox, D. J.; et al. Gaussian, Inc.: Wallingford, CT, USA*Gaussian 09*, 2009.

(13) Bisht, R.; M. K., M. F.; Singh, A. K.; Nithyanandhan, J. *J. Org. Chem.* **2017**, *82*, 1920–1930.

(14) Marinado, T.; Nonomura, K.; Nissfolk, J.; Karlsson, M. K.; Hagberg, D. P.; Sun, L.; Mori, S.; Hagfeldt, A. *Langmuir* **2010**, *26*, 2592–2598.

(15) Bisquert, J.; Cahen, D.; Hodes, G.; Rühle, S.; Zaban, A. *J. Phys. Chem. B* **2004**, *108*, 8106–8118.

(16) Ronca, E.; Pastore, M.; Belpassi, L.; Tarantelli, F.; Angelis, F. D. *Energy Environ. Sci.* **2012**, *6*, 183–193.

(17) Aghazada, S.; Gao, P.; Yella, A.; Marotta, G.; Moehl, T.; Teuscher, J.; Moser, J.-E.; De Angelis, F.; Grätzel, M.; Nazeeruddin, M. K. *Inorg. Chem.* **2016**, *55*, 6653–6659.

(18) Alagumalai, A.; M. K., M. F.; Vellimalai, P.; Sil, M. C.; Nithyanandhan, J. *ACS Appl. Mater. Interfaces* **2016**, *8*, 35353–35367.

Chapter 5

Extended Hetero-Acyloin Phototrigger and their Application in Organic Electronics: Efforts towards Developing a Photoinitiated Method for Processing Organic Molecules

5.1. INTRODUCTION

The deposition of the organic semiconductor on an organic electronic device is very important aspect along with the morphology of the formed film. The organic materials can be deposited by the various techniques. Vapor deposition is a thermal technique where molecule is evaporated and deposited on to the substrate under vacuum and/or high temperature. This technique is generally used when compound is insoluble in organic solvents.[1-2] The major disadvantages of this method are the relatively high material consumption and high initial cost for equipment setup.[3] In case of soluble organic semiconductors, solution-based processing methods are used. Solution-based methods of processing are more popular as they are easier and cheaper to carry out than vapor deposition. There are various methods by which a soluble organic semiconductor can be processed, e.g., drop-casting,[4] spin-coating,[5] doctor blading,[6,7] inkjet printing, etc.

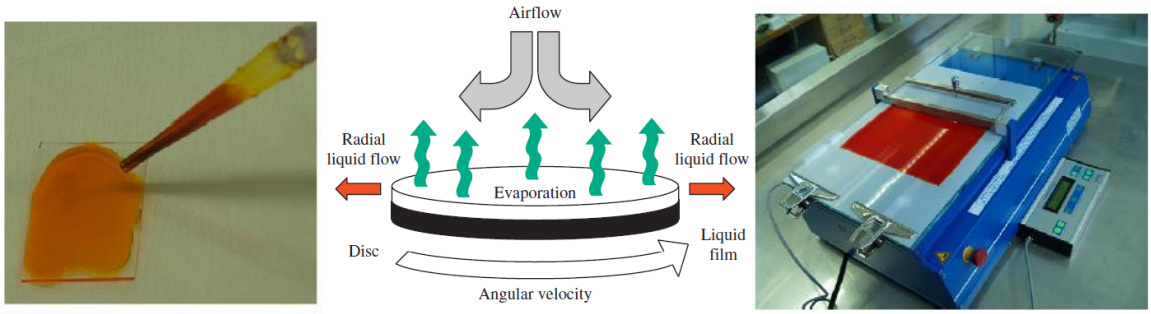

Figure 1. Processing by drop-casting (left), spin coating (middle), doctor blading (right)

In order to solution process an organic semiconductor, the solubility is a very important factor. Generally, organic semiconductors are highly conjugated molecules, and as the conjugation increases, the solubility of these molecules decreases. In order to process such molecules by solution-based processing, it is necessary to convert them into a soluble form before processing. Incorporation of the solubilizing group to the conjugated back bone is one of the methods to make molecule solution processable. Solubilizing groups help in achieving easily controllable solution based processing, however, it may hamper the favorable orientation of the molecules and hinder the π–π stacking which helps in charge conduction through the material. So it is desirable to have a molecule which can be processed in its soluble form and can be converted to its required form in a post-processing step. There

are some examples in the literature where such methods have been used to process organic semiconductors

Herwig and Müllen used a soluble derivative of pentacene to process the MISFET device.[8] They synthesized the retro-Diels alder active pentacene precursor which was coated on the FET device which was heated at 180-200 ºC, and the improved mobility was observed as the precursor converted into pentacene (Scheme 1). The highest mobility of 0.2 cm^2/Vs was obtained at a gate bias of -20 V.

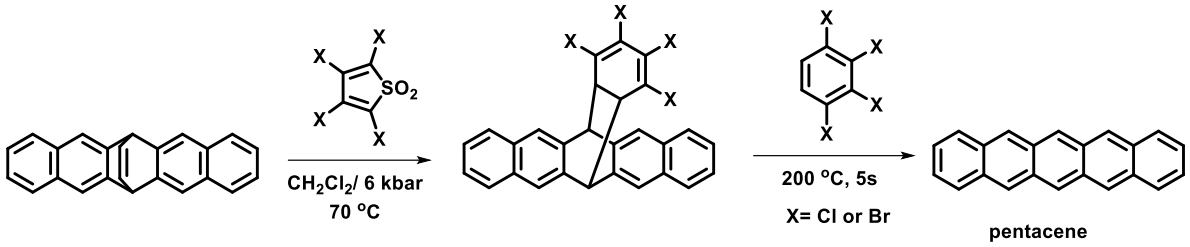

Scheme 1. Soluble precursor heated at 200 ºC for 5 sec to form insoluble pentacene

Aramaki et al. reported a tetrabenzoporphyrin based organic semiconductor for organic field effect transistors.[9] It was to be derived from its soluble bicyclo precursor which formed an amorphous film on the substrate with poor morphology. It was heated at a temperature of 150-200 C in the post-processing step and converted into an insoluble crystalline semiconductor film quantitatively. (**Scheme 2**). Field-effect transistors showed the mobility in the order of 10^{-2} cm^2/Vs.

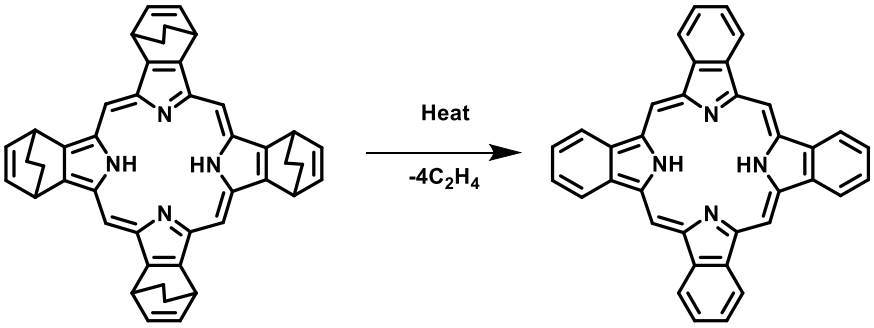

Scheme 2. Bicyclo derivative of tetrabenzoporphyrin is converted into planar and insoluble tetrabenzoporphyrin upon heating to 200 ºC.

Murphy et al. synthesized soluble sexithiophene derivative by strategically placing the solubilizing group at the terminal of the molecule.[10] Sexithiophene has a very limited solubility in its original form, and it is generally vapor deposited on to a substrate which yields mobility as high as 1 cm^2/Vs. In this work, they synthesized soluble sexithiophene derivative by attaching solubilizing chain via thermally cleavable ester link (**Scheme 3**). A film was deposited by spin-coating on the substrate, and the devices tested without annealing had low mobilities, in the order of 10^{-5} cm^2/Vs. However, after annealing the substrates at 180-200 ºC for 20 min improved mobility up to 0.05 cm^2/Vs.

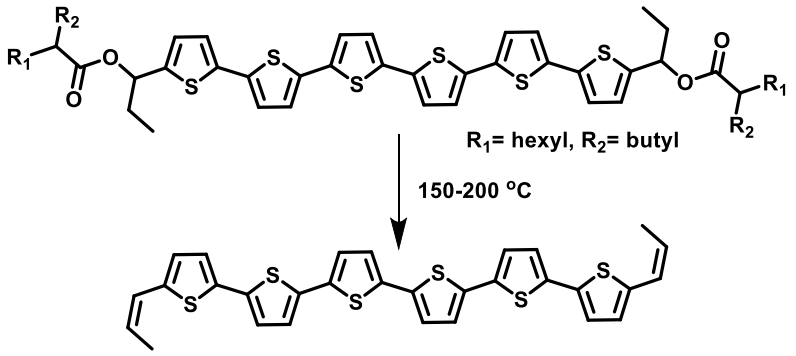

Scheme 3. Thermolysis of the soluble precursor of sexithiophene at 200 ºC yields insoluble derivative.

Krebs and Norrman used concentrated visible light to selectively heat the active material on the substrate to induce thermocleavage.[11]

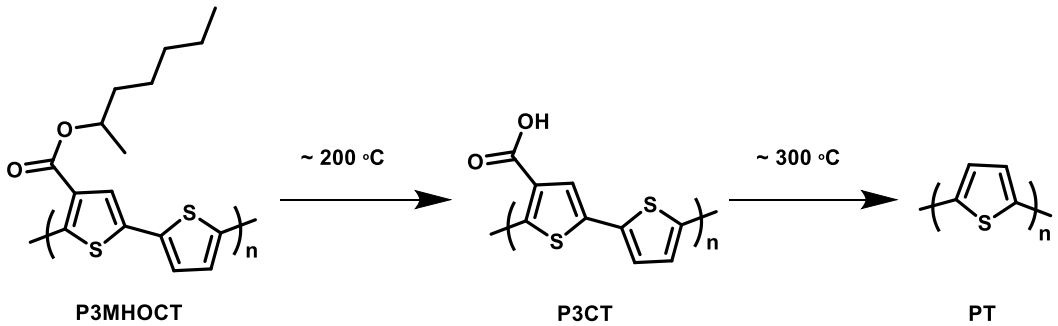

Scheme 4. The transformation of P3MHOCT to P3CT at ≈200 ºC and P3CT to PT at ≈300 ºC.

They used poly [3-(2-methylhex-2-yl)oxycarbonyldithiophene] (P3MHOCT) as a soluble polymer which upon heating eliminates an alkene to give poly (3-carboxydithiophene)

(P3CT), which is insoluble in organic solvents. Prolonged heating at higher temperature gave insoluble polythiophene (PT) (**Scheme 4**).

5.1.2 Photo-assisted Solution based Processing

The major drawback of the methods described above for the post-processing modification of the organic molecules is that the high temperatures are used, which are not always suitable for the organic molecules as it may lead to the decomposition. Photochemical approach to change the solubility of conjugated molecules gives the possibility of mild conditions and the advantage of spatiotemporal control. Such approaches have been explored in the processing of conjugated molecules which includes photo-oxidative cleavage of the conjugated polymer backbone,[12] and photopatterning of a conjugated polymer,[13] and photocleavage of solubilizing xanthate side chains.[14] There has been a recent surge in the research related to the application of photocleavable groups to the design of light-responsive polymers and surfaces.[15,16]

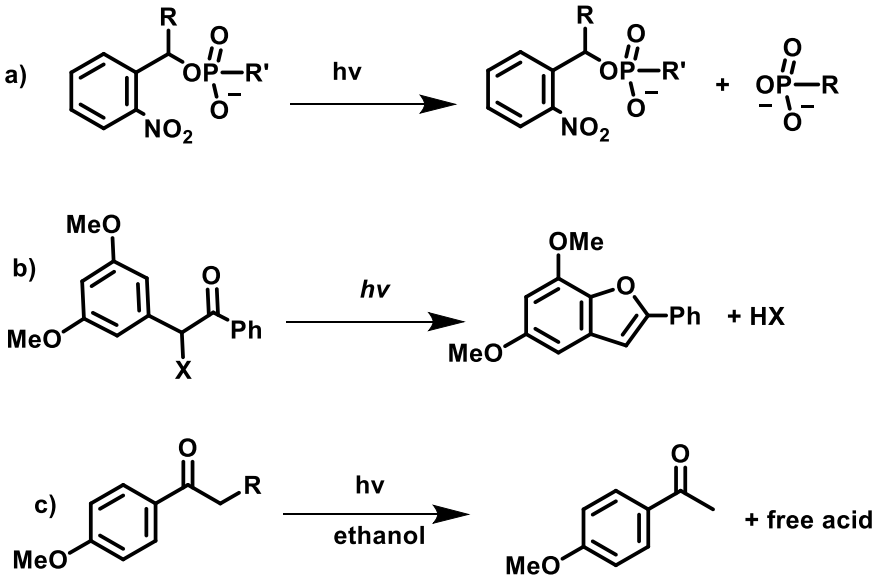

Scheme 5. Photolabile protecting groups: a) o-nitrobenzyl b) benzoin and c) phenacyl esters

In this chapter, we made an effort to explore a photochemical method by which we can post process a molecule by photochemically cleaving the solubilizing group. The choice of suitable photo-triggers for this purpose is crucial. There are several photo-labile protecting groups which can be used to protect functional groups and can be deprotected by suitable light irradiation. 3, 4-dimethoxy benzoins, o-nitrobenzyl esters, phenacyl esters are some of

the commonly used photolabile protecting groups (**Scheme 5**). The attachment of these photolabile linkers to the conjugated backbone and connecting solubilizing group to the photolabile linker can open a possibility of photochemical post-processing of OPV and OFET. Recently, a thiophene-based conjugated polymer was reported where a solubilizing alkyl chain is attached to the conjugated poly(thiophene) backbone through photolabile o-nitrobenzyl esters that cleave upon irradiation. The OFET device based on the polymer showed very little degradation in mobility when exposed to light, which shows that photolabile protecting groups can be used effectively as a processing tool in organic electronics (**Scheme 6**).[17]

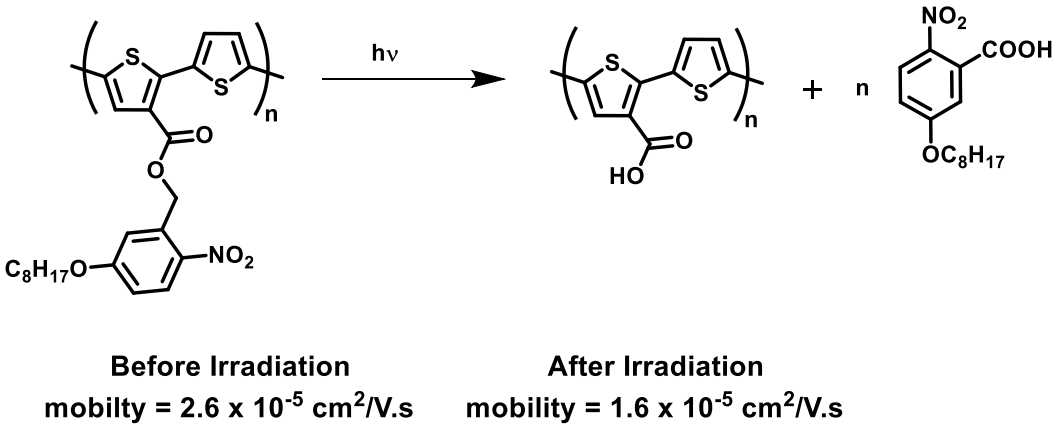

Scheme 6. The hole mobilities of *o*-nitrobenzyl linked polythiophene before and after irradiation.

We targeted a methodology for light-induced cleavage of the solubilizing group attached to phototrigger which in turn is connected to the conjugated backbone. For this purpose, we believed that benzoin type linker would be most suitable over other linkers (such as *o*-nitrobenzyl) as the benzoin do not cleave itself from the molecule and also enhance the conjugation through the formation of benzofuran (**Figure 2a)**. We aimed to design a similar photo-trigger with heteroaromatic moiety attached carbonyl group as it can help to connect the conjugated backbone selectively to the trigger (**Figure 2b**).

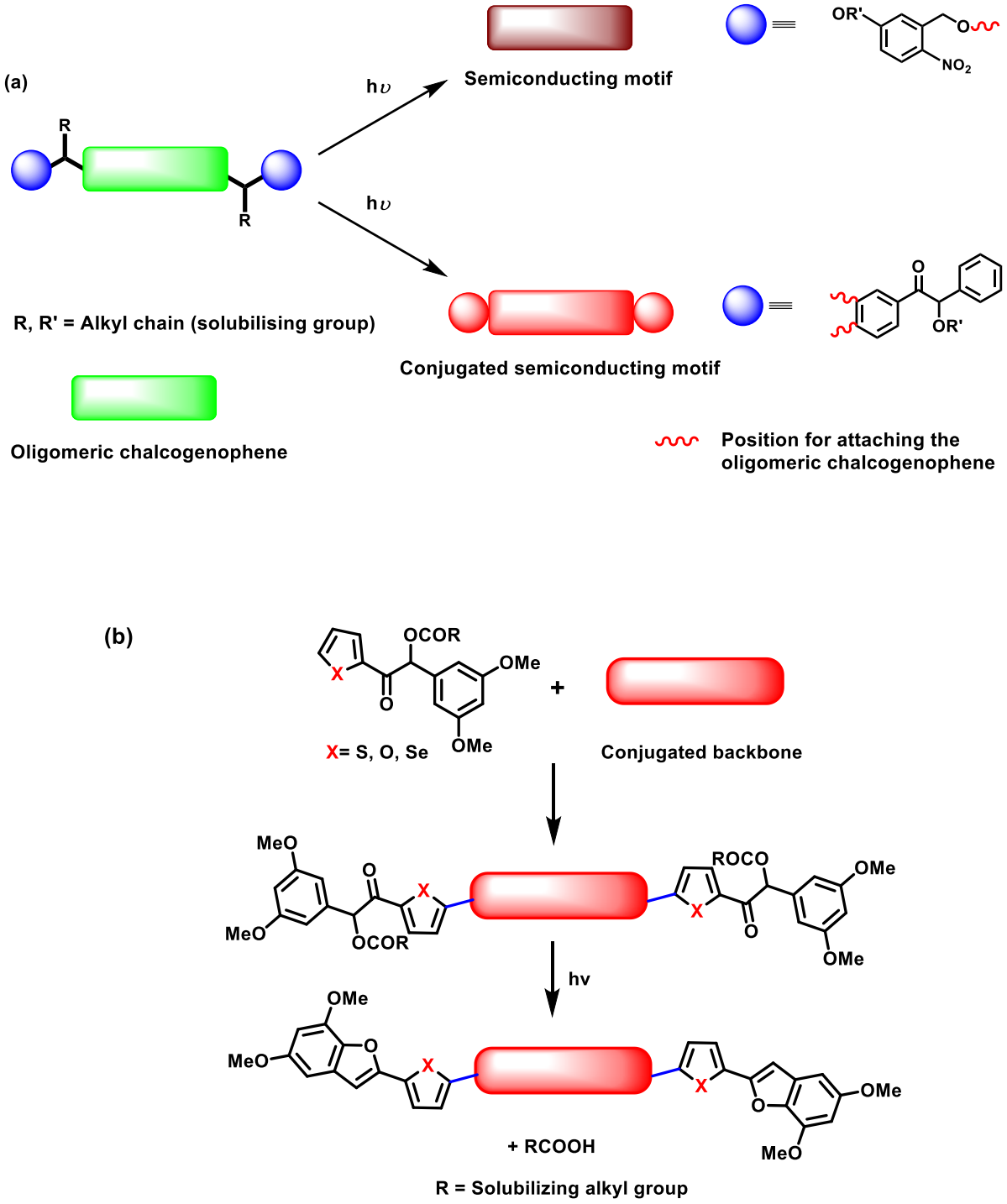

Figure 2. (a) Two possible methods of photo release of the solubilizing group- with the removal of the trigger (top) and without removal of the trigger (bottom). (b) Proposed scheme for 3',5'-dimethoxybenzoin linked photoactive triggers.

3',5'-Dimethoxy benzoin acetates (DMA) phototrigger

In 1964 Sheehan and coworkers showed that photoirradiation of benzoin acetate led to the formation of 2-substituted benzofuran with the release of acetic acid (**Scheme 7**).[18] The high quantum yield of carboxylic acid release (ϕ=0.64) makes this reaction attractive for the protection of carboxylic acids.[19]

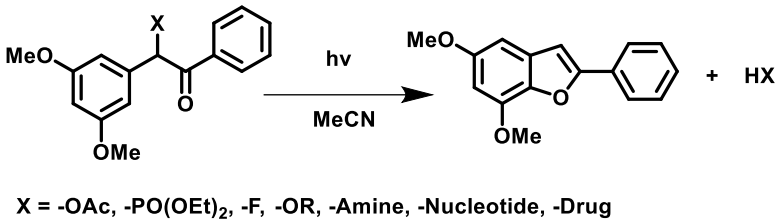

Scheme 7. Photolysis of 3',5'-Dimethoxybenzoin derivatives

In terms of structures, substitutions at the benzylic ring can modulate reaction rate and 3',5'-dimethoxybenzoin acetate led to a fast and smooth cyclization upon photolysis whereas parent benzoin acetate, and 4,4'-dimethoxybenzoin acetate only gave trace amounts of benzofuran.[19] Suitable derivatives of 3',5'-dimethoxybenzoin have been utilized to release inorganic phosphates,[20] nucleotides,[21] carboxylates,[18,22] amines[23], and alcohols which found its application in drug delivery,[24] lithographic techniques[25], biochip fabrication[26,27], and modulating the protein folding.[28,29] Releasing the targeted molecules accompanied with the fluorescent property of benzofuran unit has been used as a reporter for the photo-induced un-caging event. Besides this superior chemical reactivity, mechanism of the formation of benzofuran and release of acid draws the attention due to the involvement of singlet excited state and different intermediates such as a carbocation,[30] charge transfer complex,[31] and diradical species.[22] Mechanistic studies revealed that a clear difference between the photodeprotection pathways of parent benzoin and 3',5'-dimethoxybenzoin acetate systems, as benzoyl-localized n-π^* triplet state initiate the deprotection–cyclization reaction for the former and n-π^* singlet state character pathways proceeding via various reactive intermediates have been proposed for the later, respectively.[32–34] For 3',5'-dimethoxybenzoin systems, cyclic cation produced by ring opening of bicyclic oxetane intermediate[19] and C-X heterolytic cleavage of an intramolecular exciplex formed by dimethoxybenzylic ring to the carbonyl nπ^*singlet state were speculated.[31] Yet another cation intermediate, formed either by a direct heterolytic cleavage of the C-X bond was also postulated[30,35]. Further, a biradical intermediate is formed from a radical-based addition of the excited carbonyl oxygen to the

substituted benzylic ring further acetoxy migration, followed by re-aromatization provide the benzofuran product.[22,36] Recently, visible light absorbing ruthenium complex catalyzed deoxygenation of benzoin esters indicated the involvement of electron transfer steps.[37]

On the other hand, processing the organic molecules plays an important role in achieving the desired morphology for photovoltaic and optoelectronic applications. Such methods include side chain engineering which helps to solubilize the small molecules/polymers.[38,39] Also, studies have been attempted with chemical, and photochemical methods for processing due to the insoluble nature of conjugated organic semiconducting materials.[40–45] Owing to the semiconducting nature of poly heteroaromatic compounds, we have investigated a series of hetero-aromatic compound based benzoin type trigger molecules composed of (3',5'-dimethylphenyl)heteroaryl acyloin for its capability of photocyclization reaction to afford the benzofuran unit capped conjugated hetero-aromatic compounds (**Figure 3)**. Exploring these π-extended triggers paves the way for developing visible light sensitive triggers for releasing the relevant biologically active compounds, and also developing a conjugated benzofuran derivative with modulated photophysical property with the semiconducting property. The present investigation is concerned about the photochemical reactivity of π-extended triggers towards benzofuran capped derivatives and to make an effort towards exploring a photochemical method for solution-based processing.

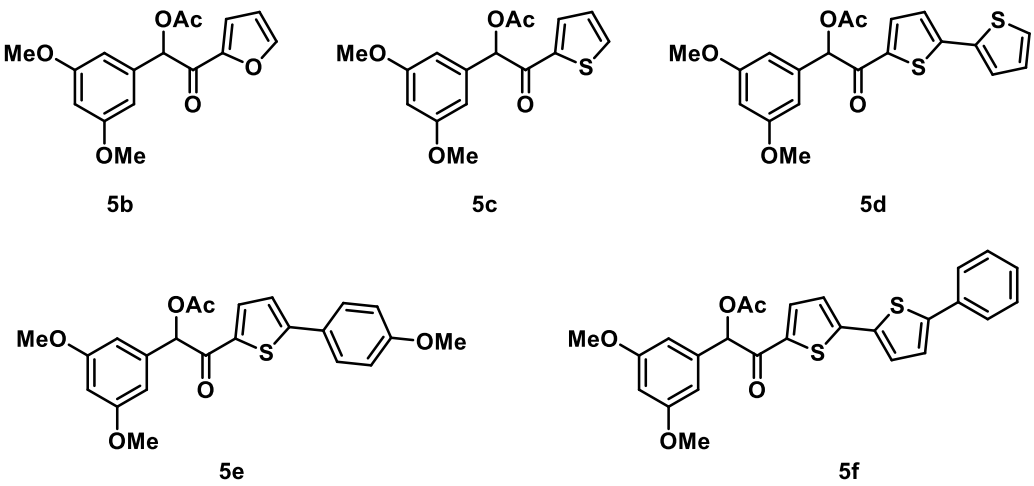

Figure 3. (3',5'-Dimethylphenyl)heteroaryl acyloin based phototriggers.

5.2. RESULTS AND DISCUSSION

5.2.1. Synthesis

The synthetic route for (3',5'-dimethylphenyl)heteroaryl acyloin based photo triggers is shown in **Scheme 8.**

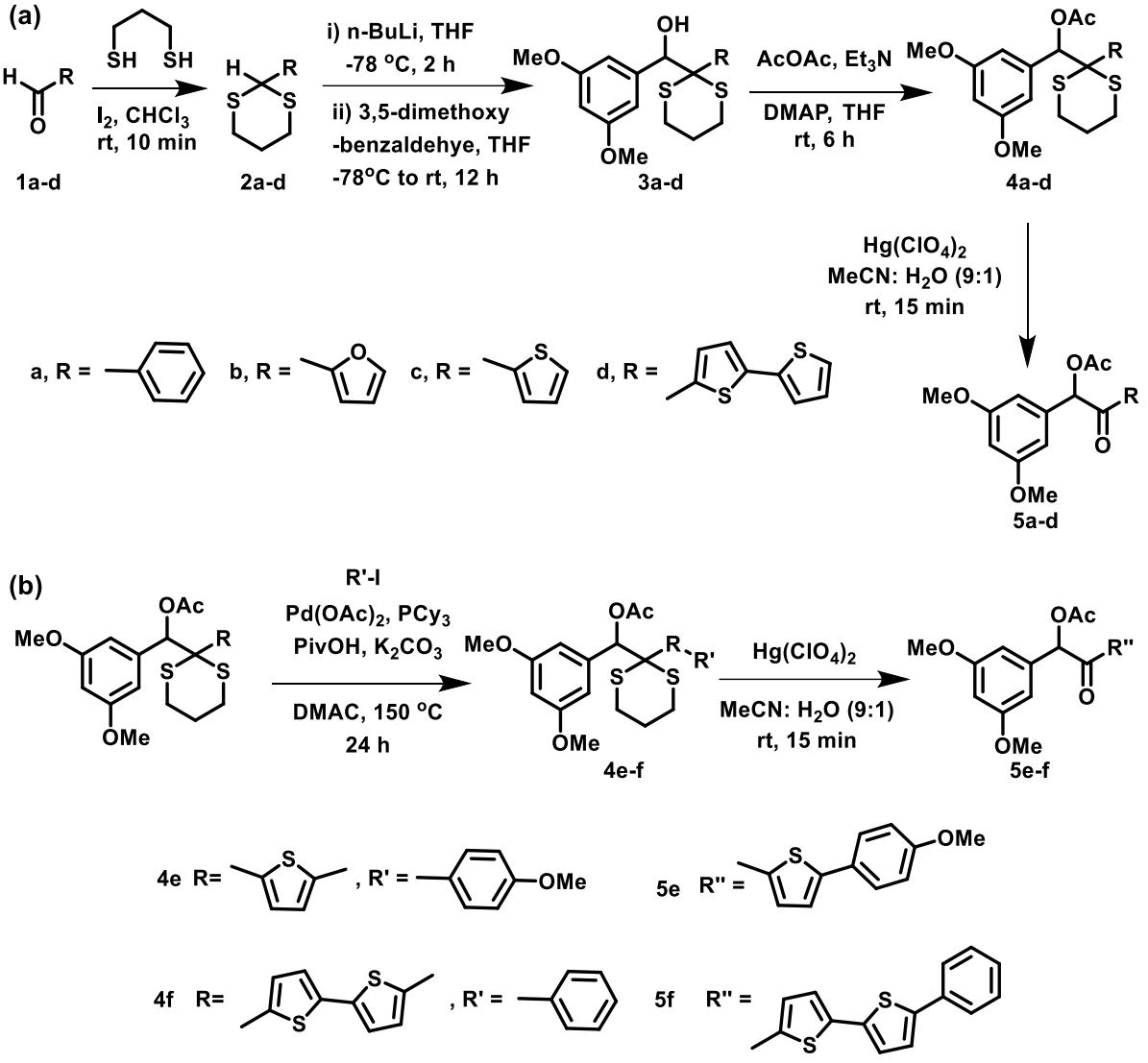

Scheme 8. (a) Synthesis of acyloin derivatives, **5a-d**, (b) synthesis of extended acyloin derivatives **5e-f.**

The hetero aromatic furan, thiophene, and bithiophene based cross-acyloin derivatives were synthesized by following umpolung-based strategies that employ dithiane protected aldehydes (**Scheme 2**). 2-heteroaromatic aldehydes were protected with 1,3-propanedithiane

by treatment with 2-propanedithiol in the presence of catalytic amount of iodine. The heteroaromatic dithianes were reacted with n-BuLi at -78 °C and the corresponding lithiated intermediates were quenched with 3,5-dimethoxybenzaldehyde to afford the carbonyl protected unsymmetrical hetero-acyloin derivatives, **3**. The acyloin derivatives (**3a-d**) were acetylated with acetic anhydride in the presence of DMAP as a catalyst. Dithiane protected O-acetylated derivatives were deprotected by using $Hg(ClO_4)_2$ to afford the unsymmetrical hetero-acyloin acetate derivatives, **5**. To synthesize the photo triggers with extended conjugation on the arylketone side, the thiophene and bithiophene based protected **4c** and **4d**, respectively, were subjected to palladium catalyzed direct arylation reactions. Coupling with iodoanisole and bromobenzene gave **5e** and **5f** respectively, which were exposed to $Hg(ClO_4)_2$ mediated deprotection to provide the π-extended triggers such as **5e** and **5f** in moderate yield.

5.2.2. Photophysical and Photochemical Investigation

The UV-Vis absorption and emission spectra of synthesized unsymmetrical acyloin derivatives were recorded in MeCN solution. The absorption spectra showed maxima (λ_{max}) at 282 nm (**5a**), 277 nm (**5b**), 287 nm (**5c**), 359 nm (**5d**), 356 nm (**5e**) and 386 nm (**5f**) (**Figure 4a** and **Table 1**). The progressively red-shifted absorption in going from **5c** to **5f** is attributed to a gradual increase in the conjugation of these acyloin derivatives. The observed fluorescence spectra showed broad emission and exhibited a similar trend as the absorption spectra (**Figure 4b** and **Table 1**). In moving from **5c** to **5f,** the spectra showed gradual red-shift in emission with maxima at 402 nm (**5a**), 387 nm (**5b**), 412 nm (**5c**), 435 nm (**5d**), 437 nm (**5e**) and 576 nm (**5f**).

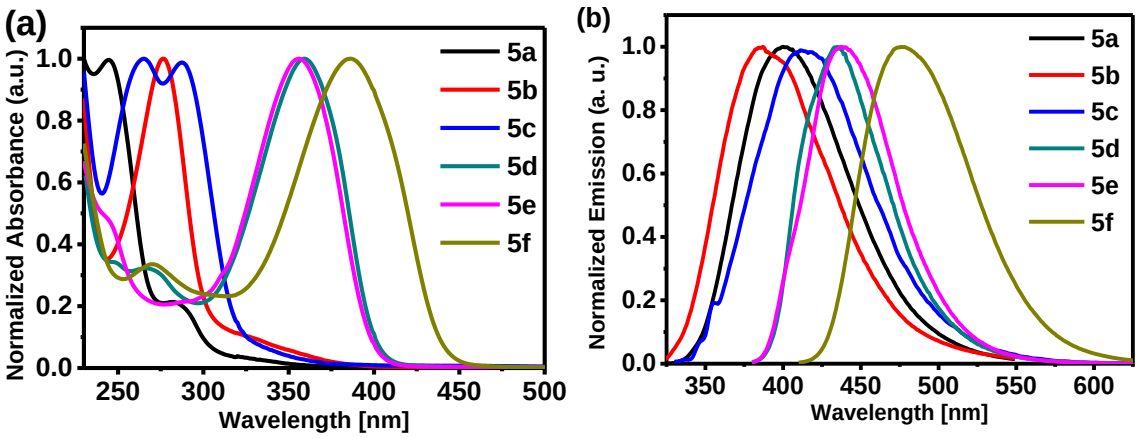

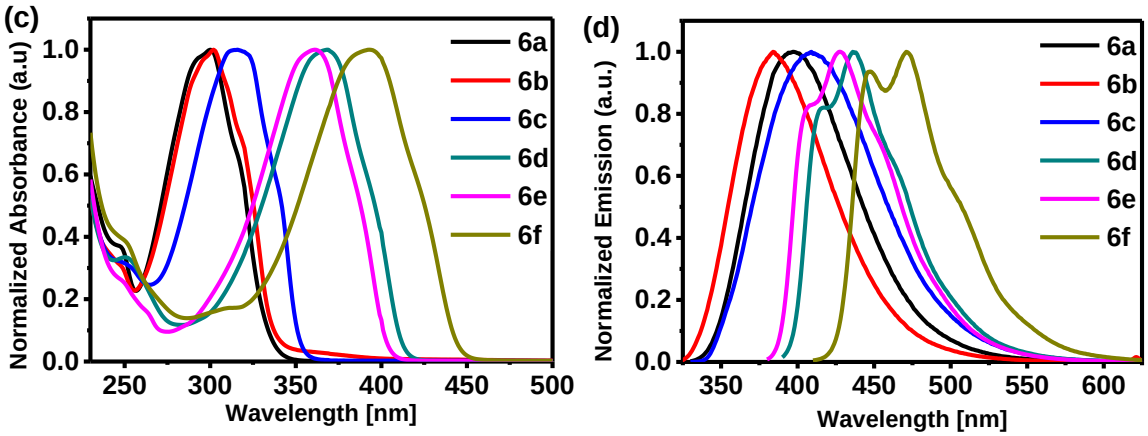

Figure 4. UV-Vis absorption (a, c) and emission (b, d) of **5a-f** and **6a-f** in MeCN

Table 1. Photophysical properties of acyloin derivatives, **5** and benzofuran, **6** derivatives in MeCN

	$\lambda_{max,}$ Phototrigger **(5)**				λ_{max} of cyclized benzofuran derivative **(6)**		
Substrate	Abs (nm)	Extinction coefficient ($M^{-1}cm^{-1}$)	Emi (nm)	Substrate	Abs (nm)	Extinction coefficient ($M^{-1}cm^{-1}$)	Emi (nm)
5a	245 282	1.15×10^4 2.6×10^3	402	**6a**	300	2.42×10^4	397
5b	277	1.24×10^4	387	**6b**	302	2.1×10^4	384
5c	265 287	0.93×10^4 0.92×10^4	412	**6c**	315	1.58×10^4	409
5d	359	2.1×10^4	435	**6d**	369	3.29×10^4	436
5e	356	2.1×10^4	437	**6e**	361	3.2×10^4	427
5f	386	2.0×10^4	476	**6f**	393	4.8×10^4	471

Photochemical reactions of acyloin triggers were carried out by irradiating under pyrex filtered UV light from a medium pressure mercury vapor lamp (**Scheme 9**).

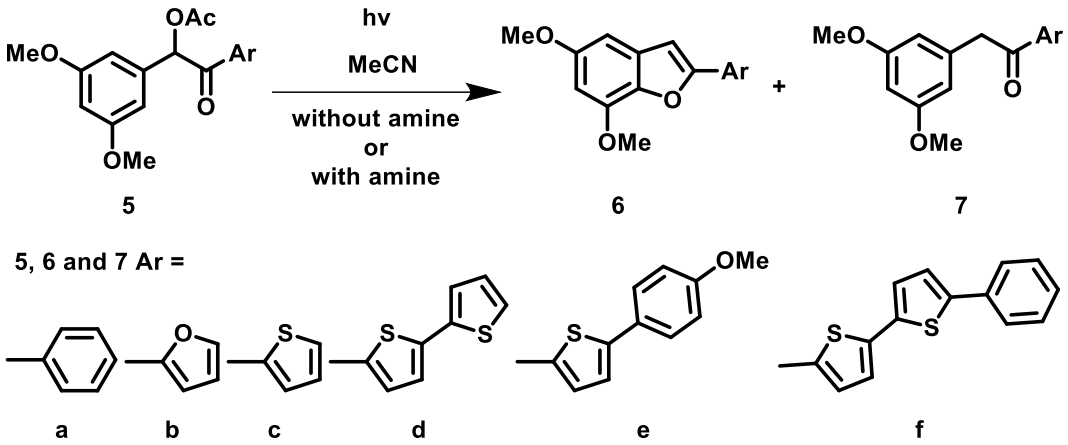

Scheme 9. Photochemical reaction of unsymmetrical acyloin derivatives **5a-f** in MeCN.

The compounds **5a**, **5b**, **5c**, and **5d** have converted efficiently into the corresponding benzofuran derivatives **6a**, **6b**, **6c**, and **6d**, respectively in quantitative yield upon photo-irradiation in MeCN under a nitrogen atmosphere (**Table 2**). This transformation occurred with the red-shifted absorption in comparison to their parent photo triggers due to increased conjugation. The absorption maxima (λ_{max}) of **6a**, **6b**, **6c,** and **6d** appeared at 300, 302, 315 and 369 nm respectively (**Figure 4c** and **Table 1**).

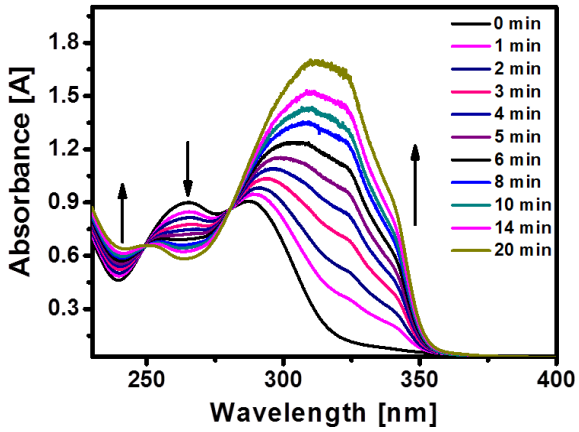

Figure 5. UV-visible absorption spectra of **5c** formed upon irradiation at 360 nm under 100 watt UV lamp in MeCN when recorded at 0, 1, 2, 3, 4, 5, 6, 8, 10, 14 and 20 min.

Figure 5 displays the change in the UV-Vis absorption spectra of **5c** recorded after a series of defined periods of photoirradiation at 360 nm. The curve exhibited two isosbestic points (at 249 and 280 nm) during the course of the reaction which is indicative of clean conversion to the benzofuran (**6c**). However, photo-irradiation of compounds **5e** and **5f** led to observe only trace amounts of the benzofuran derivatives besides photodecomposition of starting materials.

It is interesting to note that while the absorption profile for the compounds **5d** and **5e** are almost the same, a striking difference in terms of photochemical reactivity is observed. It is well known in the literature that n-π* and π-π* states of carbonyls have different reactivity towards photo-reduction of ketones due to very facile hydrogen abstraction step with n-π* carbonyl triplet state.[46] However, under electron transfer reaction conditions, both n-π* and π–π* states of carbonyls have same reactivities as the mechanism involves electron transfer followed by proton transfer.[46] In the present work, the different photochemical reactivity of **5d** and **5e** may have arisen from the change in the nature of the excited state that initiates the reaction. Hence, it was envisaged that addition of electron donor such as amines might predict whether the excited state nature of **5e** and **5f** plays any role for the observed result.

To our delight, the addition of triethylamine (TEA) to **5e** and **5f** leads to quantitative conversion of starting materials within 1 h to the required benzofuran (**6e** and **6f**) formation along with deacetoxylated product, **7e,** and **7f** (**Scheme 9**). The product ratio of benzofuran to deacetoxylated product is dependent on the equivalent of triethylamine. The bithophene based trigger **5d** provides quantitative benzofuran derivative upon irradiation in MeCN, however, in the presence of triethylamine, about 46% of deacetoxylated product is formed along with cyclized product thus indicating the electron transfer pathway is also operated under the experimental conditions.

Table 2. Photochemical results of **5a-f** in MeCN[a]

Entry	Substrate	TEA	Irradiation time (h)	Cyclized product (%)	Deacetoxylated product (%)
1	**5a**	-	1h	**6a**, 100[b]	-
2	**5a**	1 eq	1h	**6a**, 100[c]	0
3	**5b**	-	1h	**6b**, 80[b]	-
4	**5b**	1 eq	1h	-[d]	-[d]
5	**5c**	-	1h	**6c**, 90[b]	-
6	**5c**	1 eq	1h	**6c**, 70[c]	30[c]
7	**5d**	-	1.5h	**6d**, 80[b]	-
8	**5d**	1 eq	1h	**6d**, 54[c]	**7d**, 46[c]
9	**5e**	-	2.5h	**6e**, 15[b]	-
10	**5e**	1 eq	1h	**6e**, 60[b]	**7e**, 25[b]
11	**5e**	2 eq	1h	**6e**, 45[b]	**7e**, 45[b]
12	**5f**	-	2.5h	**6f**, 15[b]	-
13	**5f**	1 eq	1h	**6f**, 65[b]	**7f**, 20[b]
14	**5f**	2 eq	1h	**6f**, 50[b]	**7f**, 40[b]

[a]prior to irradiation, the solution was deoxygenated with argon for 15 min and continuously deoxygenated during the irradiation, [b]isolated yield, [c]product ratio by ^{1}H-NMR integration (see Figure 6). [d]the reactant, **5b**, was photo-decomposed in the presence of TEA.

Product formation in photochemical reaction of **5d** has been monitored by ^{1}H-NMR, where the proton from cyclized benzofuran units appeared between 6.79 ppm as a singlet and the benzylic methylene for deacetoxylated product appeared at 4.1 ppm as a singlet (**Figure 6 and 7**).

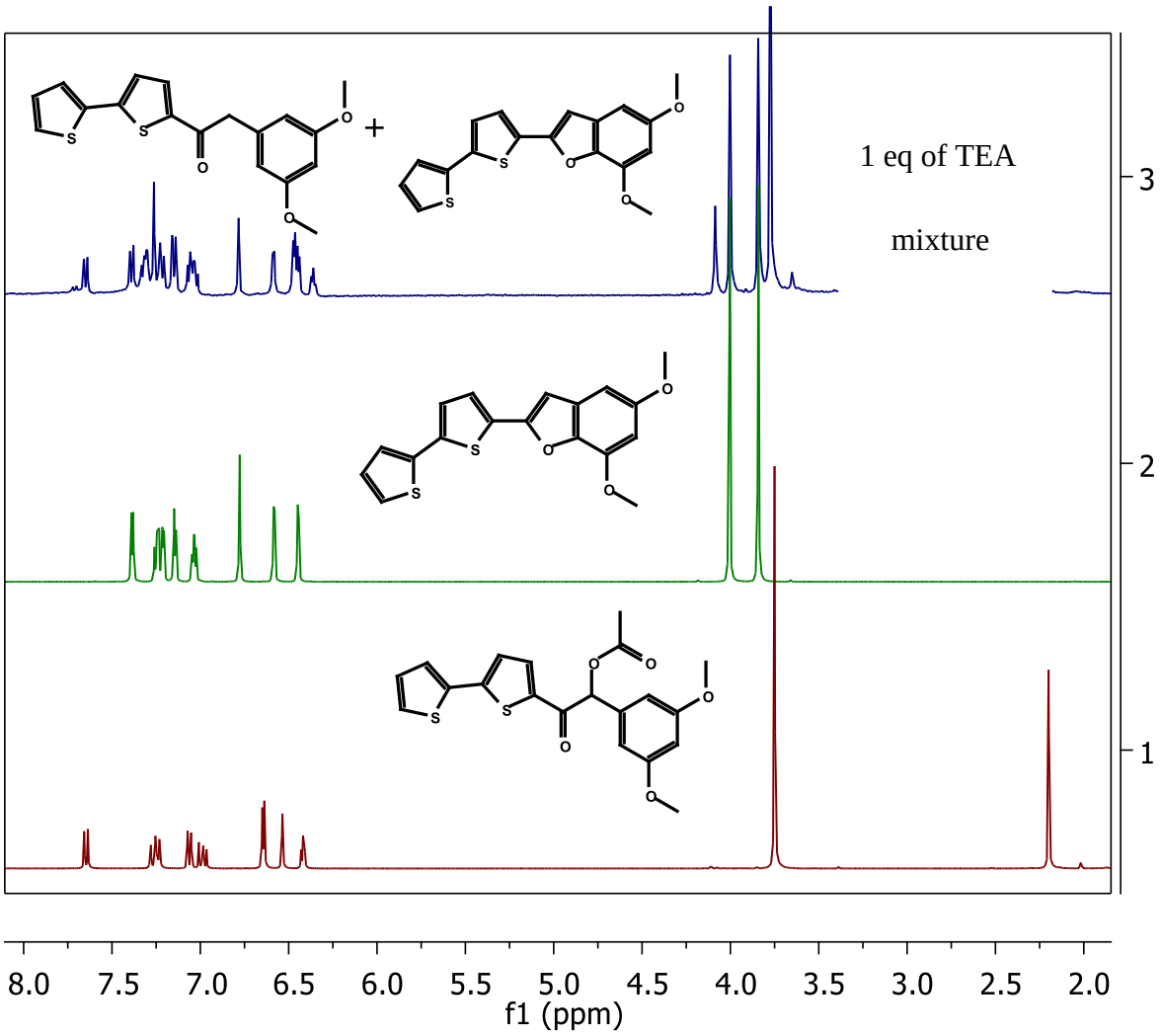

Figure 6. Stacked ^{1}H NMR spectra of **5d** (bottom), **6d** (middle) and **6d** + **7d** mixture (top)

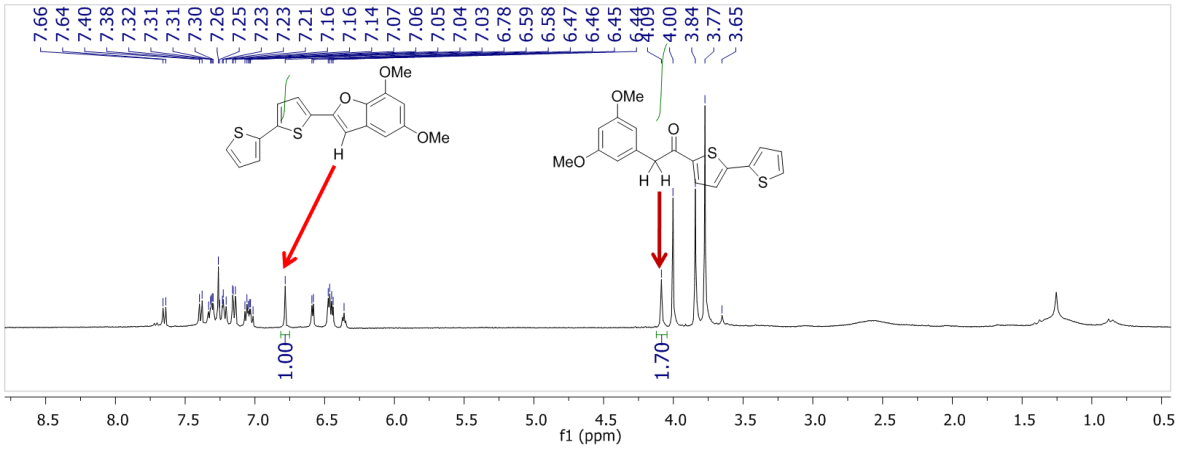

Figure 7. ^{1}H-NMR spectrum for the mixture of **6d** and **7d** obtained by the photochemical reaction of **5d** in MeCN in the presence of Et_3N (1 equiv) for 1 h and evaporated the solvent (Entry 8, **Table 2**).

The possible mechanisms for the formation of benzofuran and deacetoxylated products are provided in **Scheme 10**. The electron transfer by the amine to the excited state (either singlet or triplet) leads to the formation of the radical anion. The oxygen-centered anion can attack the 3′,5′-dimethoxybenzyl unit to provide the cyclic radical anion and triethylamine radical cation pair. The back electron transfer (BET) provides the diradical which further cyclized to benzofuran unit (Path a, **Scheme 10**).

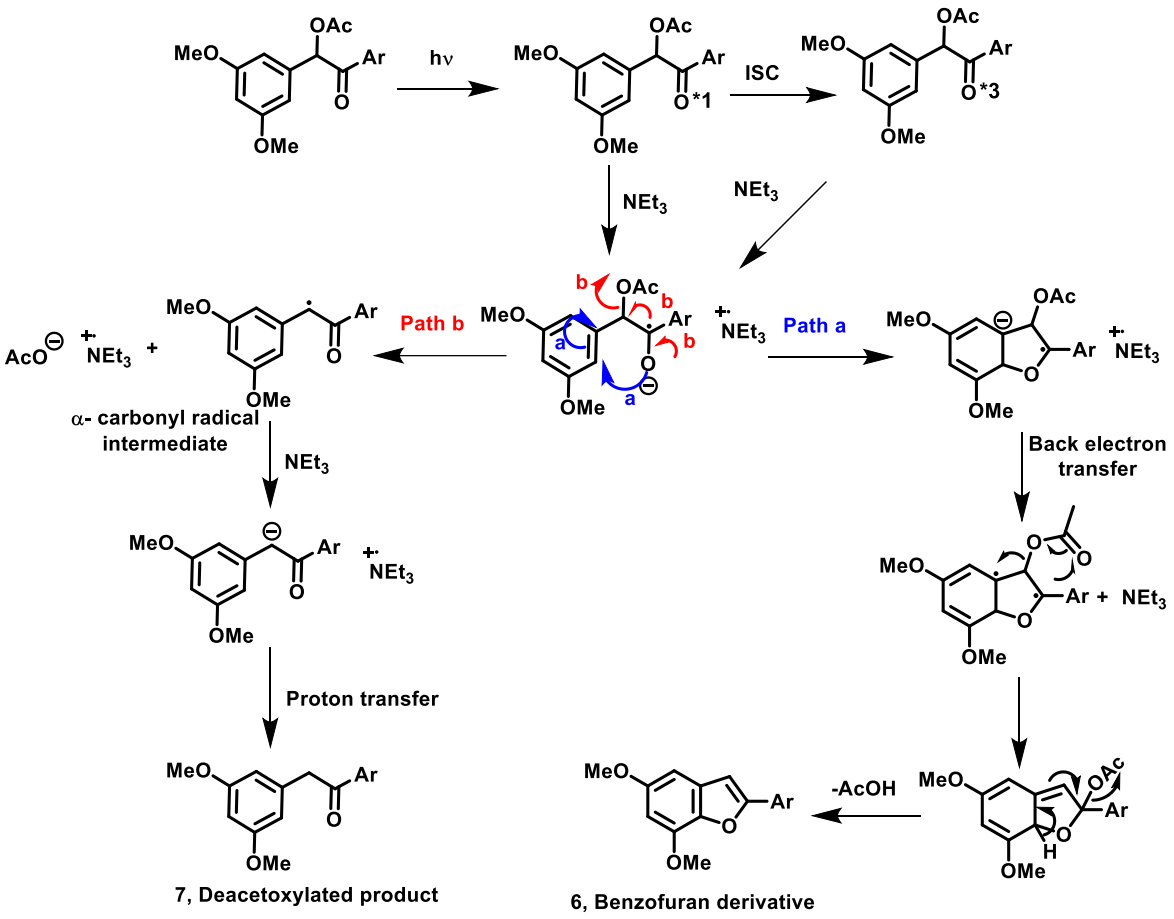

Scheme 10. Proposed mechanisms for the formation of benzofuran (**6**) and deacetoxylated (**7**) products.

On the other hand, the formation of deacetoxylated product begins with the elimination of acetate anion to afford the α-carbonyl radical intermediate. This intermediate is converted into α-carbonyl anion upon SET from the second molecule of triethylamine followed by proton transfer which provides the deacetoxylated product (Path b, S**cheme 10**). This observation presents yet another possibility of the mechanistic route in the presence of an electron transfer reagent besides existing pathways in the literature.[9,12,20-26] Such

photoinduced electron transfer based photoremovable protecting group has been demonstrated in phenacyl trigger where the electron donor is excited to initiate the triggering process.[47] Recently, visible light absorbing ruthenium complex catalyzed deoxygenation of benzoin esters indicated the involvement of electron transfer steps.[37]

To check the reactivity of triggers **5a-5c** under photoinduced electron transfer reaction conditions, experiments on **5a-c** with triethylamine have been carried out. Though the parent 3',5'-dimethoxybenzoin acetate (**5a**) provided the cyclic product exclusively (**Table 2**, Entry 2), compound **5c** provided cyclized (70%) and deacetoxylated (30%) products in the presence of triethylamine (**Table 2**, Entry 6). It is quite possible that the reactivity of the photo-excited **5a** towards cyclization is very fast compared to the electron transfer from TEA to the **5a***. Furyl based trigger, **5b**, was decomposed under the photochemical experimental conditions in the presence of triethylamine.

To test the feasibility of photoinduced electron transfer between phototriggers (A) and triethyl amine (D), the reduction potential of compounds **5d**, **5e** and **5f** were calculated by cyclic voltammetry (**Figure 8**) and formulated into the to the Rehm-Weller equation (1).

$$-\Delta G_{et} = E\,(A/A^-) - E(D^+/D) + E_{0\text{-}0} + e^2/\varepsilon a \qquad (1)$$

where $-\Delta G_{et}$ is the free energy change for forming the ion pair complex (D^+A^-) expressed in eV, E(A/A-) is reduction potential of acceptor in V, $E(D^+/D)$ is oxidation potential of donor in V, $E_{0\text{-}0}$ is the excited state energy of the electron acceptor in eV and $e^2/\varepsilon a$ is a coulomb energy term where a is the distance between D^+ and A^- ions in the complex.

The thermodynamic for the photoinduced electron transfer reaction is shown in **Table 3**. The large values of $-\Delta G_{et}$ indicates that photoinduced electron transfer in compounds **5d-f** is highly facile.

Table 3. Thermodynamics of the photoinduced electron transfer

(A)	E (A^-/A) (V vs. SCE)	$E_{0\text{-}0}$ (eV)	$-\Delta G_{et}$ (eV)
5d	-1.29 V	3.12	0.94 eV
5e	-1.31 V	3.13	0.93 eV
5f	-1.17 V	2.86	0.80 eV

$E(D^+/D)$ for triethylamine is equal to 0.98 V Vs. SCE.[48] $e^2/\varepsilon a$ is assumed to be 0.07 eV.[49] $\Delta E_{0\text{-}0}$ is calculated from the intersection point of absorption and emission curves.

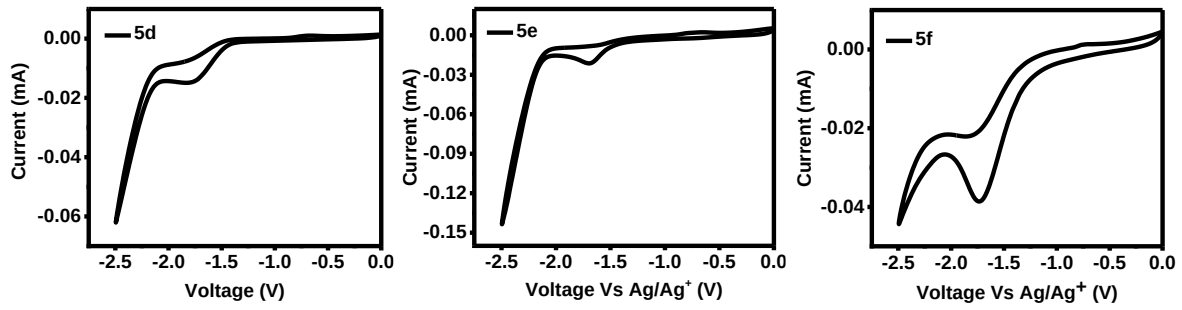

Figure 8. Cyclic voltammogram (reduction scan) of **5d**, **5e**, and **5f** measured in CH_2Cl_2

5.2.3. Organic Field Effect Transistors (OFETs) Characteristics

Small molecules based organic semiconductors have been used extensively in the fabrication of organic field effect transistors (OFETs).[50,51] Thiophene and bithiophene end-capped with benzofuran were reported to exhibit hole mobility of 1.9×10^{-4} and 4.4×10^{-3} cm^2/Vs respectively by vapor deposition method.[52] A single crystal of a naphtho[2,1-b:6,5-b′]-difuran small molecule was able to yield hole mobility up to 3.8 cm^2/Vs. These reports led our interest to explore the cyclized products of extended triggers (conjugated benzofuran molecules) in field effect transistors. To this end, the electrochemical properties of **6d**, **6e,** and **6f** were studied, and cyclic voltammograms were recorded in DCM solution with ferrocene as an external reference (**Figure 9**). HOMO energy levels were calculated from oxidation onset and found to be at -5.26 eV, -5.24 eV and -5.24 eV for **6d**, **6e,** and **6f**

respectively. LUMO energy levels were calculated by adding $E_{0\text{-}0}$ to HOMO levels and found to be at -2.18 eV, -2.09 and -2.37 eV respectively.

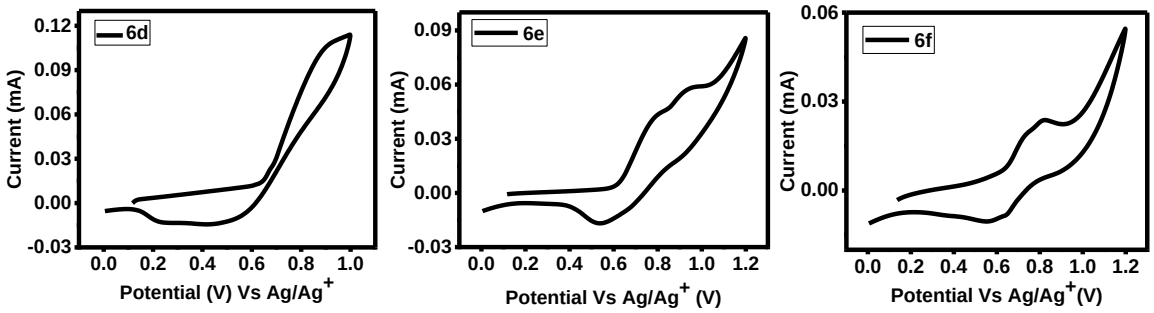

Figure 9. Cyclic voltammogram (oxidation scan) of **6d**, **6e**, and **6f** measured in CH_2Cl_2.

The charge carrier mobility of these molecules was measured in thin film form using the field effect transistor configuration. Bottom-gate bottom-contact field-effect transistor devices were fabricated by spin coating the molecules on top of SiO_2 as gate dielectric that is patterned with gold source and drain electrodes. Heavily n-doped Si was the gate electrode. OFET measurements were performed by applying negative drain and gate voltage, and all the molecules showed hole transporting properties, hole mobility (μ) values, the threshold voltage (V_T), and on/off ratio ($I_{on/off}$) were calculated for as casted film and thermally annealed films are summarized in **Table 4**. Hole mobility of molecule **6d** was found to be 1.2×10^{-8} cm^2/Vs, which increased by one order after thermal annealing at 50 ºC for 10 minutes with the maximum hole mobility calculated as $1.3\times10^{-6}cm^2/Vs$ (Figure 10). In the case of **6e**, hole mobility was calculated to be 1.2×10^{-7} cm^2/Vs (Figure 11), and the mobility values remain nearly similar for thermally annealed films. Highly extended **6f** showed the hole mobility of 4.9×10^{-9} cm^2/Vs for as casted film and 1.3×10^{-8} cm^2/Vs after thermal annealing (**Figure 12**).

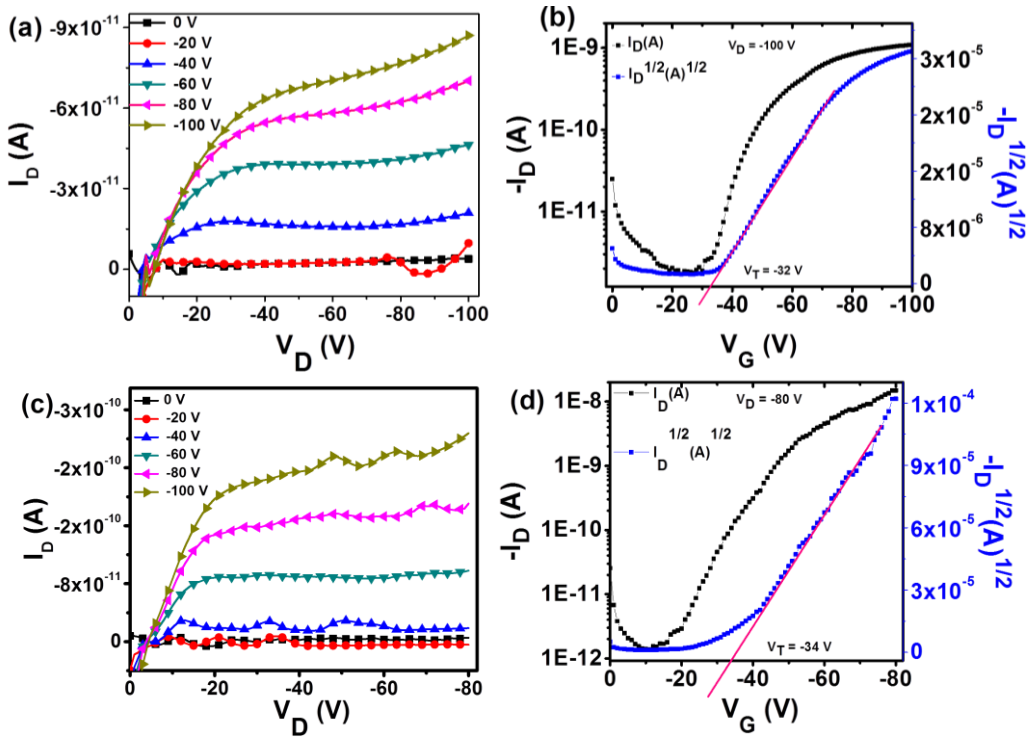

Figure 10. Output and transfer characteristics of **6d**, without annealing (a) and (b), with annealing at 50 ºC for 10 min (c) and (d). (Channel length = 5 µm.

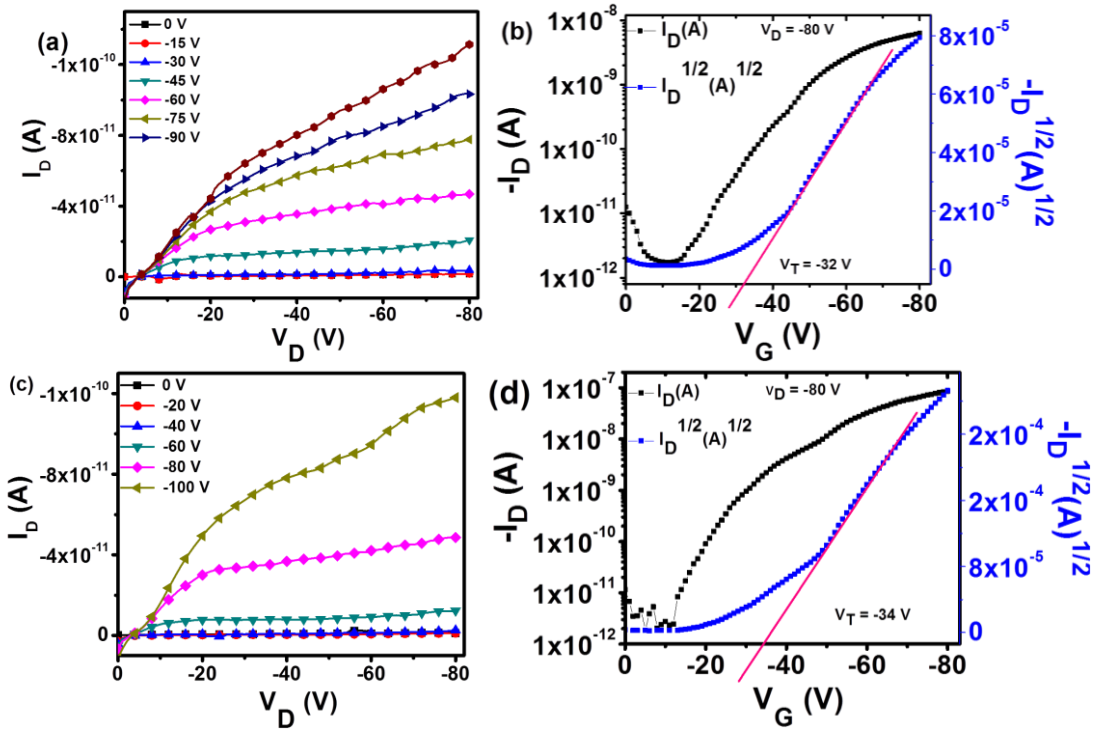

Figure 11. Output and transfer characteristics of **6e**, without annealing (a) and (b), with annealing at 50 ºC for 10 min (c) and (d). (Channel length = 2.5 µm).

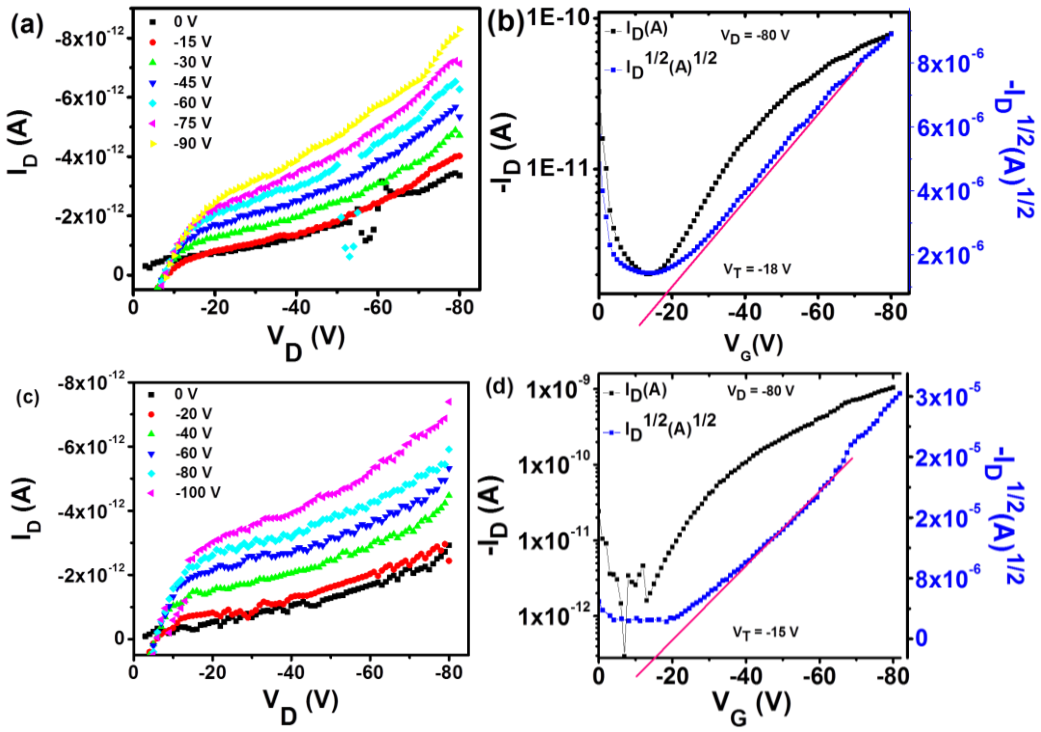

Figure 12. Output and transfer characteristics of **6f**, without annealing (a) and (b), with annealing at 50 ºC for 10 min (c) and (d). (Channel length = 2.5 µm).

Table 4. Field effect transistor device parameters for the benzofuran capped products.

Molecule	OFET properties of thin film spin coated from chlorobenzene			OFET properties of the thin film after annealing at 50 ºC for 10 min		
	μ_h (cm^2/Vs) (μ_{max})	V_T (V)	$I_{on/off}$	μ_h (cm^2/Vs) (μ_{max})	V_T (V)	$I_{on/off}$
6d	1.2×10^{-8} ($\mu_{max} = 1.7\times10^{-8}$)	-32	5×10^{2}	7.1×10^{-7} ($\mu_{max} = 1.3\times10^{-6}$)	-34	10^{4}
6e	1.2×10^{-7} ($\mu_{max} = 4.2\times10^{-7}$)	-32	4×10^{3}	1.7×10^{-7} ($\mu_{max} = 6.3\times10^{-7}$)	-33	4×10^{4}
6f	4.9×10^{-9} ($\mu_{max} = 6.7\times10^{-9}$)	- 18	40	1.3 x 10^{-8} ($\mu_{max} = 1.7\times10^{-8}$)	-15	6×10^{2}

5.3. SUMMARY

Photochemical reactivities of unsymmetrical (3',5'-dimethylphenyl)heteroaryl acyloin based phototriggers have been studied to understand the formation of benzofuran derivatives upon extending the conjugation of aromatic ketone part of the acyloin derivatives. Unsymmetrical acyloin based triggers constituted with furan, thiophene, bithiophene moieties on the ketone part exhibited facile conversion of benzofuran derivatives, quantitatively. Whereas, photolysis of triggers with extended aromatic units on the ketone part showed decomposition of starting materials with the trace formation of benzofuran capped products. However, in the presence of triethylamine, the extended trigger derivatives showed a clean conversion of starting material to the formation of a mixture of benzofuran capped and deacetylated products. Such products formation in the presence of triethylamine indicates the possible photo-induced electron transfer process involved in the reaction. The mechanism that involves photo-induced electron transfer process is proposed for the extended acyloin derivatives which may emanate from the π-π* nature of the carbonyl excited state. Furthermore, solution processed OFET devices made out of benzofuran capped products showed the hole mobility in the range of 10^{-9}-10^{-7} cm^2/Vs. This study establishes the photochemical synthesis of conjugated benzofuran derivatives by photo-induced electron transfer method and its application in organic field effect transistors. The present method could be extended to visible and NIR active phototrigger by modulating the band gap of the chromophore, nature of the excited state and the choice of electron donors. Further investigation will focus on the mechanistic aspects and development of new triggers for biologically relevant molecules and for processing organic molecules for optoelectronics.

5.4. EXPERIMENTAL

5.4.1. Materials and Methods

All the reagents and solvents were purchased from commercial sources unless otherwise noted. Tetrahydrofuran (THF) was dried and distilled over sodium/benzophenone still immediately before use. ^1H NMR and ^{13}C NMR were recorded in $CDCl_3$ in 200 MHz, 400 MHz, and 500 MHz NMR spectrometers. High-resolution mass spectrometric measurements were carried out using the ESI method and an ion-trap mass analyzer. Absorption spectra were recorded at room temperature in quartz cuvette using a UV−Visible spectrophotometer.

The photochemical reactions were carried out by pyrex filtered medium pressure mercury vapour lamp (450 W) with pyrex filter (hν > 300 nm). The cyclic voltammetry (CV) was carried out in anhydrous dichloromethane solvent by using 0.1 M tetrabutylammonium perchlorate as supporting electrolyte and Fc/Fc^+ as an internal reference at the scan rate of 50 mV s^{-1}. The experiments were performed at room temperature in a nitrogen atmosphere with a three-electrode cell consisting of a platinum foil as a counter electrode, an Ag/Ag^+ reference electrode, and a platinum wire as the working electrode. The reduction potentials of **5d-f** were calculated from the reduction onset and converted to SCE (V) by addition of 0.38 V[44] using the equation $E(A^-/A) = [\{ E_{red/onset} - E_{1/2} (Fc/Fc^+)\} + 0.38]$ V vs SCE. The HOMO energy levels cyclized product **6d-f** were calculated from oxidation onset following the equation $E_{HOMO} = -(E_{ox/onset} - E_{1/2}(Fc/Fc^+) + 4.8)$ eV. LUMO energy levels were calculated by adding $E_{0\text{-}0}$ to HOMO levels. $E_{0\text{-}0}$ for a compound is calculated from the intersection of normalized absorption and emission curves.

5.4.2. Organic Field Effect Transistors (OFET) device fabrication

Bottom-gate bottom-contact field-effect transistor substrates were purchased from Fraunhofer IPMS (interdigitated S/D electrodes, with channel lengths (L) 2.5, 5, 10 and 20 μm and channel width (W) of 10 mm. Prefabricated FET substrates consist of SiO_2 as a gate dielectric, heavily n-doped Si as a gate electrode, and gold as source and drain electrodes. FET substrates were cleaned with acetone followed by isopropanol and dried by heat gun. The device fabrication and measurements were done inside argon-filled glove box. Molecules were spin coated using chlorobenzene solution (concentration ≅ 10 mg/mL, 500 rpm for 100 seconds).OFET measurements were performed on Agilent 4156 C semiconductor probe analyzer and semi probe station. Charge carrier mobilities were calculated using the standard linear regime quadratic model equation $\mu = I_{DS}/(V_{GS}\text{-}V_{th})V_{DS} \times L/WC_{OX}$.

5.4.3. Synthetic Procedure and Characterization data

General procedure for the synthesis of dithianes (2a-2d)

Heterocyclic 2-carbaldehyde (**1a-1d**) (10 mmol) was dissolved in 30 mL chloroform, Propane-1,3-dithiol (12 mmol) and iodine (1 mmol) were added to the above solution and stirred for 15 min at room temperature. The reaction mixture was quenched with sodium thiosulphate (20 % in water) and diluted with dichloromethane (100 mL). The organic layer

was extracted and subsequently washed with aqueous NaOH (10 % weight/volume, 100 mL) followed by water (3 × 200 mL). The resultant organic layer was dried over anhydrous Na_2SO_4, concentrated under reduced pressure and purified by column chromatography over silica by eluting with petroleum ether: EtOAc.

2-Phenyl-1,3-dithiane (2a). White solid (1.8 g, 92%). Mp 66-68 ºC. 1H NMR (200 MHz, $CDCl_3$) δ 7.52 – 7.40 (m, 2H), 7.39 – 7.26 (m, 3H), 5.16 (s, 1H), 3.20 – 2.80 (m, 4H), 2.24 – 1.81 (m, 2H). ^{13}C NMR (50 MHz, $CDCl_3$) δ 139.2, 128.8, 128.5, 127.9, 51.6, 32.2, 25.2. HRMS (ESI) m/z $[M+Na]^+$ Calcd for $C_{10}H_{12}NaS_2$ 219.0278, found 219.0272.

2-(1,3-Dithian-2-yl)furan (2b). White solid (1.7 g, 89%). Mp 45-47 ºC. ^{1}H NMR (400 MHz, $CDCl_3$) δ 7.36 (d, *J* = 0.7 Hz, 1H), 6.42 – 6.36 (m, 1H), 6.34 (dd, *J* = 2.9, 1.7 Hz, 1H), 5.21 (s, 1H), 2.99 – 2.89 (m, 4H), 2.24 – 1.87 (m, 2H). ^{13}C NMR (50 MHz, $CDCl_3$) δ 151.9, 142.4, 110.7, 108.0, 42.1, 30.4, 25.4. HRMS calculated $[M + Na]^+$ for $C_8H_{10}NaOS_2$: 209.0071, found 209.0065.

2-(Thiophen-2-yl)-1,3-dithiane (2c). White solid (1.6 g, 87%). Mp 78-80 ºC. ^{1}H NMR (200 MHz, $CDCl_3$) δ 7.27 (dd, *J* = 4.7, 1.4 Hz, 3H), 7.16 (d, *J* = 3.5 Hz, 2H), 6.96 (dd, *J* = 5.1, 3.6 Hz, 2H), 5.41 (s, 2H), 3.04 – 2.92 (m, 8H), 2.22 – 1.91 (m, 4H).^{13}C NMR (50 MHz, $CDCl_3$) δ ppm 25.00, 31.0, 44.7, 76.4, 77.6, 125.6, 126.2, 126.7, 142.5. HRMS (ESI) m/z $[M-H]^+$ Calcd for $C_8H_{10}NaS_3$ 224.9842, found 224.9837.

5-(1,3-Dithian-2-yl)-2,2'-bithiophene (2d). Yellow solid (2.4 g, 85%). Mp 60-62 ºC. ^{1}H NMR (400 MHz, $CDCl_3$) δ 7.20 (dd, *J* = 5.1, 1.2 Hz, 1H), 7.14 (dd, *J* = 3.6, 1.2 Hz, 1H), 7.06 (dd, *J* = 3.7, 0.7 Hz, 1H), 7.03 – 6.98 (m, 2H), 5.34 (s, 1H), 3.02 – 2.89 (m, 4H), 2.20 – 1.86 (m, 2H). ^{13}C NMR (101 MHz, $CDCl_3$) δ 141.8, 137.8, 137.3, 127.9, 127.1, 124.7, 123.9, 123.4, 44.6, 30.7, 25.1. HRMS (ESI) m/z $[M-H]^+$ Calcd for $C_{12}H_{11}S_4$ 282.9744, found 282.9741.

General procedure for the synthesis of chalcogenophene unsymmetrical acyloin (3a-3d).

Dithiane (**2a-2d**) (10 mmol) was dissolved in 50 mL of anhydrous THF under N_2 atmosphere and cooled to -78 ºC. *n*-BuLi (1.6 M in cyclohexane, 1.1 equiv) was added to the reaction mixture dropwise and stirred at -78 ºC for 1 h. To the resultant mixture, solution of 3,5-dimethoxybenzaldehyde (1.1 equiv) in 10 mL of anhydrous THF was added dropwise and

stirred continuously at -78 ºC for another 1 h. The reaction mixture was brought to rt and stirred further for 5 h. The reaction mixture was cautiously quenched with saturated solution of NH_4Cl and extracted with EtOAc. The organic layer was separated, washed with brine solution and dried over sodium sulfate. The solvents were removed under reduced pressure and crude product was purified by column chromatography by silica gel using EtOAc and pet ether as eluents.

(3,5-Dimethoxyphenyl)(2-phenyl-1,3-dithian-2-yl)methanol (3a). Colorless sticky gum (3.2 g, 90%). ^{1}H NMR (200 MHz, $CDCl_3$) δ 7.72 (dd, *J* = 7.8, 1.7 Hz, 2H), 7.45 – 7.15 (m, 3H), 6.29 (t, *J* = 2.2 Hz, 1H), 5.99 (d, *J* = 2.2 Hz, 2H), 4.93 (d, *J* = 2.0 Hz, 1H), 3.56 (s, 6H), 3.05 (d, *J* = 2.9 Hz, 1H), 2.82 – 2.56 (m, 4H), 2.01 – 1.77 (m, 2H). ^{13}C NMR (50 MHz, $CDCl_3$) δ 159.5, 139.5, 137.6, 130.8, 128.2, 127.6, 106.1, 101.0, 81.1, 66.4, 55.2, 27.4, 27.2, 24.9. HRMS (ESI) m/z $[M+Na]^+$ Calcd for $C_{19}H_{22}NaO_3S_2$ 385.0908, found 385.0901.

(3,5-Dimethoxyphenyl)(2-(furan-2-yl)-1,3-dithian-2-yl)methanol (3b): Yellow solid (2.36 g, 67%). Mp 98-100 ºC. ^{1}H NMR (200 MHz , $CDCl_3$) δ 7.47 (dd, *J* = 0.9, 1.8 Hz, 1H), 6.53 - 6.43 (m, 1H), 6.38 (dd, *J* = 1.8, 3.3 Hz, 1H), 6.34 (t, *J* = 2.3 Hz, 1H), 6.15 (d, *J* = 2.3 Hz, 2H), 5.01 (s, 1H), 3.67 (s, 6H), 2.86 - 2.69 (m, 4H), 2.08 - 1.83 (m, 2H), ^{13}C NMR (101MHz , $CDCl_3$) δ = 159.7, 151.2, 142.7, 139.7, 113.2, 110.9, 105.2, 100.8, 79.8, 77.3, 77.2, 76.7, 59.7, 55.2, 27.6, 27.3, 24.7; HRMS (ESI) m/z $[M+Na]^+$ Calcd for $C_{17}H_{20}NaO_4S_2$: 375.0701, found 375.0695.

(3,5-Dimethoxyphenyl)(2-(thiophen-2-yl)-1,3-dithian-2-yl)methanol (3c). White solid (3.13 g, 85%). Mp 122-124 ºC. ^{1}H NMR (200MHz , $CDCl_3$) δ 7.31 (dd, *J* = 1.4, 5.1 Hz, 1H), 7.04 - 6.90 (m, 2H), 6.34 (t, *J* = 2.3 Hz, 1H), 6.14 (d, *J* = 2.3 Hz, 2H), 4.93 (s, 1H), 3.64 (s, 6H), 2.98 - 2.69 (m, 5H), 2.10 - 1.82 (m, 3H), ^{13}C NMR (50MHz , $CDCl_3$) δ = 159.6, 145.5, 139.4, 130.2, 127.5, 127.1, 105.8, 101.0, 81.6, 77.6, 76.4, 62.0, 55.2, 27.8, 27.5, 24.7. HRMS (ESI) m/z $[M+Na]^+$ Calcd for $C_{17}H_{20}NaO_3S_3$ 391.0472, found 391.0467,

(2-([2,2'-Bithiophen]-5-yl)-1,3-dithian-2-yl)(3,5-dimethoxyphenyl)methanol (3d). Yellow solid (3.61 g, 80%). Mp 138-140 ºC. ^{1}H NMR (200 MHz , $CDCl_3$) δ 7.21 (dd, *J* = 1.2, 5.1 Hz, 1H), 7.12 (dd, *J* = 1.1, 3.7 Hz, 1H), 7.06 - 6.96 (m, 2H), 6.89 (d, *J* = 3.8 Hz, 1 H), 6.45 - 6.31 (m, 1H), 6.24 (d, *J* = 2.3 Hz, 2H), 4.96 (d, *J* = 3.9 Hz, 1H), 3.64 (s, 6H), 3.10 - 2.77 (m, 4H), 2.14 - 1.78 (m, 2H). ^{13}C NMR (126 MHz, $CDCl_3$) δ = 159.9, 144.6, 139.5, 137.5, 131.3,

128.1, 124.8, 123.9, 123.7, 106.0, 101.4, 81.9, 77.5, 77.3, 62.3, 55.4, 29.9, 28.1, 27.8, 24.9. HRMS (ESI) m/z $[M+Na]^+$ Calcd for $C_{21}H_{22}O_3NaS_4$ 473.0349, found 473.0344.

General procedure for synthesis of acyloin acetates(4a-4d). To the solution of **3a-3d** (l0 mmol) in anhydrous THF (25 mL), 1.5 mL of acetic anhydride (2.14 g, 21.1 mmol), 1mL of NEt_3 (1.11 g, 11 mmol) and catalytic amount of DMAP (0.5 mol %) were added. The reaction mixture was stirred for 6 h at room temperature. The reaction mixture was diluted with EtOAc (200 mL) and washed with water (3 × 100 mL). The organic layer was separated, dried (anhydrous Na_2SO_4), concentrated under reduced pressure and purified by column chromatography by silica gel to yield pure product.

(3,5-Dimethoxyphenyl)(2-phenyl-1,3-dithian-2-yl)methyl acetate (4a). White solid (3.9 g, 95%). Mp 98-100 ºC. ^{1}H NMR (500 MHz, $CDCl_3$) δ 7.77 (d, *J* = 7.5 Hz, 2H), 7.38 – 7.23 (m, 3H), 6.32 (t, *J* = 2.2 Hz, 1H), 6.10 (s, 1H), 6.02 (d, *J* = 2.1 Hz, 2H), 3.59 (s, 6H), 2.75 – 2.58 (m, 4H), 2.12 (s, 3H), 1.98 – 1.84 (m, 2H). ^{13}C NMR (126 MHz, $CDCl_3$) δ 169.5, 159.6, 137.3, 137.1, 131.1, 128.1, 127.7, 106.7, 101.1, 80.4, 63.4, 55.3, 27.4, 27.3, 24.8, 21.0. HRMS (ESI) m/z $[M+Na]^+$ Calcd for $C_{21}H_{24}NaO_4S_2$ 427.1014, found 427.1009.

(3,5-Dimethoxyphenyl)(2-(furan-2-yl)-1,3-dithian-2-yl)methyl acetate (4b). Brown solid (3.68 g, 93%). Mp 95-97 ºC. ^{1}H NMR (200 MHz , $CDCl_3$) δ 7.47 (dd, *J* = 0.9, 1.8 Hz, 1H), 6.52 (dd, *J* = 0.8, 3.3 Hz, 1H), 6.43 - 6.33 (m, 2H), 6.18 (d, *J* = 2.3 Hz, 2H), 6.11 (s, 1H), 3.68 (s, 6H), 2.93 - 2.60 (m, 4H), 2.15 (s, 3H), 2.01 - 1.90 (m, 2H). ^{13}C NMR (50 MHz, $CDCl_3$) δ = 169.4, 159.8, 150.9, 142.7, 137.1, 113.2, 110.9, 105.9, 101.0, 79.3, 77.6, 76.4, 57.4, 55.2, 27.6, 24.6, 20.9. HRMS (ESI) m/z $[M+Na]^+$ Calcd for $C_{19}H_{22}O_5NaS_2$ 417.0806, found 417.0801.

(3,5-Dimethoxyphenyl)(2-(thiophen-2-yl)-1,3-dithian-2-yl)methyl acetate (4c). White solid (3.69 g, 90%). Mp 115-117 ºC. ^{1}H NMR (400 MHz ,$CDCl_3$) δ 7.34 (dd, *J* = 1.4, 5.0 Hz, 1 H), 7.03 (dd, *J* = 1.4, 3.7 Hz, 1H), 6.95 (dd, *J* = 3.7, 5.0 Hz, 1H), 6.35 (t, *J* = 2.3 Hz, 1H), 6.15 (d, *J* = 2.3 Hz, 2H), 6.08 (s, 1 H), 3.64 (s, 6H), 2.97 - 2.68 (m, 4H), 2.15 (s, 3H), 2.02 - 1.81 (m, 2H). ^{13}C NMR (101 MHz , $CDCl_3$) δ = 159.6, 144.3, 139.3, 139.2, 137.2, 131.0, 127.8, 124.5, 123.6, 123.4, 105.7, 101.1, 81.6, 77.3, 77.0, 76.7, 62.0, 55.2, 27.8, 27.5, 24.6. HRMS (ESI) m/z $[M+Na]^+$ Calcd for $C_{19}H_{22}O_4NaS_3$ 433.0578, found 433.0572.

(2-([2,2'-Bithiophen]-5-yl)-1,3-dithian-2-yl)(3,5-dimethoxyphenyl)methyl acetate (4d). Yellow solid (4.18 g, 85%). Mp 120-122 ºC. ^{1}H NMR (200 MHz, $CDCl_3$) δ 7.22 (dd, *J* = 5.1, 1.2 Hz, 1H), 7.15 (dd, *J* = 3.6, 1.2 Hz, 1H), 7.02 (dd, *J* = 5.0, 3.7 Hz, 2H), 6.92 (d, *J* = 3.8 Hz, 1H), 6.37 (t, *J* = 2.3 Hz, 1H), 6.25 (d, *J* = 2.2 Hz, 2H), 6.10 (s, 1H), 3.65 (s, 6H), 3.04 – 2.69 (m, 4H), 2.17 (s, 3H), 2.08 – 1.85 (m, 2H). ^{13}C NMR (101 MHz, $CDCl_3$) δ = 159.6, 144.3, 139.3, 139.2, 137.2, 131.0, 127.8, 124.5, 123.6, 123.4, 105.7, 101.1, 81.6, 77.3, 77.0, 76.7, 62.0, 55.2, 27.8, 27.5, 24.6. HRMS (ESI) m/z $[M+Na]^+$ Calcd for $C_{23}H_{24}O_4NaS_4$ 515.0455, found 515.0452.

Synthesis of extended molecules:

(3,5-Dimethoxyphenyl)(2-(5-(4-methoxyphenyl)thiophen-2-yl)-1,3-dithian-2-yl)methyl acetate (4e). In an oven dried schlenk tube, purged with nitrogen , 4-iodoanisole (0.5 mmol) was added to it followed by compound **4c** (1 mmol) , anhydrous K_2CO_3 (2.5 eq.), $Pd(OAc)_2$(10 mol%), PCy_3 (10 mol%),, PivOH(30 mol %) . DMAc was added to the above mixtutre and stirred at 120ºC for 12 h. The mixture was poured in 200 mL of brine to remove DMAc and extracted by ethyl acetate (30 mL × 5) followed by final wash by brine solution. The combined organic layer was dried over anhydrous sodium sulphate and solvent was removed under reduced pressure. The mixture was purified by column chromatography by silica gel to give pure compound **4e** as white solid (0.130 g, 50%). Mp 78-80 ºC. ^{1}H NMR (200 MHz, $CDCl_3$) δ 7.50 (d, *J* = 8.8 Hz, 2H), 7.05 (d, *J* = 3.8 Hz, 1H), 6.98 – 6.86 (m, 3H), 6.37 (t, *J* = 2.3 Hz, 1H), 6.25 (d, *J* = 2.3 Hz, 2H), 6.11 (s, 1H), 3.84 (s, 3H), 3.63 (s, 6H), 3.04 – 2.68 (m, 4H), 2.17 (s, 3H), 2.05 – 1.78 (m, 2H). ^{13}C NMR (50 MHz, $CDCl_3$) δ 169.6, 159.8, 159.5, 146.4, 142.9, 137.0, 131.7, 127.4, 127.0, 121.7, 114.5, 106.5, 101.4, 80.7, 59.6, 55.5, 55.3, 27.9, 24.7, 21.1. HRMS (ESI) m/z [M+H]+ Calcd for $C_{26}H_{29}O_5S_3$ 517.1177, found 517.1172.

(3,5-Dimethoxyphenyl)(2-(5'-phenyl-[2,2'-bithiophen]-5-yl)-1,3-dithian-2-yl)methyl acetate (4f). Follwing the same procedure as above, from **4d** (1mmol) and bromobenzene (0.5 mmol) compound **4f** was obtained as yellow solid (0.170 g, 60%). Mp 140-142 ºC. ^{1}H NMR (200 MHz, $CDCl_3$) δ 7.60 (d, *J* = 7.0 Hz, 2H), 7.46 – 7.27 (m, 3H), 7.23 (d, *J* = 3.8 Hz, 1H), 7.13 (t, *J* = 4.3 Hz, 1H), 7.04 (t, *J* = 4.3 Hz, 1H), 6.93 (d, *J* = 3.7 Hz, 1H), 6.38 (t, *J* = 2.0 Hz, 1H), 6.26 (d, *J* = 1.9 Hz, 2H), 6.11 (s, 1H), 3.66 (s, 6H), 3.13 – 2.61 (m, 4H), 2.18 (s, 3H), 2.08 – 1.84 (m, 2H). ^{13}C NMR (50 MHz, $CDCl_3$) δ 159.9, 143.9, 143.5, 139.7, 136.8,

134.1, 131.6, 129.1, 127.8, 125.8, 124.6, 124.0, 123.3, 106.6, 101.5, 80.7, 61.9, 59.4, 55.4, 27.9, 24.6, 21.1. HRMS (ESI) m/z $[M-H]^+$ Calcd for $C_{29}H_{27}O_4S_4$ 567.0792, found 567.0776.

General procedure for deprotection of dithianyl acetates (5a-5f).

To the solution of (**4a-4f**) (2 mmol) in 20 mL acetonitrile:water (9:1), mercury(II) perchlorate hydrate (2.2 mmol) was added. The solution was stirred for 15 min at room temperature and then filtered through filter paper. The filtrate was further treated with 50 mL of saturated sodium bicarbonate and extracted by 100 mL of DCM. The organic layer was dried over sodium sulphate and concentrated under vacuum. The crude product was purified by column chromatography to yield corresponding deprotected acetates (**5a-5f**)

1-(3,5-Dimethoxyphenyl)-2-oxo-2-phenylethyl acetate (5a). White solid (0.540 g , 85%). mp 105-107 ºC. ^{1}H NMR (200 MHz, $CDCl_3$) δ 7.94 (d, *J* = 7.0 Hz, 2H), 7.59 – 7.32 (m, 3H), 6.76 (s, 1H), 6.60 (d, *J* = 2.2 Hz, 2H), 6.42 (t, *J* = 2.2 Hz, 1H), 3.75 (s, 6H), 2.21 (s, 3H). ^{13}C NMR (50 MHz, $CDCl_3$) δ 193.7, 170.5, 161.3, 135.7, 134.7, 133.6, 128.9, 128.7, 106.8, 101.3, 77.8, 55.5, 20.9. HRMS (ESI) m/z $[M+Na]^+$ Calcd for $C_{18}H_{18}O_5Na$ 337.1052, found 337.1039.

1-(3,5-Dimethoxyphenyl)-2-(furan-2-yl)-2-oxoethyl acetate (5b). Yellow solid (0.396 g, 65%). Mp 100-102 ºC. ^{1}H NMR (400MHz , $CDCl_3$) δ = 7.57 (d, *J* = 1.4 Hz, 1 H), 7.27 - 7.22 (m, 1 H), 6.70 (s, 1 H), 6.64 (d, *J* = 2.3 Hz, 2 H), 6.56 (s, 1 H), 6.50 (dd, *J* = 1.8, 3.7 Hz, 1 H), 6.42 (t, *J* = 2.3 Hz, 1 H), 3.77 (s, 6 H), 2.20 (s, 3 H). ^{13}C NMR (50 MHz, $CDCl_3$) δ 182.4, 170.4, 161.2, 150.6, 147.1, 135.4, 119.2, 112.6, 106.6, 101.4, 77.4, 77.2, 55.6, 20.9. HRMS (ESI) m/z $[M+Na]^+$ Calcd for $C_{16}H_{16}O_6Na$ 327.0845, found 327.0838.

1-(3,5-Dimethoxyphenyl)-2-oxo-2-(thiophen-2-yl)ethyl acetate (5c). Light yellow solid (0.448 g, 70%). Mp 88-90 ºC. ^{1}H NMR (200 MHz, $CDCl_3$) δ 7.77 (dd, *J* = 3.9, 1.1 Hz, 1H), 7.63 (dd, *J* = 4.9, 1.1 Hz, 1H), 7.08 (dd, *J* = 4.9, 3.9 Hz, 1H), 6.65 (d, *J* = 2.2 Hz, 2H), 6.56 (s, 1H), 6.44 (t, *J* = 2.3 Hz, 1H), 3.77 (s, 6H), 2.22 (s, 3H). ^{13}C NMR (50 MHz, $CDCl_3$) δ 186.4, 170.3, 161.3, 140.6, 135.9, 134.5, 133.3, 128.3, 106.6, 101.4, 78.3, 55.5, 20.9. HRMS (ESI) m/z $[M+Na]^+$ Calcd for $C_{16}H_{16}O_5NaS$ 343.0616, found 343.0604.

2-([2,2'-Bithiophen]-5-yl)-1-(3,5-dimethoxyphenyl)-2-oxoethyl acetate (5d). Yellow solid (0.579 g, 72%). Mp 110-112 ºC. **1**H NMR (200MHz , $CDCl_3$) δ = 7.65 (d, *J* = 4.2 Hz, 1 H),

7.31 - 7.21 (m, 2 H), 7.07 (d, *J* = 4.0 Hz, 1 H), 6.99 (dd, *J* = 3.7, 5.1 Hz, 1 H), 6.65 (d, *J* = 2.3 Hz, 2 H), 6.54 (s, 1 H), 6.42 (t, *J* = 2.2 Hz, 1 H), 3.76 (s, 6 H), 2.21 (s, 3 H). ^{13}C NMR (50MHz , $CDCl_3$) δ = 198.1, 194.0, 185.8, 179.0, 170.1, 161.1, 146.4, 143.7, 138.2, 135.8, 134.1, 128.1, 126.7, 125.8, 124.2, 109.6, 106.4, 101.1, 98.3, 82.3, 77.8, 72.9, 70.2, 68.2, 55.3, 48.3, 34.4, 32.1, 29.0, 22.5, 20.6, 3.9. HRMS (ESI) m/z $[M+Na]^+$ Calcd for $C_{20}H_{18}O_5NaS_2$ 425.0493, found 425.0475.

1-(3,5-Dimethoxyphenyl)-2-(5-(4-methoxyphenyl)thiophen-2-yl)-2-oxoethyl acetate (5e). Following the general procedure of dithiane deprotection shown above, from **4e** (0.5 mmol), the compound 5e was obtained as yellow sticky gum (0.170 g, 80%). ^{1}H NMR (200 MHz, $CDCl_3$) δ 7.72 (d, *J* = 4.1 Hz, 1H), 7.54 (d, *J* = 8.9 Hz, 2H), 7.15 (d, *J* = 4.1 Hz, 1H), 6.91 (d, *J* = 8.9 Hz, 2H), 6.67 (d, *J* = 2.2 Hz, 2H), 6.57 (s, 1H), 6.44 (t, *J* = 2.2 Hz, 1H), 3.83 (s, 3H), 3.78 (s, 6H), 2.22 (s, 3H). ^{13}C NMR (50 MHz, $CDCl_3$) δ 186.1, 170.4, 161.3, 160.7, 154.0, 138.3, 136.2, 134.6, 127.9, 125.9, 123.2, 114.6, 106.6, 101.3, 78.0, 55.6, 55.5, 21.0. HRMS (ESI) m/z $[M+Na]^+$ Calcd for $C_{23}H_{22}O_6NaS$ 449.1035, found 449.1019.

1-(3,5-Dimethoxyphenyl)-2-oxo-2-(5'-phenyl-[2,2'-bithiophen]-5-yl)ethyl acetate (5f). Following the general procedure of dithiane deprotection shown above, from **4f** (0.5 mmol), the compound **5f** was obtained as yellow sticky gum (0.168 g, 70%) ^{1}H NMR (200 MHz, $CDCl_3$) δ 7.68 (d, *J* = 4.0 Hz, 1H), 7.59 (d, *J* = 6.8 Hz, 2H), 7.46 – 7.21 (m, 5H), 7.13 (d, *J* = 3.9 Hz, 1H), 6.66 (d, *J* = 2.1 Hz, 2H), 6.55 (s, 1H), 6.45 (t, *J* = 2.0 Hz, 1H), 3.79 (s, 6H), 2.23 (s, 3H). ^{13}C NMR (50 MHz, $CDCl_3$) δ 186.0, 170.4, 161.4, 146.7, 146.0, 138.4, 136.1, 135.2, 134.4, 133.7, 129.2, 128.3, 127.0, 125.9, 124.3, 106.6, 101.4, 78.1, 55.6, 21.0. HRMS (ESI) m/z $[M+Na]^+$ Calcd for $C_{26}H_{22}O_5NaS_2$ 501.0806, found 501.0801.

General procedure of photochemical irradiation of photo-triggers

(Method A): 0.5 mM solution of (**1d-4d**) (0.1 mmol) in HPLC grade acetonitrile was purged by nitrogen for 20 min and irradiated by UV light by mercury lamp fitted with Pyrex filter jacket. The reaction was monitored by TLC. After completion of reaction the solution was concentrated under reduced pressure and purified by column chromatography to give corresponding products.

5,7-Dimethoxy-2-phenylbenzofuran (6a). White solid (0.025 g, 100%). Mp 88-90 ºC. ^{1}H NMR (200 MHz, $CDCl_3$) δ 7.85 (dd, *J* = 8.2, 1.3 Hz, 2H), 7.50 – 7.26 (m, 3H), 6.93 (s, 1H),

6.61 (d, *J* = 2.2 Hz, 1H), 6.44 (d, *J* = 2.2 Hz, 1H), 4.00 (s, 3H), 3.83 (s, 3H). ^{13}C NMR (50 MHz, $CDCl_3$) δ 157.0, 156.6, 145.6, 139.6, 130.7, 130.5, 128.8, 128.6, 125.1, 102.0, 97.4, 94.6, 56.3, 56.0. HRMS (ESI) m/z $[M]^+$ Calcd for $C_{16}H_{14}O_3$ 254.0943 found 254.0935.

2-(Furan-2-yl)-5,7-dimethoxybenzofuran(6b). White solid (0.020 g, 80%). Mp 85-88 ºC. ^{1}H NMR (200 MHz, $CDCl_3$) δ 7.52 – 7.45 (m, 1H), 6.84 (s, 1H), 6.82 (s, 1H), 6.61 (d, *J* = 2.2 Hz, 1H), 6.51 (dd, *J* = 3.4, 1.8 Hz, 1H), 6.45 (d, *J* = 2.2 Hz, 1H), 3.99 (s, 3H), 3.84 (s, 3H). ^{13}C NMR (126 MHz, $CDCl_3$) δ 157.2, 148.9, 146.2, 145.5, 143.0, 139.1, 130.2, 111.8, 107.7, 101.8, 97.4, 94.6, 56.2, 56.0. HRMS (ESI) m/z $[M]^+$ Calcd for $C_{14}H_{12}O_4$ 244.0736 found 244.0725.

5,7-Dimethoxy-2-(thiophen-2-yl)benzofuran(6c). Light yellow solid (0.023 g, 90%). Mp 62-64 ºC. ^{1}H NMR (200 MHz, $CDCl_3$) δ 7.49 (dd, *J* = 3.6, 1.0 Hz, 1H), 7.32 (dd, *J* = 5.0, 0.9 Hz, 1H), 7.08 (dd, *J* = 5.0, 3.7 Hz, 1H), 6.79 (s, 1H), 6.58 (d, *J* = 2.2 Hz, 1H), 6.44 (d, *J* = 2.2 Hz, 1H), 4.00 (s, 3H), 3.84 (s, 3H). ^{13}C NMR (50 MHz, $CDCl_3$) δ 159.6, 157.2, 152.1, 145.5, 133.3, 130.6, 127.9, 125.8, 124.8, 101.9, 97.5, 94.5, 56.3, 56.0. HRMS (ESI) m/z $[M]^+$ Calcd for $C_{14}H_{12}O_3S$ 260.0507 found 260.0497.

2-([2,2'-Bithiophen]-5-yl)-5,7-dimethoxybenzofuran(6d). Light yellow solid (0.027 g, 80%). mp 126-128 ºC. ^{1}H NMR (200MHz , $CDCl_3$) δ = 7.39 (d, *J* = 3.9 Hz, 1 H), 7.28 - 7.18 (m, 2 H), 7.14 (d, *J* = 3.8 Hz, 1 H), 7.03 (dd, *J* = 3.8, 5.1 Hz, 1 H), 6.78 (s, 1 H), 6.58 (d, *J* = 2.3 Hz, 1 H), 6.44 (d, *J* = 2.1 Hz, 1 H), 4.00 (s, 3 H), 3.84 (s, 3 H). ^{13}C NMR (50MHz, $CDCl_3$) δ = 157.0, 151.4, 145.3, 137.6, 136.9, 131.6, 130.4, 127.9, 125.2, 124.8, 124.3, 124.0, 101.9, 97.4, 94.3, 56.1, 55.8. HRMS (ESI) m/z $[M]^+$ Calcd for $C_{18}H_{14}O_3S_2$ 342.0384 found 342.0371.

(Method B): To 0.5 mM solution of trigger (0.1 mmol) in HPLC grade acetonitrile was added 1 eq of TEA. The mixture was purged by nitrogen for 20 min and irradiated by UV light by mercury lamp fitted with Pyrex filter jacket. The reaction was monitored by TLC. After completion of reaction the solution was concentrated under reduced pressure and purified by column chromatography.

Following method B trigger **5e** was irradiate give two compounds **6e** and **7e**.

5,7-Dimethoxy-2-(5-(4-methoxyphenyl)thiophen-2-yl)benzofuran (6e). White solid (0.022 g, 60%). Mp 160-162 ºC. ^{1}H NMR (200 MHz, $CDCl_3$) δ 7.55 (d, *J* = 8.8 Hz, 2H), 7.43 (d, *J* = 3.8 Hz, 1H), 7.17 (d, *J* = 3.8 Hz, 1H), 6.93 (d, *J* = 8.8 Hz, 2H), 6.77 (s, 1H), 6.58 (d, *J* = 2.1 Hz, 1H), 6.44 (d, *J* = 2.1 Hz, 1H), 4.00 (s, 3H), 3.84 (s, 6H). ^{13}C NMR (50 MHz, $CDCl_3$) δ 159.7, 157.2, 152.0, 145.5, 144.8, 131.4, 130.7, 127.2, 126.9, 125.7, 122.9, 114.6, 101.6, 97.4, 94.5, 56.3, 56.0, 55.5. HRMS (ESI) m/z $[M]^+$ Calcd for $C_{21}H_{18}O_4S$ 366.0926 found 366.0912.

2-(3,5-Dimethoxyphenyl)-1-(5-(4-methoxyphenyl)thiophen-2-yl)ethan-1-one (7e). White solid (0.010 g, 25%). Mp 138-140 ºC. ^{1}H NMR (200 MHz, $CDCl_3$) δ 7.70 (d, *J* = 4.0 Hz, 1H), 7.58 (d, *J* = 8.9 Hz, 2H), 7.20 (d, *J* = 4.0 Hz, 1H), 6.93 (d, *J* = 8.9 Hz, 2H), 6.48 (d, *J* = 2.2 Hz, 2H), 6.36 (t, *J* = 2.2 Hz, 1H), 4.10 (s, 2H), 3.84 (s, 3H), 3.77 (s, 6H). ^{13}C NMR (101 MHz, $CDCl_3$) δ 190.1, 161.1, 160.6, 153.5, 141.5, 136.9, 134.1, 127.8, 126.2, 123.1, 114.7, 107.6, 99.2, 55.6, 55.5, 46.4. HRMS (ESI) m/z $[M+H]^+$ Calcd for $C_{21}H_{21}O_4S$ 369.1161 found 369.1156.

Following method B trigger **5f** was irradiated to give two compounds **6f** and **7f**.

5,7-Dimethoxy-2-(5'-phenyl-[2,2'-bithiophen]-5-yl)benzofuran (6f). Yellow solid (0.027 g, 65%). Mp 179-181 ºC. ^{1}H NMR (400 MHz, $CDCl_3$) δ 7.61 (d, *J* = 7.5 Hz, 2H), 7.39 (t, *J* = 6.4 Hz, 3H), 7.31 (d, *J* = 7.3 Hz, 1H), 7.25 (d, *J* = 3.9 Hz, 1H), 7.18 (dd, *J* = 6.3, 3.9 Hz, 2H), 6.79 (s, 1H), 6.59 (d, *J* = 1.8 Hz, 1H), 6.45 (d, *J* = 1.9 Hz, 1H), 4.01 (s, 3H), 3.85 (s, 3H). ^{13}C NMR (101 MHz, $CDCl_3$)) δ 157.2, 145.5, 139.3, 137.8, 134.1, 131.8, 129.1, 127.9, 125.8, 125.5, 125.03, 124.4, 124.1, 102.1, 97.6, 94.5, 56.3, 56.0. HRMS (ESI) m/z $[M]^+$ Calcd for $C_{24}H_{18}O_3S_2$ 418.0697 found 418.0690.

2-(3,5-Dimethoxyphenyl)-1-(5'-phenyl-[2,2'-bithiophen]-5-yl)ethan-1-one (7f). Yellow solid (0.009, 20%). Mp 136-138 ºC. ^{1}H NMR (500 MHz, $CDCl_3$) δ 7.66 (d, *J* = 4.0 Hz, 1H), 7.60 (d, *J* = 7.6 Hz, 2H), 7.40 (t, *J* = 7.6 Hz, 2H), 7.32 (d, *J* = 7.3 Hz, 1H), 7.29 (d, *J* = 3.8 Hz, 1H), 7.26 (d, *J* = 4.5 Hz, 1H), 7.17 (d, *J* = 3.9 Hz, 1H), 6.48 (d, *J* = 1.7 Hz, 2H), 6.36 (t, *J* = 1.7 Hz, 1H), 4.09 (s, 2H), 3.78 (s, 6H). ^{13}C NMR (126 MHz, $CDCl_3$) δ 190.0, 161.1, 146.2, 145.8, 141.6, 136.7, 135.5, 133.9, 133.7, 129.2, 128.3, 126.8, 125.9, 124.3, 124.2, 107.6, 99.2, 55.5, 46.5. HRMS (ESI) m/z $[M+H]^+$ Calcd for $C_{24}H_{21}O_3S_2$ 421.0932 found 421.0921.

5.5. NMR Spectra of Selected Compounds

^{1}H and ^{13}C NMR spectra of 5a

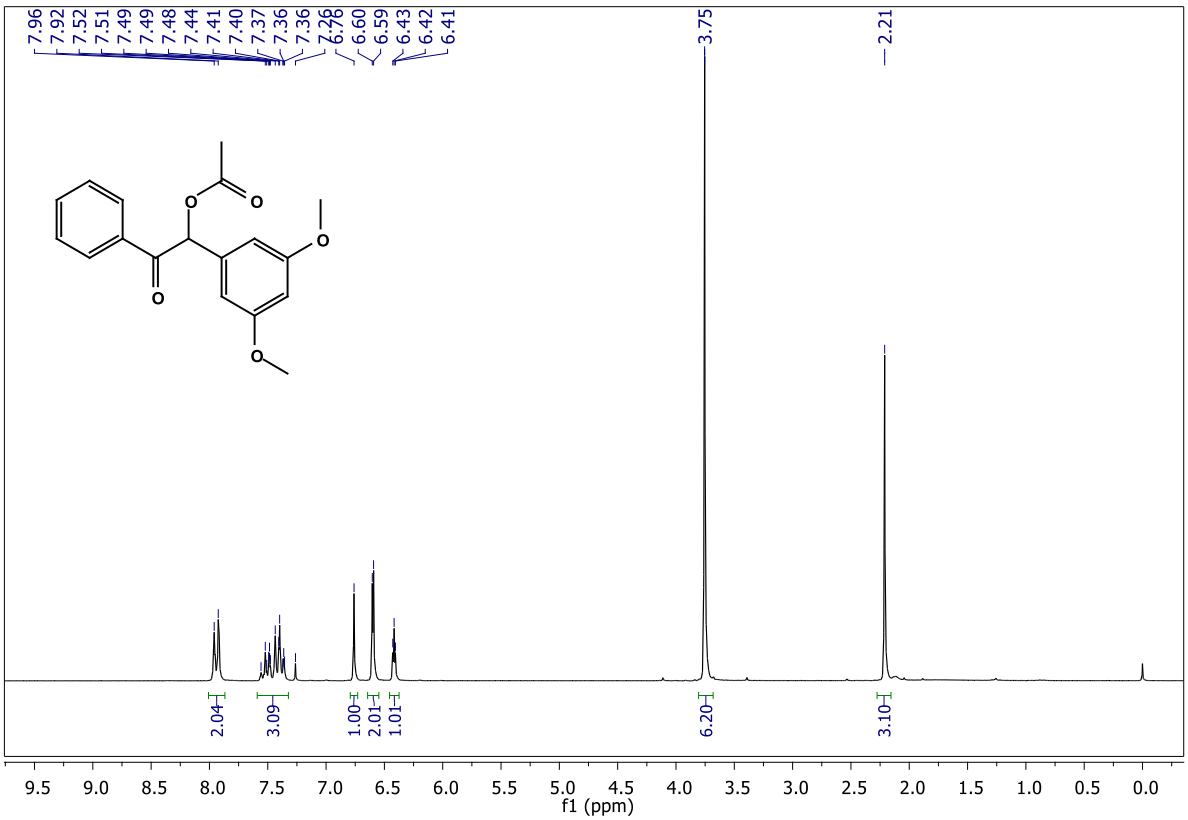

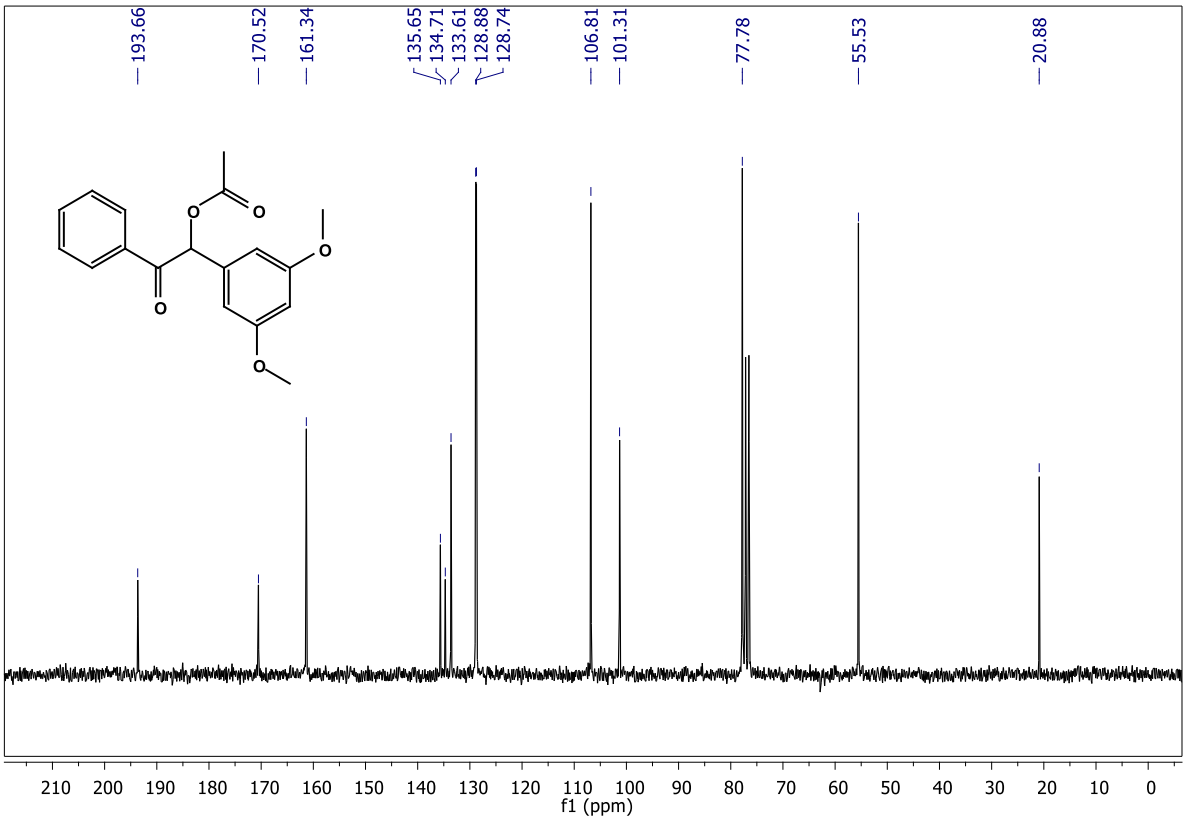

^{1}H and ^{13}C NMR spectra of 5b

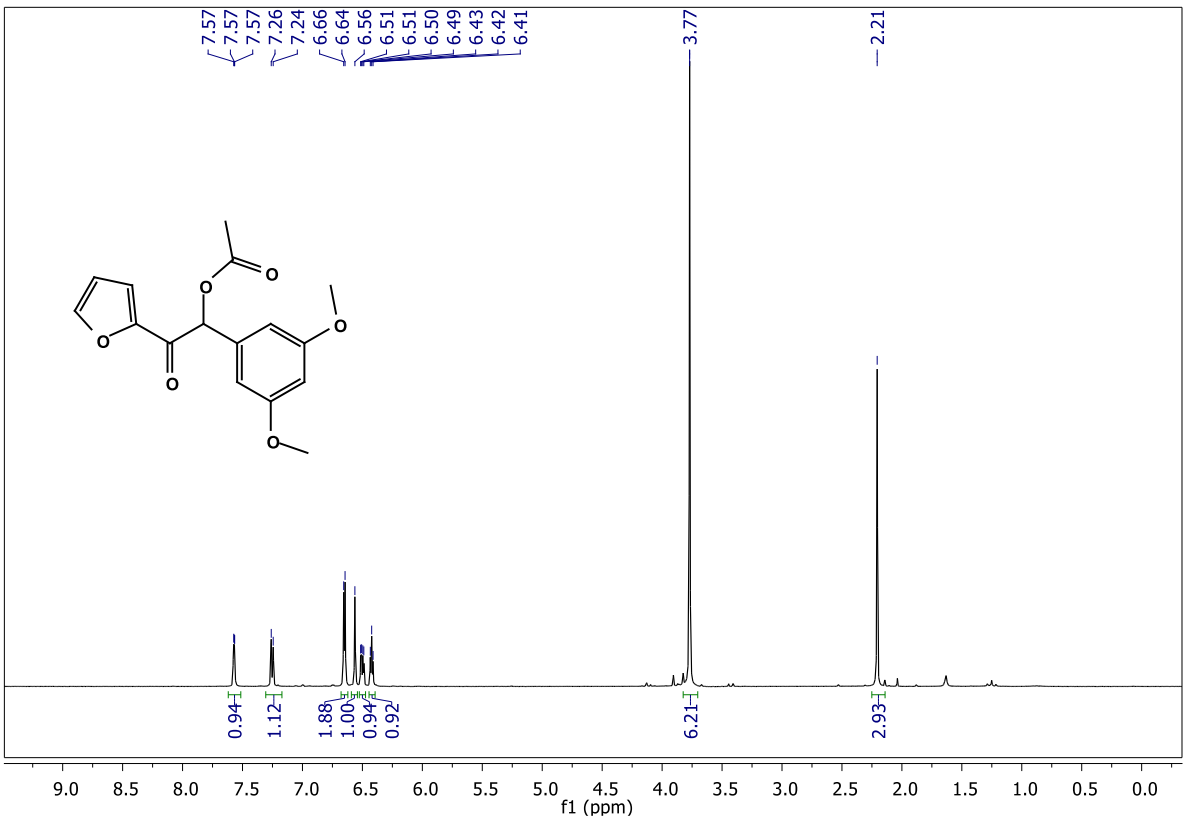

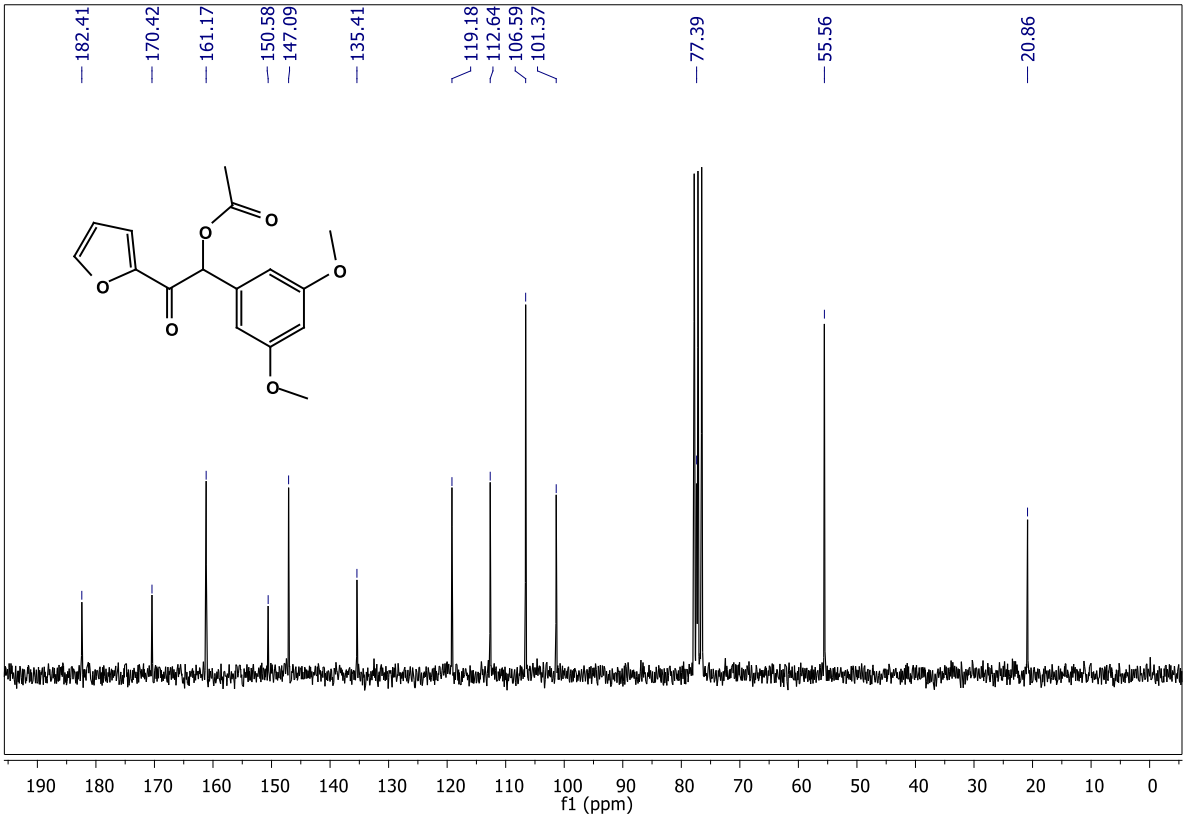

^{1}H and ^{13}C NMR spectra of 5c

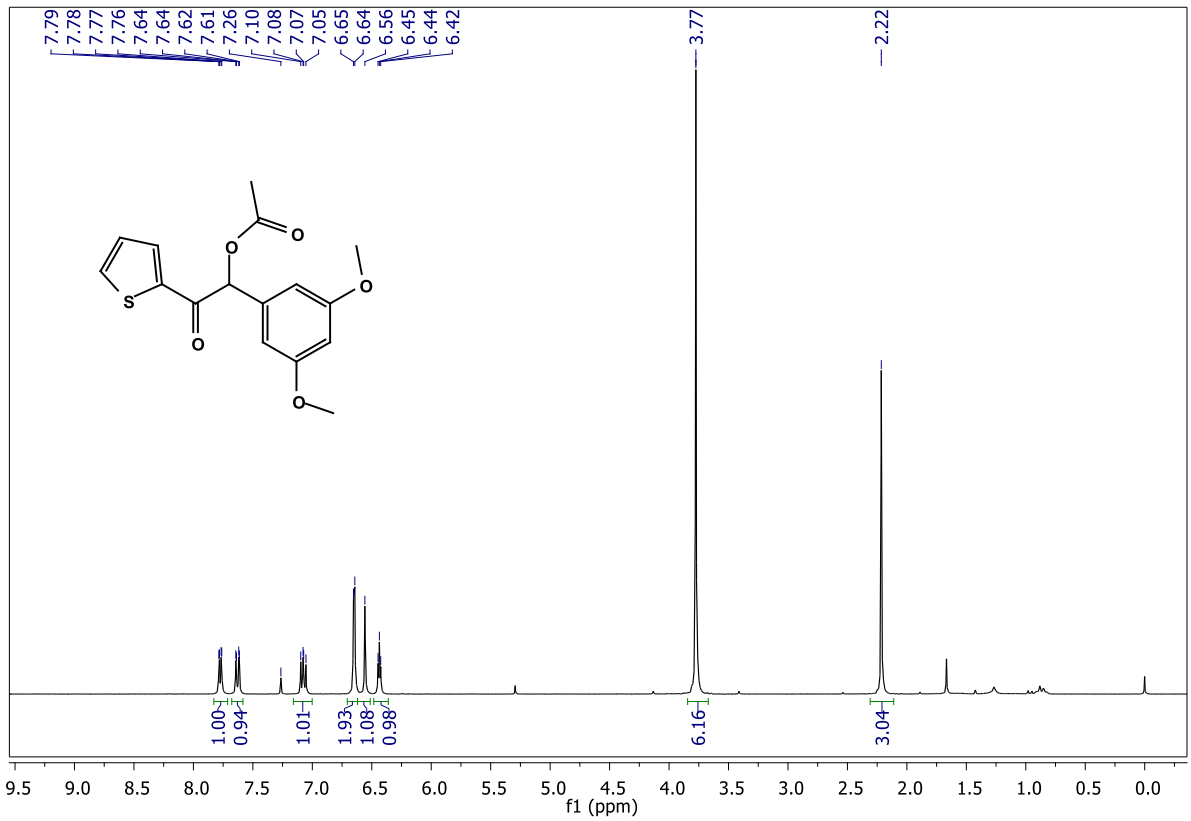

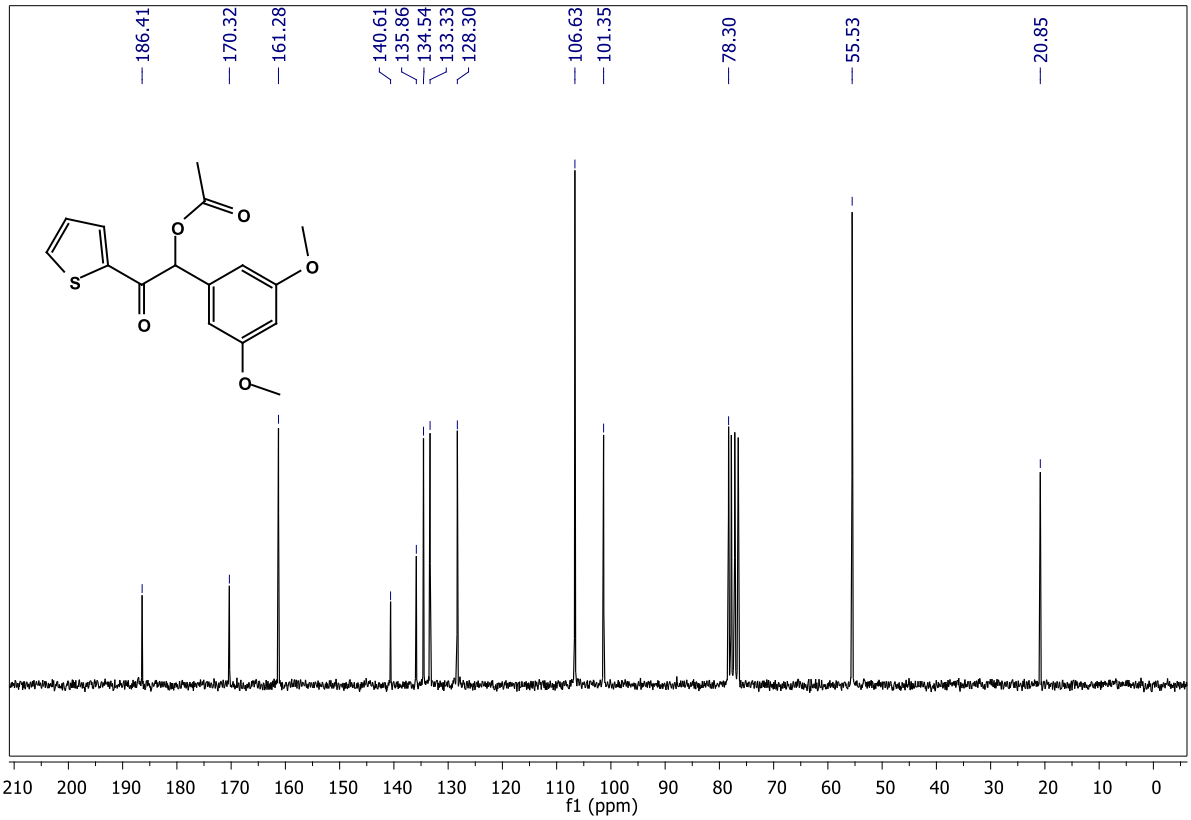

^{1}H and ^{13}C NMR spectra of 5d

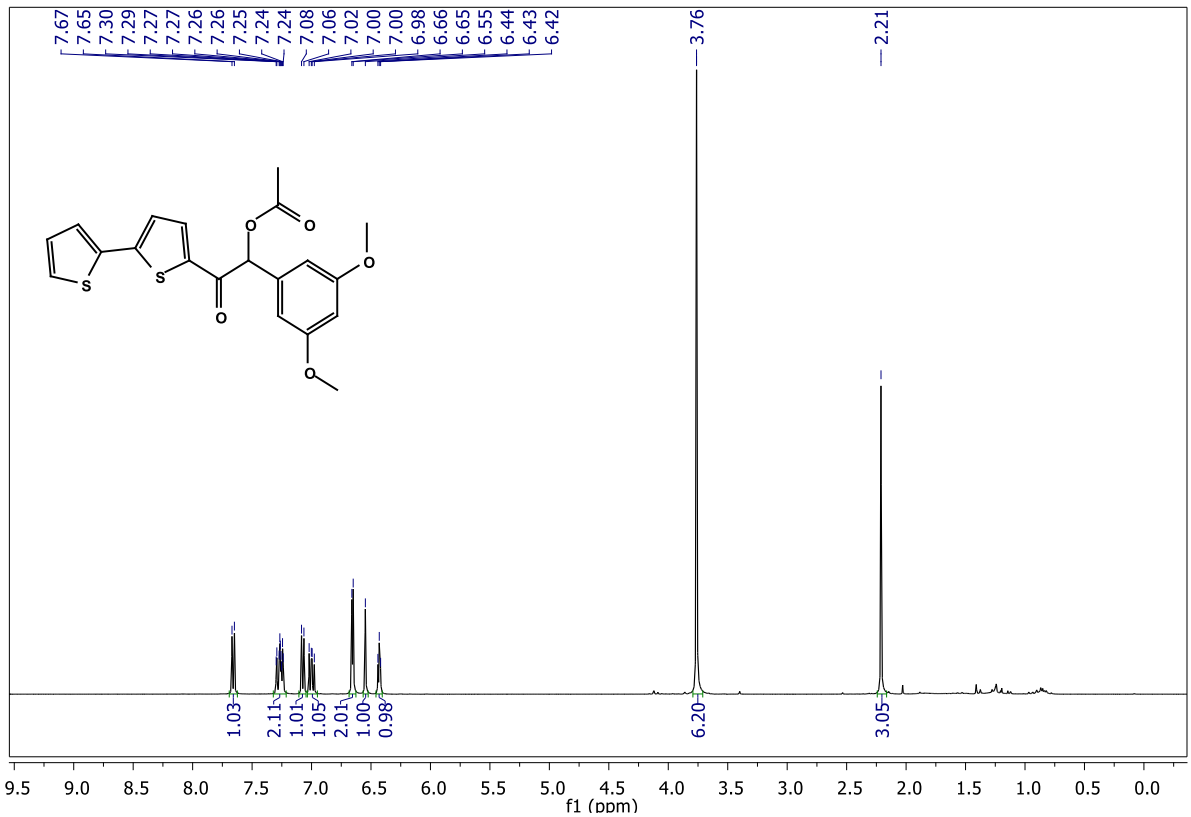

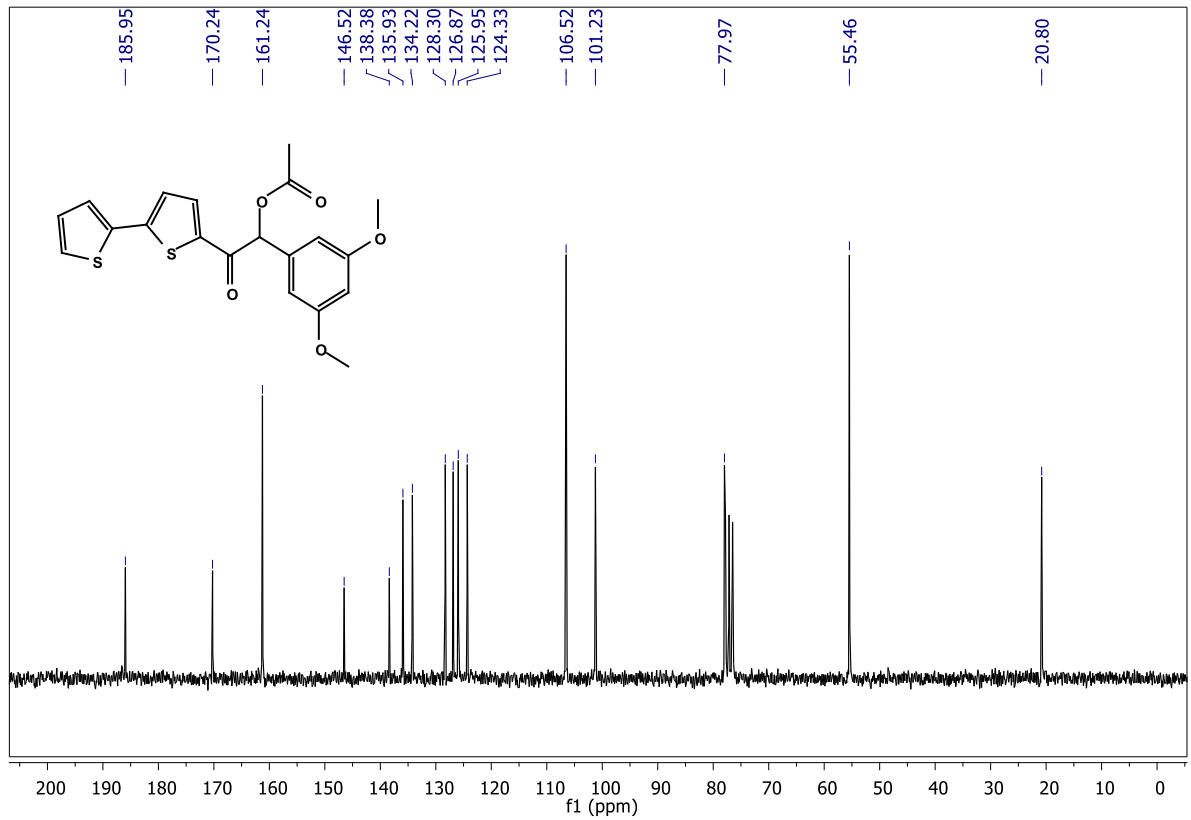

^{1}H and ^{13}C NMR spectra of 5e

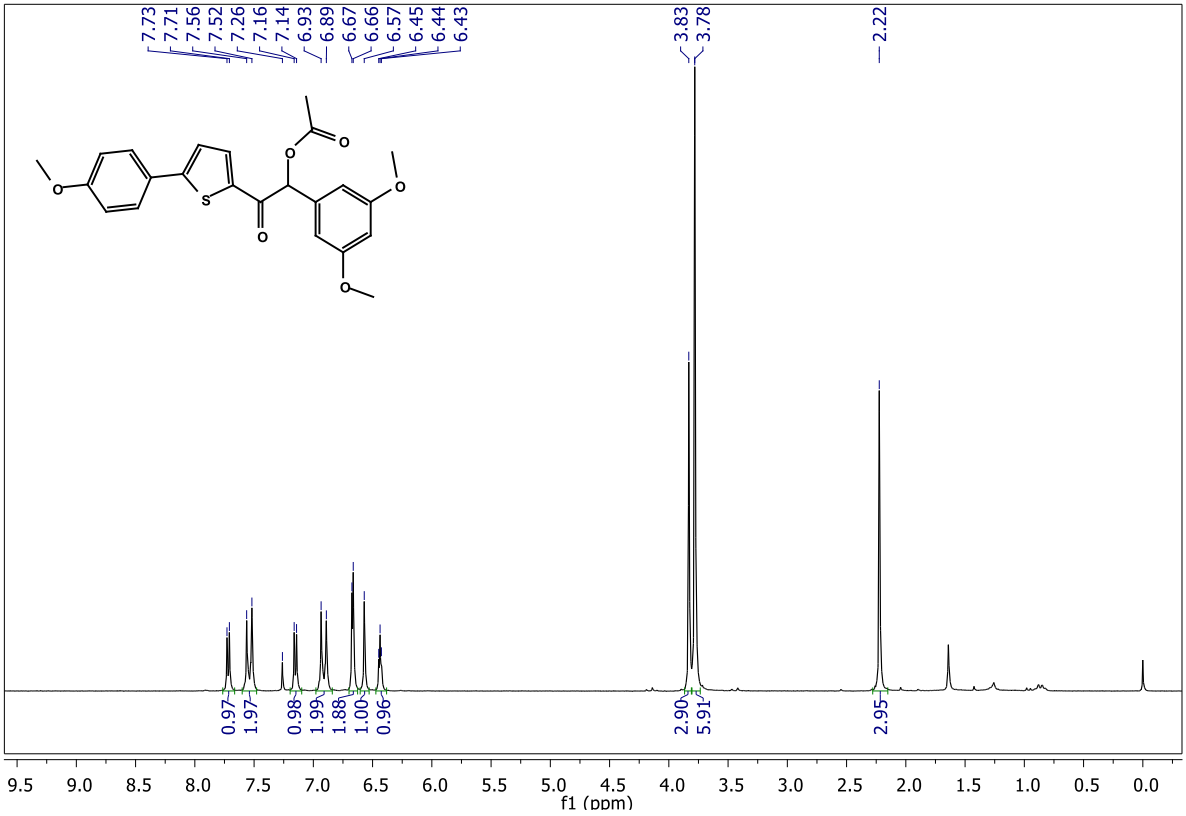

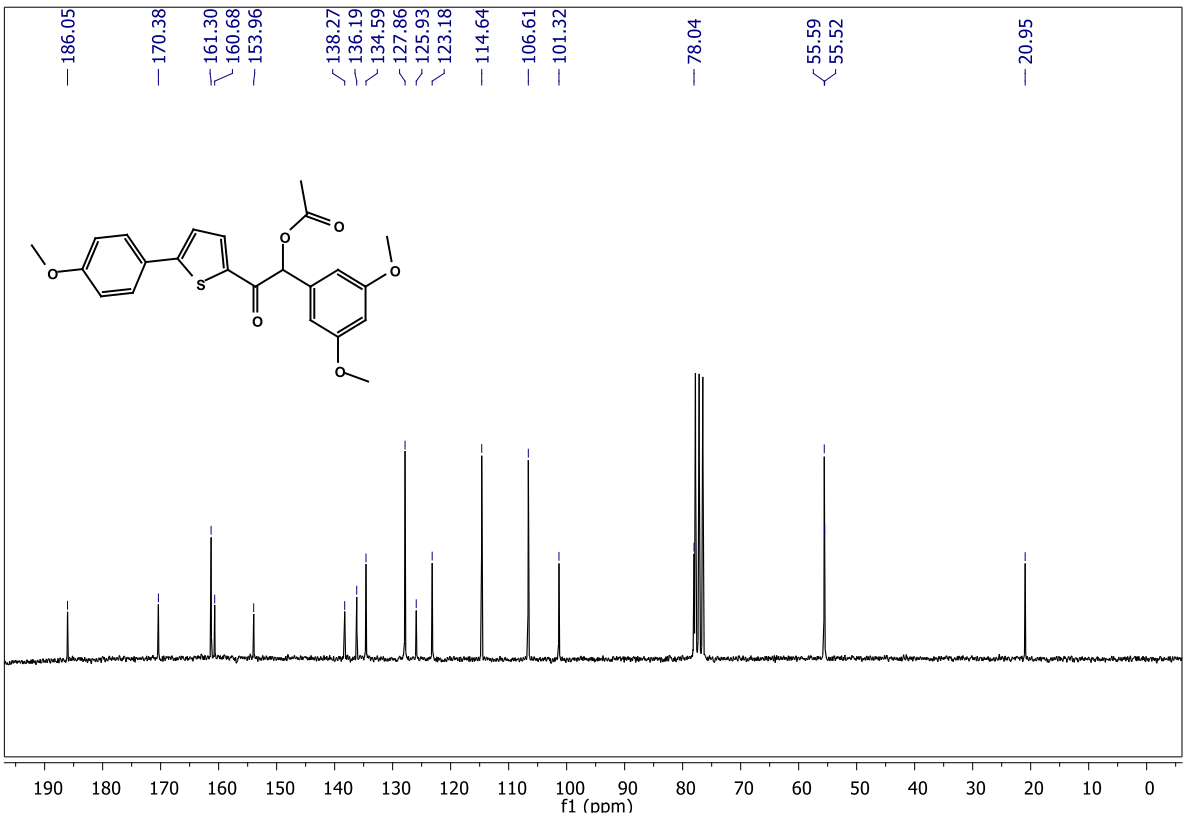

^{1}H and ^{13}C NMR spectra 5f

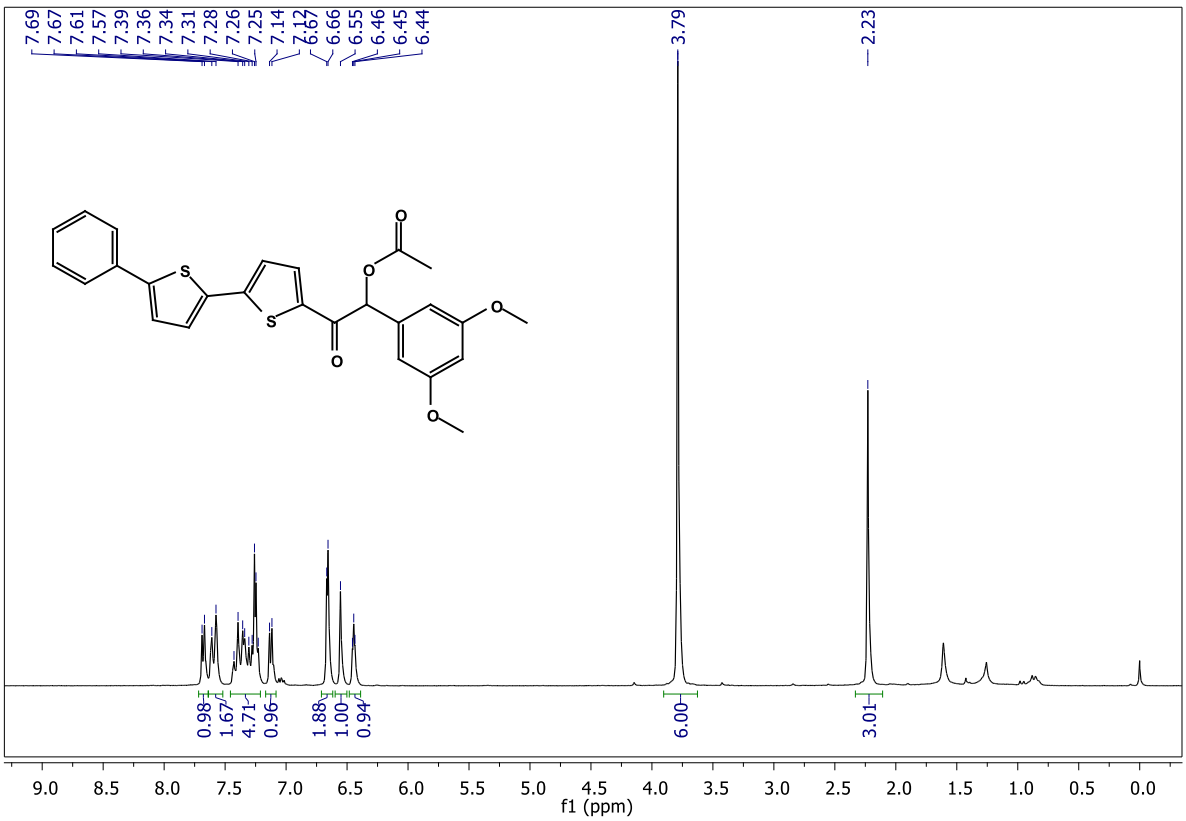

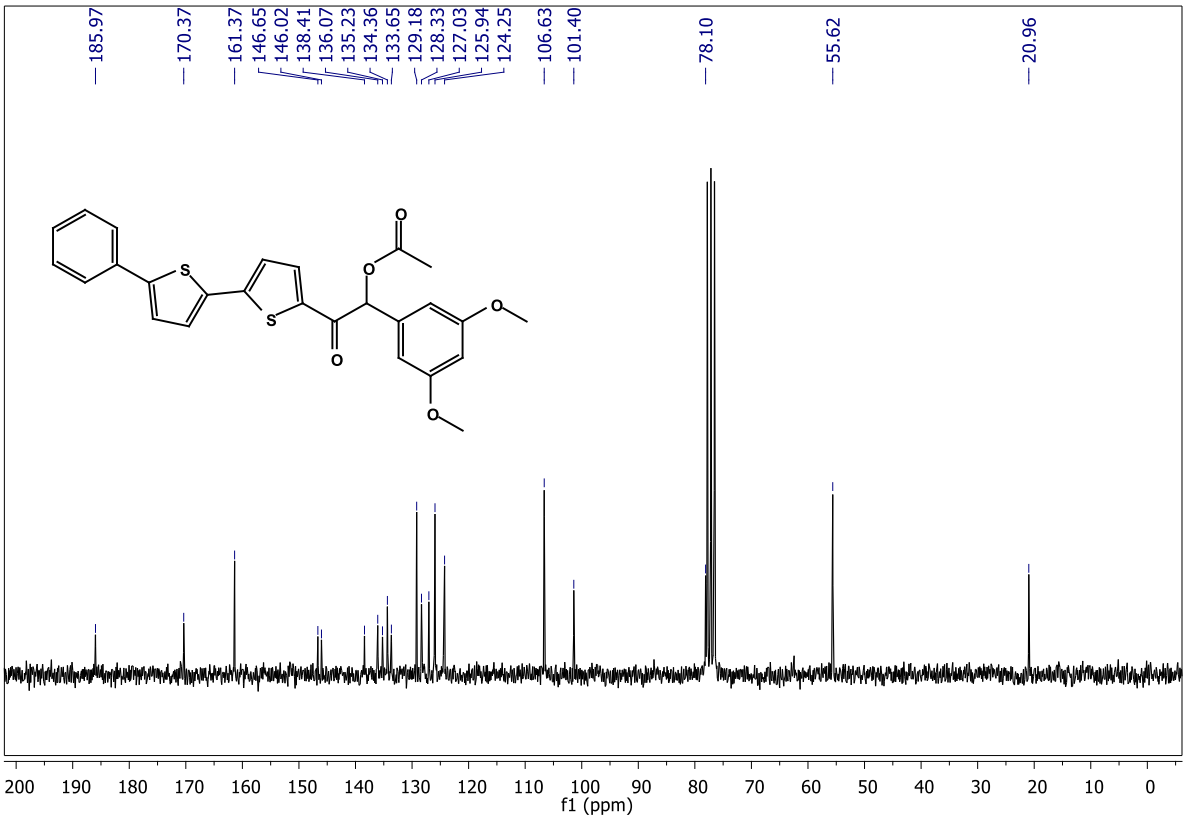

^{1}H and ^{13}C NMR spectra of 6a

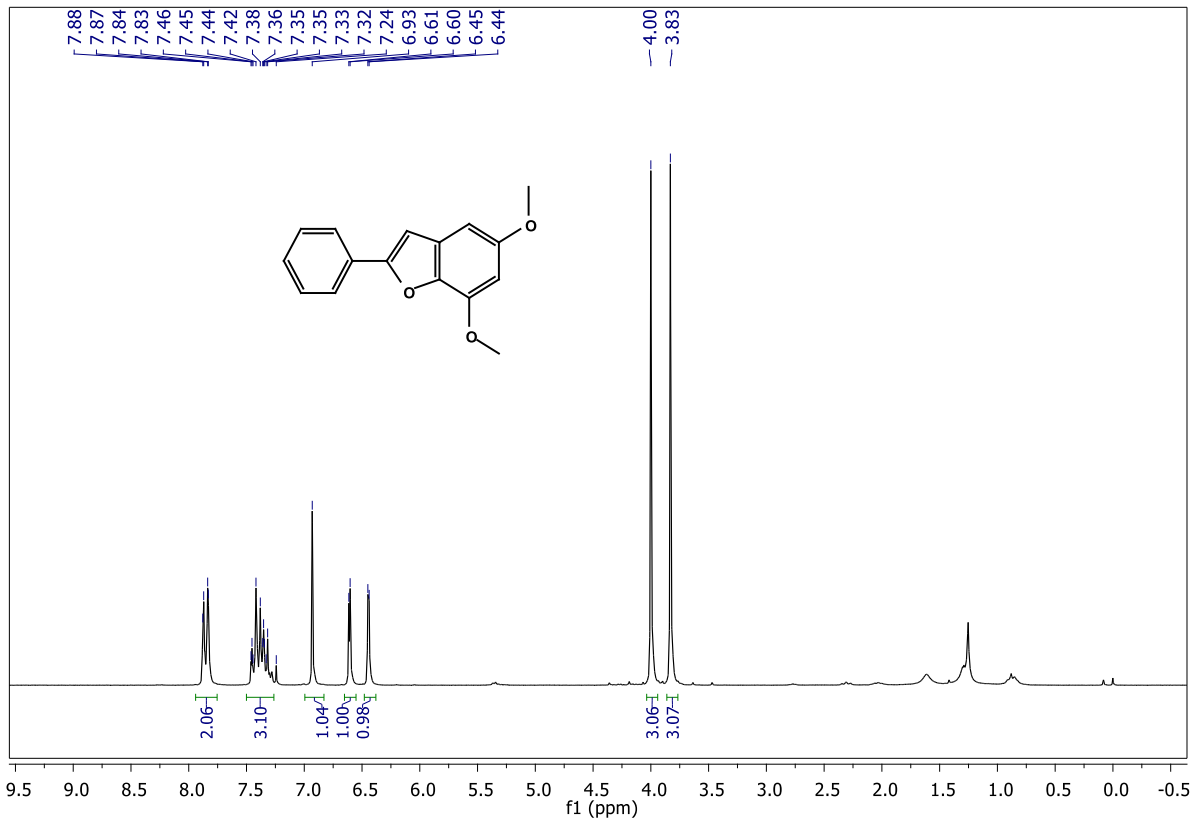

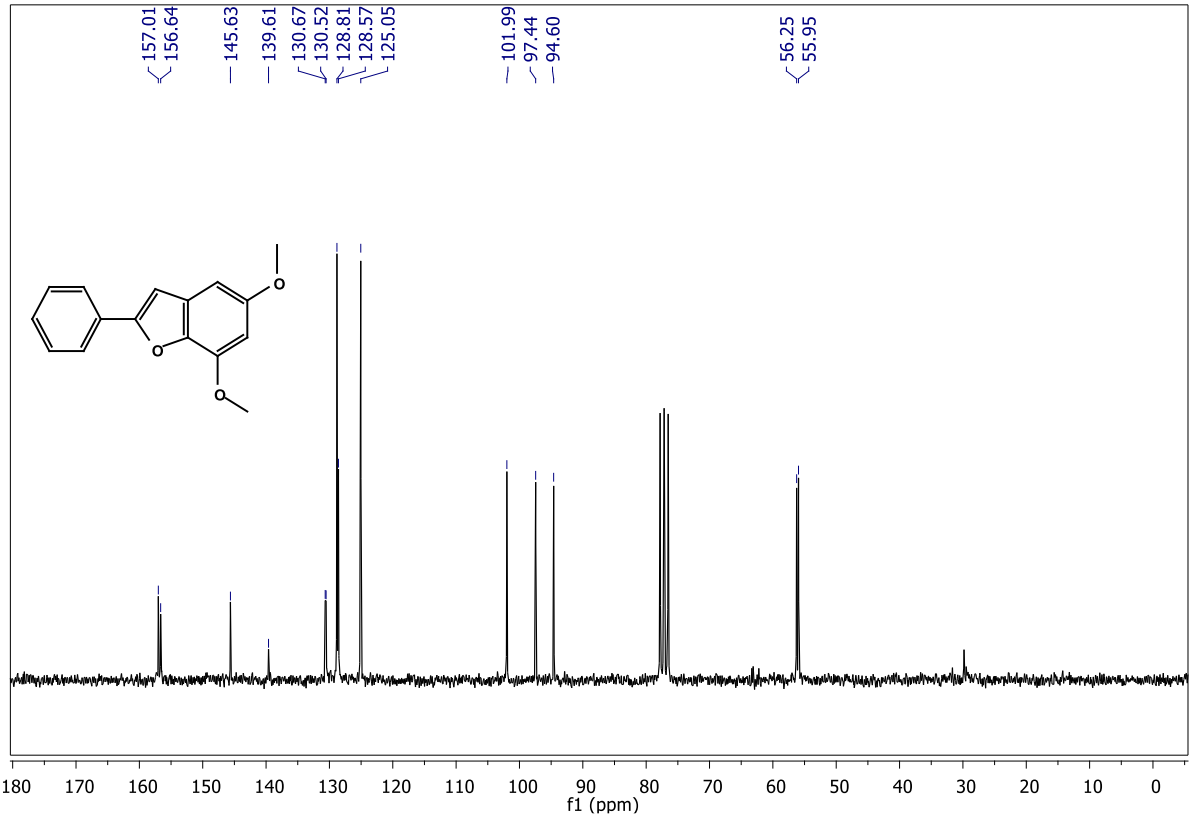

^{1}H and ^{13}C NMR spectra of 6b

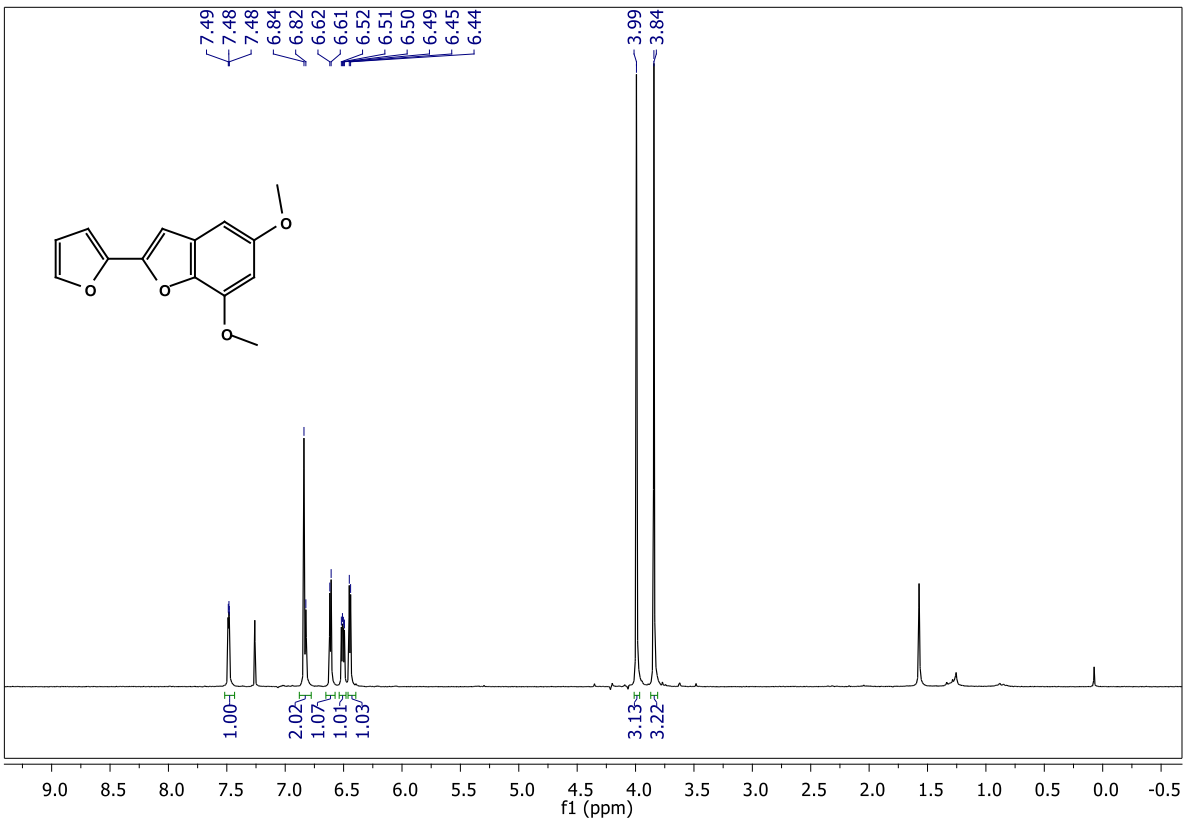

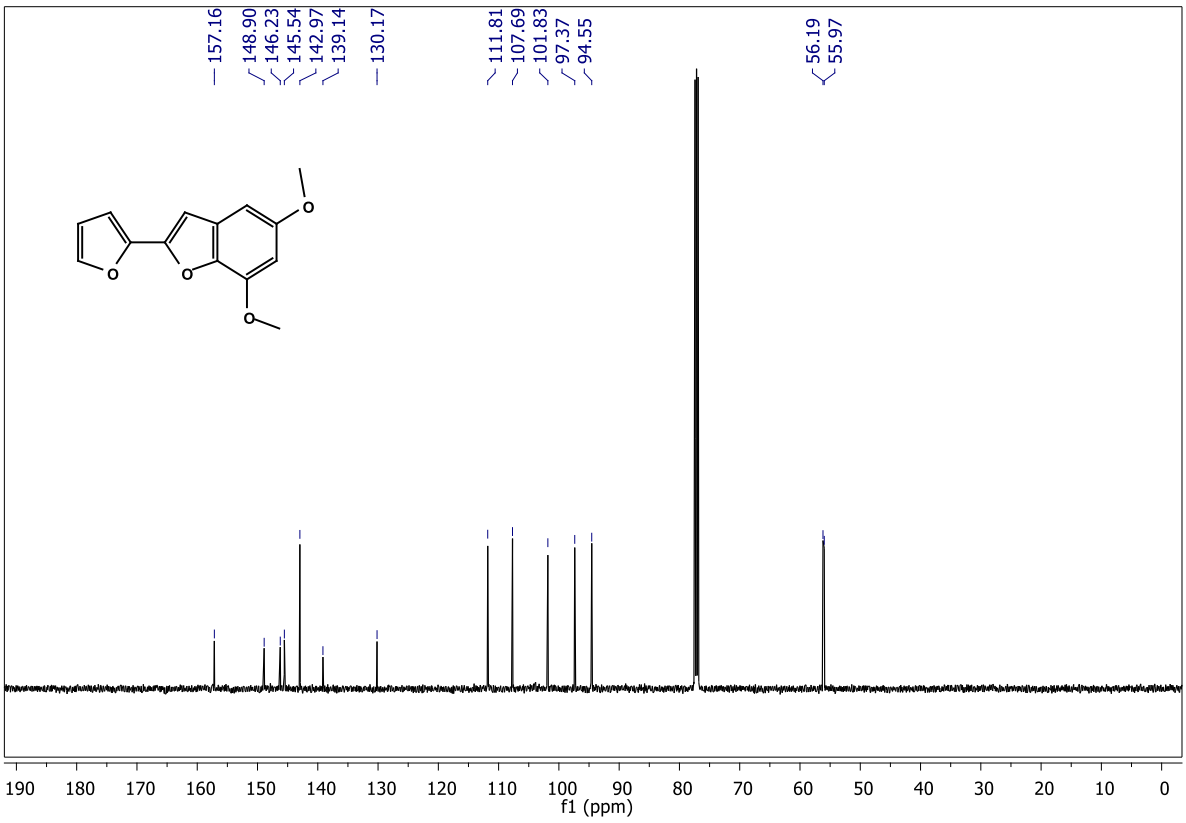

^{1}H and ^{13}C NMR spectra of 6c

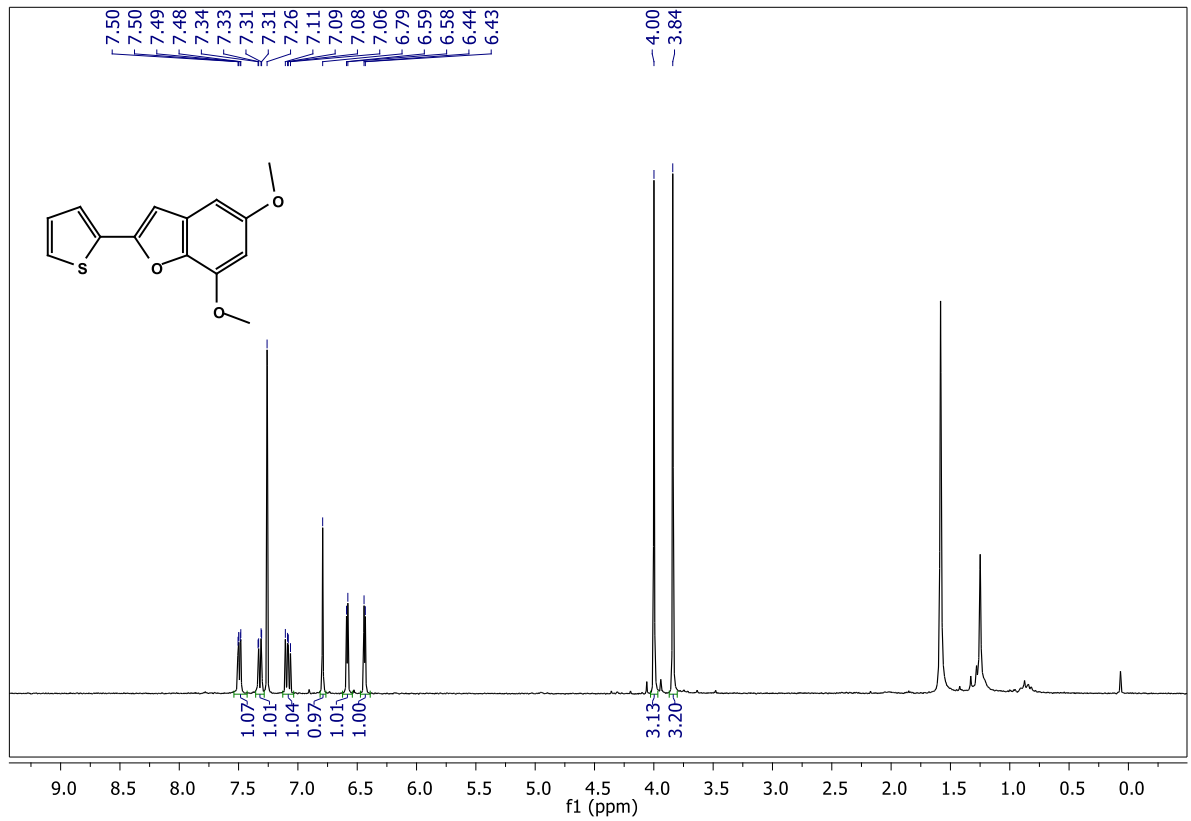

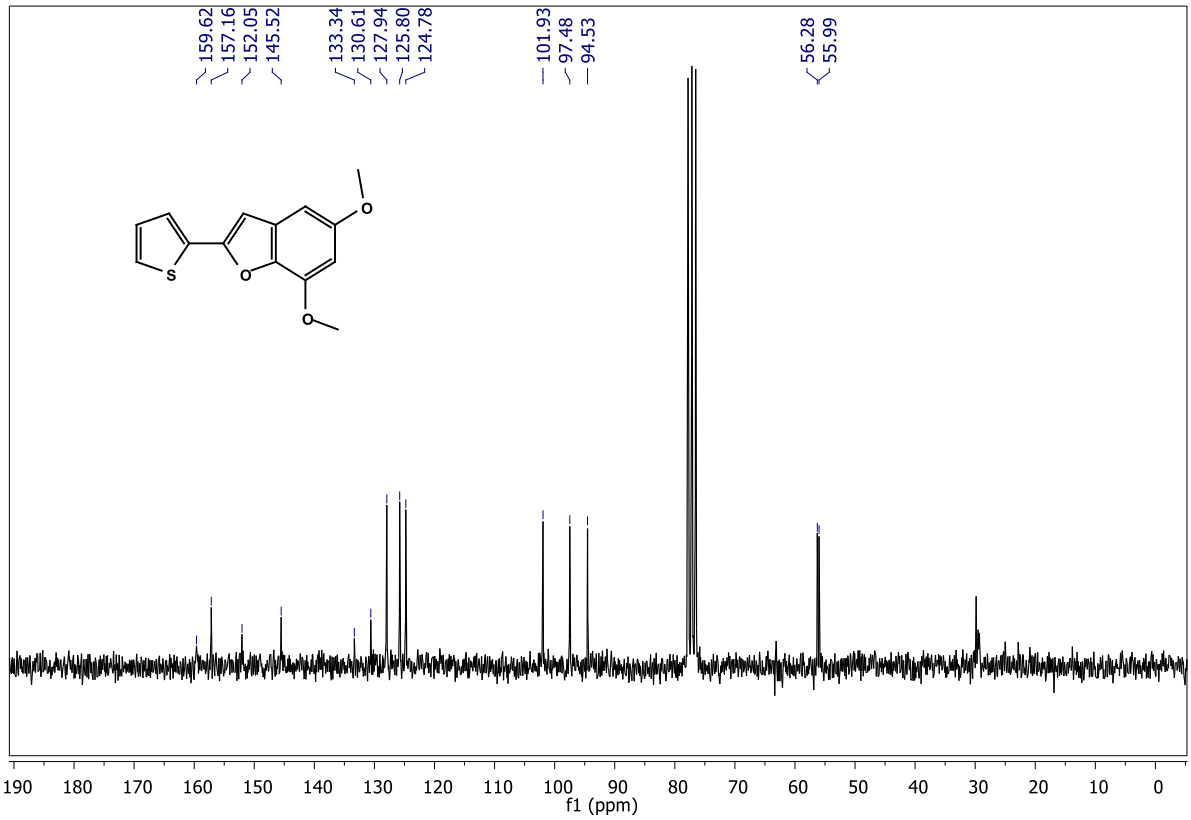

^{1}H and ^{13}C NMR spectra of 6d

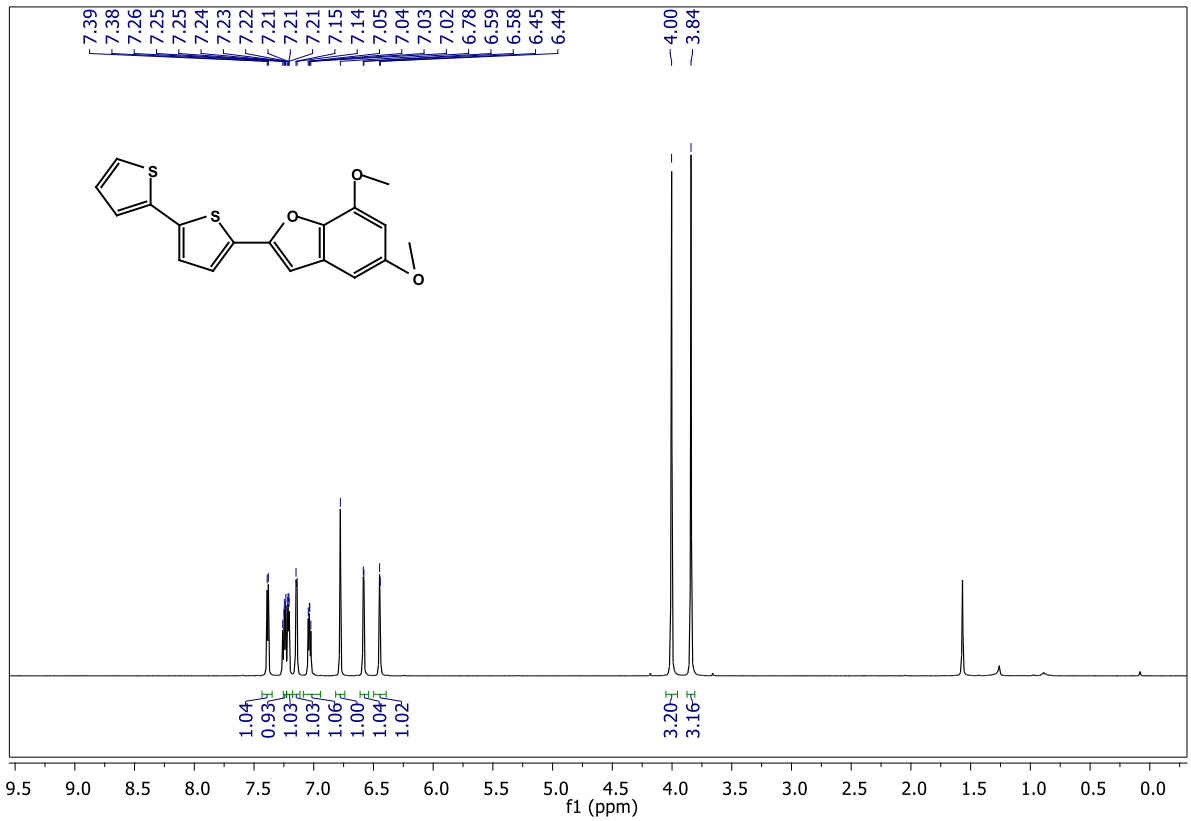

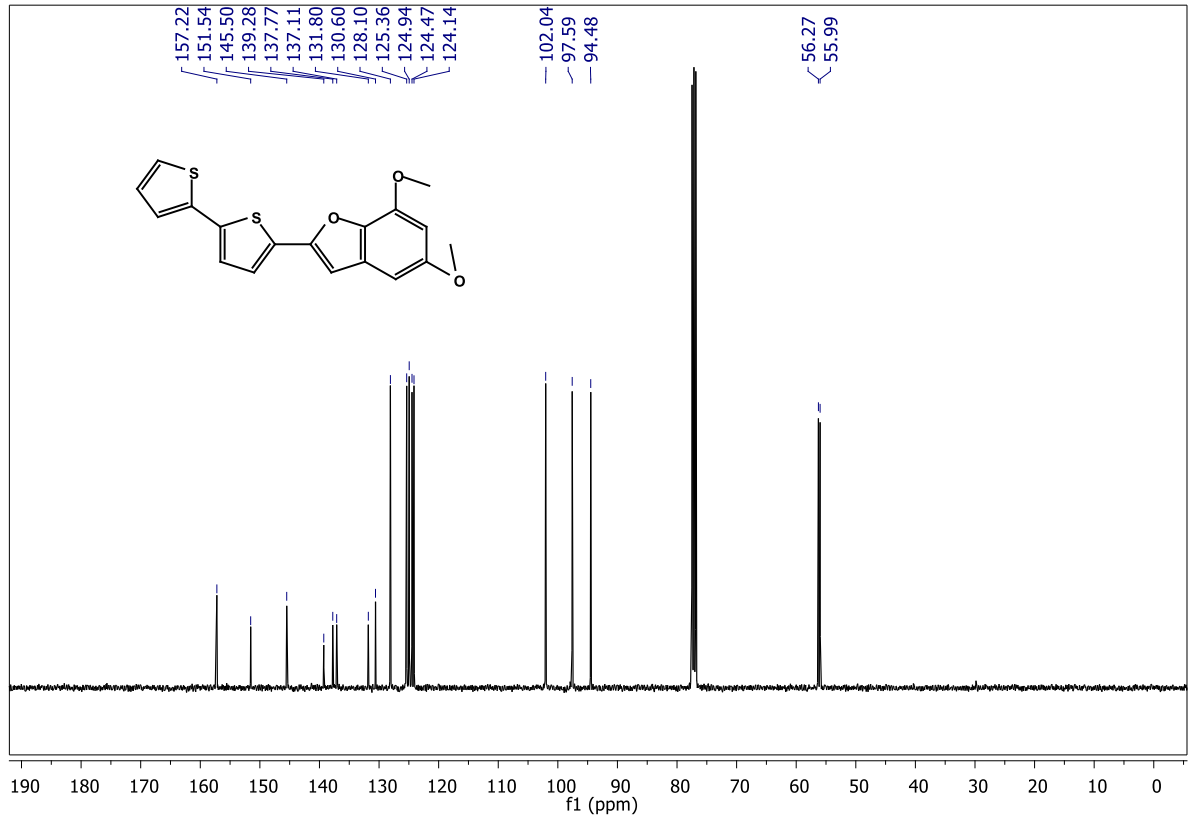

^{1}H and ^{13}C NMR spectra of 6e

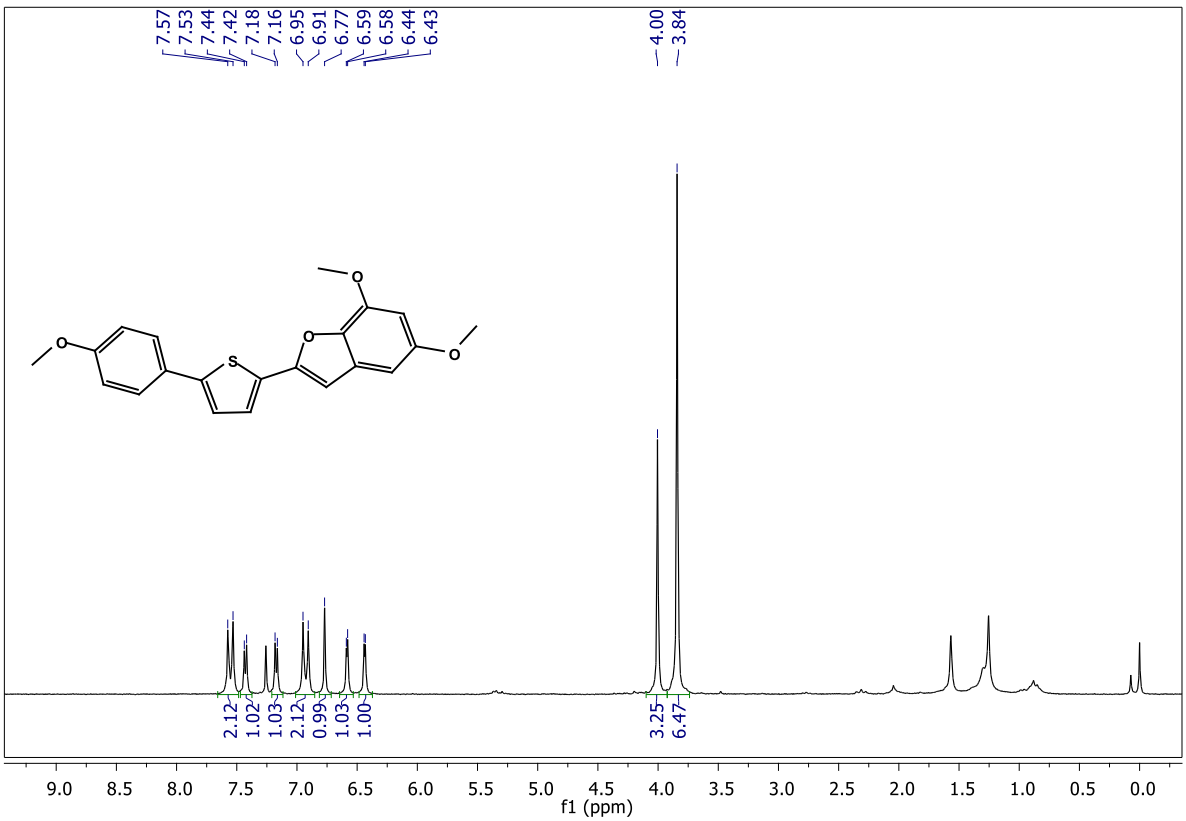

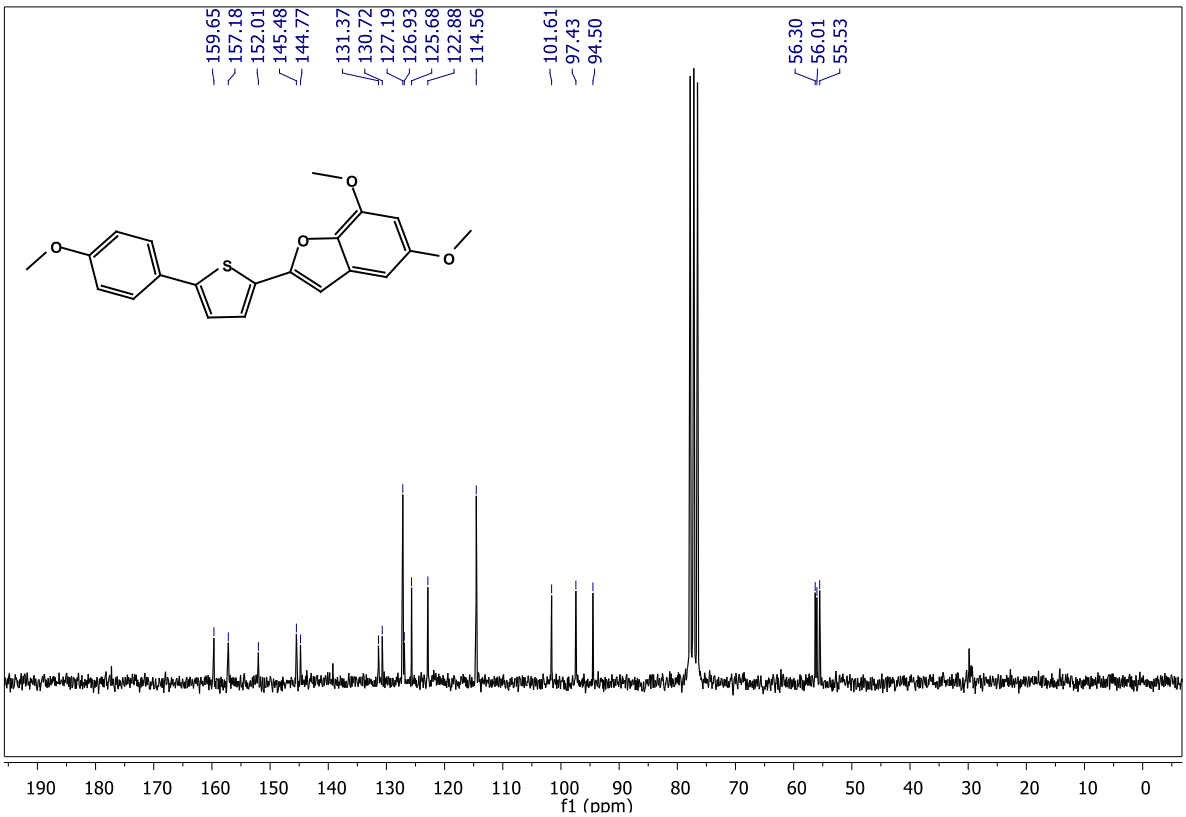

^{1}H and ^{13}C NMR spectra of 7e

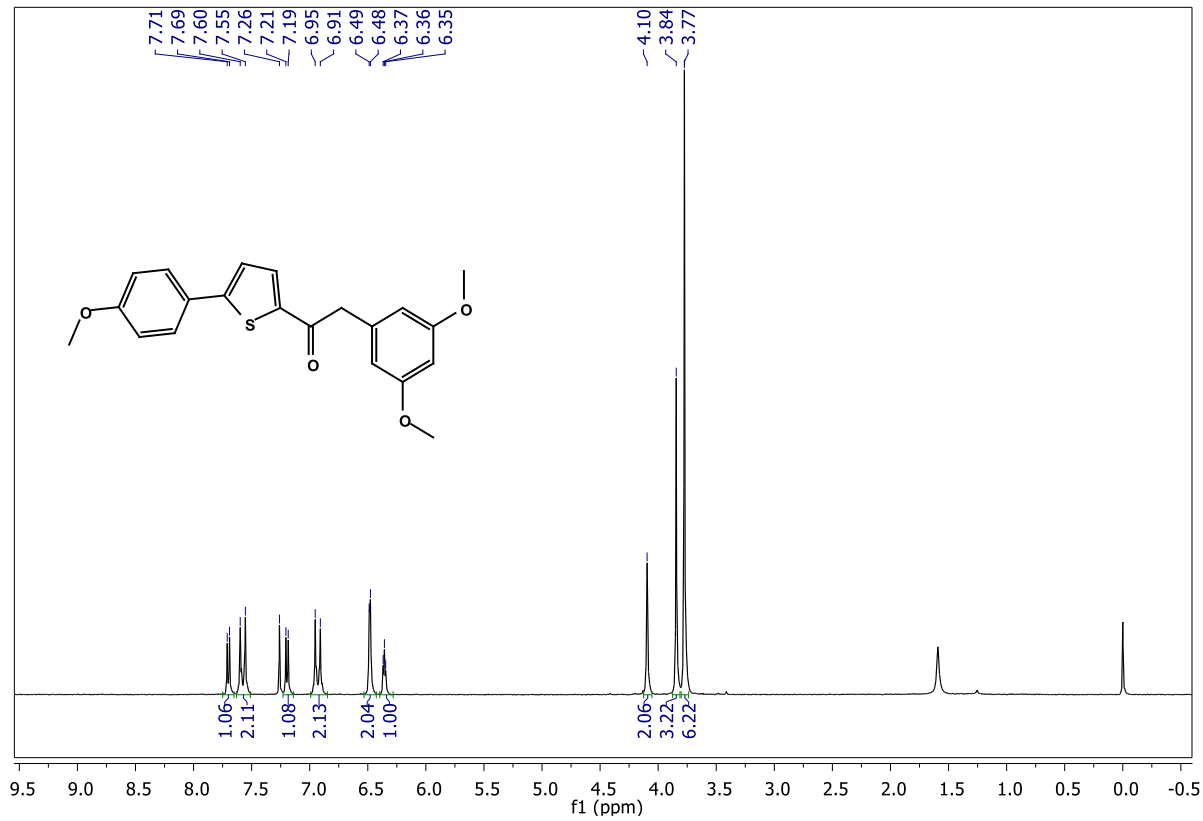

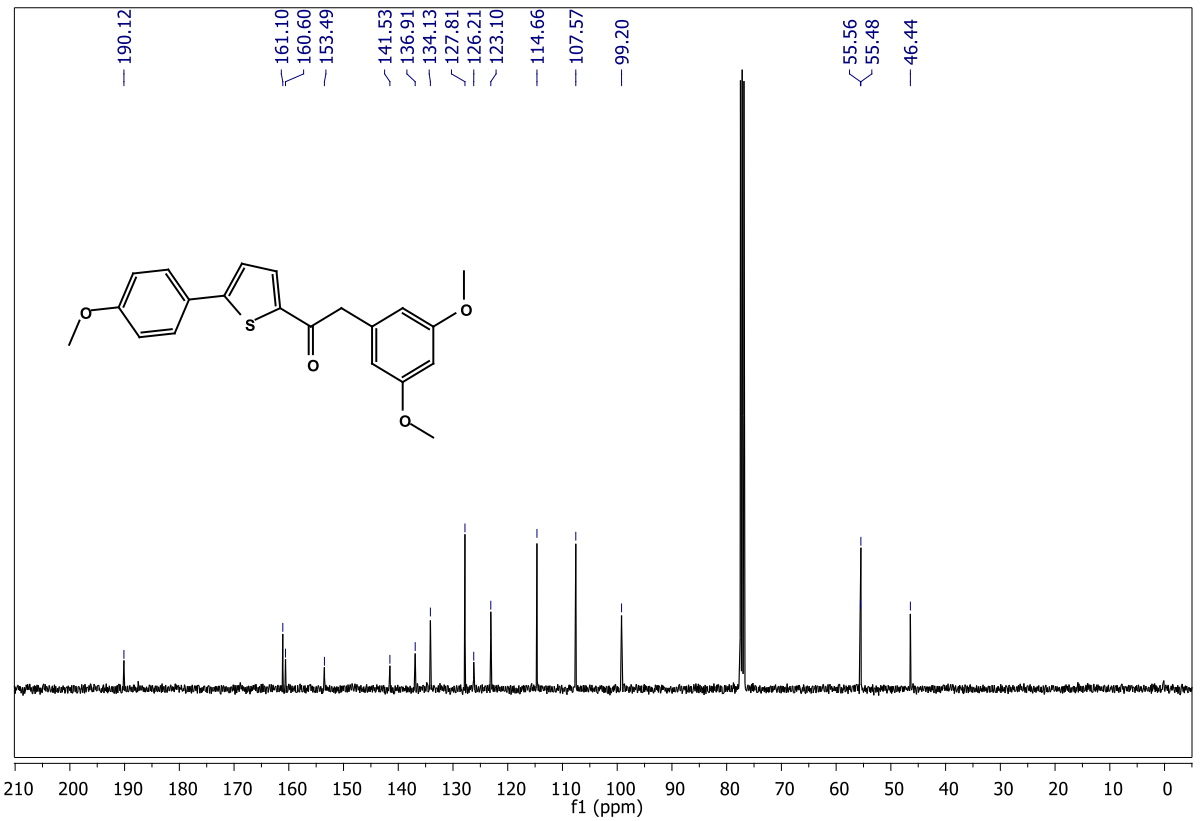

^{1}H and ^{13}C NMR spectra of 6f

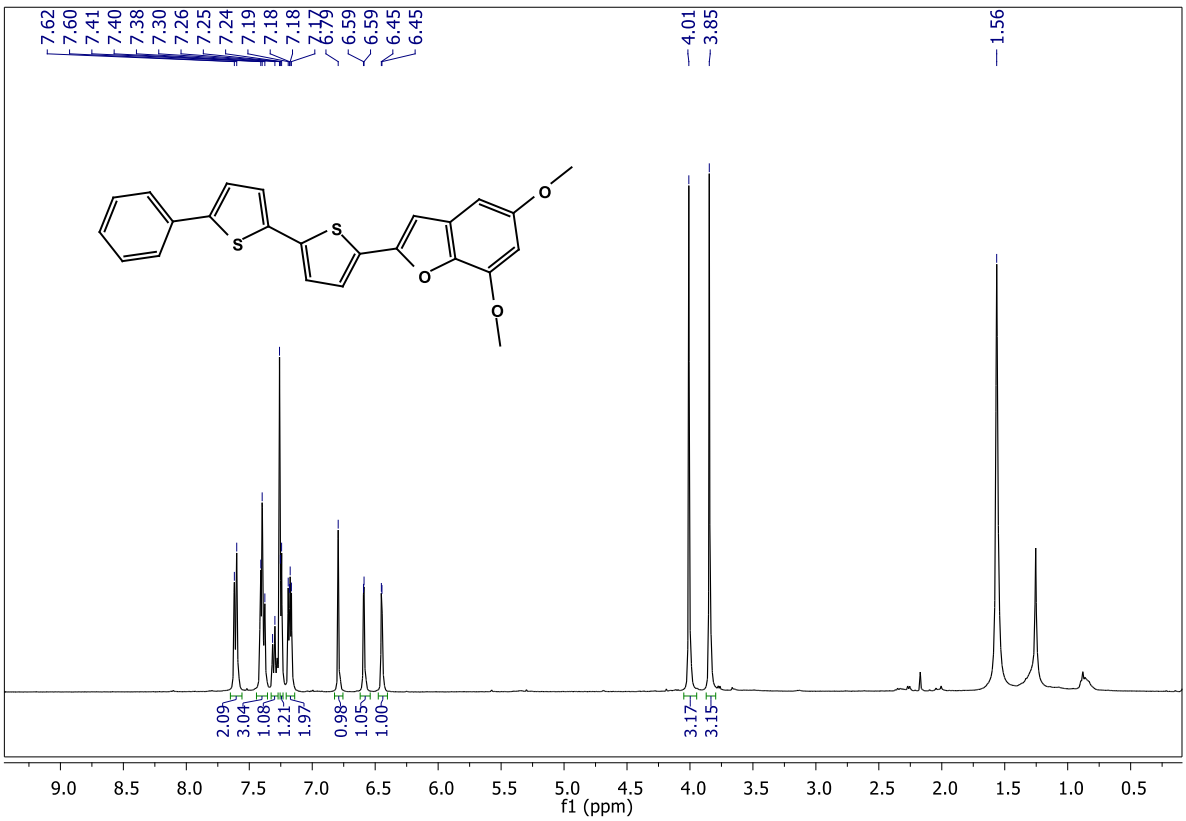

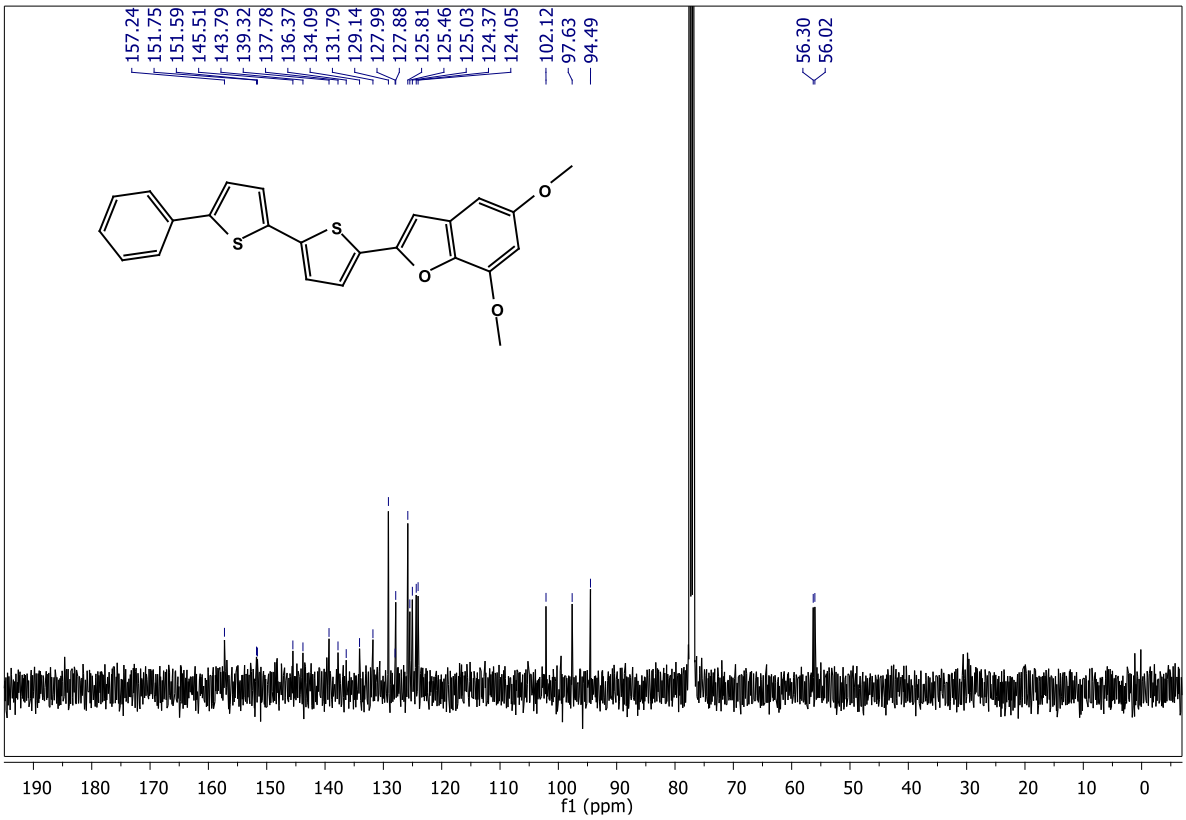

^{1}H and ^{13}C NMR spectra of 7f

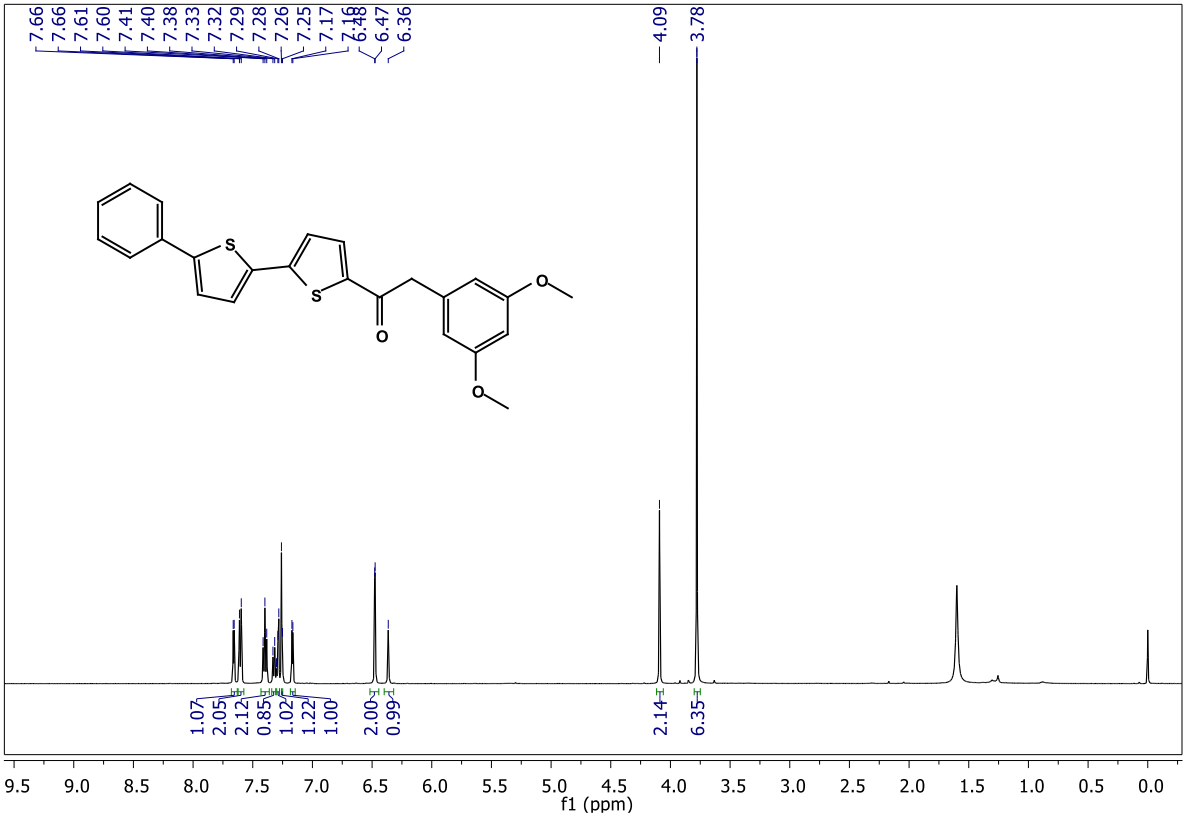

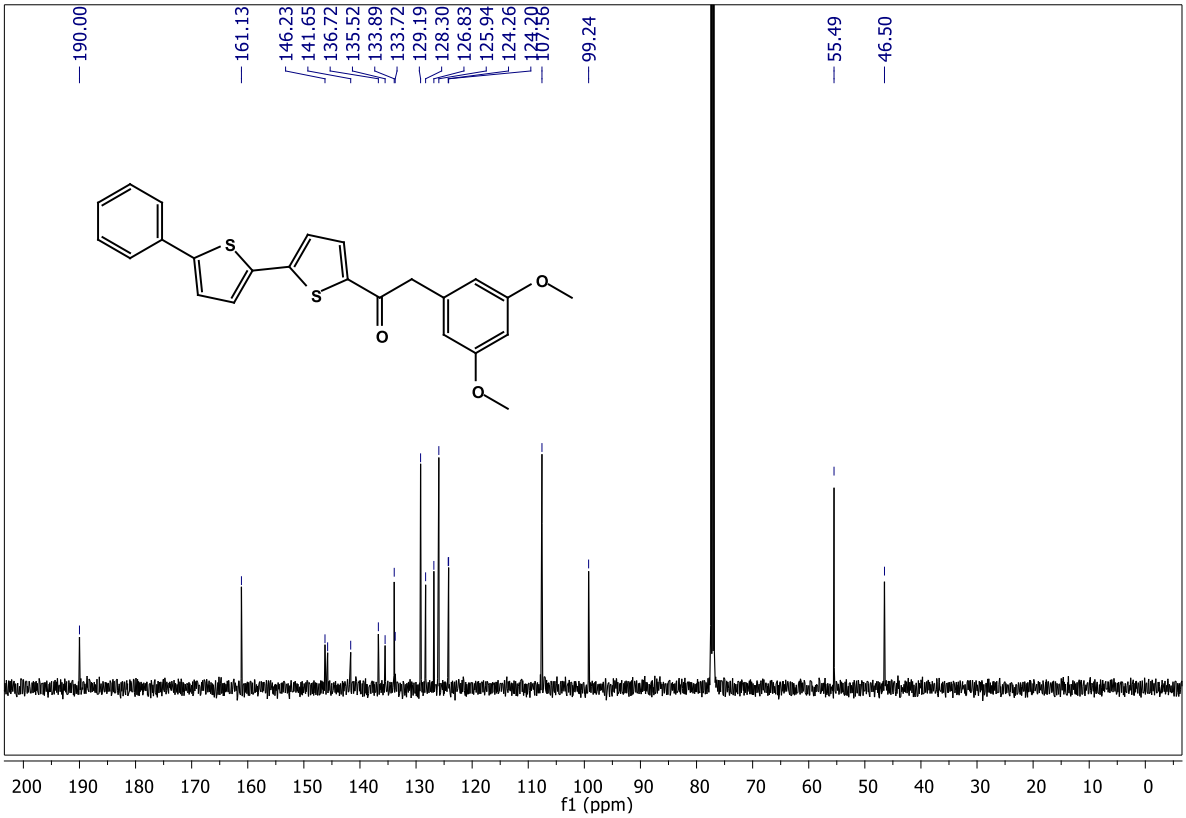

5.6. REFERENCES

(1) Forrest, S. R. *Chem. Rev.* **1997**, *97*, 1793–1896.

(2) Forrest, S. R. *Nature* **2004**, *428*, 911–918.

(3) Locklin, J.; Roberts, M. E.; Mannsfeld, S. C. B.; Bao, Z. *J. Macromol. Sci. Part C Polym. Rev.* **2006**, *46*, 79–101.

(4) Krebs, F. C. *Sol. Energy Mater. Sol. Cells* **2009**, *93*, 394–412.

(5) Norrman, K.; Ghanbari-Siahkali, A.; Larsen, N. B. *Annu. Rep. Sect. C Phys. Chem.* **2005**, *101*, 174–201.

(6) Mens, R.; Adriaensens, P.; Lutsen, L.; Swinnen, A.; Bertho, S.; Ruttens, B.; D'Haen, J.; Manca, J.; Cleij, T.; Vanderzande, D.; Gelan, J. *J. Polym. Sci. Part Polym. Chem.* **2008**, *46*, 138–145.

(7) Schilinsky, P.; Waldauf, C.; Brabec, C. J. *Adv. Funct. Mater.* **2006**, *16*, 1669–1672.

(8) Herwig, P. T.; Müllen, K. *Adv. Mater.* **1999**, *11*, 480–483.

(9) Aramaki, S.; Sakai, Y.; Ono, N. *Appl. Phys. Lett.* **2004**, *84*, 2085–2087.

(10) Murphy, A. R.; Fréchet, J. M. J.; Chang, P.; Lee, J.; Subramanian, V. *J. Am. Chem. Soc.* **2004**, *126*, 1596–1597.

(11) Krebs, F. C.; Norrman, K. *ACS Appl. Mater. Interfaces* **2010**, *2*, 877–887.

(12) Johnson Ross S.; Haworth Jacob J.; Finnegan Patrick S.; Wheeler David R.; Dirk Shawn M. *Macromol. Rapid Commun.* **2014**, *35*, 1116–1120.

(13) Lee, S. K.; Jung, B.-J.; Ahn, T.; Song, I.; Shim, H.-K. *Macromolecules* **2003**, *36*, 9252–9256.

(14) Johnson, R. S.; Finnegan, P. S.; Wheeler, D. R.; Dirk, S. M. *Chem. Commun.* **2011**, *47*, 3936–3938.

(15) Gumbley, P.; Koylu, D.; Pawle, R. H.; Umezuruike, B.; Spedden, E.; Staii, C.; Thomas, S. W. *Chem. Mater.* **2014**, *26*, 1450–1456.

(16) Thomas Samuel W. *Macromol. Chem. Phys.* **2012**, *213*, 2443–2449.

(17) Smith, Z. C.; Meyer, D. M.; Simon, M. G.; Staii, C.; Shukla, D.; Thomas, S. W. *Macromolecules* **2015**, *48*, 959–966.

(18) Sheehan, J. C.; Wilson, R. M. *J. Am. Chem. Soc.* **1964**, *86*, 5277–5281.

(19) Sheehan, J. C.; Wilson, R. M.; Oxford, A. W. *J. Am. Chem. Soc.* **1971**, *93*, 7222–7228.

(20) Givens, R. S.; Kueper, L. W. *Chem. Rev.* **1993**, *93*, 55–66.

(21) Peach, J. M.; Pratt, A. J.; Snaith, J. S. *Tetrahedron* **1995**, *51*, 10013–10024.

(22) Rock, R. S.; Chan, S. I. *J. Am. Chem. Soc.* **1998**, *120*, 10766–10767.

(23) Pirrung, M. C.; Huang, C.-Y. *Tetrahedron Lett.* **1995**, *36*, 5883–5884.

(24) McCoy, C. P.; Rooney, C.; Edwards, C. R.; Jones, D. S.; Gorman, S. P. *J. Am. Chem. Soc.* **2007**, *129*, 9572–9573.

(25) Pirrung, M. C.; Bradley, J.-C. *J. Org. Chem.* **1995**, *60*, 6270–6276.

(26) Pirrung, M. C.; Fallon, L.; Lever, D. C.; Shuey, S. W. *J. Org. Chem.* **1996**, *61*, 2129–2136.

(27) Pirrung, M. C.; Bradley, J.-C. *J. Org. Chem.* **1995**, *60*, 1116–1117.

(28) Rock, R. S.; Chan, S. I. *J. Org. Chem.* **1996**, *61*, 1526–1529.

(29) Rock, R. S.; Hansen, K. C.; Larsen, R. W.; Chan, S. I. *Chem. Phys.* **2004**, *307*, 201–208.

(30) Pirrung, M. C.; Shuey, S. W. *J. Org. Chem.* **1994**, *59*, 3890–3897.

(31) Shi, Y.; Corrie, J. E.; Wan, P. *J. Org. Chem.* **1997**, *62*, 8278–8279.

(32) Rajesh, C. S.; Givens, R. S.; Wirz, J. *J. Am. Chem. Soc.* **2000**, *122*, 611–618.

(33) Ma, C.; Kwok, W. M.; An, H.-Y.; Guan, X.; Fu, M. Y.; Toy, P. H.; Phillips, D. L. *Chem. - Eur. J.* **2010**, *16*, 5102–5118.

(34) Ma, C.; Du, Y.; Kwok, W. M.; Phillips, D. L. *Chem. – Eur. J.* **2007**, *13*, 2290–2305.

(35) Cameron, J. F.; Willson, C. G.; Fréchet, J. M. J. *J. Chem. Soc. Chem. Commun.* **1995**, *0*, 923–924.

(36) Pirrung, M. C.; Ye, T.; Zhou, Z.; Simon, J. D. *Photochem. Photobiol.* **2006**, *82*, 1258–1264.

(37) Speckmeier, E.; Padié, C.; Zeitler, K. *Org. Lett.* **2015**, *17*, 4818–4821.

(38) Mei, J.; Bao, Z. *Chem. Mater.* **2014**, *26*, 604–615.

(39) Mei, J.; Kim, D. H.; Ayzner, A. L.; Toney, M. F.; Bao, Z. *J. Am. Chem. Soc.* **2011**, *133*, 20130–20133.

(40) Gordon, T. J.; Yu, J.; Yang, C.; Holdcroft, S. *Chem. Mater.* **2007**, *19*, 2155–2161.

(41) Videlot-Ackermann, C.; Ackermann, J.; Brisset, H.; Kawamura, K.; Yoshimoto, N.; Raynal, P.; El Kassmi, A.; Fages, F. *J. Am. Chem. Soc.* **2005**, *127*, 16346–16347.

(42) Smith, Z. C.; Pawle, R. H.; Thomas, S. W. *ACS Macro Lett.* **2012**, *1*, 825–829.

(43) Bjerring, M.; Nielsen, J. S.; Nielsen, N. C.; Krebs, F. C. *Macromolecules* **2007**, *40*, 6012–6013.

(44) S. Johnson, R.; S. Finnegan, P.; R. Wheeler, D.; M. Dirk, S. *Chem. Commun.* **2011**, *47*, 3936–3938.

(45) Nicolas, Y.; Blanchard, P.; Roncali, J.; Allain, M.; Mercier, N.; Deman, A.-L.; Tardy, J. *Org. Lett.* **2005**, *7*, 3513–3516.

(46) Turro, N. J.; Ramamurthy, V.; Scaiano, J. C. University Science Books*Modern Molecular Photochemistry of Organic Molecules*, 2010.

(47) Banerjee, A.; Lee, K.; Falvey, D. E. *Tetrahedron* **1999**, *55*, 12699–12710.

(48) Ballardini, R.; Varani, G.; Indelli, M. T.; Scandola, F.; Balzani, V. *J. Am. Chem. Soc.* **1978**, *100*, 7219–7223.

(49) Yip, R. W.; Loutfy, R. O.; Chow, Y. L.; Magdzinski, L. K. *Can. J. Chem.* **1972**, *50*, 3426–3431.

(50) Wu, W.; Liu, Y.; Zhu, D. *Chem. Soc. Rev.* **2010**, *39*, 1489–1502.

(51) Mas-Torrent, M.; Rovira, C. *Chem. Soc. Rev.* **2008**, *37*, 827–838.

(52) Mallet, C.; Didane, Y.; Watanabe, T.; Yoshimoto, N.; Allain, M.; Videlot-Ackermann, C.; Frère, P. *ChemPlusChem* **2013**, *78*, 459–466.

(53) Mitsui, C.; Soeda, J.; Miwa, K.; Tsuji, H.; Takeya, J.; Nakamura, E. *J. Am. Chem. Soc.* **2012**, *134*, 5448–5451.

Chapter 6

Summary and Future Outlooks

6.1. Summary

Due to unrestricted population growth and rampant urbanization, energy security and global warming have become a severe problem for the current and future generation. Photovoltaic devices or solar cells are one of the tools which can tap the solar energy for clean and sustainable energy supply. Dye-sensitized solar cells (DSSC) have shown great potential as an alternative to silicon-based solar cells for future demand of clean and renewable energy. Developments in the various key components have significantly improved the efficiency of DSSCs in past two decades. Sensitizers or dyes are one of the crucial components in DSSC which absorbs the light and helps in generating current.

Among sensitizers, NIR-absorbing dyes are highly desirable in DSSCs to utilize the low energy photons. Squaraine dyes are among the few chromophores which have potential to absorb in NIR region. However, very few squaraine based dyes have absorption beyond 750 nm. There are two major strategies to extend the absorption of squaraine dyes further into the NIR region, i) covalently linking an additional π-spacer to squaraine dye (Chapter 2), and ii) modifying the donor flanking the central squaraine unit(Chapter 3 and 4). Increasing the conjugation of squaraine dyes also leads to increased aggregation which is detrimental to DSSC performance. Hence proper strategy to control aggregation is also vital for optimum cell performance.

A series of squaraine based dyes (**RSQ1-2**) were synthesized in which BDT unit was appended to squaraine unit towards anchoring end (**Chapter 2**). BDT unit was functionalized with -OMe and -OEthylhexyl groups to compare and understand the effect of alkyl chains on aggregation of these dyes. Since both the dyes possess similar conjugated backbone, they have similar electronic properties which are evident from the identical absorption profile of both dyes in solution. However, the spectra on thin film show the greater aggregation of methyl substituted (**RSQ1**) dye compared to ethylhexyl substituted dye (**RSQ2**) which suggest the ability of branched ethylhexyl chain to restrict aggregation. It also provides surface passivation to TiO_2 and restricts charge recombination which is supported by EIS studies. As a result, **RSQ2** showed better V_{OC} than **RSQ1** which lead to the efficiency of 672 % without co-adsorbent. The dyes showed good response towards NIR region with IPCE extending up to 770 nm.

The π-extended donors in squaraine dyes can significantly enhance the absorption in NIR region. However, the increased planarity also increases the aggregation by providing larger π-surface. Hence in C**hapter 3**, we discussed the design of a fused fluorene and indole-based donor, fluorenylindoleine, which can accommodate four out-of-plane alkyl chains to control aggregation and can also increase absorption towards NIR region. A series of four dyes **XSQ1-4** were synthesized using the donor. The out-of-plane alkyl chains helped to manage the aggregation efficiently, and the dyes showed IPCE onset up to 800 nm with best PCE of 6.57 %. We also systematically investigated the effect of branched alkyl chains on the performance of DSSC. The addition of 3 equiv CDCA gave significant improvement in J_{SC} for all the dyes without considerable change in the dye loading. This suggests that excessive branched chains around the dyes create a void between dye molecules which can be occupied by CDCA. As a result, the dyes provide effective surface passivation and reduced self-quenching of excition, without compromising the dye loading. **XSQ3** showed IPCE response up to 800 nm with the highest efficiency of 6.57 %.

To further extend the response of squaraine dyes in NIR region, we explored the possibility of fusing fluorene with donor stronger than indolenine such as quinaldine. So in **Chapter 4**, we described the synthesis and properties of fused fluorene and quinaldine based donor, indenoquinaldine, which was appended with two C-12 alkyl chain in the out-of-plane direction. Towards the anchoring end, the donor was changed to indoleine, benze[e]indolenine and quinaldine to form a series of squaraine dye **ISQ1**, **ISQ2** and **ISQ3** respectively. Despite possessing long branched alkyl chains, the dyes showed extensive aggregation. The addition of CDCA exhibited a different response in different dyes. The efficiency of **ISQ1** was decreased significantly due to a drastic decrease in dye loading whereas **ISQ2** and **ISQ3** showed improvement in efficiency with the addition of CDCA. The results suggest that the difference in the donor moieties towards anchoring end dictates their dye-dye and dye-TiO_2 interaction. The formation of dye monolayer by **ISQ1** on TiO_2 is easily disturbed by adding the even slight amount of CDCA which was ascribed to weak dye-dye interaction in **ISQ1**. Due to good panchromatic IPCE response with onset up to 880 nm, **FSQ3** showed the highest efficiency of 4.1 % in the presence of 10 equiv CDCA.

Apart from squaraine dyes for DSSC, we also explored the benzoin type phototriggers for their possible application in the photochemical solution-based processing in organic

electronics. The removal of solubilizing groups in the conjugated molecules in post-processing step has shown promising results in organic electronics. However, these methods involve high temperatures in which compound may not be stable. Hence, we tried to explore the application of phototriggers in a photochemical method for removal of the solubilizing group in a post-processing step.

Several phototriggers have been reported in the literature and have been used for the various application. However, their application in material processing, except photo patterning, is very limited. The known 3',5'-dimethoxy benzoin acetate trigger cyclizes into benzofuran derivative upon irradiation with the release of carboxylic acid. Hence, it provides the advantage over other triggers in that it can extend the conjugation in addition to removal of the solubilizing group. We proposed that such benzoin type trigger can be included in the conjugated molecules which can help in photochemical processing. Thus in **Chapter 5**, we explored a photochemical method for solution based processing using benzoin type phtotriggers. For this purpose, we synthesized a set of heteroaromatic cross acyloin derivatives and tested their photoreactivity. The small conjugated phototrigger reacted as expected to give benzofuran derivatives in good yields but the phototriggers with extended conjugation did not give the desired product and most of the reactant decomposed. However, in the presence of triethylamine (Et_3N), the extended triggers exhibited modulated photoreactivity. Addition of one equiv Et_3N resulted in cyclization to benzofuran as major product and deacetoxylated derivatives as a minor product. Further addition of Et_3N resulted in a change in the ratio of the two photoproducts, with an increase in deacetoxylated product and decrease in cyclized product. We also tested the cyclized photoproducts of extended triggers in organic field effect transistors and moderate mobilities in the order of 10^{-6}-10^{-8} cm^2/Vs was obtained.

6.2. Future outlooks

Based on the finding of this work, several squaraine dyes with strong NIR absorption can be designed for efficient DSSC. The extended donors with out-of-plane branched chains can be condensed with various semi-squaric acid derivatives to form new dye that can control aggregation. As these dyes have strong absorption in NIR region, they can be co-sensitized with dyes having strong absorption in the visible region to form a panchromatic DSSC. Also, the absorption of XSQ type of dye can be further extended by attaching covalently linked π-

bridge with cyanoacrylic acid as anchoring group. The HOMO levels of indenoquinaldine dyes are comparatively high which may restrict dye regeneration. Suitable modification and substitution, such as incorporating an electron withdrawing group towards anchoring group can help to rectify the issue. This research can also help in designing visible light responsive phototriggers for various applications.

List of Publications

1. Bisht, R.; M. K., M. F.; Singh, A. K.; Nithyanandhan, J. Panchromatic Sensitizer for Dye-Sensitized Solar Cells: Unsymmetrical Squaraine Dyes Incorporating Benzodithiophene π-Spacer with Alkyl Chains to Extend Conjugation, Control the Dye Assembly on TiO2, and Retard Charge Recombination. *J. Org. Chem.* **2017**, *82*, 1920–1930.

2. Bisht, R.; Sudhakar, V.; Mele Kavungathodi, M. F.; Karjule, N.; Nithyanandhan, J. Fused Fluorenylindolenine-Donor-Based Unsymmetrical Squaraine Dyes for Dye-Sensitized Solar Cells. *ACS Appl. Mater. Interfaces* **2018**, *10*, 26335–26347.

3. Bisht, R.; Mele Kavungathodi, M. F.; Nithyanandhan, J. Indenoquinaldine Based Unsymmetrical Squaraine Dyes for Near-Infrared Absorption: Investigating the Steric and Electronic Effects in Dye-Sensitized Solar Cells. *Chemistry – A European Journal* **2018** .(https://doi.org/10.1002/chem.201803062)

4. Bisht, R.; Singh, S.; Krishnamoorthy, K.; Nithyanandhan, J. Modulated Photochemical Reactivities of O-Acetylated (3′,5′-Dimethoxyphenyl)Heteroaryl Acyloin Derivatives under Direct Irradiation and Photo-Induced Electron Transfer Conditions. *Photochem. Photobiol. Sci.* **2018**, *17*, 835–845.

5. Thangaraj, M.; Bhojgude, S. S.; **Bisht, R.** H.; Gonnade, R. G.; Biju, A. T. Diels–Alder Reaction of Tropones with Arynes: Synthesis of Functionalized Benzobicyclo[3.2.2]Nonatrienones. *J. Org. Chem.* **2014**, *79*, 4757–4762.

Erratum